UNIVERSITY OF SOUTHAMPTON

FACULTY OF ENGINEERING AND PHYSICAL SCIENCES

Active Vibration Control for Asymmetric Systems by Pole Assignment

by

Rittirong Ariyatanapol

Thesis for the degree of Doctor of Philosophy

December 2018

UNIVERSITY OF SOUTHAMPTON

ABSTRACT

FACULTY OF ENGINEERING AND PHYSICAL SCIENCES

Doctor of Philosophy

ACTIVE VIBRATION CONTROL FOR ASYMMETRIC SYSTEMS BY POLE ASSIGNMENT

by Rittirong Ariyatanapol

Most structural systems are symmetric and naturally stable but some are asymmetric and prone to instability. The asymmetric system is defined by a non-symmetric matrix and generated by a non-conservative force. When the force is bigger than a critical point, poles are shifted from the left-hand side to the right-hand side of the complex plane leading to instability. To stabilise the unstable asymmetric system, partial pole assignment by using an unobservability condition is implemented to assign unstable poles and keep others unchanged. It requires both unassigned poles and mode shapes in order to keep the poles unchanged. Nonetheless, the mode shapes of the asymmetric system is difficult to evaluate. This thesis proposes a new algorithm of partial pole assignment by using the unobservability condition which requires only unassigned poles to keep them unchanged. Both single and couple time delays are also included in the control algorithm to avoid spill-over effect.

The algorithm of partial pole assignment with and without time delay can assign the required closed-loop poles precisely when the non-conservative force is a certain value. However, it is changeable and makes the closed-loop poles shifted away from desired locations. The closed-loop system may be unstable if the force is highly uncertain. To deal with this problem, sensitivities of the closed-loop poles must be minimised by using the robust pole assignment. A former algorithm is available for a case of friction-induced vibration by using the single-input control. In this thesis, a novel method of robust pole assignment to minimise sensitivities by using multiple-input control is proposed. Both friction-induced vibration and aerodynamic flutter problems are considered. Furthermore, a new concept to minimise magnitudes of vibration responses by evaluating the optimal closed-loop poles is focused. The power flow mode theory based on damping distribution may reveal the optimal locations of poles by maximising the time-averaged power dissipation per unit characteristic velocity.

Contents

List of Figures

List of Tables

Declaration of Authorship

I, Rittirong Ariyatanapol , declare that the thesis entitled *Active Vibration Control for Asymmetric Systems by Pole Assignment* and the work presented in the thesis are both my own, and have been generated by me as the result of my own original research. I confirm that:

- this work was done wholly or mainly while in candidature for a research degree at this University;
- where any part of this thesis has previously been submitted for a degree or any other qualification at this University or any other institution, this has been clearly stated;
- where I have consulted the published work of others, this is always clearly attributed;
- where I have quoted from the work of others, the source is always given. With the exception of such quotations, this thesis is entirely my own work;
- I have acknowledged all main sources of help;
- where the thesis is based on work done by myself jointly with others, I have made clear exactly what was done by others and what I have contributed myself;
- parts of this work have been published as: Ariyatanapol et al. (2018)

Signed:.....Rittirong Ariyatanapol.....

Date:.....20 December 2018.....

Acknowledgements

I would like to take this opportunity to thank many people who supported me over the past four years as a researcher at University of Southampton. Without the following names, this research has not been successful.

First of all, I would like to thank the supervisory team of this project, Associate Prof Yeping Xiong from University of Southampton and Prof Huajiang Ouyang from University of Liverpool, for their valuable guidance and encouragement in every aspect. I am also grateful to Dr Khemapat Tontiwattanakul, Dr Kantapon Tanakitkorn and Dr Ponprot Boonpratpai for their help and support since my master degree study.

Special thanks to my wife for making me feel at home in UK, reducing my stress and supporting my study all the time. Special thanks are extended to my friends Krongboon Singhanat, Kantida Pancharoen and Trewut Anurakpandit for sharing experience of PhD study. I am particularly grateful for the financial support provided by Royal Thai Navy.

Finally, I wish to express my gratitude to my parents for understanding and support through the duration of my studies.

Nomenclature

$\mathbf{a}$	Acceleration gain vector
a_{w}	Lift curve slope
$\mathbf{b}$	Actuator distribution vector
$\mathbf{B}$	Actuator distribution matrix
c	Damping coefficient
c_{c}	Contact damping coefficient
C	Wing chord
$\mathbf{C}$	Damping matrix
$\mathbf{C}_{\mathrm{as}}$	Asymmetric damping matrix
$\mathbf{C}_{\mathrm{s}}$	Symmetric damping matrix
e	Aero-centre
E	Energy index
$\mathbf{E}$	Asymmetric matrix containing only one non-zero element
EI	Bending rigidity
$\mathbf{f}$	Velocity gain vector
$\mathbf{F}$	Velocity gain matrix
$\mathbf{g}$	Displacement gain vector
GJ	Torsional rigidity
$\mathbf{G}$	Displacement gain matrix
$\mathbf{H}_{\mathrm{as}}$	Asymmetric receptance matrix of the open-loop system
$\widehat{\mathbf{H}}_{\mathrm{as}}$	Asymmetric receptance matrix of the closed-loop system
$\mathbf{H}_{\mathrm{s}}$	Symmetric receptance matrix of the open-loop system
$\mathbf{I}$	Identity matrix
k	Stiffness coefficient
k_{c}	Contact stiffness coefficient
$\mathbf{K}$	Stiffness matrix
$\mathbf{K}_{\mathrm{as}}$	Asymmetric stiffness matrix
$\mathbf{K}_{\mathrm{s}}$	Symmetric stiffness matrix
m	Mass or mass per unit area
$M_{\dot{\theta}}$	Eccentricity between flexural axis and aero-centre

$\mathbf{M}$	Mass matrix
p	External force
$\mathbf{p}$	External force vector
P	Instantaneous power
$\bar{P}$	Time-averaged power
$\bar{P}_{\mathrm{d}}$	Time-averaged power dissipation
$\bar{P}_{\mathrm{i}}$	Time-averaged input power
$\bar{P}_j$	Mode of power
$\bar{P}_u$	Power dissipation per unit characteristic velocity
s	Laplace domain
S	Wing span
$S_{\mu_{\mathrm{c}}}$	Sensitivity of the closed-loop pole with respect to the friction coefficient
$S_{c_{\mathrm{c}}}$	Sensitivity of the closed-loop pole with respect to the contact damping
$S_{k_{\mathrm{c}}}$	Sensitivity of the closed-loop pole with respect to the contact stiffness
S_ρ	Sensitivity of the closed-loop pole with respect to the air density
S_V	Sensitivity of the closed-loop pole with respect to the air speed
$\mathbf{S}$	Sensitivity matrix of the closed-loop pole
t	Time
T	Kinetic energy
u	Single-input control
$\mathbf{u}$	Multiple-input control
$\mathbf{v}$	Velocity vector
V	Air speed
x	Displacement in horizontal direction
x_{f}	Elastic axis location
$\mathbf{x}$	Displacement vector
y	Displacement in vertical direction
β	Control effort margin
η	Control effort
λ	Unchanged pole
μ	Required closed-loop pole
μ_{c}	Friction coefficient
ρ	Air density
τ	Time delay
τ_{f}	Time delay associated with velocity state feedback
τ_{g}	Time delay associated with displacement state feedback
$\bar{\tau}$	Critical time delay

Chapter 1

Introduction

1.1 Engineering backgrounds

Vibration mostly generated from machines and natural sources may lead to degradation of machine performances, failure of structures, and health deterioration of humans. The vibration severity is classified by International Organization for Standardization (ISO) such as vibration severity of machinery (ISO 2372), of structures (ISO DP 4866) and of human (ISO 2631). The level of the severity depends on both amplitudes and frequencies. According to the standards, the vibration severity in large machines with rigid foundation, is graded as good and satisfactory conditions when the velocity range is between 0.11-6.00 mm/s within frequency 10-1000 Hz. The acceptable and minor damage conditions of structures are between 3-5 and 5-30 mm/s respectively within frequency 1-100 Hz. The vibration sensitivity of whole body in 24 hours is limited between 4-8 Hz with acceleration below 0.01 mm/s^2 (Rao (2004)). If the vibration responses and frequencies are higher than the above criteria, the structure and machine will be damaged as well as human life will be in danger. Therefore, it is essential to control the vibration.

Resonance is a phenomenon, which occurs when an excitation frequency corresponds to a natural frequency leading to a large amplitude of oscillation. An example of the impact of resonance is Tacoma Narrow Bridge as it was collapsed due to the natural frequency of the bridge matching with the excitation frequency of the wind (Billah and Scanlan (1991)). Therefore, the resonances should be avoided. A typical method to control the vibration is to avoid a resonant frequency by changing a natural frequency of a system. For passive control, the natural frequency can be changed by modifying mass and stiffness of a material.

Another method to control the vibration is to reduce the level of the vibration response at the resonance. It can be achieved by adding a damper into the system. The use of damping always prevents excessive vibration responses efficiently. In term of structural vibration control, most structures contain internal damping (loss factor) but it is not sufficient to prevent the excessive vibration. To increase damping in the structures, an external damping with viscoelastic material (high loss factor) is installed on the host structures.

Obviously, the passive vibration control is to modify mass, stiffness and damping to suppress the vibration by avoiding the resonance and preventing excessive vibration. Although the passive control strategies usually guarantee stability and no energy supply is required, the exactly desired response cannot be achieved due to some limitations such as uncontrollable and unpredictable changing mass, stiffness and damping parameters. To deal this problem, the active vibration control is considered to be more effective.

The active vibration control normally adopts the concept of feedback control consisting three main devices e.g. sensors, actuators and controllers. The sensors measure the vibration responses (displacement or velocity or acceleration) and feed to a controller. The controller does some calculation according to a given control rule then generates and sends control signals to the actuators. The actuators convert electrical signals into control forces to suppress the vibration. Pole assignment, a type of feedback control, is capable to shift natural frequencies away from the excitation frequencies for avoiding resonances and/or to add damping for preventing excessive vibration by relocating poles or changing characteristics of the system.

1.2 Motivations

Active pole assignment was firstly formulated in the first-order differential equation or widely called state space (Wonham (1967); Andry et al. (1983); Kautsky et al. (1985)) and it has been implemented in the second-order differential equation (Juang and Maghami (1992); Chu and Datta (1996); Chu (2002)). Although the first-order differential equation is a general approach and mostly used in a general control theory, the second-order differential equation is the natural formulation for vibration problems and maintains some good properties of the second-order equation of motion such as the symmetry of the structural matrices. Many researchers extended pole assignment with the second-order differential equation to partial pole assignment (Datta et al. (1997); Datta and Sarkissian (1999)), partial pole assignment with time delay (Pratt et al. (2009); Bai et al. (2012)) and robust pole assignment (Xu and Qian (2008)).

Normally, pole assignment requires the knowledge of mass, damping and stiffness matrices. These particular matrices can be evaluated by the finite element method (FEM). Ram and Mottershead (2007) pointed out that finite element models always make some errors because several assumptions must be made when these models are constructed, for example, damping is neglected (or proportional damping assumed) and model reduction methods are applied. To deal with this problem, the receptance method for a single-input control was proposed (Ram and Mottershead (2007)). The idea of this method is to measure receptance from experiment rather than evaluating mass, damping and stiffness matrices from FEM. So modelling errors from FEM can be avoided. The receptance method, however, may contain errors because a curve fitting method. It was extended to pole-zero assignment (Mottershead et al. (2008)), pole assignment with time delay (Ram et al. (2009, 2011)), robust pole assignment (Mottershead et al. (2009); Tehrani et al. (2011)), partial pole assignment by using the uncontrollability condition (Tehrani et al. (2010)), partial pole assignment by using the unobservability condition (Ram and Mottershead (2013)) and eigenstructure assignment (Liu et al. (2015)).

The aforementioned works studied pole assignment for symmetric systems. Nonetheless, some systems are asymmetric due to non-conservative forces such as friction and aerodynamic forces. They are affected by asymmetric damping and/or stiffness matrices and prone to instability reflected by some positive real parts of poles. Friction-induced vibration being an example of the asymmetric system was stabilised by pole assignment using the receptance method (Ouyang (2010, 2011)). In practice, time delay always exists in active vibration control systems due to sensing and actuating in the feedback loop. It may destabilise the closed-loop system because the closed-loop poles are accidentally moved from the left-hand side to the right-hand side of the complex plane (spill-over effect). To handle the time delay, pole assignment with a single time delay

was introduced by Singh and Ouyang (2013). In practice, pole assignment contains a couple of time delays associated with displacement and velocity feedback. So, pole assignment with a couple of time delays remains open and challenge.

Furthermore, partial pole assignment by using the uncontrollability condition for the asymmetric system was proposed by Tehrani and Ouyang (2012) in order to prevent the spill-over effect due to unassigned poles. Then, Liang et al. (2016) adopted the concept of the unobservability condition to keep unassigned poles unchanged. It requires both unchanged eigenvalues (poles) and unchanged eigenvectors (mode shapes) but the eigenvectors of the asymmetric systems are difficult to evaluate. Thus, partial pole assignment by using the unobservability condition should be improved.

Existing algorithms of pole assignment yield the high accuracy only when perturbations are disregarded. In fact, the perturbations always exist in the systems and make the closed-loop poles shifted from the desired position. They may destabilise the systems when the closed-loop poles shift from the left-hand side to the right-hand side of the complex plane. Therefore, Liang et al. (2017) proposed robust pole assignment for the single-input control which allows to assign both closed-loop poles and their sensitivities. However, both of them are not assigned precisely because the number of equations is more than the number of control gains. The solution must be rearranged in the least-square problem and solved by using an optimisation method. Thus, it is challenging to develop the algorithm of robust pole assignment for both single-input and multiple-input controls to assign the closed-loop poles with their minimum sensitivities.

In addition, most researchers provide various algorithms to assign poles, partial poles and robust poles in order to avoid resonances, prevent excessive vibration and minimise the sensitivities of the closed-loop poles. There is no method to evaluate the optimal closed-loop poles to minimise vibration responses. However, they may be evaluated by using power flow mode theory based on damping distribution (Xiong et al. (2005)). This theory provides a method to maximise the time-averaged power dissipation per unit characteristic velocity leading to vibration minimisation. It was successfully applied to find optimal material layout which minimises vibrational power flow responses (Xiong (2015)). Therefore, it is interesting to apply this theory into active pole assignment to determine the optimal poles for minimising vibration responses.

1.3 Aim and objectives

This thesis aims to investigate the optimal poles for minimising the vibration responses, to improve partial pole assignment with and without time delays for the asymmetric system by using the unobservability condition and to propose a new method of robust pole assignment for the asymmetric system which allows to assign the closed-loop poles with their minimum sensitivities. To achieve the aim, the brief objectives are

- to investigate the power flow mode theory in passive and active vibration control for minimising vibration and determining optimal poles,
- to improve partial pole assignment for the asymmetric system by using the unobservability condition which requires only unassigned poles to keep them unchanged,
- to investigate three control strategies such as (i) velocity and displacement feedback, (ii) acceleration and velocity feedback, and (iii) acceleration and displacement feedback as well as determine the most effective control strategy for minimising the energy consumed by the actuators,
- to evaluate the optimal actuator distribution vector (locations of actuators) for minimising the energy supplied to the actuators,
- to combine both single and multiple time delays in the algorithm of partial pole assignment for the asymmetric system by using the unobservability condition,
- to analyse the stability of the closed-loop system including time delays by using a root finding method and a frequency-sweeping test for determining the closed-loop poles and the critical time delay respectively,
- to avoid modelling errors from the finite element method (FEM) by using the receptance method,
- to develop a new robust pole assignment for the asymmetric system by using both single-input and multiple-input state feedback control,
- to apply the genetic algorithm for minimising the sensitivities of the closed-loop poles with respect to uncertain parameters.

1.4 Thesis outline

In Chapter 2, power flow analysis approaches and feedback control methods are briefly reviewed. Three main approaches of the power flow analysis such as analytical, numerical and experimental are described to understand benefits and drawbacks of each approach. The state feedback control methods such as pole assignment and active damping are also discussed. Comparison of both methods are provided.

In Chapter 3, fundamental concept of the power flow mode theory based on damping distribution is introduced (Xiong et al. (2005)). This theory provides a method to minimise vibration responses by maximising the time-averaged power dissipation per unit characteristic velocity which may reveal the optimal location of poles. Both passive damping modification and active velocity feedback control are considered. The numerical example show that the passive control is capable to apply this theory to minimise the vibration responses but the active control is unsuitable. Therefore, the optimal poles for minimising the vibration responses cannot be determined by using this theory.

In Chapter 4, the algorithm of partial pole assignment for the asymmetric system by using the unobservability condition is developed from Liang et al. (2016). The unobservability condition normally requires both poles (eigenvalues) and mode shapes (eigenvectors) to keep the unassigned poles unchanged. However, it is difficult to evaluate the mode shapes of the the asymmetric system. So, the algorithm of partial pole assignment which requires only unassigned poles for keeping them unchanged is proposed. Three control strategies of the single-input state-feedback control such as velocity and displacement feedback, acceleration and velocity feedback, and acceleration and displacement feedback are considered to determine the most effective control strategy for minimising the energy supplied to the actuators. The receptance method is implemented without any knowledge of mass, damping and stiffness matrices. The solution is formulated based on Sherman-Morrison formula and solved by linear equations. The optimal actuation is investigated to minimise the energy supplied to the actuators.

In Chapter 5, the single and multiple time delays in the feedback loop are considered on the algorithm of partial pole assignment for the asymmetric system in order to avoid spill-over effect. The unobservability condition is also applied to handle this case. The stability is analysed by applying a Tool for Robust Analysis and Characteristic Equations for Delay Differential Equations (TRACE-DDE), which is a toolbox in MATLAB (Breda et al. (2009)) to compute the first few dominant poles of the closed-loop system and a frequency-sweeping test (Gu et al. (2003)) to determine the critical time delay.

In Chapter 6, a new method of robust pole assignment for the asymmetric system is proposed. Both single-input and multiple-input controls are considered. The receptance method, Sherman-Morrison formula and Jacobi formula are applied to obtain sensitivities of the closed-loop poles with respect to uncertain parameters such as the friction coefficient, the contact damping, the control stiffness (friction-induced vibration), the air density and the air speed (aerodynamic flutter). The solution is formulated in the optimisation problem and solved by the genetic algorithm. Two nonlinear constraints such as stability guarantee and control effort confinement are considered. The proposed method allows to assign the closed-loop poles with their minimum sensitivities.

In Chapter 7, some conclusions are drawn and future research ideas are given.

Chapter 2

Literature Review

This chapter aims to review both power flow analysis (PFA) and feedback control in order to understand fundamental and advanced knowledge of both topics. PFA is a technique to describe vibration in term of power by combining forces and velocities into a single quantity. Three main approaches are considered such as analytical, numerical and experimental. The active vibration control based on the feedback control is considered to attenuate the magnitude of vibration. Two control methods such as pole assignment (model-based feedback) and active damping, are discussed.

2.1 Power flow analysis

PFA is a technique to describe vibration responses in term of power by combining forces and velocities into a single quantity. It is widely implemented in many applications such as vibration control (Goyder and White (1980a,c,b); Gardonio et al. (1997a,b); Xiong et al. (2005)), noise reduction (Gardonio and Elliott (1999)), damage detection (Li et al. (2001); Huh et al. (2015); Wong et al. (2009)) and loss factor evaluation (Clarkson (1991); Mace and Shorter (2000)). In this thesis, only the vibration control is considered. The basic concept of the power flow is discussed to understand the technical terms of the instantaneous and time-averaged power. The power flow analysis approaches such as analytical, numerical and experimental are reviewed to discuss the benefits and drawbacks of each approaches.

2.1.1 Fundamental concept of power flow

Basic concept of power flow was proposed by Xing and Price (1999). It is a product of forces and velocities measuring in both instantaneous and average values. The instantaneous power for a single degree-of-freedom (SDOF) system is given by

$$P(t) = p(t)v(t), \tag{2.1}$$

$$p(t) = p\cos(\omega t), \tag{2.2}$$

$$v(t) = v\cos(\omega t + \theta), \tag{2.3}$$

where p and v are respectively amplitudes of force and velocity, ω denotes frequency, θ is relative phase angle and t is time. Alternatively, the power can be represented in term of complex notations as:

$$P(t) = \Re\big(\tilde{p}(t)\big)\Re\big(\tilde{v}(t)\big), \tag{2.4}$$

$$\tilde{p}(t) = p\mathrm{e}^{\mathrm{i}\omega t} = \tilde{p}\mathrm{e}^{\mathrm{i}\omega t}, \tag{2.5}$$

$$\tilde{v}(t) = v\mathrm{e}^{\mathrm{i}(\omega t+\theta)} = \tilde{v}\mathrm{e}^{\mathrm{i}\omega t}, \tag{2.6}$$

where $\tilde{p}$ and $\tilde{v}$ are respectively force and velocity presented in a complex exponential function and $\Re(\bullet)$ denotes a real part.

The time-averaged power by the single excitation force over a period $\omega/2\pi$ is written below:

$$\bar{P} = \frac{\omega}{2\pi}\int_0^{2\pi/\omega} \Re(\tilde{p}\mathrm{e}^{\mathrm{i}\omega t})\Re(\tilde{v}\mathrm{e}^{\mathrm{i}\omega t})\,\mathrm{d}t, \tag{2.7}$$

$$\bar{P} = \frac{1}{2}\Re(\tilde{p}^*\tilde{v}) = \frac{1}{2}\Re(\tilde{p}\tilde{v}^*) = \frac{1}{2}\big(\Re(\tilde{p}\tilde{v}) + \Im(\tilde{p}\tilde{v})\big), \tag{2.8}$$

where $\bar{P}$ is the time-averaged power, the superscript asterisk $(*)$ represents the complex conjugate and $\Im(\bullet)$ denotes a imaginary part.

In general, the time-averaged power by the multiple excitation forces or the multiple degrees-of-freedom (MDOF) system is expressed by

$$\bar{P} = \frac{1}{2}\Re(\tilde{\mathbf{p}}^{\mathrm{H}}\tilde{\mathbf{v}}) = \frac{1}{2}\Re(\tilde{\mathbf{v}}^{\mathrm{H}}\tilde{\mathbf{p}}) = \frac{1}{4}\Re(\tilde{\mathbf{p}}^{\mathrm{H}}\tilde{\mathbf{v}} + \tilde{\mathbf{v}}^{\mathrm{H}}\tilde{\mathbf{p}}), \tag{2.9}$$

where $\tilde{\mathbf{p}}$, $\tilde{\mathbf{v}} \in \mathbb{C}^{n\times 1}$ are the complex force and velocity vectors, and superscript H is the conjugate transpose.

As can be seen, the time-average power considers only on the real part. This is because the real part provides physical meaning of the power but the average value of the complex power is meaningless as described in Eq.(2.10)

$$\bar{\tilde{P}} = \frac{\omega}{2\pi} \int_0^{2\pi/\omega} \tilde{p}\mathrm{e}^{\mathrm{i}\omega t}\tilde{v}\mathrm{e}^{\mathrm{i}\omega t}\,\mathrm{d}t = 0. \tag{2.10}$$

2.1.2 Power flow analysis approaches

In this section, three main approaches such as analytical, numerical and experimental, are reviewed to discuss the benefits and drawbacks of each approaches. For the analytical approach, modal and wave methods are applied to determine internal forces, internal moments, translational velocities and angular velocities, and processed these parameters to predict vibrational power flow. Although the analytical approach provides efficient calculation and no convergence issues, it is suitable for only simple structures.

Alternatively, the numerical approach e.g. finite element method (FEM), is presented for complex structures. This method separates the structures into small elements in order to evaluate mass, damping and stiffness matrices. Then, the forces and the velocities are numerically calculated leading to prediction of the vibrational power flow. Although FEM is a useful technique to estimate the vibrational power flow in the complex systems, it contains numerical errors due to several assumptions and model reduction methods. Lastly, the experimental approach is considered. Transducer arrays and the finite different method are applied to approximate the flow of power in the structures.

2.1.2.1 Analytical approach

Power flow is a technique to describe vibration responses in term of power for locating sources, sinks and propagation of the vibration. It is usually obtained by using modal and wave methods. For the modal method, frequency response function (FRF) such as receptance (relationship between displacement and force) and mobility (relationship between velocity and force) are considered. By applying modal parameters (natural frequencies and mode shapes) to the exact solutions, internal forces and moments as well as translational and angular velocities are determined and processed to power flow. Many researchers applied this concept to investigate vibrational power flow of rigid and flexural supported beams (Cuschieri (1990b)), a coupled beam (Clarkson (1991); Farag and Pan (1996)), a coupled plate (Cuschieri (1990a); Clarkson (1991); Beshara and Keane (1998)), a coupled cylindrical shell (Ming et al. (1999)) and a thin circular plate (Zhang and Li (2016)).

Although the modal method is more convenient to predict the power flow in a structure, it is efficient in the low frequency region. This is because the modal method cannot present the responses of the structure with the superposition for all eigenmodes. In high frequency, eigenmodes are truncated. Moreover, the power flow analysis by using the modal method contains errors due to inaccurate in higher order derivatives of the displacement response, such as bending moment and shear force. Pan and Pan (1998) also stated that the modal method inaccurately predicts the power flow near a driving force.

To deal with this problem, the wave method is considered. It naturally describes energy propagation through structures and provides accurate prediction in the high frequency region. Wu and White (1995) applied the flexural wave to predict vibrational power flow in a multi-supported uniform beam. Both far field (travelling) and near field (evanescent) waves are considered to determine input power and power transmission. This study indicates that an increase of internal damping (loss factor) can suppress the power flow around resonant frequencies. On the other hand, it is amplified around off-resonant frequencies. Another way to reduce the power flow is to locate the supporters near the excitation forces. The supporters act as dampers to absorb the power.

The power flow predicted by the flexural wave is accurate in the low frequency region. In high frequency, however, it contains errors because the longitudinal wave is not included. Park et al. (2001) and Kessissoglou (2004) investigated the power transmission of L-shaped plates by using both flexural and longitudinal waves. The results show that the longitudinal wave is not effective to the power transmission in the low frequency range in comparison with the flexural wave but it significantly influences to the power transmission in the high frequency range.

For a structural system, Goyder and White (1980a,c,b) applied PFA to study the power transmitted from a rigid machine through a spring-like isolator to infinite flexural structures (beam and plate). Many formulae was provided to estimate the power flow based on mobility transfer function. The power flow normally requires excitations and velocity responses at the interesting point. Alternatively, it can be obtained by using the excitations and mobility matrix. Two vibration isolation methods, single and two stages of the spring-like isolator, are demonstrated to passively reduce the power transmitted to the foundation. Even though these formulae are convenient to estimate the power flow, the spring-like isolator of this model is impractical.

To improve this model, Pan et al. (1992); Gardonio et al. (1997a); Li and Lavrich (1999); Sun et al. (2007) used an elastic mount instead of the spring-like isolator. Three main components of the power are discussed such as the input power generated by the machine and the power transmitted to the elastic mounts and the flexible supporting structures.

Both force and moment excitations are applied to investigate the power input to the structures. It is found that the force excitation influences to the power in the low frequency range whereas the moment excitation is less significant. Nonetheless, in the high frequency range, the power flow by the moment excitation becomes more important than the force excitation.

In order to reduce the power transmission at the supporting structure, two control algorithms such as passive and active are considered. In passive control, Koh and White (1996a,b,c) proposed a method to determine the optimal moment arm of a seating mount placed between the machine and the supporting structure. It is capable to reduce the power transmission at a specific frequency. This is because the displacement caused by the force excitation is counteracted (cancelled) by the displacement caused by the moment excitation. In active control, Pan et al. (1993) applied the feedforward control algorithm to minimise the power transmitted to the supporting structure. The actuator are placed in parallel with the elastic mounts. Both numerical and experimental results shown that power transmission is reduced.

Then Gardonio et al. (1997b) extended the work of Pan et al. (1993) to minimise the power transmitted to the supporting structure. Five control strategies such as (i) total power minimisation, (ii) velocity cancellation, (iii) force cancellation, (iv) axial power minimisation and (v) velocity and force minimisation are applied. The simulation results show that the total power minimisation is the most effective control strategy. It is capable to reduce the power transmission with the all frequency range. The other control strategies are effective to reduce the power transmission in the high frequency range but they give poor results in the low frequency range particularly with the frequency of the rigid body modes of the elastic mounts.

Xiong et al. (2001) proposed two progressive methods, namely equivalent mobility and equivalent impedance matrices to describe dynamic behaviours between substructures in term of power flow. These methods reduce the complexity of the isolation systems. However, they may be less accurate because the isolators are modelled as linear springs. The numerical example is demonstrated the power transmission of a floating raft isolation system which composed of five substructures such as machines, a flexible raft, a flexible foundation, isolators between the machines and the raft, and isolators between the raft and the foundation. The results show that an increase of the raft stiffness can reduce the power transmission to the foundation. Then Choi et al. (2009) continued applying this method to investigate the transmission power of the sandwich raft isolation system.

Another method is considered on the power flow mode theory. Ji et al. (2003) proposed the mobility-characterised power flow mode to estimate the input power at the flexible

foundation. It is derived by eigenvalues and eigenvectors of the mobility matrix of the structure. The expressions of upper bound, lower bound and mean value of the input power are provided in term of power flow modes. To achieve this method, full knowledge of excitation forces are required. However, in some applications such as a bridge excited by pedestrians and a ship hull excited by sea waves, the forces cannot be measured. In order to avoid this problem, Xiong et al. (2005) proposed the damping-characterised power flow mode to estimate the input power by considering on the damping matrix. This method requires a damping matrix instead of full knowledge of a force vector. In addition, it also describes a way to achieve maximum power dissipation. Xiong (2015) continued applying this method to determine optimal material layout to minimise vibrational transmission power.

2.1.2.2 Numerical approach

Although the analytical approach provides effective calculation of the vibrational power flow between substructures, it is merely suitable for the simple structures. Unfortunately, exact solutions are difficult to derive for the complex structure. To overcome with this problem, the numerical approach e.g. finite element method (FEM) is pointed out. FEM is a technique to discretise the structures into small elements in order to evaluate mass, damping and stiffness matrices as well as estimate velocities and internal forces. Hambric (1990) applied FEM to predict the power flow of a simple truss and a beam-stiffened cantilever plate. A software package, namely NASTRAN, is implemented to estimate the velocities and the forces for all elements and post process to evaluate the power flow. Then Hambric and Taylor (1994) continued investigating the vibrational power flow though the uniform beam and validated the results with the experimental approach (Pavić (1976)).

FEM with many small elements provides good agreement results but it requires high computational cost. To deal with this problem, the substructure method was proposed to reduce the number of degrees of freedom. It separates the structure into several sub-structures instead of the elements. Free-free interface conditions are assumed to deduct displacement contribution of the external and boundary coupling forces and predict the vibrational power flow between the substructures. Many researches implemented this method to determine the input power and power transmission of spring-coupled beams and rigid-coupled beams (Shankar and Keane (1995b,a)), two- and three-dimensional structural networks (Shankar and Keane (1995b, 1997); Wang et al. (2002b)), L-shaped plates (Wang et al. (2002a)) and coupled plate-cylindrical shell systems (Wang et al. (2004)).

2.1.2.3 Experimental approach

The vibrational power flow based on experimental approach was firstly proposed by Noiseux (1970) to estimate the path of the bending wave power in the uniform structures i.e. beams and plates. Two accelerometers are implemented to measure rotational and transverse velocities which allow to calculate the vibrational power flow. However, this technique is only considered on the far field region. Pavić (1976) continued investigating the vibrational power flow of the simple structures by considering both far field and near field regions. Four and eight accelerometers are respectively applied to measure vibration responses of beams and plates and then the finite difference method is implemented to estimate vibrational power at the centre of the accelerometer array. Verheij (1980) and Linjama and Lahti (1992) modified the previous work based on time domain into the frequency domain by using the cross spectral density method. Wu and White (1995) applied this technique to validate the vibrational power transmission of a multi-supported beam.

2.2 Feedback control

The feedback control algorithms that are generally used in an active vibration control problem can be divided into two main types: pole assignment (model based feedback) and active damping. A brief introduction is given in the following.

2.2.1 Pole assignment

The pole assignment is a technique to control the vibration by relocating poles or changing the characteristics of the systems. Many researchers provided various algorithms i.e. pole assignment formulated in the first-order and the second-order differential equations as well as pole assignment by using the receptance method. Pole assignment formulated in the first-order differential equation (state space) is a general approach and mostly used in general control theory. However, it is not suitable for structural vibration control because the symmetry and sparseness of matrices are destroyed.

Then, an improvement approach, pole assignment for the second-order differential equation is proposed to deal with vibration problem. Generally, pole assignment requires full knowledge of mass, damping and stiffness matrices evaluated by the finite element method (FEM). The numerical errors always occur in finite element models because several assumptions must be made when these models were constructed. To avoid the

errors, pole assignment by using the receptance method is applied for measuring the frequency response function in term of the receptance instead of evaluating mass, damping and stiffness matrices from FEM.

2.2.1.1 First-order differential equation

During 1970s to 1990s, a modern control theory had been discovered and extensively improved. Wonham (1967) studied a method to assign poles by using the multiple-input state feedback control. The closed-loop poles can be arbitrarily assigned if the system is controllability. This method is widely known in pole assignment (pole placement). The pole assignment can be formed in the first-order differential equation or state space as shown below.

$$\dot{\mathbf{z}}(t) = \mathbf{A}\mathbf{z}(t) + \mathbf{B}\mathbf{u}(t), \tag{2.11}$$

$$\mathbf{u}(t) = \mathbf{F}\mathbf{z}(t), \tag{2.12}$$

where $\mathbf{z} \in \mathbb{R}^{n\times 1}$ is the state vector; $\mathbf{u} \in \mathbb{R}^{m\times 1}$ is the input (control) vector; $\mathbf{A} \in \mathbb{R}^{n\times n}$ is the state (system) matrix; $\mathbf{B} \in \mathbb{R}^{n\times m}$ is the control distribution matrix and $\mathbf{F} \in \mathbb{R}^{m\times n}$ is the feedback control gain matrix. The characteristics of the open-loop system are governed by the poles of the matrix $\mathbf{A}$.

By combining Eq.(2.11) and Eq.(2.12), it yields,

$$\dot{\mathbf{z}}(t) = (\mathbf{A} + \mathbf{B}\mathbf{F})\mathbf{z}(t), \tag{2.13}$$

which allows to relocate poles in order to change the characteristics (natural frequencies and damping ratios) of a system. Wonham (1967) stated that the poles can be assigned by using the state feedback if the system is controllable or satisfied with the following equation.

$$\text{rank}\begin{bmatrix}\mathbf{B} & \mathbf{A}\mathbf{B} & \mathbf{A}^2\mathbf{B} & \dots & \mathbf{A}^{n-1}\mathbf{B}\end{bmatrix} = n. \tag{2.14}$$

Then Davison and Wang (1975) and Kimura (1975) proposed pole assignment by using the output feedback.

$$\mathbf{u}(t) = \mathbf{F}\mathbf{y}(t), \tag{2.15}$$

$$\mathbf{y}(t) = \mathbf{D}\mathbf{z}(t), \tag{2.16}$$

where $\mathbf{y} \in \mathbb{R}^{l\times 1}$ is the output vector and $\mathbf{D} \in \mathbb{R}^{l\times n}$ is the output matrix. It is achieved if the system is controllable and observable. In other word, pole assignment by using the output feedback can be assigned the poles if the system is satisfied with Eq.(2.14)

and Eq.(2.17).

$$\text{rank}\begin{bmatrix}\mathbf{D}\\ \mathbf{DA}\\ \mathbf{DA}^2\\ \vdots\\ \mathbf{DA}^{n-1}\end{bmatrix} = n. \tag{2.17}$$

Moore (1975) and Srinathkumar (1978) extended the previous works to eigenstructure assignment which allows to assign both poles (eigenvalues) and mode shapes (eigenvectors). Andry et al. (1983) reviewed the feedback control theory i.e. full state, output and constrained output feedback including both the single-input and the multiple-input systems. They also considered on eigenstructure assignment and provided a numerical example involving flight control for giving direction to the application of eigenstructure assignment in different areas. For the multiple-input state feedback control, the inverse eigenvalue problem contains many solutions (control gains). Some solutions may induce the sensitivity of the assigned poles to perturbations. So, it is important to select the solution with insensitivity. Kautsky et al. (1985) proposed the robustness analysis to determine the well-conditioned solution for minimising the sensitivity of the assigned poles and reducing perturbations in the system.

2.2.1.2 Second-order differential equation

The pole assignment is normally formed in the first-order differential equation rather than the second-order differential equation in order to reduce complexity of the mathematical expressions and allow to combine different sources simultaneously. However, this form is not suitable for the structural vibration control because the symmetry and sparseness of the matrices are destroyed. Therefore, many researchers (Juang and Maghami (1992); Datta et al. (1997); Chu (2002)) turned to focus on pole assignment formulated in the second-order differential equation. For the single-input state feedback control, the second order dynamic equation is given by

$$\mathbf{M}\ddot{\mathbf{x}}(t) + \mathbf{C}\dot{\mathbf{x}}(t) + \mathbf{K}\mathbf{x}(t) = \mathbf{b}u(t) + \mathbf{p}(t), \tag{2.18}$$

$$u(t) = -\mathbf{f}^{\mathrm{T}}\dot{\mathbf{x}}(t) - \mathbf{g}^{\mathrm{T}}\mathbf{x}(t). \tag{2.19}$$

where $\mathbf{M}$, $\mathbf{C}$ and $\mathbf{K} \in \mathbb{R}^{n\times n}$ are respectively real mass, damping and stiffness matrices; $\mathbf{x}$, $\mathbf{p}$, $\mathbf{b}$, $\mathbf{f}$ and $\mathbf{g} \in \mathbb{R}^{n\times 1}$ are respectively real displacement, excitation force, actuator distribution, velocity gain and displacement gain vectors; $u \in \mathbb{R}^{1\times 1}$ is a single-input control; and superscript T denotes matrix transposition.

The open-loop (λ) and closed-loop (μ) poles can be respectively obtained by the roots of the following equations.

$$\lambda^2\mathbf{M} + \lambda\mathbf{C} + \mathbf{K} = 0. \tag{2.20}$$

$$\mu^2\mathbf{M} + \mu(\mathbf{C} + \mathbf{bf}^{\mathrm{T}}) + \mathbf{K} + \mathbf{bg}^{\mathrm{T}} = 0. \tag{2.21}$$

The stability is the major concern of the pole assignment technique. To ensure that, all poles must be negative real values or located on the left-hand side of the complex plane. The use of pole assignment to a structural system containing an infinite number of degrees of freedom does not guarantee stability due to unassigned (residue) poles. They may get unintentionally shifted from the left-hand side to the right-hand side of the complex plane leading to instability. To overcome this so-called spill-over problem, Datta et al. (1997) proposed partial pole assignment by using the single-input control. The orthogonal properties were implemented to assign some poles and keep others unchanged. Ram (1998) applied this technique to control vibration of a rod.

Then, Datta and Sarkissian (1999) and Ram and Elhay (2000) continued investigating partial pole assignment for multiple-input symmetric system. Ram and Elhay (2000) indicated that pole assignment by using the multiple-input control is able to reduce a control effort in comparison with the single-input control. Chu (2002) modified the work of Juang and Maghami (1992) and proposed the robust pole assignment with the output feedback. Xu and Qian (2008) continued studying robust partial pole assignment using state feedback control. They explained that this control algorithm is able to not only assign partial poles but also provide robustness (insensitive to perturbations). Brahma and Datta (2009) developed a control algorithm of robust partial pole assignment by using an optimisation method to minimise the condition number and the norm of the control gains.

Pratt et al. (2009) and Bai et al. (2012) proposed partial pole assignment with time delay using the single-input and the multiple-input controls in order to prevent the spill-over effect generated by the unassigned poles and the time delay in the feedback loop. However, the stability of the closed-loop system was not investigated and discussed in these works. Singh and Ouyang (2013) demonstrated various methods e.g. Taylor series expansion, Newton's eigenvalue iteration method (Singh and Ram (2002)) and graphical root-finding algorithm (Vyhlidal and Zitek (2009)), to determine the first few dominant poles of the closed-loop system (the closed-loop system with time delay has an infinite number of poles) and implemented a frequency-sweeping method (Gu et al. (2003)) to determine the critical time delay. Moreover, Singh et al. (2014) used a Tool for Robust Analysis and Characteristic Equations for Delay Differential Equations (TRACE-DDE),

which is a toolbox in MATLAB (Breda et al. (2009)) to evaluate the first twenty closed-loop poles and applied a Cluster Treatment of Characteristic Roots (CTCR) technique (Olgac and Sipahi (2002)) to determine the critical time delay.

Most pole assignment algorithms are focused on the displacement-velocity feedback. However, they can be achieved by using the acceleration-displacement feedback, and the acceleration-velocity feedback. Zhang et al. (2014) investigated partial pole assignment of an undamped vibration system by using the acceleration-displacement feedback with the multiple-input control. Then, Zhang et al. (2015) continued studying partial pole assignment by using the acceleration-velocity feedback with the multiple-input control. Besides the main purpose to assign partial poles, minimisation of the control gains is also included in the control algorithm. The norm of the control gains is minimised to reduce energy supplied to actuators.

2.2.1.3 Receptance method

Generally pole assignment by using the receptance method is widely known in passive structural modification by adding mass and/or stiffness and/or damping into the system in order to change the characteristics of the system. In term of active control, the receptance method was firstly implemented by Ram and Mottershead (2007). It takes advantage over the model based approach by avoiding numerical errors from FEM but it may contain the errors from a curve fitting method. This technique requires receptance measurement from an experiment rather than evaluating mass, damping and stiffness matrices by FEM.

By taking Laplace transform and using Sherman-Morrison formula, Eq.(2.15) can be expressed as

$$\widehat{\mathbf{H}}(s) = \mathbf{H}(s) - \frac{\mathbf{H}(s)\mathbf{b}(s\mathbf{f}^{\mathrm{T}} + \mathbf{g}^{\mathrm{T}})\mathbf{H}(s)}{1 + s\mathbf{f}^{\mathrm{T}} + \mathbf{g}^{\mathrm{T}})\mathbf{H}(s)\mathbf{b}}, \tag{2.22}$$

where $\mathbf{H}$ and $\widehat{\mathbf{H}}$ are respectively open-loop and closed-loop receptances. It can be seen that the poles of the closed-loop system are obtained by

$$(s\mathbf{f}^{\mathrm{T}} + \mathbf{g}^{\mathrm{T}})\mathbf{H}(s)\mathbf{b} = -1. \tag{2.23}$$

Then, Mottershead et al. (2008) extended the previously work from the single-input state feedback to the output feedback. They provided numerical and experimental examples to show vibration suppression by using pole/zero assignment with receptance measurements. The receptance method was extensively applied to pole assignment with time delay (Ram et al. (2009)), partial pole assignment by using the uncontrollability condition (Tehrani et al. (2010)), partial pole assignment by using the unobservability

condition (Ram and Mottershead (2013); Wei et al. (2014)) and partial pole assignment with time delay (Ram et al. (2011); Xiang et al. (2016)).

Existing algorithms of pole/partial pole assignment with and without time delay yields the high accuracy when perturbations are disregarded. Nonetheless, the perturbations, which may destabilise the system, are inevitable because of uncertain parameters such the receptance measurement and the control gains. Influences of the perturbations can be reduced by decreasing sensitivities of the poles. Mottershead et al. (2009) proposed a method to assign both poles and their sensitivities with respect to the control gains. Tehrani et al. (2011) introduced robust pole assignment to assign the closed-loop poles and minimise their sensitivities with respect to the receptance measurement. For a nonlinear system, Tehrani et al. (2013, 2015) applied the receptance method into pole assignment to control a duffing oscillator.

Although most systems are symmetric, some systems are asymmetric and prone to instability. Ouyang (2010)) continued applying pole assignment by using the receptance method to stabilise an asymmetric system exemplified by a friction-induced vibration. Three control strategies such as displacement and velocity feedback, velocity and acceleration feedback as well as displacement and acceleration feedback, are investigated. The results show that the first two cases can be applied to assign the poles precisely but the last case is incapability to assign the poles due to an ill-conditioned equation. Ouyang (2011) proposed a hybrid pole assignment (a combination of passive structural modification and active pole assignment) to reduce the energy supplied to the actuators.

Ouyang et al. (2013) extended the concept of pole assignment using the receptance method for the friction-induced vibration system to control flexible link mechanisms. The system contains asymmetric matrices of damping and stiffness which are generated by the coupling between rigid-body motion and elastic motion. The receptance method is applied to increase reliability and efficiency of the control algorithms. The results are compared with Ackerman's formula and the robust algorithm 'place' function in MATLAB. As a result, the algorithm of pole assignment using the receptance method are the most accurate. Singh and Ouyang (2013) continued applying the receptance method to pole assignment with the single time delay to avoid the spill-over effect. The stability of the closed-loop system is analysed by determining the first few dominant poles and the critical time delay.

The receptance method was also implemented to partial pole assignment by using the uncontrollability condition for the asymmetric system (Tehrani and Ouyang (2012)). This method requires a particular set of the actuator distribution vector for making the unassigned poles unchanged (uncontrollable). Then, Liang et al. (2016) proposed partial pole assignment by using the unobservability condition which allows to use various sets

of the actuator distribution vectors. Nonetheless, it requires both poles (eigenvalues) and mode shapes (eigenvectors) to keep the poles unchanged. In practice, this method is difficult to implement because the mode shapes of the asymmetric system are hard to evaluate. Liang et al. (2017) studied robust pole assignment which allows to assign both closed-loop poles and their sensitivities with respect to the friction coefficient. Zhen et al. (2018) proposed a new algorithm of pole assignment for nonlinear vibration problems.

2.2.2 Active damping

Active damping is a type of the feedback control, such as velocity feedback, aiming to suppress the vibration responses around resonances by adding damping ration into the system. Jayachandran and Sun (1997) and Preumont (2011) stated that the system controlled by active damping is unconditionally stable when the sensors and the actuators are placed at the same location (collocation) as well as forces and vibration responses are matched (dual condition) such as force-velocity and moment-angular velocity. Jayachandran and Sun (1997) described that the non-collocated sensor-actuator pairs changes the property of poles and zeros pattern (called pole-zero flipping) which makes Root Locus plotted in the right-hand side of the complex plane.

In practice, the system may be unstable even if the concepts of the sensor-actuator collocation and the dual condition are applied because of the dynamic effects of an inertial actuator and a piezoelectric patch actuator. Elliott et al. (2001) and citebaumann2007destabilization explained that the control force produced by the inertial actuator may react on a base structure and a proof mass. When the high control gain is applied to generate the large control force, the proof mass will hit the actuator protective case and produce another force which disturbs the control force and destabilises the system. Gardonio and Elliott (2005) also described that the collocation of the sensor-actuator pair is impractical when the piezoelectric patch is applied. It normally produces moments at its edges but it measures velocities at the centre. Hong et al. (2007) and Gatti et al. (2007) also showed that the non-collocated sensor-actuator pair induces the instability problem when the control gain is high enough. This indicates that the limitation of the control gain degrades the control performance.

To improve the stability and control performance, Gardonio et al. (2004) applied a phase lag compensator into velocity feedback. It allows to apply the large control gain which increases the control performance and maintains the stability. Hong et al. (2007) proposed a triangle-shape piezoceramic actuator which generates the forces at the three tips and the moments along the three edges. The velocity sensor is placed at a tip of the actuator to nearly achieve the sensor-actuator collocation. Gatti et al. (2007) used a point mass attached at the accelerometer location in order to enlarge the control gain

for maintaining the stability. Shin et al. (2013) proposed a novel technique namely, filtered-velocity feedback control to stabilize the control system with the non-collocated velocity sensor and moment actuator.

In addition, decentralised velocity feedback control is also applied to improve the control performance. It is the multiple loops of the velocity feedback control using the concept of the sensor-actuator collocation. Gardonio et al. (2004) and Zilletti et al. (2010) applied the piezoelectric actuators to control the vibration with both the single and the decentralised multiple velocity feedback loops. The results show that the control performance of the multiple loops is better than the single one. Baumann and Elliott (2007) confirmed that the control performance depends on the number of the control loops. The stability of the decentralised velocity feedback control is investigated by Nyquist criterion. All control loops must be stable. If one of them is unstable, the system will be destabilised.

2.3 Summary

Benefits and drawbacks of PFA and the feedback control are respectively summarised in Table 2.1 and Table 2.2. The main purpose of PFA is to describe vibration responses in term of power. Three approaches such as analytical, numerical and experimental, are considered. The analytical approach provides efficient calculation but it is confined in the simple structures. For complex structures, the numerical approach is taken into account but it contains numerical errors. Finally, the experimental approach is implemented to validate the results of the first two approaches.

In order to suppress the vibration, the feedback control methods such as pole assignment and active damping are discussed. The active damping is applied to control the vibration without using the plant model (mass, damping and stiffness matrices). Theoretically, it guarantees the stability when the collocated sensor-actuator pairs and the dual condition are applied. Nonetheless, this method is effective only around the resonances. To deal with this problem, the pole assignment is applied to control the vibration by relocating the closed-loop poles. This means that natural frequencies are shifted away from the excitation frequencies for avoiding resonances and/or damping is added for preventing excessive vibration. Three different formulations of pole assignment are summarised in Table 2.3.

Table 2.1: Comparison of power flow analysis approaches

Approach	Benefit	Drawback
Analytical	• Efficient calculation • No convergence issues	• Limited in simple structures
Numerical	• Available in various software package • Suitable for complex structures	• Numerical errors due to several assumptions and model reduction
Experimental	• Experimental based data to validate	• Dynamic effect of sensors • Contain noises

Table 2.2: Comparison of feedback control methods

Method	Benefit	Drawback
Pole assignment	• Global method • Relocate the poles	• Require accurate plant model • Spill-over effect
Active damping	• Do not require accurate plant model • Simple to implement • Guarantee stability (collocated sensor-actuator pairs and dual condition)	• Effective only around resonant frequencies

Table 2.3: Comparison of pole assignment in different formulations

Formulation	Benefit	Drawback
First-order	• Reduce complexity of the mathematical expressions	• Do not suitable for structure vibration control
	• Widely use in software package e.g. 'place' and 'acker' in MATLAB	• Damage symmetry and sparseness of the matrices
	• Allow to use data from different sources simultaneously	• Require full knowledge of mass, damping and stiffness matrices
		• Contain numerical errors from evaluating the matrices by FEM
Second-order	• Widely used in the structural vibration control	• Require full knowledge of mass, damping and stiffness matrices
	• Maintain symmetry and sparseness of the matrices	• Contain numerical errors from evaluating the matrices by FEM
Receptance	• No need FEM and model reduction method to evaluate the matrices	• Contain errors from a curve fitting method

Chapter 3

Application of Power Flow Mode Theory to Minimisation of Vibration

The power flow mode theory to minimise the vibration responses is discussed. It was firstly proposed by Ji et al. (2003) to estimate the input power at the flexible structural foundation. Eigenvalues and eigenvectors of the mobility matrix are determined and full knowledge of excitation forces are required to calculate the modes of the power flow. Nonetheless, it is difficult to measure the forces in some applications such as a bridge excited by pedestrians and a ship hull excited by sea waves. In order to overcome this problem, a power flow mode theory by using damping distribution was proposed (Xiong et al. (2005)). It requires a damping matrix instead of the excitation forces to determine the modes of the power flow. This theory also provides a method to minimise the vibrational power flow by maximising the time-averaged power dissipation per unit characteristic velocity or the trace of the damping matrix. Then, Xiong (2015) combined this theory into topology optimisation to determine the optimal material layout for minimising the power flow responses of a clamped plate.

In this chapter, power flow mode theory based on damping distribution (Xiong et al. (2005)) is applied into the passive and the active vibration controls to minimise the vibration responses. This theory provides a method to maximise the time-averaged power dissipation per unit characteristic velocity that may minimise the vibration and revel the optimal locations of poles. In the passive vibration control, the maximum time-averaged power dissipation per unit characteristic velocity is obtained by maximising damping coefficients. Alternatively, in the active vibration control, the maximum time-averaged power dissipation per unit characteristic velocity is obtained by maximising

velocity gains. Both single-input and multiple-input state feedback controls are considered.

3.1 Introductory of power flow mode theory based on damping distributions

The time-averaged input power generally is given by

$$\bar{P}_{\mathrm{i}} = \frac{1}{2}\Re(\mathbf{p}^{\mathrm{H}}\mathbf{v}), \tag{3.1}$$

where $\bar{P}_{\mathrm{i}} \in \mathbb{R}^{1\times 1}$ is the time-averaged input power, $\mathbf{p}$ and $\mathbf{v} \in \mathbb{C}^{n\times 1}$ are excitation force and velocity vectors presented in the complex number, $\Re(\bullet)$ indicates a real part of the complex number and superscript H denotes a conjugate matrix transposition. Alternatively, the time-averaged input power can be formulated by considering on damping matrix instead of the excitation force vector as shown below

$$\bar{P}_{\mathrm{i}} = \bar{P}_{\mathrm{d}} = \frac{1}{2}\Re(\mathbf{v}^{\mathrm{H}}\mathbf{C}\mathbf{v}), \tag{3.2}$$

$$\mathbf{C} = \mathbf{C}_{\mathrm{s}} = \frac{1}{2}\left(\mathbf{C}_{\mathrm{as}} + \mathbf{C}_{\mathrm{as}}^{\mathrm{T}}\right), \tag{3.3}$$

where $\bar{P}_{\mathrm{d}} \in \mathbb{R}^{1\times 1}$ is the time-averaged power dissipation, $\mathbf{C}_{\mathrm{s}}$, $\mathbf{C}_{\mathrm{as}} \in \mathbb{R}^{n\times n}$ are symmetric and asymmetric damping matrices and superscript T denotes the matrix transposition. It should be noted that Eq.(3.2) can be achieved when the mass and stiffness matrices are symmetric. By applying the power flow mode theory (Xiong et al. (2005)), the mode of power dissipation is expressed as

$$\bar{P}_{\mathrm{d}} = \sum_{j=1}^{n} \bar{P}_j, \tag{3.4}$$

$$\bar{P}_j = \frac{1}{2}\lambda_j |q_j|^2, \tag{3.5}$$

$$q_j = \boldsymbol{\varphi}_j^{\mathrm{T}}\mathbf{v}, \tag{3.6}$$

where $\bar{P}_j \in \mathbb{R}^{1\times 1}$ is the power flow mode, $q_j \in \mathbb{C}^{1\times 1}$ is the characteristic velocity, $\lambda_j \in \mathbb{R}^{1\times 1}$ and $\boldsymbol{\varphi}_j \in \mathbb{R}^{n\times 1}$ are the eigenvalue and the eigenvector of the damping matrix. Based on Eq.(3.4), the time-averaged power dissipation per unit characteristic velocity is given by

$$\bar{P}_{\mathrm{u}} = \frac{1}{2}\sum_{j=1}^{n}\lambda_j = \frac{1}{2}\mathrm{tr}(\mathbf{C}), \tag{3.7}$$

where tr(•) is the trace of matrix. This indicates that the time-averaged power dissipation per unit characteristic velocity can be calculated from the trace of the damping matrix. Xiong (2015) claimed that the vibration responses can be minimised by maximising the trace of the damping matrix.

$$\bar{P}_{\mathrm{u,max}} = \max(\mathrm{tr}(\mathbf{C})), \tag{3.8}$$

where max(•) indicates the maximum value.

3.2 Passive vibration control

The dynamic equation including with damping modification presented in s-domain is written by

$$\big(s^2\mathbf{M} + s(\mathbf{C} + \triangle\mathbf{C}) + \mathbf{K}\big)\mathbf{x}(s) = \mathbf{p}(s), \tag{3.9}$$

where $\mathbf{M}$, $\triangle\mathbf{C}$ and $\mathbf{K} \in \mathbb{R}^{n\times n}$ are respectively real mass, damping modification and stiffness matrices, $\mathbf{x} \in \mathbb{C}^{n\times 1}$ is a displacement vector presented in complex numbers. By using the power flow mode theory (Eq.(3.8)), the vibration is minimised by

$$\bar{P}_{\mathrm{u,max}} = \max(\mathrm{tr}(\mathbf{C} + \triangle\mathbf{C})). \tag{3.10}$$

Due to the constant damping matrix $\mathbf{C}$, Eq.(3.10) can be expressed by

$$\bar{P}_{\mathrm{u,max}} = \max(\mathrm{tr}(\triangle\mathbf{C})) = \max(\sum_{j=1}^{n} \triangle c_{jj}), \tag{3.11}$$

where $\triangle c_{jj}$ is the added damping coefficient to the diagonal matrix.

3.3 Active vibration control

3.3.1 Single-input control

The dynamic equation including the single-input velocity feedback control presented in s-domain is written by

$$\big(s^2\mathbf{M} + s\mathbf{C} + \mathbf{K}\big)\mathbf{x}(s) = \mathbf{b}u(s) + \mathbf{p}(s), \tag{3.12}$$

$$u(s) = -s\mathbf{f}^{\mathrm{T}}\mathbf{x}(s), \tag{3.13}$$

where $\mathbf{b}$ and $\mathbf{f} \in \mathbb{R}^{n\times 1}$ are actuator distribution and velocity gain vectors and $u \in \mathbb{C}^{1\times 1}$ is the single-input control. Combining Eq.(3.12) and Eq.(3.13), it yields,

$$\big(s^2\mathbf{M} + s(\mathbf{C} + \mathbf{b}\mathbf{f}^{\mathrm{T}}) + \mathbf{K}\big)\mathbf{x}(s) = \mathbf{p}(s). \tag{3.14}$$

By using the power flow mode theory (Eq.(3.8)), the maximum power dissipation per unit characteristic velocity is expressed by

$$\bar{P}_{\mathrm{u,max}} = \max(\mathrm{tr}(\mathbf{b}\mathbf{f}^{\mathrm{T}})). \tag{3.15}$$

3.3.2 Multiple-input control

The dynamic equation including the multiple-input velocity feedback control presented in s-domain is written by

$$\big(s^2\mathbf{M} + s\mathbf{C} + \mathbf{K}\big)\mathbf{x}(s) = \mathbf{B}\mathbf{u}(s) + \mathbf{p}(s), \tag{3.16}$$

$$\mathbf{u}(s) = -s\mathbf{F}^{\mathrm{T}}\mathbf{x}(s), \tag{3.17}$$

where $\mathbf{B}$ and $\mathbf{F} \in \mathbb{R}^{n\times m}$ are actuator distribution and velocity gain matrices and $\mathbf{u} \in \mathbb{C}^{m\times 1}$ is the multiple-input control. Combining Eq.(3.16) and Eq.(3.17), it yields,

$$\big(s^2\mathbf{M} + s(\mathbf{C} + \mathbf{B}\mathbf{F}^{\mathrm{T}}) + \mathbf{K}\big)\mathbf{x}(s) = \mathbf{p}(s). \tag{3.18}$$

By using the power flow mode theory (Eq.3.8), the maximum power dissipation per unit characteristic velocity is expressed by

$$\bar{P}_{\mathrm{u,max}} = \max(\mathrm{tr}(\mathbf{B}\mathbf{F}^{\mathrm{T}})). \tag{3.19}$$

3.4 Control performance

After applying the control methods, the control performance should be investigated to guarantee vibration reduction. It is presented by the frequency integrated kinetic energy without and with control methods.

$$\mathrm{R_T} = \frac{\int_0^{\omega} \widehat{\mathrm{T}}}{\int_0^{\omega} \mathrm{T}}, \tag{3.20}$$

$$\mathrm{T} = \frac{1}{4}\mathbf{v}^{\mathrm{H}}\mathbf{M}\mathbf{v}, \tag{3.21}$$

$$\widehat{\mathrm{T}} = \frac{1}{4}\widehat{\mathbf{v}}^{\mathrm{H}}\mathbf{M}\widehat{\mathbf{v}}, \tag{3.22}$$

where $\mathrm{R_T}$ is the kinetic energy ratio, T and $\widehat{\mathrm{T}}$ are respectively kinetic energy without and with control.

3.5 Numerical examples

A two-degree-of-freedom mass-spring-damper system is excited by a unit impules force; $p = 1$ N at mass m_2 as shown in Figure 3.1. This system has mass, $m_i = 1$ kg; damping, $c_i = 0.1$ Ns/m; and stiffness, $k_i = 25$ N/m where $i = 1, 2$. The mass, damping and stiffness matrices as well as the excitation force vector are given by

$$\mathbf{M} = \begin{bmatrix} m_1 & 0 \\ 0 & m_2 \end{bmatrix}, \mathbf{C} = \begin{bmatrix} c_1 + c_2 & -c_2 \\ -c_2 & c_2 \end{bmatrix}, \mathbf{K} = \begin{bmatrix} k_1 + k_2 & -k_2 \\ -k_2 & k_2 \end{bmatrix}, \mathbf{p} = \begin{Bmatrix} 0 \\ p \end{Bmatrix}.$$

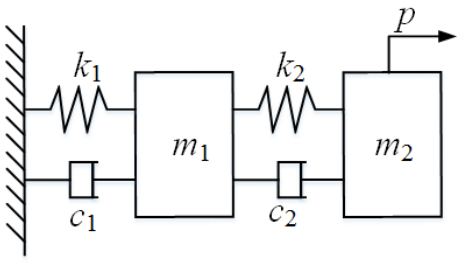

Figure 3.1: A two-degree-of-freedom mass-spring-damper system

3.5.1 Vibration minimisation by passive control

For the passive vibration control, the damping modification matrix is given by

$$\triangle\mathbf{C} = \begin{bmatrix} \triangle c_1 + \triangle c_2 & -\triangle c_2 \\ -\triangle c_2 & \triangle c_2 \end{bmatrix}.$$

Assuming $\triangle c = \triangle c_1 = \triangle c_2$ and varying $\triangle c$ from 0-10 Ns/m, the kinetic energy ratio decreases from 0 to -20.51 dB and the power dissipation per unit characteristic velocity increases from 0.3 to 30.3 when the added damping increases from 0 to 10 Ns/m (see Figure 3.2). Figure 3.3 shows the kinetic energy becomes flatter when the added damping increases. This indicates that the maximum added damping or the maximum power dissipation per unit characteristic velocity can minimise the vibration response.

Therefore, this theory can be applied into the passive control to minimise the vibration. However, it should be noted that when the added damping is significantly high, the underdamped system will be changed to the overdamped system.

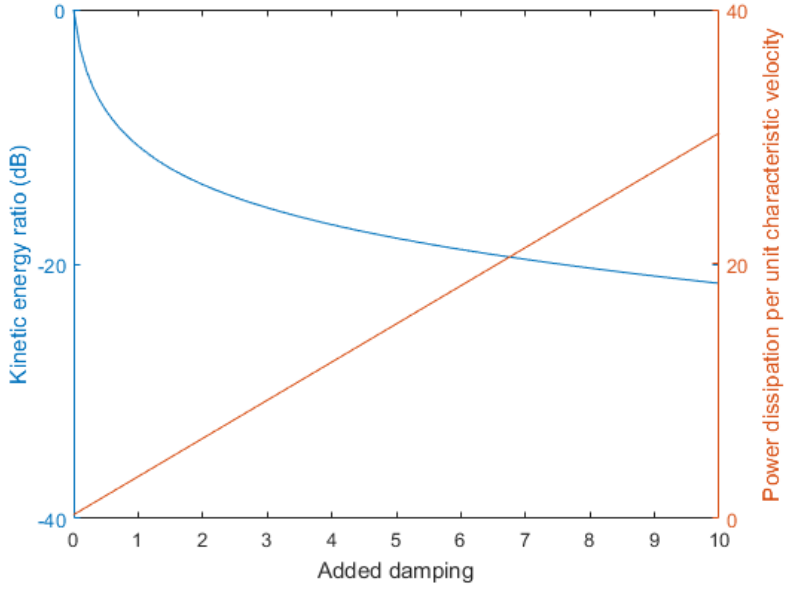

Figure 3.2: Relationship of the kinetic energy ratio, the power dissipation per unit charteristic velocity and the added damping of the two-degree-of-freedom system

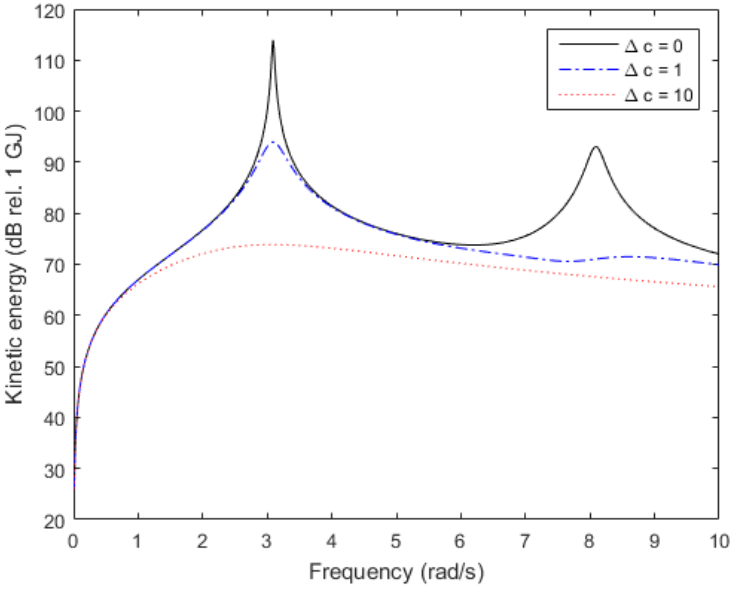

Figure 3.3: Kinetic energy with and without added damping of the two-degree-of-freedom system

3.5.2 Vibration minimisation by active control

For the single-input velocity feedback control, the actuator distribution and velocity gain vectors are given by

$$\mathbf{b} = \begin{Bmatrix} 1 \\ 1 \end{Bmatrix} \text{ and } \mathbf{f} = \begin{Bmatrix} f \\ f \end{Bmatrix}.$$

Applying the power flow mode theory (Eq.(3.15)), $\bar{P}_{\mathrm{u,max}}$ is obtained by maximising the velocity gain (f). The gain is varied from 0-10. As a result, the kinetic energy ratio drops from 0 to -13.89 dB when the the velocity gain raises from 0 to 2.60 and it gradually increases to -12.02 dB when the velocity gain rises to 10. The power dissipation per unit characteristic velocity continuously rises from 0.3 to 20.3 corresponding to an increase velocity gain (see Figure 3.4). This means that the velocity gain at 2.60 is the optimal value to minimise the vibration. In addition, Figure 3.5 shows that the kinetic energy with the optimal velocity gain becomes flatter (blue dash line) whereas the kinetic energy with the maximum velocity gain slightly increases (red dotted line). This indicates that the power flow mode theory is not able to minimise the vibration by using the single-input velocity feedback control because the maximum power dissipation per unit characteristic velocity cannot minimise the vibration. However, the vibration of this control system can be minimised by using the optimal velocity gain.

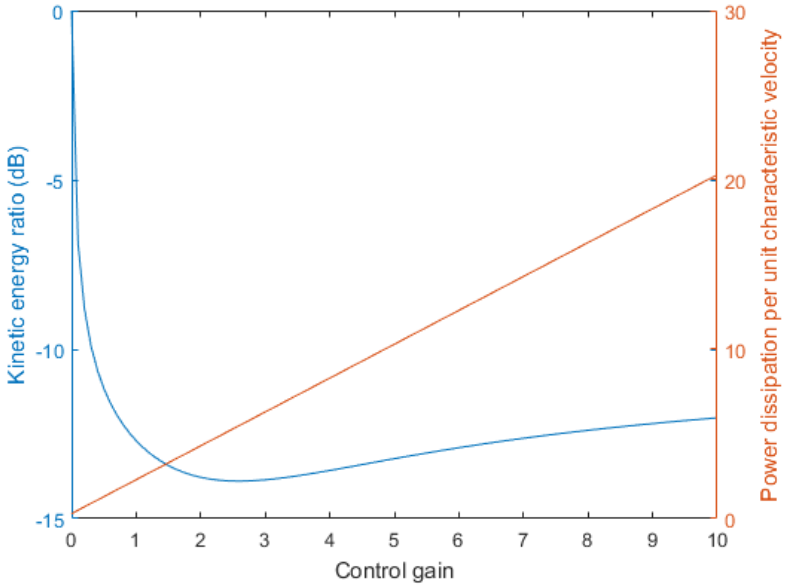

Figure 3.4: Relationship of the kinetic energy ratio, power dissipation per unit characteristic velocity and the velocity gain (single-input control) of the two-degree-of-freedom system

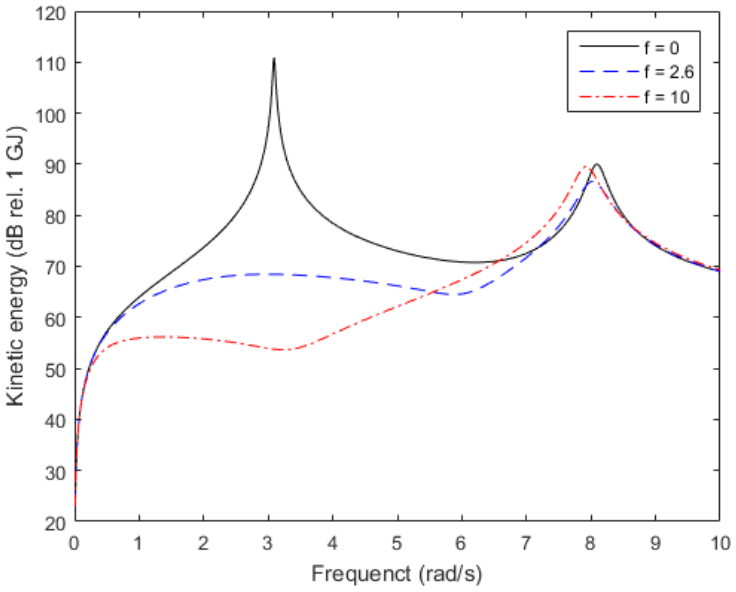

Figure 3.5: Kinetic energy with and without velocity gain (single-input control) of the two-degree-of-freedom system

For the multiple-input velocity feedback control, the actuator distribution and velocity gain matrices are assumed to be the diagonal matrix.

$$\mathbf{B}_1 = \begin{bmatrix} 1 & 0 \\ 0 & 1 \end{bmatrix}, \mathbf{F}_1 = \begin{bmatrix} f & 0 \\ 0 & f \end{bmatrix}.$$

Applying the power flow mode theory (Eq.(3.19)), $\bar{P}_{\mathrm{u,max}}$ is obtained by maximising the velocity gain (f). The gain is increased from 0-10. Obviously, this result is similar with the passive control. The kinetic energy ratio decreases from 0 to -27.31 dB and the power dissipation per unit characteristic velocity increases from 0.3 to 20.3 when the velocity gain increases from 0 to 10 (see Figure 3.6). Moreover, the kinetic energy becomes flatter when the velocity gain increases (see Figure 3.7). This means that the power flow mode theory can be applied into the multiple-input velocity feedback control to minimise the vibration when the actuator distribution and velocity gain are the diagonal matrices. However, it should be concerned that increasing high velocity gain is expensive and has the limitation.

Alternatively, the assumptions are changed to

$$\mathbf{B}_2 = \begin{bmatrix} 1 & 1 \\ 1 & 1 \end{bmatrix}, \mathbf{F}_2 = \begin{bmatrix} f & f \\ f & f \end{bmatrix}.$$

The gain is varied from 0-10. As can be seen, this result is similar with the single-input control. The kinetic energy ratio drops from 0 to -13.89 dB when the velocity gain increases from 0 to 1.30. It gradually raises when the velocity gain is larger than 1.30 (see Figure 3.8). In contrast, the power dissipation per unit characteristic velocity continuously increases from 0.3 to 40.3. In addition, Figure 3.5 shows that the kinetic energy with the optimal velocity gain becomes flatter (blue dash line) whereas the kinetic energy with the maximum velocity gain slightly increases (red dotted line). This means that the power flow mode theory cannot minimise the vibration by using the multiple-input velocity feedback control when the actuator distribution and velocity gain are non-diagonal matrices. Nonetheless, the vibration can be minimised by using the optimal velocity gain.

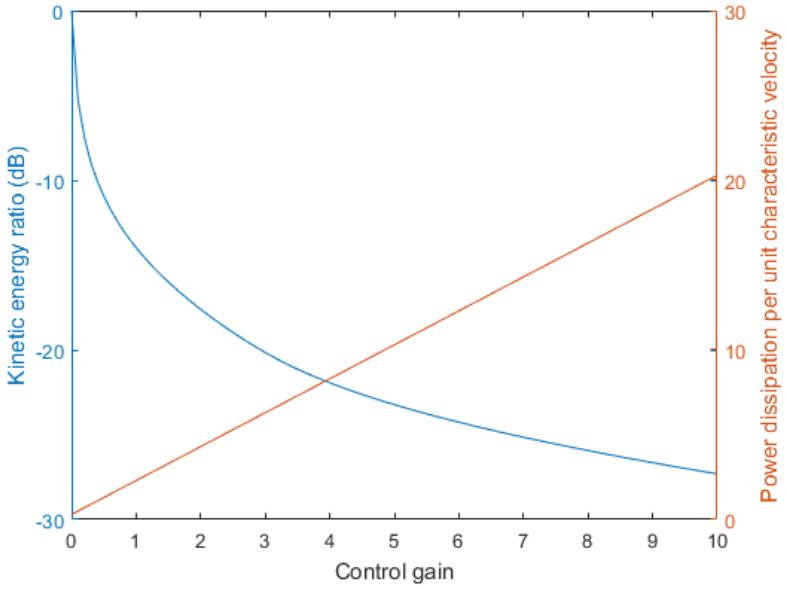

Figure 3.6: Relationship of the kinetic energy ratio, power dissipation per unit charateristic velocity and the velocity gain (multiple-input control with $\mathbf{B}_1$ and $\mathbf{F}_1$) of the two-degree-of-freedom system

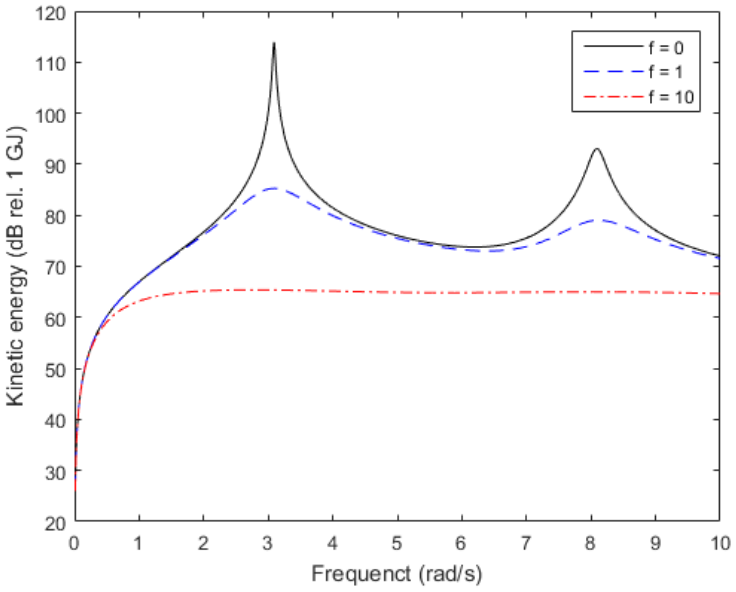

Figure 3.7: Kinetic energy with and without velocity gain (multiple-input control with $\mathbf{B}_1$ and $\mathbf{F}_1$) of the two-degree-of-freedom system

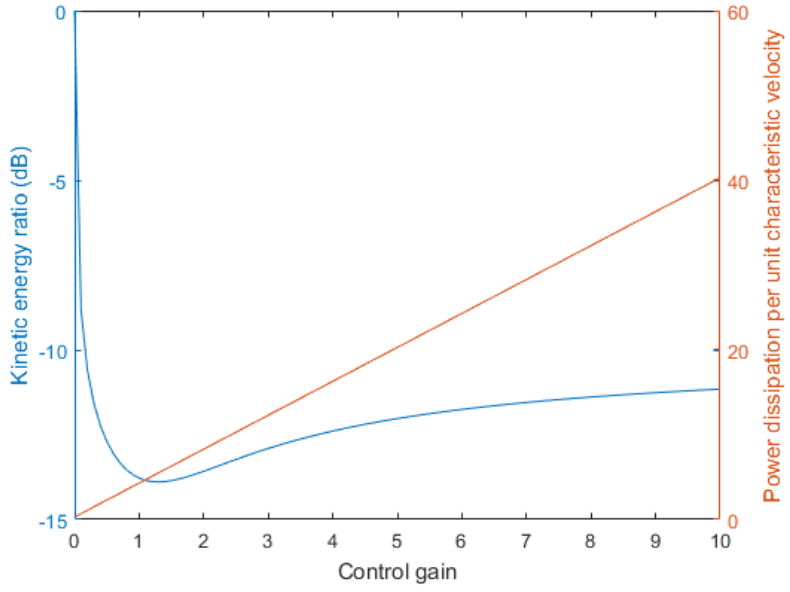

Figure 3.8: Relationship of the kinetic energy ratio, power dissipation per unit characteristic velocity and the velocity gain (multiple-input control with $\mathbf{B}_2$ and $\mathbf{F}_2$) of the two degrees-of-freedom system

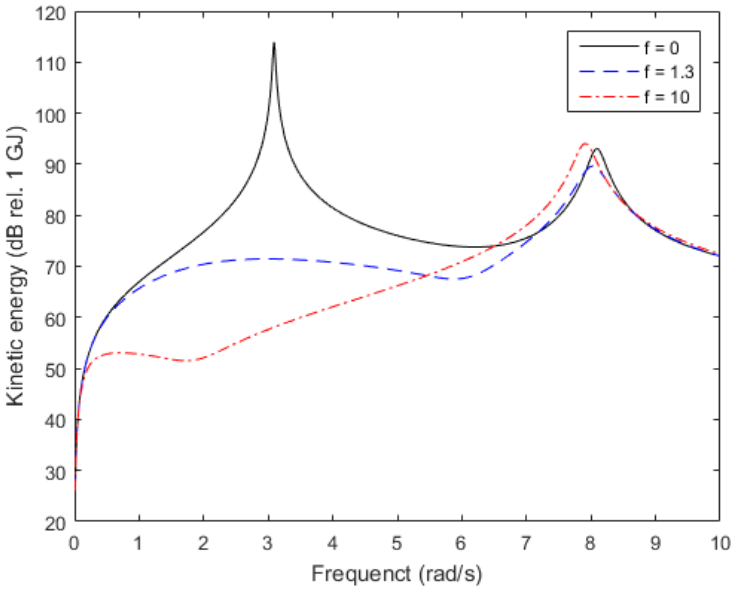

Figure 3.9: Kinetic energy with and without velocity gain (multiple-input control with $\mathbf{B}_2$ and $\mathbf{F}_2$) of the two degrees-of-freedom system

3.6 Summary

The power flow mode theory based on damping distribution provides the method to minimise the vibration responses by maximising the time-averaged power dissipation per unit characteristic velocity or the trace of the damping matrix. It is applied into both passive and active controls. The maximum time-averaged power dissipation per unit characteristic velocity is obtained by maximising the added damping (passive control) and the velocity gain (active control). As a result, the theory works properly for the passive control and the multiple-input velocity feedback with diagonal matrices of the actuator distribution and velocity gain because maximum added damping/velocity gain minimise the vibration. Nonetheless, when the added damping/velocity gain is high enough, the underdamped system will be changed to the overdamped system.

For single-input control and multiple-input control without the diagonal matrices, the vibration is minimised by using the optimal gain. The results show that the vibration is rapidly dropped by increasing the velocity gain from zero to the optimal value and it is gradually raised when the velocity gain is higher than the optimal value. This study indicates that the power flow mode theory cannot minimise the vibration for all cases. It is suitable for some such as passive control and multiple-input control with the diagonal matrices. For the others, the vibration can be minimised by using the optimal velocity gain.

Chapter 4

Partial Pole Assignment for Asymmetric Systems

This chapter reports a study of partial pole assignment by using the single-input control for stabilising the asymmetric system, exemplified by the friction-induced vibration. The control strategies are considered on velocity and displacement feedback, acceleration and velocity feedback, as well as acceleration and displacement feedback. The unobservability condition is implemented to keep unassigned poles unchanged. The receptance method is applied to avoid modelling errors from evaluating mass, damping and stiffness matrices by the finite element method (FEM). The solution is formulated in linear equations which allow to determine the control gains directly. The locations of actuators are taken into account to minimise the energy supplied to the actuators.

For symmetric systems, partial pole assignment was firstly proposed by Datta et al. (1997). Orthogonality conditions were applied to assign some poles and keep others unchanged. Tehrani et al. (2010) proved that partial pole assignment can be achieved by using unobservability condition and its concept is similar with partial pole assignment by using orthogonality conditions. However, unobservability condition requires sensors at every degrees of freedom. Then, Tehrani et al. (2010) applied uncontrollability condition in partial pole assignment by using receptance method to avoid numerical errors evaluated by FEM. Nonetheless, the errors still contain in the system due to a curve fitting method for estimating receptances.

For asymmetric systems, Tehrani and Ouyang (2012) implemented the receptance-based method of partial pole assignment by using the uncontrollability condition. It requires a particular set of the actuator distribution vector to keep unassigned poles unchanged. Then, Liang et al. (2016) proposed partial pole assignment by using the unobservability condition. This method allows to select various sets of the actuator distribution vectors

but it requires both the poles (eigenvalues) and the mode shapes (eigenvectors) to make unassigned poles unchanged. However, the mode shapes are difficult to evaluate in the asymmetric system. Therefore, this algorithm should be improved.

In this chapter, an alternative method of partial pole assignment for the asymmetric system by using the unobservability condition is improved from Liang et al. (2016). It requires only unassigned poles to keep them unchanged. The receptance method is implemented to avoid the modelling errors from FEM. The solution is determined by using Sherman-Morrison formula and formulated in the linear equations, which can be solved directly. Three control methods such as velocity and displacement feedback, acceleration and velocity feedback, as well as acceleration and displacement feedback are investigated to determine the most effective method for saving the energy consumed by the actuators. The optimal actuator locations are also considered to minimise the energy. The numerical examples show that the proposed method is capable of making partial pole assignment in the asymmetric systems and minimising the energy.

4.1 Pole assignment

The dynamic equation of the asymmetric system including the state feedback control presented in Ouyang (2010) can be written as

$$\mathbf{M}\ddot{\mathbf{x}}(t) + \mathbf{C}\dot{\mathbf{x}}(t) + \mathbf{K}\mathbf{x}(t) = \mathbf{b}u(t) + \mathbf{p}(t), \tag{4.1}$$

$$\mathbf{C} = \mathbf{C}_{\mathrm{s}} + \mathbf{C}_{\mathrm{as}}, \tag{4.2}$$

$$\mathbf{K} = \mathbf{K}_{\mathrm{s}} + \mathbf{K}_{\mathrm{as}}, \tag{4.3}$$

$$u(t) = -\mathbf{a}^{\mathrm{T}}\ddot{\mathbf{x}}(t) - \mathbf{f}^{\mathrm{T}}\dot{\mathbf{x}}(t) - \mathbf{g}^{\mathrm{T}}\mathbf{x}(t). \tag{4.4}$$

Substituting Eq.(4.2) - Eq.(4.4) into Eq.(4.1) and taking Laplace transform gives

$$\left(s^2\mathbf{M} + s(\mathbf{C}_{\mathrm{s}} + \mathbf{C}_{\mathrm{as}}) + \mathbf{K}_{\mathrm{s}} + \mathbf{K}_{\mathrm{as}} + \mathbf{b}(s^2\mathbf{a}^{\mathrm{T}} + s\mathbf{f}^{\mathrm{T}} + \mathbf{g}^{\mathrm{T}})\right)\mathbf{x}(\mathbf{s}) = \mathbf{p}(s). \tag{4.5}$$

where $\mathbf{M}$, $\mathbf{C}_{\mathrm{s}}$ and $\mathbf{K}_{\mathrm{s}} \in \mathbb{R}^{n\times n}$ are respectively real symmetric mass, damping and stiffness matrices; $\mathbf{C}_{\mathrm{as}}$ and $\mathbf{K}_{\mathrm{as}} \in \mathbb{R}^{n\times n}$ are respectively real asymmetric damping and stiffness matrices generated by non-conservative forces such as friction forces; $\mathbf{x}$ and $\mathbf{p} \in \mathbb{C}^{n\times 1}$ are respectively complex displacement and excitation force vectors; $\mathbf{b}$, $\mathbf{a}$, $\mathbf{f}$ and $\mathbf{g} \in \mathbb{R}^{n\times 1}$ are respectively real actuator distribution, acceleration gain, velocity gain and displacement gain vectors; $u \in \mathbb{C}^{1\times 1}$ is a single-input control; and superscript T denotes matrix transposition.

Define

$$\mathbf{H}_{\text{as}}(s) = \left(s^2\mathbf{M}_{\text{s}} + s(\mathbf{C}_{\text{s}} + \mathbf{C}_{\text{as}}) + \mathbf{K}_{\text{s}} + \mathbf{K}_{\text{as}}\right)^{-1}. \tag{4.6}$$

$$\widehat{\mathbf{H}}_{\text{as}}(s) = \left(\mathbf{H}_{\text{as}}^{-1}(s) + \mathbf{b}(s^2\mathbf{a}^{\text{T}} + s\mathbf{f}^{\text{T}} + \mathbf{g}^{\text{T}})\right)^{-1}. \tag{4.7}$$

Apparently $\mathbf{H}_{\text{as}}$ and $\widehat{\mathbf{H}}_{\text{as}}$ are (asymmetric) receptance matrices of the open-loop and closed-loop systems. It should be pointed out (Tehrani and Ouyang (2012)) that $\mathbf{H}_{\text{as}}$ is difficult to measure in practice, for example, measuring $\mathbf{H}_{\text{as}}$ in a disc brake requires a torque to rotate the disc while the brake is engaged. So, $\mathbf{H}_{\text{as}}$ should be rearranged and expressed in term of the open-loop symmetric receptance matrix $\mathbf{H}_{\text{s}}$, which is easier to measure.

$$\mathbf{H}_{\text{as}}(s) = \left(\mathbf{I} + \mathbf{H}_{\text{s}}(s)(s\mathbf{C}_{\text{as}} + \mathbf{K}_{\text{as}})\right)^{-1}\mathbf{H}_{\text{s}}(s). \tag{4.8}$$

$$\mathbf{H}_{\text{s}}(s) = (s^2\mathbf{M} + s\mathbf{C}_{\text{s}} + \mathbf{K}_{\text{s}})^{-1}. \tag{4.9}$$

Using Sherman-Morrison formula, Eq.(4.7) can be expressed as

$$\widehat{\mathbf{H}}_{\text{as}}(s) = \mathbf{H}_{\text{as}}(s) - \frac{\mathbf{H}_{\text{as}}(s)\mathbf{b}(s^2\mathbf{a}^{\text{T}} + s\mathbf{f}^{\text{T}} + \mathbf{g}^{\text{T}})\mathbf{H}_{\text{as}}(s)}{1 + (s^2\mathbf{a}^{\text{T}} + s\mathbf{f}^{\text{T}} + \mathbf{g}^{\text{T}})\mathbf{H}_{\text{as}}(s)\mathbf{b}}. \tag{4.10}$$

It can be seen that the poles of the closed-loop system (that are different from the poles of the open-loop system) satisfy the following characteristic equation:

$$(s^2\mathbf{a}^{\text{T}} + s\mathbf{f}^{\text{T}} + \mathbf{g}^{\text{T}})\mathbf{H}_{\text{as}}(s)\mathbf{b} = -1. \tag{4.11}$$

In order to assign $2n$ poles, they are substituted into Eq.(4.11) which give $2n$ equations. Two-thirds of the control gain vectors must be chosen. Therefore, three control strategies such as velocity and displacement feedback, acceleration and velocity feedback, as well as acceleration and displacement feedback are considered to solve the pole assignment problem and expressed below.

$$\begin{bmatrix} \mathbf{r}_1^{\text{T}} & \mu_1\mathbf{r}_1^{\text{T}} \\ \mathbf{r}_2^{\text{T}} & \mu_2\mathbf{r}_2^{\text{T}} \\ \vdots & \vdots \\ \mathbf{r}_{2n}^{\text{T}} & \mu_{2n}\mathbf{r}_{2n}^{\text{T}} \end{bmatrix} \begin{pmatrix} \mathbf{g} \\ \mathbf{f} \end{pmatrix} = \begin{pmatrix} -1 \\ -1 \\ \vdots \\ -1 \end{pmatrix}, \tag{4.12}$$

$$\begin{bmatrix} \mu_1^2\mathbf{r}_1^{\text{T}} & \mu_1\mathbf{r}_1^{\text{T}} \\ \mu_2^2\mathbf{r}_2^{\text{T}} & \mu_2\mathbf{r}_2^{\text{T}} \\ \vdots & \vdots \\ \mu_{2n}^2\mathbf{r}_{2n}^{\text{T}} & \mu_{2n}\mathbf{r}_{2n}^{\text{T}} \end{bmatrix} \begin{pmatrix} \mathbf{a} \\ \mathbf{f} \end{pmatrix} = \begin{pmatrix} -1 \\ -1 \\ \vdots \\ -1 \end{pmatrix}, \tag{4.13}$$

$$\begin{bmatrix} \mu_1^2\mathbf{r}_1^{\mathrm{T}} & \mathbf{r}_1^{\mathrm{T}} \\ \mu_2^2\mathbf{r}_2^{\mathrm{T}} & \mathbf{r}_2^{\mathrm{T}} \\ \vdots & \vdots \\ \mu_{2n}^2\mathbf{r}_{2n}^{\mathrm{T}} & \mathbf{r}_{2n}^{\mathrm{T}} \end{bmatrix} \begin{pmatrix} \mathbf{a} \\ \mathbf{g} \end{pmatrix} = \begin{pmatrix} -1 \\ -1 \\ \vdots \\ -1 \end{pmatrix}, \tag{4.14}$$

$$\mathbf{r}_i = \mathbf{H}_{\mathrm{as}}(\mu_i)\mathbf{b}. \tag{4.15}$$

where μ_i is the required closed-loop pole.

4.2 Partial pole assignment by unobservability condition

The previous section demonstrates the algorithms of pole assignment for assigning $2n$ poles. In this section, partial pole assignment by using the unobservability condition is considered, which allow to assign some poles and keep others unchanged. According to Eq.(4.10), a particular pole λ_i can make the closed-loop receptance matrix equal to the open-loop receptance matrix ($\widehat{\mathbf{H}}_{\mathrm{as}} = \mathbf{H}_{\mathrm{as}}$) when either

$$\mathbf{H}_{\mathrm{as}}(\lambda_i)\mathbf{b} = \mathbf{0}, \quad \text{for } i = p+1, p+2, ..., 2n, \tag{4.16}$$

or

$$(\lambda_i^2\mathbf{a}^{\mathrm{T}} + \lambda_i\mathbf{f}^{\mathrm{T}} + \mathbf{g}^{\mathrm{T}})\mathbf{H}_{\mathrm{as}}(\lambda_i) = \mathbf{0}, \quad \text{for } i = p+1, p+2, ..., 2n, \tag{4.17}$$

where λ_i is the unchanged pole.

Eq.(4.16) and Eq.(4.17) are respectively called the uncontrollability and the unobservability conditions. Partial pole assignment by using the uncontrollability condition was proposed by Tehrani and Ouyang (2012). Then, Liang et al. (2016) continued using the unobservability condition which requires both the unchanged eigenvalues and the unchanged eigenvectors. However, it is difficult to evaluate the eigenvectors of the asymmetric system. To deal with the problem, the algorithm of partial pole assignment by using the unobservability condition which requires only unchanged eigenvalues is developed.

4.2.1 Unobservability condition

Partial pole assignment by using the unobservability condition is derived from Eq.(4.17). Post-multiplying by $\mathbf{b}$, it implies that

$$(\lambda_i^2\mathbf{a}^{\mathrm{T}} + \lambda_i\mathbf{f}^{\mathrm{T}} + \mathbf{g}^{\mathrm{T}})\mathbf{H}_{\mathrm{as}}(\lambda_i)\mathbf{b} = 0, \quad \text{for } i = p+1, p+2, ..., 2n. \tag{4.18}$$

Combining Eq.(4.11) and Eq.(4.18), algorithms of partial pole assignment by using velocity and displacement feedback, acceleration and velocity feedback, as well as acceleration and displacement feedback are respectively given by

$$\begin{bmatrix} \mathbf{r}_1^{\mathrm{T}} & \mu_1\mathbf{r}_1^{\mathrm{T}} \\ \vdots & \vdots \\ \mathbf{r}_p^{\mathrm{T}} & \mu_p\mathbf{r}_p^{\mathrm{T}} \\ \mathbf{r}_{p+1}^{\mathrm{T}} & \lambda_{p+1}\mathbf{r}_{p+1}^{\mathrm{T}} \\ \vdots & \vdots \\ \mathbf{r}_{2n}^{\mathrm{T}} & \lambda_{2n}\mathbf{r}_{2n}^{\mathrm{T}} \end{bmatrix} \begin{pmatrix} \mathbf{g} \\ \mathbf{f} \end{pmatrix} = \begin{pmatrix} -1 \\ \vdots \\ -1 \\ 0 \\ \vdots \\ 0 \end{pmatrix}. \tag{4.19}$$

$$\begin{bmatrix} \mu_1^2\mathbf{r}_1^{\mathrm{T}} & \mu_1\mathbf{r}_1^{\mathrm{T}} \\ \vdots & \vdots \\ \mu_p^2\mathbf{r}_p^{\mathrm{T}} & \mu_p\mathbf{r}_p^{\mathrm{T}} \\ \lambda_{p+1}^2\mathbf{r}_{p+1}^{\mathrm{T}} & \lambda_{p+1}\mathbf{r}_{p+1}^{\mathrm{T}} \\ \vdots & \vdots \\ \lambda_{2n}^2\mathbf{r}_{2n}^{\mathrm{T}} & \lambda_{2n}\mathbf{r}_{2n}^{\mathrm{T}} \end{bmatrix} \begin{pmatrix} \mathbf{a} \\ \mathbf{f} \end{pmatrix} = \begin{pmatrix} -1 \\ \vdots \\ -1 \\ 0 \\ \vdots \\ 0 \end{pmatrix}. \tag{4.20}$$

$$\begin{bmatrix} \mu_1^2\mathbf{r}_1^{\mathrm{T}} & \mathbf{r}_1^{\mathrm{T}} \\ \vdots & \vdots \\ \mu_p^2\mathbf{r}_p^{\mathrm{T}} & \mathbf{r}_p^{\mathrm{T}} \\ \lambda_{p+1}^2\mathbf{r}_{p+1}^{\mathrm{T}} & \mathbf{r}_{p+1}^{\mathrm{T}} \\ \vdots & \vdots \\ \lambda_{2n}^2\mathbf{r}_{2n}^{\mathrm{T}} & \mathbf{r}_{2n}^{\mathrm{T}} \end{bmatrix} \begin{pmatrix} \mathbf{a} \\ \mathbf{g} \end{pmatrix} = \begin{pmatrix} -1 \\ \vdots \\ -1 \\ 0 \\ \vdots \\ 0 \end{pmatrix}. \tag{4.21}$$

To validate the result, the required closed-loop poles, the control gain vectors and the actuator distribution vector are substituted back into Eq.(4.22). If $|D|$ is close to zero, the partial poles are successfully assigned by using the unobservability condition.

$$D = \det\big(s^2(\mathbf{M} + \mathbf{b}\mathbf{a}^{\mathrm{T}}) + s(\mathbf{C} + \mathbf{b}\mathbf{f}^{\mathrm{T}}) + \mathbf{K} + \mathbf{b}\mathbf{g}^{\mathrm{T}}\big). \tag{4.22}$$

It should be noted that the proposed method is also applied to the symmetric system when $\mathbf{r}_i = \mathbf{H}_{\mathrm{s}}(\mu_i)\mathbf{b}$.

4.3 Optimal actuation

In this section, the optimal actuator distribution vector for minimising the energy consumed by the actuators is determined by using an optimisation method. Generally, the minimum control effort (control gain) is required to prevent an excessive control force and save energy supplied to the actuators. For pole assignment problems, the locations of actuators are normally assumed. Some sets of the actuator distribution vectors require low energy for assigning the poles but some of them require high energy.

So, it is important to determine the optimal actuator distribution vector. The algorithm of pole assignment to minimise the control effort by using the optimal actuation was proposed by Guzzardo et al. (2013). However, the energy consumed by the actuators does not depend only on the control effort. It is also influenced by the control forces (Soong (1990)).

$$E = \int_0^t u^2 \mathbf{b}^{\mathrm{T}} \mathbf{b} \, \mathrm{d}t, \tag{4.23}$$

where E is an indicator to measure the energy consumed by the actuators and t is the time. Substituting Eq.(4.4) into Eq.(4.23), the energy index was rewritten by (Ouyang (2011))

$$E = \int_0^t \left(\mathbf{a}^{\mathrm{T}} \ddot{\mathbf{x}} + \mathbf{f}^{\mathrm{T}} \dot{\mathbf{x}} + \mathbf{g}^{\mathrm{T}} \mathbf{x}\right)^2 \mathbf{b}^{\mathrm{T}} \mathbf{b} \, \mathrm{d}t. \tag{4.24}$$

In the cases of pole assignment and partial pole assignment for the asymmetric system, the optimal actuator distribution vector is determined by

$$\min_{b_i \in \mathbf{b}} E \text{ subjected to}$$
$$\begin{cases} \text{Eq.(4.12) for pole assignment by using velocity and displacement feedback,} \\ \text{Eq.(4.13) for pole assignment by using acceleration and velocity feedback,} \\ \text{Eq.(4.14) for pole assignment by using acceleration and displacement feedback,} \\ \text{Eq.(4.19) for partial pole assignment by using velocity and displacement feedback,} \\ \text{Eq.(4.20) for partial pole assignment by using acceleration and velocity feedback,} \\ \text{Eq.(4.21) for partial pole assignment by using acceleration and displacement feedback.} \end{cases} \tag{4.25}$$

Note that b_i is assumed to be either 0 or 1.

4.4 Numerical examples

In this section, algorithms of pole assignment and partial pole assignment are applied into a friction-induced vibration problem in order to assign the given poles. Three control strategies such as velocity and displacement feedback, acceleration and velocity feedback, as well as acceleration and displacement feedback are demonstrated. Various sets of the actuator distribution vectors are implemented in order to investigate the minimum energy supplied to the actuators. In addition, the genetic algorithm is also applied to determine the optimal actuation.

A disc brake is modelled by a mass-spring-damper system on a conveyor belt as illustrated in Figure 4.1 (Ouyang (2010)). The system consists of three masses with m_1 having a degree-of-freedom in the horizontal direction, m_3 having a degree-of-freedom in the vertical direction and m_2 having degrees-of-freedom in both directions attached with linear spring k_3 at 45° relative to the vertical direction. When the belt is moving, a friction force is generated between the belt and the slider. To simplify the problem, Coulomb friction is considered and stick-slip phenomenon is avoided. $\mathbf{M}$, $\mathbf{C}_\mathrm{s}$, $\mathbf{K}_\mathrm{s}$, and $\mathbf{K}_\mathrm{as}$ corresponding to the displacement vector, $\mathbf{x} = \{x_1, y_3, x_2, y_2\}^\mathrm{T}$ are given by,

$$\mathbf{M} = \begin{bmatrix} m_1 & 0 & 0 & 0 \\ 0 & m_3 & 0 & 0 \\ 0 & 0 & m_2 & 0 \\ 0 & 0 & 0 & m_2 \end{bmatrix}, \mathbf{C}_\mathrm{s} = \begin{bmatrix} c_1 & 0 & -c_1 & 0 \\ 0 & 0 & 0 & 0 \\ -c_1 & 0 & c_1 & 0 \\ 0 & 0 & 0 & c_0 \end{bmatrix},$$

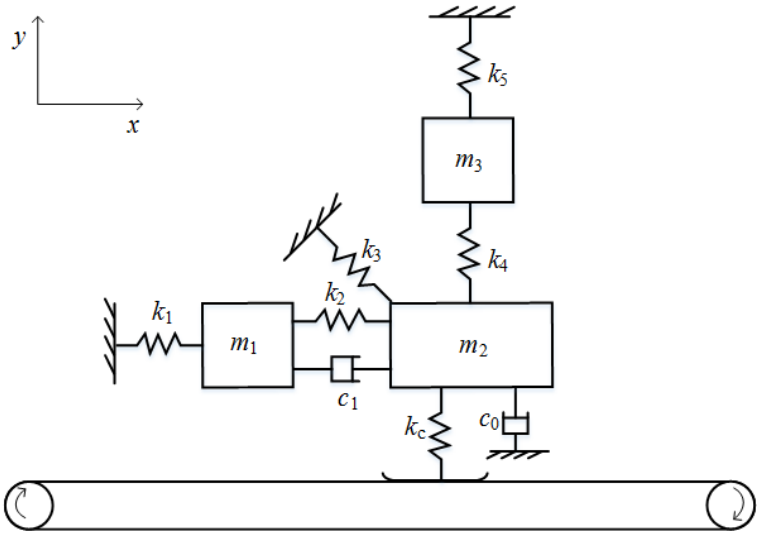

Figure 4.1: A disc brake model

$$\mathbf{K}_{\mathrm{s}} = \begin{bmatrix} k_1 + k_2 & 0 & -k_2 & 0 \\ 0 & k_4 + k_5 & 0 & -k_4 \\ -k_2 & 0 & k_2 + 0.5k_3 & -0.5k_3 \\ 0 & -k_4 & -0.5k_3 & k_4 + 0.5k_3 + k_{\mathrm{c}} \end{bmatrix},$$

$$\mathbf{K}_{\mathrm{as}} = \begin{bmatrix} 0 & 0 & 0 & 0 \\ 0 & 0 & 0 & 0 \\ 0 & 0 & 0 & \mu_{\mathrm{c}} k_{\mathrm{c}} \\ 0 & 0 & 0 & 0 \end{bmatrix},$$

where x_1 and x_2 are respectively the displacement in horizontal direction of mass m_1 and m_2, and y_2 and y_3 are respectively the displacement in vertical direction of mass m_2 and m_3. Assume that sensors and actuators can be located at every degrees of freedom.

Parameters used are taken from Ouyang (2010): mass, $m_i = 1$ kg $(i = 1, 2, 3)$; damping, $c_i = 0.5$ Ns/m $(i = 0, 1)$; stiffness, $k_i = 100$ N/m $(i = 1, 2, ..., 5)$; contact stiffness, $k_{\mathrm{c}} = 200$ N/m; and friction coefficient, $\mu_{\mathrm{c}} = 0.5$. The open-loop poles are determined by using 'polyeig' function in MATLAB. As can be seen, the open-loop system is unstable because of the positive real parts of the first pair of poles. In order to demonstrate the proposed method, four cases of required closed-loop poles are considered (see Table 4.1) and various sets of actuator distribution vectors are applied (see Table 4.2).

$$\{\lambda\}_1^8 = \begin{Bmatrix} 0.0070 \pm 8.9462\mathrm{i} \\ -0.0553 \pm 12.1336\mathrm{i} \\ -0.5259 \pm 16.8229\mathrm{i} \\ -0.1757 \pm 19.7336\mathrm{i} \end{Bmatrix}.$$

Table 4.1: Required closed-loop poles of the disc brake model

Case I	Case II	Case III	Case IV
$-1.0000 \pm 9.0000\mathrm{i}$	$-1.0000 \pm 9.0000\mathrm{i}$	$-1.0000 \pm 9.0000\mathrm{i}$	$-1.0000 \pm 9.0000\mathrm{i}$
$-1.0000 \pm 12.5000\mathrm{i}$	$-1.0000 \pm 12.5000\mathrm{i}$	$-1.0000 \pm 12.5000\mathrm{i}$	$-0.0553 \pm 12.1336\mathrm{i}$
$-1.0000 \pm 17.0000\mathrm{i}$	$-1.0000 \pm 17.0000\mathrm{i}$	$-0.5259 \pm 16.8229\mathrm{i}$	$-0.5259 \pm 16.8229\mathrm{i}$
$-1.0000 \pm 20.0000\mathrm{i}$	$-0.1757 \pm 19.7336\mathrm{i}$	$-0.1757 \pm 19.7336\mathrm{i}$	$-0.1757 \pm 19.7336\mathrm{i}$

Table 4.2: Various set of actuator distribution vectors

$\mathbf{b}_1 = \{0,0,0,1\}^{\mathrm{T}}$	$\mathbf{b}_2 = \{0,0,1,0\}^{\mathrm{T}}$	$\mathbf{b}_3 = \{0,1,0,0\}^{\mathrm{T}}$
$\mathbf{b}_4 = \{1,0,0,0\}^{\mathrm{T}}$	$\mathbf{b}_5 = \{0,0,1,1\}^{\mathrm{T}}$	$\mathbf{b}_6 = \{0,1,0,1\}^{\mathrm{T}}$
$\mathbf{b}_7 = \{1,0,0,1\}^{\mathrm{T}}$	$\mathbf{b}_8 = \{0,1,1,0\}^{\mathrm{T}}$	$\mathbf{b}_9 = \{1,0,1,0\}^{\mathrm{T}}$
$\mathbf{b}_{10} = \{1,1,0,0\}^{\mathrm{T}}$	$\mathbf{b}_{11} = \{1,1,0,1\}^{\mathrm{T}}$	$\mathbf{b}_{12} = \{1,0,1,1\}^{\mathrm{T}}$
$\mathbf{b}_{13} = \{0,1,1,1\}^{\mathrm{T}}$	$\mathbf{b}_{14} = \{1,1,1,0\}^{\mathrm{T}}$	$\mathbf{b}_{15} = \{1,1,1,1\}^{\mathrm{T}}$

4.4.1 Velocity and displacement feedback

Algorithms of pole assignment (Eq.(4.12)) and partial pole assignment (Eq.(4.19)) by using velocity and displacement feedback are applied to assign the required closed-loop poles with various sets of the actuator distribution vectors. The velocity and displacement gain vectors are obtained as shown in Table 4.3 - Table 4.6 for Case I - Case IV respectively. These results are validated by using Eq.(4.22). It is found that $|D|$ is close to zero for all cases. Therefore, the algorithms of pole assignment and partial pole assignment by using velocity and displacement feedback are capable to assign poles and partial poles precisely.

The energy index within the time period 0-5 s (Eq.(4.24)) is also determined in order to investigate the optimal actuator distribution vector. The initial conditions are zero displacement and zero velocity except the displacement, $x_2 = 0.01$ m. The displacement responses with the minimum and maximum energy indexes are plotted as illustrated in Figure 4.2 - Figure 4.5 for Case I - Case IV respectively. It is clear that the responses with the minimum energy index slightly oscillate whereas the responses with the maximum energy index highly oscillate. This means that slightly vibration requires low energy supplied to the actuators.

The results in Table 4.3 - Table 4.6 indicate that the velocity and displacement gains as well as the energy indexes are totally different when various sets of the actuator distribution vectors are applied. Some of them require the large energy index leading to plenty energy supplied to the actuators. To save the energy, the optimal actuator distribution vector for the smallest energy index must be chosen. For example, the optimal actuator distribution vectors: $\mathbf{b}_8$, $\mathbf{b}_4$, $\mathbf{b}_9$ and $\mathbf{b}_9$ are selected to assign the required closed-loop poles in Case I - Case IV respectively. It can be seen that the actuators should be located on mass m_1 and m_2 in the horizontal direction in order to minimise the energy. On the other hand, the control system requires the maximum energy when the actuators are located on mass m_2 and m_3 in the vertical direction such as $\mathbf{b}_6$, $\mathbf{b}_6$, $\mathbf{b}_{11}$ and $\mathbf{b}_{11}$ for Case I - Case IV respectively.

Alternatively, the optimal actuator distribution vector for minimising the energy index (see Table 4.7) can be obtained by using the genetic algorithm to solve Eq.(4.25). These results are the same with the previous method. They also indicate that the energy index depends on the number of the assigned closed-loop pole. For example, the largest energy index, 0.0436, is required when all poles (Case I) are assigned. On the other hand, the smallest energy index, 0.0048, is required when only one pair of poles (Case IV) are assigned.

By using the results in Table 4.7, amplitudes and phases of the closed-loop receptances are compared with the open-loop receptance (see Figure 4.6). For Case I, the closed-loop receptance becomes flatter for all resonances because all poles are assigned with high damp. For Case II, the closed-loop receptance drops for the first three resonances and keep the last resonance unchanged because the first three pairs of poles are assigned with high damp and the last pair of poles is kept unchanged. Similarly, for Case III and Case IV, the closed-loop receptance reduces at the resonances corresponding to the assigned poles and maintains unchanged corresponding to the unchanged poles.

Table 4.3: Velocity gain and displacement gain vectors associated with the energy index for assigning the required closed-loop poles in Case I

$\mathbf{b}$	$\mathbf{g}$	$\mathbf{f}$	E
$\mathbf{b}_1$	$\{64.67, 0.03, -37.55, 47.25\}^{\mathrm{T}}$	$\{-5.17, 4.34, -13.15, 6.50\}^{\mathrm{T}}$	0.2074
$\mathbf{b}_2$	$\{5.75, -55.75, 45.28, -161.29\}^{\mathrm{T}}$	$\{3.94, -12.23, 6.50, -12.13\}^{\mathrm{T}}$	0.0645
$\mathbf{b}_3$	$\{-25.58, 44.00, 57.92, -42.68\}^{\mathrm{T}}$	$\{-13.62, 6.50, -8.02, 0.94\}^{\mathrm{T}}$	0.2071
$\mathbf{b}_4$	$\{46.54, -161.61, -54.62, 165.91\}^{\mathrm{T}}$	$\{6.50, -11.60, 1.42, 1.89\}^{\mathrm{T}}$	0.1182
$\mathbf{b}_5$	$\{-27.73, 28.59, -7.52, 54.59\}^{\mathrm{T}}$	$\{0.35, 3.88, 3.56, 2.94\}^{\mathrm{T}}$	0.0560
$\mathbf{b}_6$	$\{75.52, -39.89, -61.63, 84.48\}^{\mathrm{T}}$	$\{-19.56, 5.33, 6.76, 1.17\}^{\mathrm{T}}$	1.7560
$\mathbf{b}_7$	$\{-14.44, 51.81, -27.32, 60.40\}^{\mathrm{T}}$	$\{2.74, 5.65, 2.58, 3.76\}^{\mathrm{T}}$	0.0583
$\mathbf{b}_8$	$\{-22.95, 38.52, 6.96, -19.56\}^{\mathrm{T}}$	$\{1.10, 2.45, 4.05, -1.36\}^{\mathrm{T}}$	0.0436
$\mathbf{b}_9$	$\{30.77, 49.08, 13.23, -196.39\}^{\mathrm{T}}$	$\{6.60, -1.88, -0.10, -11.02\}^{\mathrm{T}}$	0.3974
$\mathbf{b}_{10}$	$\{-6.24, 50.15, -6.17, -38.24\}^{\mathrm{T}}$	$\{3.50, 3.00, 3.68, -2.73\}^{\mathrm{T}}$	0.0711
$\mathbf{b}_{11}$	$\{3.28, -10.07, -29.29, 51.68\}^{\mathrm{T}}$	$\{7.00, -1.24, 5.94, 0.74\}^{\mathrm{T}}$	0.2253
$\mathbf{b}_{12}$	$\{-16.44, 128.75, -52.07, 117.2\}^{\mathrm{T}}$	$\{-0.11, 13.77, -2.77, 9.38\}^{\mathrm{T}}$	0.1453
$\mathbf{b}_{13}$	$\{-6.46, -45.82, -29.17, 121.53\}^{\mathrm{T}}$	$\{3.68, -2.25, 4.09, 4.67\}^{\mathrm{T}}$	0.2141
$\mathbf{b}_{14}$	$\{-136.64, 78.82, 101.83, -38.25\}^{\mathrm{T}}$	$\{-7.20, 5.71, 7.98, -2.56\}^{\mathrm{T}}$	1.1312
$\mathbf{b}_{15}$	$\{100.55, -48.42, -104.21, 98.62\}^{\mathrm{T}}$	$\{7.98, -1.92, -4.64, 5.08\}^{\mathrm{T}}$	1.1680

Table 4.4: Velocity gain and displacement gain vectors associated with the energy index for assigning the required closed-loop poles in Case II

b	**g**	**f**	E
$\mathbf{b}_1$	$\{63.49, 13.76, -41.23, 27.45\}^{\mathrm{T}}$	$\{-6.14, 4.77, -11.58, 4.85\}^{\mathrm{T}}$	0.2144
$\mathbf{b}_2$	$\{17.57, -113.28, 25.23, -69.29\}^{\mathrm{T}}$	$\{4.45, -12.88, 4.85, -7.35\}^{\mathrm{T}}$	0.0325
$\mathbf{b}_3$	$\{-33.07, 25.03, 48.59, 0.32\}^{\mathrm{T}}$	$\{-12.08, 4.85, -9.01, 3.16\}^{\mathrm{T}}$	0.2026
$\mathbf{b}_4$	$\{25.8, -61.97, -4.29, -32.08\}^{\mathrm{T}}$	$\{4.85, -7.61, 3.30, -4.12\}^{\mathrm{T}}$	0.0200
$\mathbf{b}_5$	$\{-34.47, 48.70, 4.83, 22.38\}^{\mathrm{T}}$	$\{0.50, 4.11, 3.69, 1.16\}^{\mathrm{T}}$	0.0576
$\mathbf{b}_6$	$\{2.03, 6.66, 3.49, 17.75\}^{\mathrm{T}}$	$\{-18.84, 6.08, 6.88, -1.23\}^{\mathrm{T}}$	2.0131
$\mathbf{b}_7$	$\{-14.39, 65.64, -21.81, 40.35\}^{\mathrm{T}}$	$\{2.48, 5.45, 2.99, 2.37\}^{\mathrm{T}}$	0.0560
$\mathbf{b}_8$	$\{-20.15, 23.64, 2.32, 10.15\}^{\mathrm{T}}$	$\{1.53, 1.45, 3.40, 0.03\}^{\mathrm{T}}$	0.0354
$\mathbf{b}_9$	$\{69.00, -53.81, -43.98, -13.66\}^{\mathrm{T}}$	$\{6.75, -5.90, -1.90, -1.48\}^{\mathrm{T}}$	0.3082
$\mathbf{b}_{10}$	$\{4.30, 21.11, -20.33, 16.79\}^{\mathrm{T}}$	$\{3.68, 1.17, 2.92, 0.36\}^{\mathrm{T}}$	0.0539
$\mathbf{b}_{11}$	$\{2.80, 11.50, -17.39, 10.14\}^{\mathrm{T}}$	$\{6.31, -0.42, 6.42, -1.04\}^{\mathrm{T}}$	0.2108
$\mathbf{b}_{12}$	$\{-15.42, 147.99, -49.55, 93.53\}^{\mathrm{T}}$	$\{-0.51, 12.89, -1.71, 7.06\}^{\mathrm{T}}$	0.1487
$\mathbf{b}_{13}$	$\{-21.15, 16.43, 3.98, 5.39\}^{\mathrm{T}}$	$\{2.92, 0.38, 5.33, -0.86\}^{\mathrm{T}}$	0.1159
$\mathbf{b}_{14}$	$\{-144.20, 65.03, 104.20, -7.46\}^{\mathrm{T}}$	$\{-4.40, 3.81, 5.44, -0.40\}^{\mathrm{T}}$	1.2527
$\mathbf{b}_{15}$	$\{103.06, -12.06, -94.52, 29.32\}^{\mathrm{T}}$	$\{5.44, -0.02, -2.12, 1.55\}^{\mathrm{T}}$	1.1788

Table 4.5: Velocity gain and displacement gain vectors associated with the energy index for assigning the required closed-loop poles in Case III

b	**g**	**f**	E
$\mathbf{b}_1$	$\{0.11, 31.00, 4.78, 17.56\}^{\mathrm{T}}$	$\{-8.12, 4.94, -9.26, 3.90\}^{\mathrm{T}}$	0.1130
$\mathbf{b}_2$	$\{33.16, -121.09, 15.17, -68.66\}^{\mathrm{T}}$	$\{4.78, -11.64, 3.90, -6.37\}^{\mathrm{T}}$	0.0252
$\mathbf{b}_3$	$\{6.49, 15.61, 8.88, 8.81\}^{\mathrm{T}}$	$\{-9.23, 3.90, -10.83, 3.64\}^{\mathrm{T}}$	0.1591
$\mathbf{b}_4$	$\{15.72, -61.74, 6.56, -35.23\}^{\mathrm{T}}$	$\{3.90, -6.66, 3.68, -3.88\}^{\mathrm{T}}$	0.0174
$\mathbf{b}_5$	$\{-15.73, 45.38, -8.80, 25.51\}^{\mathrm{T}}$	$\{1.69, 3.31, 2.70, 1.21\}^{\mathrm{T}}$	0.0309
$\mathbf{b}_6$	$\{1.93, 10.55, 3.52, 5.97\}^{\mathrm{T}}$	$\{-4.28, 2.09, -4.97, 1.82\}^{\mathrm{T}}$	0.0662
$\mathbf{b}_7$	$\{-23.03, 69.53, -12.47, 38.89\}^{\mathrm{T}}$	$\{2.06, 4.84, 3.42, 1.85\}^{\mathrm{T}}$	0.0531
$\mathbf{b}_8$	$\{-8.60, 21.27, -5.30, 11.85\}^{\mathrm{T}}$	$\{2.11, 1.08, 2.82, 0.09\}^{\mathrm{T}}$	0.0262
$\mathbf{b}_9$	$\{10.85, -40.93, 4.76, -23.29\}^{\mathrm{T}}$	$\{2.07, -4.20, 1.83, -2.37\}^{\mathrm{T}}$	0.0093
$\mathbf{b}_{10}$	$\{-10.12, 25.29, -6.13, 13.99\}^{\mathrm{T}}$	$\{2.74, 1.16, 3.62, 0.00\}^{\mathrm{T}}$	0.0424
$\mathbf{b}_{11}$	$\{-7.61, 14.49, -4.55, 7.46\}^{\mathrm{T}}$	$\{5.49, -0.35, 6.79, -1.24\}^{\mathrm{T}}$	0.2064
$\mathbf{b}_{12}$	$\{-46.65, 158.63, -23.56, 88.69\}^{\mathrm{T}}$	$\{-1.71, 11.62, -0.11, 5.73\}^{\mathrm{T}}$	0.0646
$\mathbf{b}_{13}$	$\{-7.02, 13.24, -4.67, 7.16\}^{\mathrm{T}}$	$\{3.62, 0.06, 4.53, -0.69\}^{\mathrm{T}}$	0.0930
$\mathbf{b}_{14}$	$\{-10.21, 31.37, -5.55, 17.55\}^{\mathrm{T}}$	$\{0.61, 2.16, 1.14, 0.88\}^{\mathrm{T}}$	0.0105
$\mathbf{b}_{15}$	$\{-6.04, 16.24, -3.53, 9.06\}^{\mathrm{T}}$	$\{1.14, 0.96, 1.59, 0.22\}^{\mathrm{T}}$	0.0177

Table 4.6: Velocity gain and displacement gain vectors associated with the energy index for assigning the required closed-loop poles in Case IV

b	**g**	**f**	E
$\mathbf{b}_1$	$\{-3.81, 1.68, -6.38, 3.00\}^{\mathrm{T}}$	$\{-6.29, 1.68, -7.54, 2.01\}^{\mathrm{T}}$	0.1098
$\mathbf{b}_2$	$\{1.40, -0.55, 2.16, -0.92\}^{\mathrm{T}}$	$\{1.68, -0.45, 2.01, -0.54\}^{\mathrm{T}}$	0.0080
$\mathbf{b}_3$	$\{-4.50, 1.99, -7.57, 3.58\}^{\mathrm{T}}$	$\{-7.54, 2.01, -9.04, 2.42\}^{\mathrm{T}}$	0.1581
$\mathbf{b}_4$	$\{1.79, -0.69, 2.73, -1.14\}^{\mathrm{T}}$	$\{2.01, -0.54, 2.41, -0.64\}^{\mathrm{T}}$	0.0116
$\mathbf{b}_5$	$\{2.10, -0.80, 3.18, -1.32\}^{\mathrm{T}}$	$\{2.29, -0.61, 2.75, -0.73\}^{\mathrm{T}}$	0.0302
$\mathbf{b}_6$	$\{-2.06, 0.91, -3.46, 1.63\}^{\mathrm{T}}$	$\{-3.43, 0.92, -4.11, 1.10\}^{\mathrm{T}}$	0.0653
$\mathbf{b}_7$	$\{3.04, -1.12, 4.49, -1.81\}^{\mathrm{T}}$	$\{2.96, -0.79, 3.55, -0.95\}^{\mathrm{T}}$	0.0506
$\mathbf{b}_8$	$\{1.95, -0.75, 2.95, -1.24\}^{\mathrm{T}}$	$\{2.16, -0.58, 2.59, -0.69\}^{\mathrm{T}}$	0.0268
$\mathbf{b}_9$	$\{0.79, -0.31, 1.21, -0.51\}^{\mathrm{T}}$	$\{0.92, -0.24, 1.10, -0.29\}^{\mathrm{T}}$	0.0048
$\mathbf{b}_{10}$	$\{2.74, -1.02, 4.08, -1.66\}^{\mathrm{T}}$	$\{2.75, -0.73, 3.29, -0.88\}^{\mathrm{T}}$	0.0434
$\mathbf{b}_{11}$	$\{6.36, -2.21, 9.02, -3.41\}^{\mathrm{T}}$	$\{4.86, -1.29, 5.83, -1.55\}^{\mathrm{T}}$	0.2106
$\mathbf{b}_{12}$	$\{0.97, -0.37, 1.47, -0.61\}^{\mathrm{T}}$	$\{1.07, -0.29, 1.28, -0.34\}^{\mathrm{T}}$	0.0099
$\mathbf{b}_{13}$	$\{3.48, -1.27, 5.11, -2.05\}^{\mathrm{T}}$	$\{3.29, -0.88, 3.94, -1.05\}^{\mathrm{T}}$	0.0951
$\mathbf{b}_{14}$	$\{0.93, -0.36, 1.42, -0.59\}^{\mathrm{T}}$	$\{1.04, -0.28, 1.25, -0.33\}^{\mathrm{T}}$	0.0093
$\mathbf{b}_{15}$	$\{1.19, -0.45, 1.79, -0.74\}^{\mathrm{T}}$	$\{1.25, -0.33, 1.50, -0.40\}^{\mathrm{T}}$	0.0180

Table 4.7: Optimal actuator distribution vector for velocity and displacement feedback obtained by the genetic algorithm

Caes	**b**	**g**	**f**	E
I	$\mathbf{b}_8$	$\{-22.95, 38.52, 6.96, -19.56\}^{\mathrm{T}}$	$\{1.10, 2.45, 4.05, -1.36\}^{\mathrm{T}}$	0.0436
II	$\mathbf{b}_4$	$\{25.8, -61.97, -4.29, -32.08\}^{\mathrm{T}}$	$\{4.85, -7.61, 3.30, -4.12\}^{\mathrm{T}}$	0.0200
III	$\mathbf{b}_9$	$\{10.85, -40.93, 4.76, -23.29\}^{\mathrm{T}}$	$\{2.07, -4.20, 1.83, -2.37\}^{\mathrm{T}}$	0.0093
IV	$\mathbf{b}_9$	$\{0.79, -0.31, 1.21, -0.51\}^{\mathrm{T}}$	$\{0.92, -0.24, 1.10, -0.29\}^{\mathrm{T}}$	0.0048

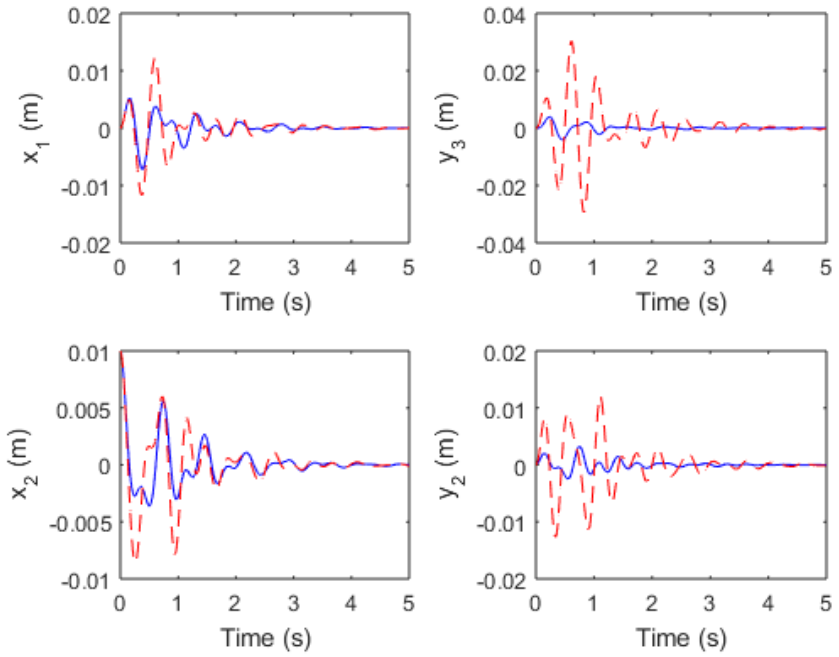

Figure 4.2: Displacement responses obtained by velocity and displacement feedback for Case I with $\mathbf{b}_8$ (blue solid line) and $\mathbf{b}_6$ (red dashed line)

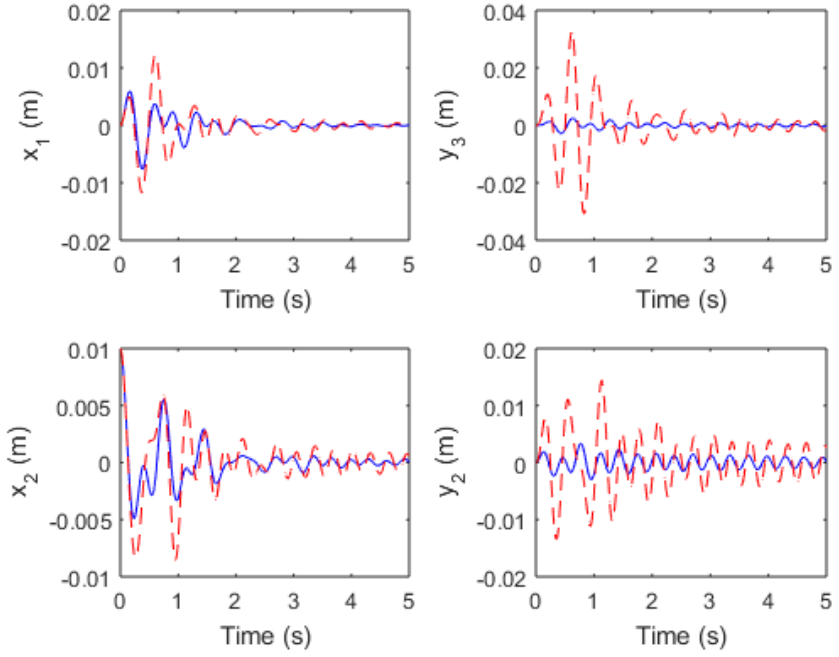

Figure 4.3: Displacement responses obtained by velocity and displacement feedback for Case II with $\mathbf{b}_4$ (blue solid line) and $\mathbf{b}_6$ (red dashed line)

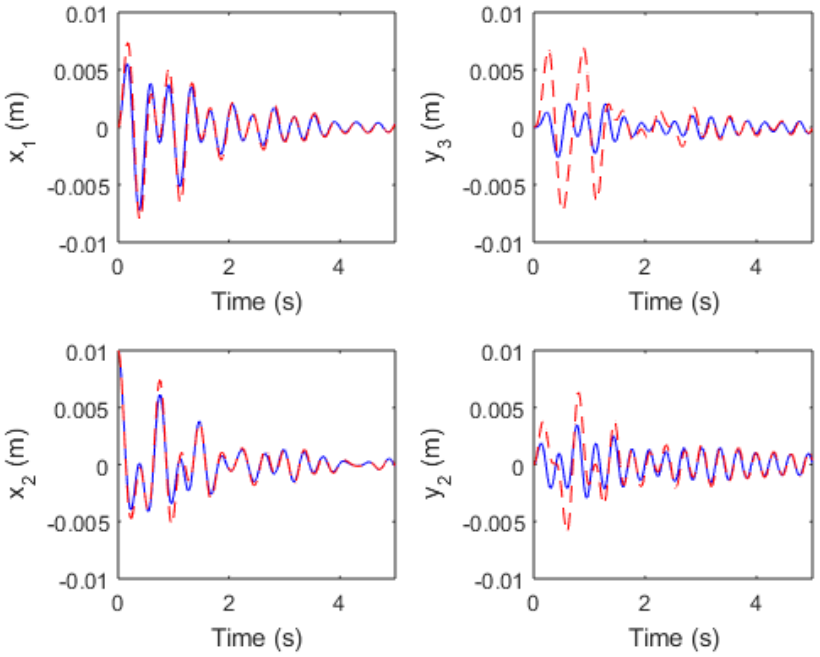

Figure 4.4: Displacement responses obtained by velocity and displacement feedback for Case III with $\mathbf{b}_9$ (blue solid line) and $\mathbf{b}_{11}$ (red dashed line)

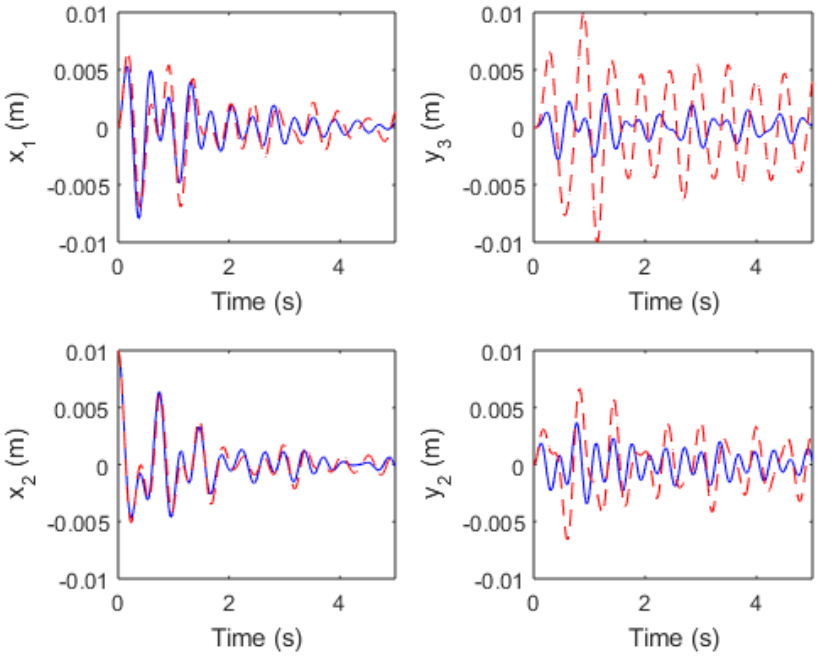

Figure 4.5: Displacement responses obtained by velocity and displacement feedback for Case IV with $\mathbf{b}_9$ (blue solid line) and $\mathbf{b}_{11}$ (red dashed line)

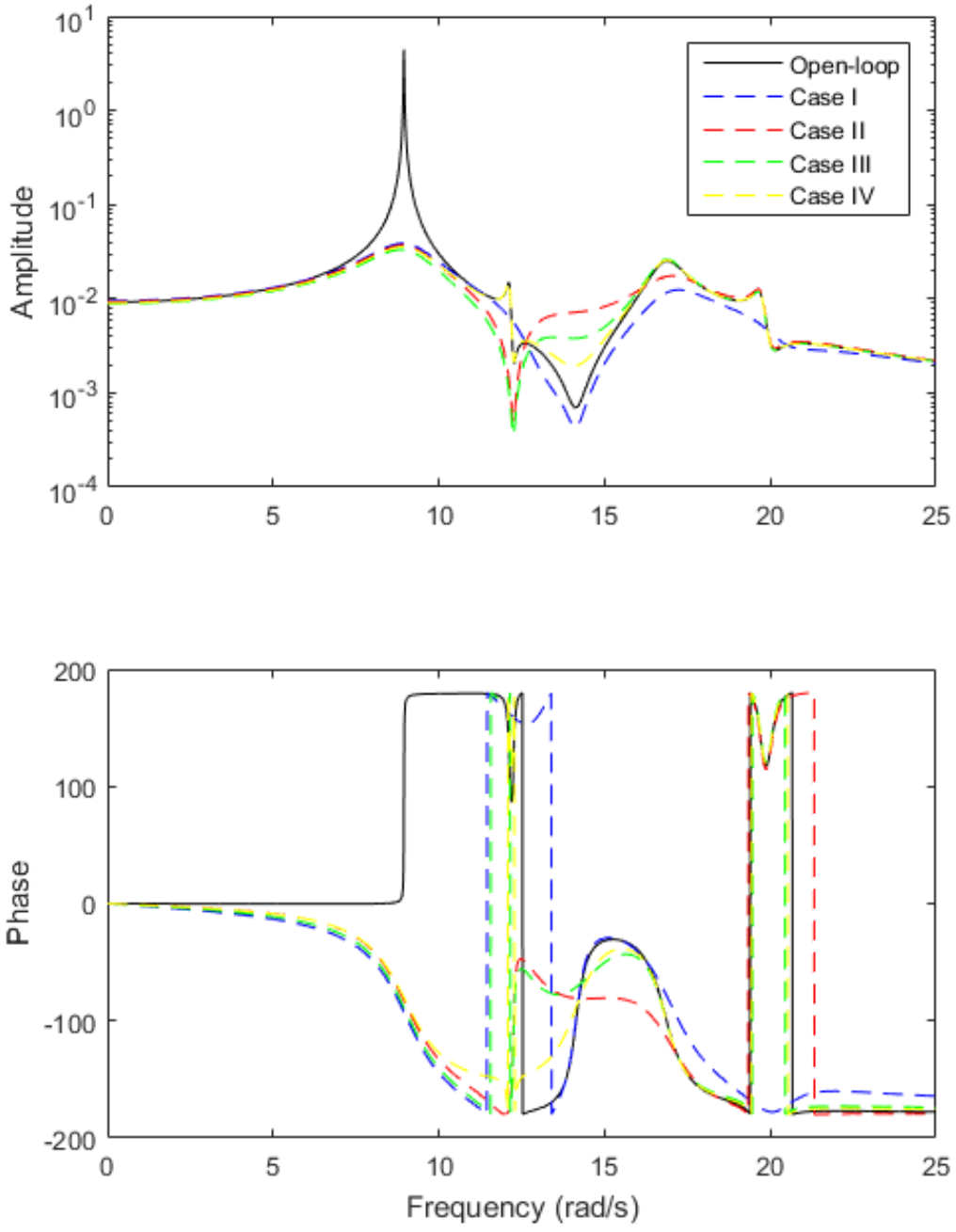

Figure 4.6: Amplitude and phase of open-loop (black solid line) and closed-loop receptances; h_{33} and $\widehat{h}_{33}$, obtained by velocity and displacement feedback for Case I with $\mathbf{b}_8$ (blue dashed line), Case II with $\mathbf{b}_4$ (red dashed line), Case III with $\mathbf{b}_9$ (green dashed line) and Case IV with $\mathbf{b}_9$ (yellow dashed line)

4.4.2 Acceleration and velocity feedback

Similar with the previous section, algorithms of pole assignment (Eq.(4.13)) and partial pole assignment (Eq.(4.20)) by using acceleration and velocity feedback are applied to assign the required closed-loop poles with various sets of the actuator distribution vectors. The energy index (Eq.(4.24)) is also determined with the same conditions as mentioned in Section 4.4.1. The acceleration and velocity gains are shown in Table 4.8 - Table 4.11 for Case I - Case IV respectively and validated by using Eq.(4.22). It is found that $|D|$ is close to zero for all cases. Therefore, the algorithms of pole assignment and partial pole assignment by using acceleration and velocity feedback are capable to assign poles and partial poles precisely.

The displacement responses with the minimum and maximum energy indexes are plotted as illustrated in Figure 4.7 - Figure 4.10 for Case I - Case IV respectively. It can be seen that the vibration responses with the minimum energy index slightly oscillate. In order to save the energy, the optimal actuator distribution vector for the smallest energy index must be chosen. For example, the optimal actuator distribution vectors: $\mathbf{b}_8$, $\mathbf{b}_4$, $\mathbf{b}_9$ and $\mathbf{b}_9$ are selected to assign the required closed-loop poles in Case I - Case IV respectively. These results are also obtained by using the genetic algorithm to solve Eq.(4.25) as shown in Table 4.12.

Table 4.8: Acceleration gain and velocity gain vectors associated with the energy index for assigning the required closed-loop poles in Case I

b	**a**	**f**	E
$\mathbf{b}_1$	$\{-0.29, -0.07, -0.02, -0.13\}^{\mathrm{T}}$	$\{-4.61, 3.76, -11.26, 5.57, \}^{\mathrm{T}}$	0.2074
$\mathbf{b}_2$	$\{-0.09, 0.53, -0.13, 0.57\}^{\mathrm{T}}$	$\{3.44, -10.60, 5.61, -10.23\}^{\mathrm{T}}$	0.0645
$\mathbf{b}_3$	$\{-0.06, -0.13, -0.33, 0.12\}^{\mathrm{T}}$	$\{-11.67, 5.64, -7.09, 0.87\}^{\mathrm{T}}$	0.2073
$\mathbf{b}_4$	$\{-0.13, 0.57, 0.14, -0.27\}^{\mathrm{T}}$	$\{5.50, -10.06, 1.37, 1.51\}^{\mathrm{T}}$	0.1182
$\mathbf{b}_5$	$\{0.16, -0.23, 0.08, -0.21\}^{\mathrm{T}}$	$\{0.34, 3.36, 3.05, 2.44\}^{\mathrm{T}}$	0.0560
$\mathbf{b}_6$	$\{-0.27, 0.07, 0.10, -0.20\}^{\mathrm{T}}$	$\{-17.15, 4.62, 6.05, 0.92\}^{\mathrm{T}}$	1.7564
$\mathbf{b}_7$	$\{0.14, -0.36, 0.16, -0.28\}^{\mathrm{T}}$	$\{2.37, 4.90, 2.24, 3.12\}^{\mathrm{T}}$	0.0583
$\mathbf{b}_8$	$\{0.12, -0.17, 0.04, -0.01\}^{\mathrm{T}}$	$\{0.99, 2.13, 3.47, -1.18\}^{\mathrm{T}}$	0.0435
$\mathbf{b}_9$	$\{-0.13, 0.04, 0.00, 0.50\}^{\mathrm{T}}$	$\{5.65, -1.63, -0.02, -9.30\}^{\mathrm{T}}$	0.3974
$\mathbf{b}_{10}$	$\{0.07, -0.21, 0.09, 0.02\}^{\mathrm{T}}$	$\{3.02, 2.60, 3.20, -2.36\}^{\mathrm{T}}$	0.0711
$\mathbf{b}_{11}$	$\{0.07, -0.04, 0.16, -0.16\}^{\mathrm{T}}$	$\{6.02, -1.08, 5.20, 0.56\}^{\mathrm{T}}$	0.2249
$\mathbf{b}_{12}$	$\{0.19, -0.84, 0.24, -0.56\}^{\mathrm{T}}$	$\{-0.12, 11.94, -2.38, 7.85\}^{\mathrm{T}}$	0.1454
$\mathbf{b}_{13}$	$\{0.09, 0.05, 0.13, -0.31\}^{\mathrm{T}}$	$\{3.17, -1.95, 3.56, 3.89\}^{\mathrm{T}}$	0.2140
$\mathbf{b}_{14}$	$\{0.46, -0.32, -0.27, 0.04\}^{\mathrm{T}}$	$\{-5.87, 4.95, 6.56, -2.20\}^{\mathrm{T}}$	1.1295
$\mathbf{b}_{15}$	$\{-0.27, 0.07, 0.33, -0.27\}^{\mathrm{T}}$	$\{6.62, -1.66, -3.72, 4.27\}^{\mathrm{T}}$	1.1694

Table 4.9: Acceleration gain and velocity gain vectors associated with the energy index for assigning the required closed-loop poles in Case II

b	**a**	**f**	E
$\mathbf{b}_1$	$\{-0.27, -0.12, 0.03, -0.11\}^{\mathrm{T}}$	$\{-5.63, 4.26, -10.19, 4.28\}^{\mathrm{T}}$	0.2144
$\mathbf{b}_2$	$\{-0.13, 0.70, -0.11, 0.39\}^{\mathrm{T}}$	$\{3.96, -11.49, 4.34, -6.37\}^{\mathrm{T}}$	0.0325
$\mathbf{b}_3$	$\{0.01, -0.11, -0.28, 0.01\}^{\mathrm{T}}$	$\{-10.64, 4.33, -8.18, 2.82\}^{\mathrm{T}}$	0.2029
$\mathbf{b}_4$	$\{-0.11, 0.37, 0.02, 0.19\}^{\mathrm{T}}$	$\{4.27, -6.79, 3.01, -3.59\}^{\mathrm{T}}$	0.0200
$\mathbf{b}_5$	$\{0.17, -0.29, 0.04, -0.15\}^{\mathrm{T}}$	$\{0.51, 3.66, 3.23, 0.96\}^{\mathrm{T}}$	0.0576
$\mathbf{b}_6$	$\{-0.04, -0.06, -0.07, -0.05\}^{\mathrm{T}}$	$\{-16.80, 5.43, 6.13, -1.12\}^{\mathrm{T}}$	2.0130
$\mathbf{b}_7$	$\{0.13, -0.41, 0.14, -0.24\}^{\mathrm{T}}$	$\{2.22, 4.87, 2.67, 1.99\}^{\mathrm{T}}$	0.0560
$\mathbf{b}_8$	$\{0.11, -0.14, 0.03, -0.07\}^{\mathrm{T}}$	$\{1.40, 1.30, 3.00, -0.01\}^{\mathrm{T}}$	0.0354
$\mathbf{b}_9$	$\{-0.24, 0.29, 0.13, 0.10\}^{\mathrm{T}}$	$\{5.84, -5.26, -1.51, -1.28\}^{\mathrm{T}}$	0.3083
$\mathbf{b}_{10}$	$\{0.04, -0.14, 0.11, -0.10\}^{\mathrm{T}}$	$\{3.25, 1.04, 2.65, 0.27\}^{\mathrm{T}}$	0.0539
$\mathbf{b}_{11}$	$\{0.04, -0.08, 0.11, -0.07\}^{\mathrm{T}}$	$\{5.60, -0.37, 5.77, -0.96\}^{\mathrm{T}}$	0.2106
$\mathbf{b}_{12}$	$\{0.19, -0.93, 0.24, -0.54\}^{\mathrm{T}}$	$\{-0.48, 11.50, -1.50, 6.04\}^{\mathrm{T}}$	0.1489
$\mathbf{b}_{13}$	$\{0.11, -0.10, 0.04, -0.05\}^{\mathrm{T}}$	$\{2.65, 0.34, 4.72, -0.79\}^{\mathrm{T}}$	0.1158
$\mathbf{b}_{14}$	$\{0.49, -0.30, -0.30, -0.02\}^{\mathrm{T}}$	$\{-3.53, 3.40, 4.46, -0.37\}^{\mathrm{T}}$	1.2516
$\mathbf{b}_{15}$	$\{-0.30, -0.01, 0.32, -0.12\}^{\mathrm{T}}$	$\{4.55, -0.02, -1.58, 1.32\}^{\mathrm{T}}$	1.1803

Table 4.10: Acceleration gain and velocity gain vectors associated with the energy index for assigning the required closed-loop poles in Case III

b	**a**	**f**	E
$\mathbf{b}_1$	$\{-0.04, -0.18, -0.09, -0.09\}^{\mathrm{T}}$	$\{-7.40, 4.52, -8.48, 3.52\}^{\mathrm{T}}$	0.1131
$\mathbf{b}_2$	$\{-0.19, 0.76, -0.09, 0.41\}^{\mathrm{T}}$	$\{4.32, -10.64, 3.62, -5.62\}^{\mathrm{T}}$	0.0252
$\mathbf{b}_3$	$\{-0.09, -0.09, -0.13, -0.03\}^{\mathrm{T}}$	$\{-8.42, 3.57, -9.91, 3.31\}^{\mathrm{T}}$	0.1592
$\mathbf{b}_4$	$\{-0.09, 0.39, -0.03, 0.21\}^{\mathrm{T}}$	$\{3.54, -6.09, 3.39, -3.44\}^{\mathrm{T}}$	0.0174
$\mathbf{b}_5$	$\{0.11, -0.29, 0.07, -0.16\}^{\mathrm{T}}$	$\{1.56, 3.02, 2.45, 1.02\}^{\mathrm{T}}$	0.0309
$\mathbf{b}_6$	$\{-0.04, -0.06, -0.05, -0.03\}^{\mathrm{T}}$	$\{-3.90, 1.91, -4.55, 1.65\}^{\mathrm{T}}$	0.0663
$\mathbf{b}_7$	$\{0.15, -0.44, 0.10, -0.24\}^{\mathrm{T}}$	$\{1.91, 4.43, 3.09, 1.57\}^{\mathrm{T}}$	0.0531
$\mathbf{b}_8$	$\{0.06, -0.14, 0.05, -0.08\}^{\mathrm{T}}$	$\{1.93, 0.99, 2.57, 0.04\}^{\mathrm{T}}$	0.0262
$\mathbf{b}_9$	$\{-0.06, 0.26, -0.02, 0.14\}^{\mathrm{T}}$	$\{1.87, -3.84, 1.69, -2.09\}^{\mathrm{T}}$	0.0093
$\mathbf{b}_{10}$	$\{0.07, -0.16, 0.06, -0.09\}^{\mathrm{T}}$	$\{2.51, 1.06, 3.30, -0.05\}^{\mathrm{T}}$	0.0423
$\mathbf{b}_{11}$	$\{0.06, -0.09, 0.05, -0.05\}^{\mathrm{T}}$	$\{5.03, -0.32, 6.20, -1.16\}^{\mathrm{T}}$	0.2063
$\mathbf{b}_{12}$	$\{0.29, -0.99, 0.16, -0.54\}^{\mathrm{T}}$	$\{-1.50, 10.62, -0.17, 4.96\}^{\mathrm{T}}$	0.0646
$\mathbf{b}_{13}$	$\{0.06, -0.09, 0.05, -0.05\}^{\mathrm{T}}$	$\{3.31, 0.05, 4.14, -0.65\}^{\mathrm{T}}$	0.0929
$\mathbf{b}_{14}$	$\{0.07, -0.20, 0.04, -0.11\}^{\mathrm{T}}$	$\{0.57, 1.97, 1.03, 0.75\}^{\mathrm{T}}$	0.0105
$\mathbf{b}_{15}$	$\{0.04, -0.10, 0.03, -0.06\}^{\mathrm{T}}$	$\{1.05, 0.87, 1.45, 0.17\}^{\mathrm{T}}$	0.0177

Table 4.11: Acceleration gain and velocity gain vectors associated with the energy index for assigning the required closed-loop poles in Case IV

b	**a**	**f**	E
$\mathbf{b}_1$	$\{0.05, -0.02, 0.07, -0.02\}^{\mathrm{T}}$	$\{-6.15, 1.64, -7.35, 1.95\}^{\mathrm{T}}$	0.1098
$\mathbf{b}_2$	$\{-0.02, 0.01, -0.02, 0.01\}^{\mathrm{T}}$	$\{1.64, -0.44, 1.96, -0.52\}^{\mathrm{T}}$	0.0080
$\mathbf{b}_3$	$\{0.06, -0.02, 0.08, -0.03\}^{\mathrm{T}}$	$\{-7.37, 1.97, -8.82, 2.34\}^{\mathrm{T}}$	0.1580
$\mathbf{b}_4$	$\{-0.02, 0.01, -0.03, 0.01\}^{\mathrm{T}}$	$\{1.97, -0.52, 2.35, -0.62\}^{\mathrm{T}}$	0.0116
$\mathbf{b}_5$	$\{-0.03, 0.01, -0.04, 0.01\}^{\mathrm{T}}$	$\{2.24, -0.60, 2.68, -0.71\}^{\mathrm{T}}$	0.0303
$\mathbf{b}_6$	$\{0.03, -0.01, 0.04, -0.01\}^{\mathrm{T}}$	$\{-3.35, 0.89, -4.01, 1.07\}^{\mathrm{T}}$	0.0653
$\mathbf{b}_7$	$\{-0.04, 0.01, -0.05, 0.02\}^{\mathrm{T}}$	$\{2.90, -0.77, 3.46, -0.92\}^{\mathrm{T}}$	0.0506
$\mathbf{b}_8$	$\{-0.03, 0.01, -0.03, 0.01\}^{\mathrm{T}}$	$\{2.11, -0.56, 2.52, -0.67\}^{\mathrm{T}}$	0.0268
$\mathbf{b}_9$	$\{-0.01, 0.00, -0.01, 0.00\}^{\mathrm{T}}$	$\{0.90, -0.24, 1.07, -0.28\}^{\mathrm{T}}$	0.0048
$\mathbf{b}_{10}$	$\{-0.04, 0.01, -0.05, 0.01\}^{\mathrm{T}}$	$\{2.68, -0.71, 3.21, -0.85\}^{\mathrm{T}}$	0.0434
$\mathbf{b}_{11}$	$\{-0.08, 0.03, -0.10, 0.03\}^{\mathrm{T}}$	$\{4.76, -1.26, 5.68, -1.50\}^{\mathrm{T}}$	0.2109
$\mathbf{b}_{12}$	$\{-0.01, 0.00, -0.02, 0.01\}^{\mathrm{T}}$	$\{1.05, -0.28, 1.25, -0.33\}^{\mathrm{T}}$	0.0099
$\mathbf{b}_{13}$	$\{-0.05, 0.02, -0.06, 0.02\}^{\mathrm{T}}$	$\{3.22, -0.86, 3.84, -1.02\}^{\mathrm{T}}$	0.0951
$\mathbf{b}_{14}$	$\{-0.01, 0.00, -0.02, 0.01\}^{\mathrm{T}}$	$\{1.02, -0.27, 1.22, -0.32\}^{\mathrm{T}}$	0.0093
$\mathbf{b}_{15}$	$\{-0.02, 0.01, -0.02, 0.01\}^{\mathrm{T}}$	$\{1.22, -0.33, 1.46, -0.39\}^{\mathrm{T}}$	0.0180

Table 4.12: Optimal actuator distribution vector for acceleration and velocity feedback

Caes	**b**	**a**	**f**	E
I	$\mathbf{b}_8$	$\{0.12, -0.17, 0.04, -0.01\}^{\mathrm{T}}$	$\{0.99, 2.13, 3.47, -1.18\}^{\mathrm{T}}$	0.0435
II	$\mathbf{b}_4$	$\{-0.11, 0.37, 0.02, 0.19\}^{\mathrm{T}}$	$\{4.27, -6.79, 3.01, -3.59\}^{\mathrm{T}}$	0.0200
III	$\mathbf{b}_9$	$\{-0.06, 0.26, -0.02, 0.14\}^{\mathrm{T}}$	$\{1.87, -3.84, 1.69, -2.09\}^{\mathrm{T}}$	0.0093
IV	$\mathbf{b}_9$	$\{-0.01, 0.00, -0.01, 0.00\}^{\mathrm{T}}$	$\{0.90, -0.24, 1.07, -0.28\}^{\mathrm{T}}$	0.0048

By using the results in Table 4.12, amplitudes and phases of the closed-loop receptances are compared with the open-loop receptance (see Figure 4.11). The closed-loop receptance becomes flatter corresponding to the assigned poles with high damp. It should be noted that the optimal actuator distribution vectors and energy indexes obtained by using acceleration and velocity feedback (Table 4.12) are the same with velocity and displacement feedback (Table 4.7). Therefore, the energy efficiencies of both control methods are the same. In term of robustness, the velocity and displacement feedback is more robust than the acceleration and velocity feedback. The displacement gains are very large in comparison with the the acceleration gains. This means that the displacement gains are more robust than the acceleration gains.

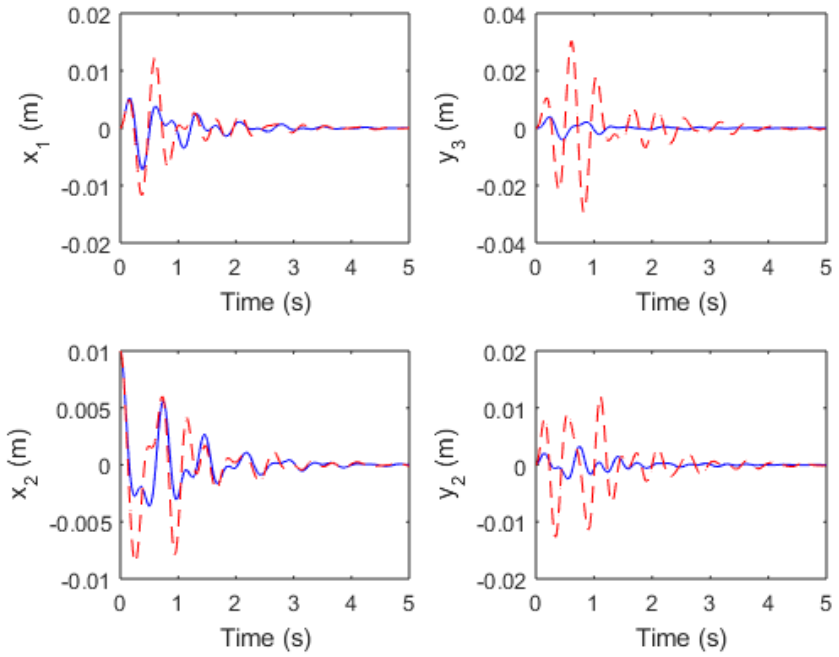

Figure 4.7: Displacement responses obtained by acceleration and velocity feedback for Case I with $\mathbf{b}_8$ (blue solid line) and $\mathbf{b}_6$ (red dashed line)

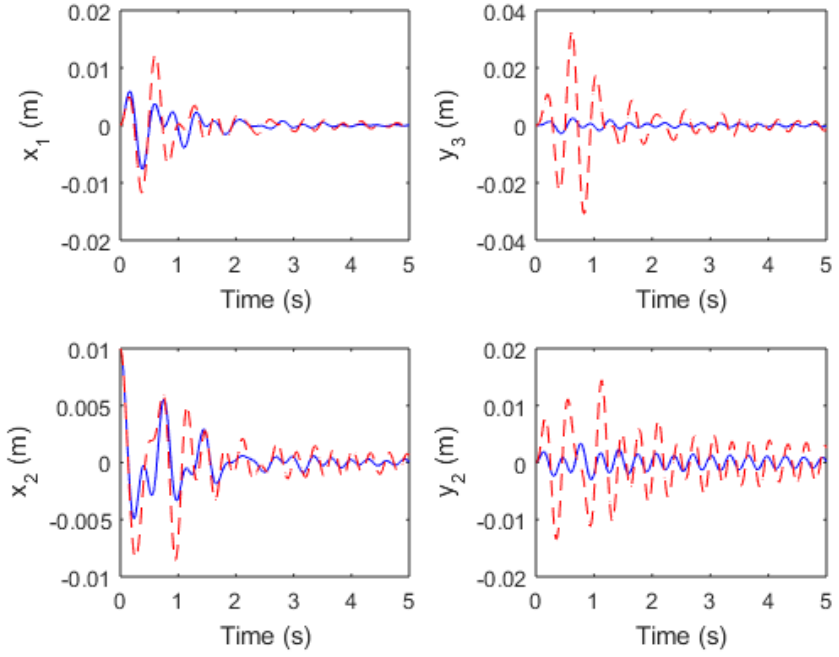

Figure 4.8: Displacement responses obtained by acceleration and velocity feedback for Case II with $\mathbf{b}_4$ (blue solid line) and $\mathbf{b}_6$ (red dashed line)

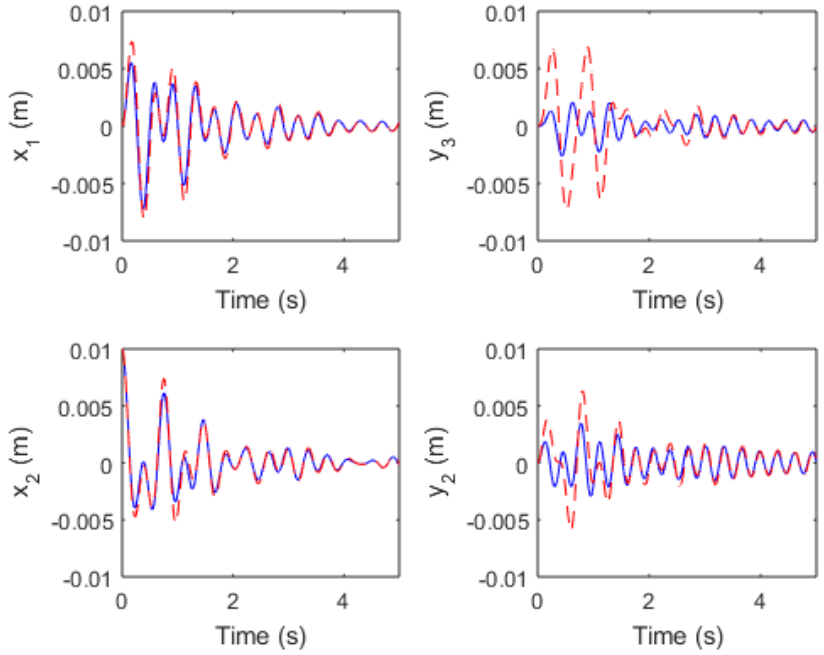

Figure 4.9: Displacement responses obtained by acceleration and velocity feedback for Case III with $\mathbf{b}_9$ (blue solid line) and $\mathbf{b}_{11}$ (red dashed line)

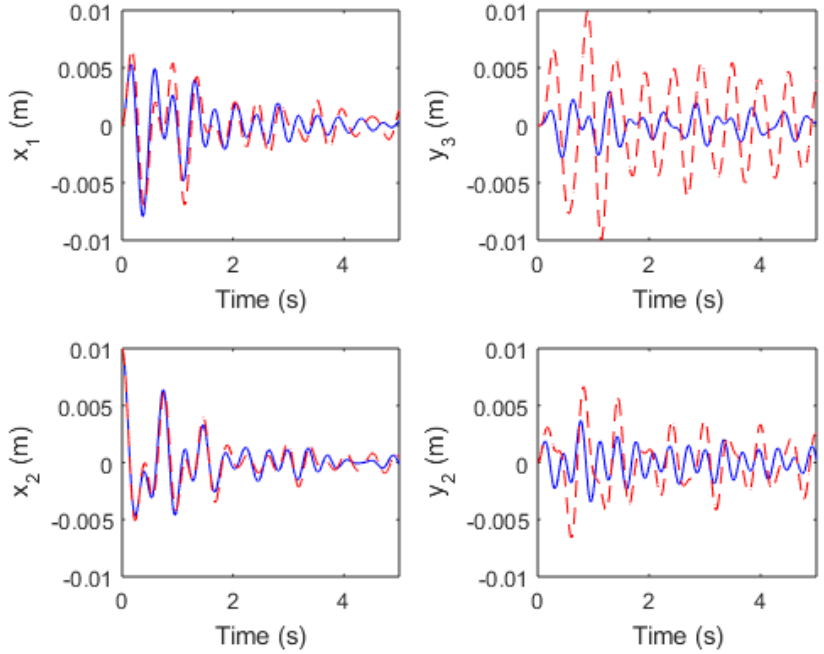

Figure 4.10: Displacement responses obtained by acceleration and velocity feedback for Case IV with $\mathbf{b}_9$ (blue solid line) and $\mathbf{b}_{11}$ (red dashed line)

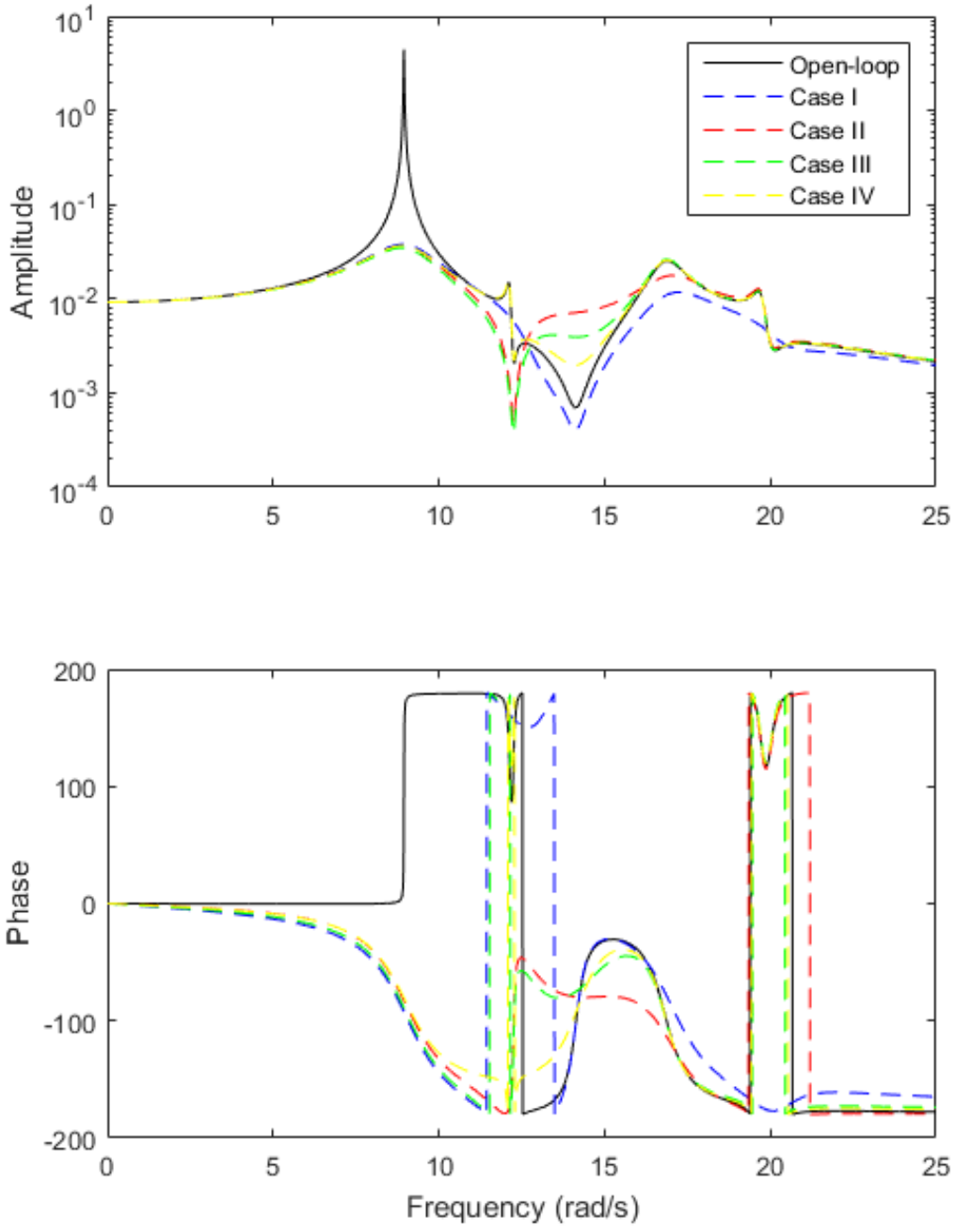

Figure 4.11: Amplitude and phase of open-loop (black solid line) and closed-loop receptances; h_{33} and $\widehat{h}_{33}$, obtained by acceleration and velocity feedback for Case I with $\mathbf{b}_8$ (blue dashed line), Case II with $\mathbf{b}_4$ (red dashed line), Case III with $\mathbf{b}_9$ (green dashed line) and Case IV with $\mathbf{b}_9$ (yellow dashed line)

4.4.3 Acceleration and displacement feedback

Unfortunately, algorithms of pole assignment (Eq.(4.14)) and partial pole assignment (Eq.(4.21)) by using acceleration and displacement feedback cannot be implemented to assign the required closed-loop poles because they are ill-conditioned for the under-damped system. Generally, acceleration and displacement gains are applied to modify mass and stiffness respectively (see Eq.(4.26)). This means that these algorithms can assign only natural frequencies. In addition, Ouyang (2010) also stated that it is impossible to assign the closed-loop poles into an under-damped system by using acceleration and displacement feedback.

$$\left(s^2(\mathbf{M}+\mathbf{b}\mathbf{a}^{\mathrm{T}})+s(\mathbf{C}_{\mathrm{s}}+\mathbf{C}_{\mathrm{as}})+\mathbf{K}_{\mathrm{s}}+\mathbf{K}_{\mathrm{as}}+\mathbf{b}\mathbf{g}^{\mathrm{T}}\right)\mathbf{x}(s)=\mathbf{p}(s). \tag{4.26}$$

4.5 Summary

According to Liang's work (Liang et al. (2016)), the algorithm of partial pole assignment for the asymmetric system by using the unobservability condition requires both poles and mode shapes for keeping unassigned poles unchanged. Nonetheless, the mode shapes for the asymmetric system are hard to evaluate. So, the algorithm of partial pole assignment for the asymmetric system by using the unobservability condition, which requires only the assigned poles, is proposed. Three control strategies such as velocity and displacement feedback, acceleration and velocity feedback, as well as acceleration and displacement feedback are considered. The receptance method is used to avoid modelling errors from FEM. Sherman-Morrison formula is applied to formulate the partial pole assignment problem in linear equations which can be solved directly. The energy index is also determined to estimate the amount of energy supplied to the actuators.

Numerical examples show that the algorithms of pole assignment and partial pole assignment by using acceleration and displacement feedback cannot be implemented to assigned the required closed-loop poles due to the ill-conditioned equations. However, they can be applied to assign the natural frequencies for the undamped system. For other control methods, velocity and displacement feedback and acceleration and velocity feedback, they can be implemented to assign the required closed-loop poles precisely with various sets of the actuator distribution vectors. The results also indicate that both control methods require the energy supplied to the actuators equally. Although velocity and displacement feedback requires the same energy with acceleration and velocity feedback, it is usually applied in practice. This is because the displacement gains are less sensitive than the acceleration gains. Therefore, the following chapters will consider only on velocity and displacement feedback.

Chapter 5

Partial Pole Assignment with Time Delays for Asymmetric Systems

This chapter reports a study of partial pole assignment with time delays for stabilising the asymmetric system, exemplified by friction-induced vibration and aerodynamic flutter. The control strategy is a single-input state feedback including constant single and multiple time delays in the feedback loop. The concept of the unobservability condition and the receptance method from Chapter 4 are also applied to keep the unassigned poles unchanged and prevent the numerical errors from FEM. The stability of the closed-loop system is analysed by evaluating the first few dominant poles and determining a critical time delay. The numerical examples show that the proposed method is capable of making partial pole assignment with time delays. Since many structures and systems with non-conservative forces can be represented by asymmetric systems, this work is widely applicable.

Algorithms of partial pole assignment based on the single-input and multiple-input controls were proposed by Datta et al. (1997); Datta and Sarkissian (1999); Ram and Elhay (2000) in order to assign some poles and keep others unchanged. Pratt et al. (2009) and Bai et al. (2012) combined the time delay in the feedback loop to partial pole assignment but the stability is not investigated. To analyse the stability, the root-finding methods, such as Taylor series expansion, Newton's eigenvalue iteration method (Singh and Ram (2002)), graphical root-finding algorithm (Vyhlidal and Zitek (2009)) and TRACE-DDE toolbox in MATLAB (Breda et al. (2009)), are considered to determine the first few dominant poles of the closed-loop system. However, theses methods donot guarantee the stability because the residual poles generated by the time delays are unidentified.

In order to ensure the stability, Olgac and Sipahi (2002) and Gu et al. (2003) respectively proposed Cluster Treatment of Characteristic Roots (CTCR) technique and the frequency-sweeping method to determine the critical time delay.

Ram and Mottershead (2007) proposed receptance method in active pole assignment to avoid modelling errors from FEM. The receptance measurement obtained from the experiment is used instead of mass, damping and stiffness matrices. It was extended to pole-zero assignment (Mottershead et al. (2008)), pole assignment with time delay (Ram et al. (2009, 2011)), robust pole assignment (Mottershead et al. (2009) and Tehrani et al. (2011)) and eigenstructure assignment (Liu et al. (2015)). It was also applied to partial pole assignment to shift some poles and keep others unchanged by using the uncontrollability condition (Tehrani et al. (2010)) and the unobservability condition (Ram and Mottershead (2013)). Furthermore, Ram and Mottershead (2013) extended single-input partial pole assignment to the multiple-input receptance-based method.

All mentions above studied pole assignment for the symmetric system. Nonetheless some systems are asymmetric because of non-conservative forces such as friction and aerodynamic forces. These forces induce vibration themselves and may destabilise the system. Ouyang (2010, 2011) applied the receptance method into pole assignment for stabilising the friction-induced vibration system modelled by a disc brake. Many researchers extended the previous works to pole assignment with time delay (Singh and Ouyang (2013)), partial pole assignment by using the uncontrollability condition (Tehrani and Ouyang (2012)) and the unobservability condition (Liang et al. (2016)). It is clear that partial pole assignment with time delay for the asymmetric system has not been done yet.

Therefore, partial pole assignment with time delay for the asymmetric system by using the single-input state-feedback control is proposed in this chapter. The receptance method is implemented which requires no knowledge of mass, damping and stiffness matrices. The unobservability condition is also applied to keep the poles unchanged. The solution is determined by using Sherman-Morrison formula and formulated in linear equations which can be solved directly. Both single and multiple time delays in the feedback loop are considered. The stability is analysed by using TRACE-DDE toolbox in MATLAB (Breda et al. (2009)) to compute the first few dominant poles of the closed-loop system and the frequency-sweeping test (Gu et al. (2003)) to determine the critical time delay. Three numerical examples, such as friction-induced vibration with single and multiple friction forces as well as aerodynamic flutter, show that the algorithm of partial pole assignment with the time delays as proposed in this chapter can assign the required closed-loop poles precisely. The dominant closed-loop poles and the critical time delay are determined to ensure that the closed-loop system is stable.

5.1 Pole assignment with time delay

The dynamic equation of the asymmetric system including velocity and displacement feedback with the time delays presented in Singh and Ouyang (2013) can be written as

$$\mathbf{M}\ddot{\mathbf{x}}(t) + \mathbf{C}\dot{\mathbf{x}}(t) + \mathbf{K}\mathbf{x}(t) = \mathbf{b}u(t-\tau) + \mathbf{p}(t), \tag{5.1}$$

$$\mathbf{C} = \mathbf{C}_{\mathrm{s}} + \mathbf{C}_{\mathrm{as}}, \tag{5.2}$$

$$\mathbf{K} = \mathbf{K}_{\mathrm{s}} + \mathbf{K}_{\mathrm{as}}, \tag{5.3}$$

$$u(t-\tau) = -\mathbf{f}^{\mathrm{T}}\dot{\mathbf{x}}(t-\tau_{\mathrm{f}}) - \mathbf{g}^{\mathrm{T}}\mathbf{x}(t-\tau_{\mathrm{g}}). \tag{5.4}$$

Laplace transform of Eq.(5.1) gives

$$\big(s^2\mathbf{M} + s(\mathbf{C}_{\mathrm{s}} + \mathbf{C}_{\mathrm{as}}) + \mathbf{K}_{\mathrm{s}} + \mathbf{K}_{\mathrm{as}}\big)\mathbf{x}(s) = -\mathbf{b}(s\mathrm{e}^{-s\tau_{\mathrm{f}}}\mathbf{f}^{\mathrm{T}} + \mathrm{e}^{-s\tau_{\mathrm{g}}}\mathbf{g}^{\mathrm{T}})\mathbf{x}(s) + \mathbf{p}(s), \tag{5.5}$$

$$\big(s^2\mathbf{M} + s(\mathbf{C}_{\mathrm{s}} + \mathbf{C}_{\mathrm{as}}) + \mathbf{K}_{\mathrm{s}} + \mathbf{K}_{\mathrm{as}} + \mathbf{b}(s\mathrm{e}^{-s\tau_{\mathrm{f}}}\mathbf{f}^{\mathrm{T}} + \mathrm{e}^{-s\tau_{\mathrm{g}}}\mathbf{g}^{\mathrm{T}})\big)\mathbf{x}(\mathbf{s}) = \mathbf{p}(s), \tag{5.6}$$

where τ_{f} and τ_{g} are time delays associated with the velocity and displacement feedback.

Rearranging Eq.(5.6), the closed-loop receptance is expressed by

$$\widehat{\mathbf{H}}_{\mathrm{as}}(s) = \big(\mathbf{H}_{\mathrm{as}}^{-1}(s) + \mathbf{b}(s\mathrm{e}^{-s\tau_{\mathrm{f}}}\mathbf{f}^{\mathrm{T}} + \mathrm{e}^{-s\tau_{\mathrm{g}}}\mathbf{g}^{\mathrm{T}})\big)^{-1}. \tag{5.7}$$

Applying Sherman-Morrison formula to Eq.(5.7), it yields

$$\widehat{\mathbf{H}}_{\mathrm{as}}(s) = \mathbf{H}_{\mathrm{as}}(s) - \frac{\mathbf{H}_{\mathrm{as}}(s)\mathbf{b}(s\mathrm{e}^{-s\tau_{\mathrm{f}}}\mathbf{f}^{\mathrm{T}} + \mathrm{e}^{-s\tau_{\mathrm{g}}}\mathbf{g}^{\mathrm{T}})\mathbf{H}_{\mathrm{as}}(s)}{1 + (s\mathrm{e}^{-s\tau_{\mathrm{f}}}\mathbf{f}^{\mathrm{T}} + \mathrm{e}^{-s\tau_{\mathrm{g}}}\mathbf{g}^{\mathrm{T}})\mathbf{H}_{\mathrm{as}}(s)\mathbf{b}}. \tag{5.8}$$

It can be seen that the poles of the closed-loop system satisfy the following characteristic equation:

$$(s\mathrm{e}^{-s\tau_{\mathrm{f}}}\mathbf{f}^{\mathrm{T}} + \mathrm{e}^{-s\tau_{\mathrm{g}}}\mathbf{g}^{\mathrm{T}})\mathbf{H}_{\mathrm{as}}(s)\mathbf{b} = -1. \tag{5.9}$$

Rearranging Eq.(5.9), the velocity and displacement gain vectors to assign the poles are determined by

$$\begin{bmatrix} \mathrm{e}^{-\mu_1\tau_{\mathrm{g}}}\mathbf{r}_1^{\mathrm{T}} & \mu_1\mathrm{e}^{-\mu_1\tau_{\mathrm{f}}}\mathbf{r}_1^{\mathrm{T}} \\ \mathrm{e}^{-\mu_2\tau_{\mathrm{g}}}\mathbf{r}_2^{\mathrm{T}} & \mu_2\mathrm{e}^{-\mu_2\tau_{\mathrm{f}}}\mathbf{r}_2^{\mathrm{T}} \\ \vdots & \vdots \\ \mathrm{e}^{-\mu_{2n}\tau_{\mathrm{g}}}\mathbf{r}_{2n}^{\mathrm{T}} & \mu_{2n}\mathrm{e}^{-\mu_{2n}\tau_{\mathrm{f}}}\mathbf{r}_{2n}^{\mathrm{T}} \end{bmatrix} \begin{pmatrix} \mathbf{g} \\ \mathbf{f} \end{pmatrix} = \begin{pmatrix} -1 \\ -1 \\ \vdots \\ -1 \end{pmatrix}, \tag{5.10}$$

$$\mathbf{r}_i = \mathbf{H}_{\mathrm{as}}(\mu_i)\mathbf{b}. \tag{5.11}$$

5.2 Partial pole assignment with time delay

According to Eq.(5.8), the unobservability condition is expressed by

$$(\lambda_i \mathrm{e}^{-\lambda_i \tau_\mathrm{f}} \mathbf{f}^\mathrm{T} + \mathrm{e}^{-\lambda_i \tau_\mathrm{g}} \mathbf{g}^\mathrm{T}) \mathbf{H}_\mathrm{as}(\lambda_i) = \mathbf{0}, \quad \text{for } i = p+1, p+2, ..., 2n \tag{5.12}$$

Post-multiplying Eq.(5.12) by $\mathbf{b}$, it implies that

$$(\lambda_i \mathrm{e}^{-\lambda_i \tau_\mathrm{f}} \mathbf{f}^\mathrm{T} + \mathrm{e}^{-\lambda_i \tau_\mathrm{g}} \mathbf{g}^\mathrm{T}) \mathbf{H}_\mathrm{as}(\lambda_i) \mathbf{b} = 0, \text{for } \ i = p+1, p+2, ..., 2n \tag{5.13}$$

Rearranging Eq.(5.13) yields,

$$\begin{bmatrix} \mathrm{e}^{-\lambda_{p+1}\tau_\mathrm{g}} \mathbf{r}_{p+1}^\mathrm{T} & \lambda_{p+1} \mathrm{e}^{-\lambda_{p+1}\tau_\mathrm{f}} \mathbf{r}_{p+1}^\mathrm{T} \\ \mathrm{e}^{-\lambda_{p+2}\tau_\mathrm{g}} \mathbf{r}_{p+2}^\mathrm{T} & \lambda_{p+2} \mathrm{e}^{-\lambda_{p+2}\tau_\mathrm{f}} \mathbf{r}_{p+2}^\mathrm{T} \\ \vdots & \vdots \\ \mathrm{e}^{-\lambda_{2n}\tau_\mathrm{g}} \mathbf{r}_{2n}^\mathrm{T} & \lambda_{2n} \mathrm{e}^{-\lambda_{2n}\tau_\mathrm{f}} \mathbf{r}_{2n}^\mathrm{T} \end{bmatrix} \begin{pmatrix} \mathbf{g} \\ \mathbf{f} \end{pmatrix} = \begin{pmatrix} 0 \\ 0 \\ \vdots \\ 0 \end{pmatrix}. \tag{5.14}$$

Combining Eq.(5.10) and Eq.(5.14), the velocity gain and displacement gain vectors for the partial pole assignment with the time delays by using the unobservability condition are derived by

$$\begin{bmatrix} \mathrm{e}^{-\mu_1\tau_\mathrm{g}} \mathbf{r}_1^\mathrm{T} & \mu_1 \mathrm{e}^{-\mu_1\tau_\mathrm{f}} \mathbf{r}_1^\mathrm{T} \\ \vdots & \vdots \\ \mathrm{e}^{-\mu_p\tau_\mathrm{g}} \mathbf{r}_p^\mathrm{T} & \mu_p \mathrm{e}^{-\mu_p\tau_\mathrm{f}} \mathbf{r}_p^\mathrm{T} \\ \mathrm{e}^{-\lambda_{p+1}\tau_\mathrm{g}} \mathbf{r}_{p+1}^\mathrm{T} & \lambda_{p+1} \mathrm{e}^{-\lambda_{p+1}\tau_\mathrm{f}} \mathbf{r}_{p+1}^\mathrm{T} \\ \vdots & \vdots \\ \mathrm{e}^{-\lambda_{2n}\tau_\mathrm{g}} \mathbf{r}_{2n}^\mathrm{T} & \lambda_{2n} \mathrm{e}^{-\lambda_{2n}\tau_\mathrm{f}} \mathbf{r}_{2n}^\mathrm{T} \end{bmatrix} \begin{pmatrix} \mathbf{g} \\ \mathbf{f} \end{pmatrix} = \begin{pmatrix} -1 \\ \vdots \\ -1 \\ 0 \\ \vdots \\ 0 \end{pmatrix}. \tag{5.15}$$

To validate the result, the required closed-loop poles, the control gains, the actuator distribution vector and the time delays are substituted back into Eq.(5.16). If $|D|$ is close to zero, the partial poles are successfully assigned by using the unobservability condition.

$$D = \det\big(s^2\mathbf{M} + s(\mathbf{C} + \mathrm{e}^{-s\tau_\mathrm{f}} \mathbf{b}\mathbf{f}^\mathrm{T}) + \mathbf{K} + \mathrm{e}^{-s\tau_\mathrm{g}} \mathbf{b}\mathbf{g}^\mathrm{T}\big). \tag{5.16}$$

It should be noted that time delay can vary with time or state. When it varies with time, an analytical mathematical expression of Laplace transform of $u(t-\tau)$, such as in Eq.(5.5), cannot be obtained. This means that pole assignment as a frequency-domain method cannot be used. When time delay varies with state, Eq.(5.1) becomes a nonlinear

dynamic problem. Again pole assignment cannot be used. Therefore, in this chapter, the time delay is assumed to be a constant.

5.3 Stability analysis

In this section, two methods of stability analysis are provided i.e. root-finding method and frequency-sweeping test. The root-finding method is to determine the closed-loop poles which can identify the stability of the system. If all closed-loop poles have negative real parts, the system will be stable. However, this method does not guarantee the stability because the time delays produce an infinite number of the closed-loop poles. To ensure the stability, the frequency-sweeping test is implemented to evaluate the critical time delay. If the time delay in the feedback loop is smaller than the critical one, the system will be stable.

5.3.1 Root-finding methods

The stability must be investigated after applying the feedback control. The time delays in the feedback loop may destabilise the system. Without the time delay ($\tau = 0$), the characteristic equation of the closed-loop system given by

$$\widehat{\mathbf{H}}_{\text{as}}^{-1}(s) = s^2\mathbf{M} + s(\mathbf{C} + \mathbf{b}\mathbf{f}^{\text{T}}) + \mathbf{K} + \mathbf{b}\mathbf{g}^{\text{T}}, \tag{5.17}$$

is generally formulated in a polynomial which has $2n$ poles for the n-dimensional system. The stability of the system is defined by pole locations. All negative real parts of the poles indicate a stable system and any positive real part of the pole indicates an unstable system. Nonetheless, the characteristic equation of the closed-loop system with the time delays given by

$$\widehat{\mathbf{H}}_{\text{as}}^{-1}(s) = s^2\mathbf{M} + s(\mathbf{C} + \mathrm{e}^{-s\tau_{\text{f}}}\mathbf{b}\mathbf{f}^{\text{T}}) + \mathbf{K} + \mathrm{e}^{-s\tau_{\text{g}}}\mathbf{b}\mathbf{g}^{\text{T}}, \tag{5.18}$$

has an infinite number of poles. Various methods were proposed, i.e., Taylor series expansion, Newton's eigenvalue iteration method (Singh and Ram (2002)) and graphical method (Vyhlidal and Zitek (2009)) to approximate the first few dominant poles (closest to the imaginary axis of the complex plane) of the closed-loop system. In this section, TRACE-DDE toolbox in MATLAB (Breda et al. (2009)) is applied to evaluate the dominant closed-loop poles.

5.3.2 Frequency-sweeping test

Although the root-finding methods can determine the first few dominant closed-loop poles, they cannot guarantee stability because the residual poles are unidentified. To ensure stability, the frequency-sweeping test (Gu et al. (2003)) is implemented. The closed-loop system with the time delays is classified by delay-independent stability, delay-dependent stability and instability. Delay-independent stability means the system is stable for any time delay: $\tau = [0, \infty]$. Delay-dependent stability indicates the system is stable within a limited range of time delay: $\tau = [0, \overline{\tau}]$ where $\overline{\tau}$ is the critical time delay. Instability means an unstable system for any time delay.

In this section, only commensurate delays are considered. The closed-loop system

$$\mathbf{M}\ddot{\mathbf{x}}(t) + \mathbf{C}\dot{\mathbf{x}}(t) + \mathbf{K}\mathbf{x}(t) = -\mathbf{b}\mathbf{f}^{\mathrm{T}}\dot{\mathbf{x}}(t - \tau_{\mathrm{f}}) - \mathbf{b}\mathbf{g}^{\mathrm{T}}\mathbf{x}(t - \tau_{\mathrm{g}}), \tag{5.19}$$

can be studied in cases of two specific time delays:

$$\dot{\mathbf{z}}(t) = \mathbf{A}_0\mathbf{z}(t) + \mathbf{A}_1\mathbf{z}(t - \tau), \text{for } \tau_{\mathrm{f}} = \tau_{\mathrm{g}} = \tau \geq 0, \tag{5.20}$$

where

$$\mathbf{z} = \begin{pmatrix} \mathbf{x} \\ \dot{\mathbf{x}} \end{pmatrix}, \quad \mathbf{A}_0 = \begin{bmatrix} \mathbf{0} & \mathbf{I} \\ -\mathbf{M}^{-1}\mathbf{K} & -\mathbf{M}^{-1}\mathbf{C} \end{bmatrix}, \mathbf{A}_1 = \begin{bmatrix} \mathbf{0} & \mathbf{0} \\ -\mathbf{M}^{-1}\mathbf{b}\mathbf{g}^{\mathrm{T}} & -\mathbf{M}^{-1}\mathbf{b}\mathbf{f}^{\mathrm{T}} \end{bmatrix},$$

or

$$\dot{\mathbf{z}}(t) = \mathbf{A}_0\mathbf{z}(t) + \mathbf{A}_1\mathbf{z}(t - \tau) + +\mathbf{A}_2\mathbf{z}(t - 2\tau), \text{for } \tau_{\mathrm{f}} = \tau \text{ and } \tau_{\mathrm{g}} = 2\tau \geq 0, \tag{5.21}$$

where

$$\mathbf{z} = \begin{pmatrix} \mathbf{x} \\ \dot{\mathbf{x}} \end{pmatrix}, \quad \mathbf{A}_0 = \begin{bmatrix} \mathbf{0} & \mathbf{I} \\ -\mathbf{M}^{-1}\mathbf{K} & -\mathbf{M}^{-1}\mathbf{C} \end{bmatrix},$$
$$\mathbf{A}_1 = \begin{bmatrix} \mathbf{0} & \mathbf{0} \\ \mathbf{0} & -\mathbf{M}^{-1}\mathbf{b}\mathbf{f}^{\mathrm{T}} \end{bmatrix}, \quad \mathbf{A}_2 = \begin{bmatrix} \mathbf{0} & \mathbf{0} \\ -\mathbf{M}^{-1}\mathbf{b}\mathbf{g}^{\mathrm{T}} & \mathbf{0} \end{bmatrix}.$$

For the single time delay, $\tau_{\mathrm{f}} = \tau_{\mathrm{g}} = \tau$, Gu et al. (2003) stated that the closed-loop system is delay-independent stable if and only if

$$\Re\big(\lambda(\mathbf{A}_0)\big) < 0 \ \ (\mathbf{A}_0 \text{ is stable}), \tag{5.22}$$

$$\Re\big(\lambda(\mathbf{A}_0 + \mathbf{A}_1)\big) < 0 \ \ (\mathbf{A}_0 + \mathbf{A}_1 \text{ is stable}), \tag{5.23}$$

$$\rho\big(\mathrm{i}\omega\mathbf{I}-\mathbf{A}_0)^{-1}\mathbf{A}_1\big)<1,\ \ \forall\omega>0, \tag{5.24}$$

where ρ is spectral radius: $\rho(\mathbf{A})=\max_{1\le k\le 2n}|\lambda(\mathbf{A})|$, $\lambda(\mathbf{A})$ denotes eigenvalues of matrix $\mathbf{A}$.

If one of them is not satisfied, the closed-loop system is not regarded as delay-independent stable (may be either delay-dependent stable or unstable). For the delay-dependent stable system, if the closed-loop system without the time delay is stable (Eq.(5.23) is satisfied), the critical time delay is determined by

$$\overline{\tau}:=\min_{1\le i\le q}\overline{\tau}_i,\ \ \text{for}\ \ q=\operatorname{rank}(\mathbf{A}_1), \tag{5.25}$$

$$\begin{gathered}\overline{\tau}_i=\min\nolimits_{1\le k\le 2n}\frac{\theta_k^i}{\omega_k^i}\ \ \text{if}\ \ \lambda\big((\mathrm{i}\omega_k^i\mathbf{I}-\mathbf{A}_0),\mathbf{A}_1\big)=\mathrm{e}^{-\mathrm{i}\theta_k^i},\\ \text{for some}\ \ \omega_k^i\in(0,\infty),\theta_k^i\in[0,2\pi].\end{gathered} \tag{5.26}$$

For the multiple commensurate time delays (for example, $\tau_{\mathrm{f}}=\tau$ and $\tau_{\mathrm{g}}=2\tau$), Gu et al. (2003) stated that the closed-loop system is delay-independent stable if and only if

$$\Re\big(\lambda(\mathbf{A}_0)\big)<0\ \ (\mathbf{A}_0\ \text{is stable}), \tag{5.27}$$

$$\Re\big(\lambda(\mathbf{A}_0+\mathbf{A}_1+\mathbf{A}_2)\big)<0\ \ (\mathbf{A}_0+\mathbf{A}_1+\mathbf{A}_2\ \text{is stable}), \tag{5.28}$$

$$\rho\left(\begin{bmatrix}(\mathrm{i}\omega\mathbf{I}-\mathbf{A}_0)^{-1}\mathbf{A}_1 & (\mathrm{i}\omega\mathbf{I}-\mathbf{A}_0)^{-1}\mathbf{A}_2\\ \mathbf{I} & \mathbf{0}\end{bmatrix}\right)<1,\ \ \forall\omega>0. \tag{5.29}$$

If one of them is not satisfied, the closed-loop system is not delay-independent stable (may be either delay-dependent stable or unstable). For the delay-dependent stable system, if the closed-loop system without time delay is stable (Eq.(5.28) is satisfied), the critical time delay is determined by

$$\overline{\tau}:=\min_{1\le i\le q+2n}\overline{\tau}_i,\ \ \text{for}\ \ q=\operatorname{rank}(\mathbf{A}_2), \tag{5.30}$$

$$\begin{gathered}\overline{\tau}_i=\min\nolimits_{1\le k\le 2n}\frac{\theta_k^i}{\omega_k^i}\ \ \text{if}\ \ \lambda\left(\begin{bmatrix}\mathbf{0} & \mathbf{I}\\ -(\mathrm{i}\omega_k^i\mathbf{I}-\mathbf{A}_0) & \mathbf{A}_1\end{bmatrix},\begin{bmatrix}\mathbf{I} & \mathbf{0}\\ \mathbf{0} & -\mathbf{A}_2\end{bmatrix}\right)=\mathrm{e}^{-\mathrm{i}\theta_k^i},\\ \text{for some}\ \ \omega_k^i\in(0,\infty),\theta_k^i\in[0,2\pi].\end{gathered} \tag{5.31}$$

Consequently, the closed-loop system with time delays is stable if $\tau<\overline{\tau}$ but it becomes unstable if $\tau>\overline{\tau}$.

5.4 Numerical examples

In this section, three numerical examples of unstable asymmetric systems exemplified by the friction-induced vibration with the single and the multiple friction forces as well as the aerodynamic flutter are demonstrated. Partial pole assignment by using the unobservability condition with time delays is applied to relocate unstable poles from positive to negative real parts and keep stable poles unchanged. Both single and multiple time delays are considered. Two stability analysis methods are implemented i.e. root-finding method and frequency-sweeping test, in order to determine the dominant poles and the critical time delay respectively.

5.4.1 Friction-induced vibration with the single friction force

The friction-induced vibration with the single friction force exemplified by the disc brake model (Figure 4.1) is the first example. The parameters are used as the same with Section 4.5 which make the system unstable. To stabilise the system, four cases of the required closed-loop poles are applied (see Table 4.2). Pole assignment and partial pole assignment with the single time delay ($\tau_{\mathrm{f}} = \tau_{\mathrm{g}} = 0.05$ and 0.10) and the multiple time delays ($\tau_{\mathrm{f}} = 0.05, \tau_{\mathrm{g}} = 2\tau_{\mathrm{f}}$) are applied. The actuator distribution vector; $\mathbf{b} = \{0, 0, 1, 1\}^{\mathrm{T}}$ is assumed. Velocity and displacement gain vectors for assigning the required closed-loop poles including the time delays are determined by solving the linear equations expressed in Eq.(5.10) for pole assignment and Eq.(5.15) for partial pole assignment (see Table 5.1).

The control gains are substituted back into Eq.(5.16). It is found that $|D|$ is close to zero for all cases. Hence, the algorithms of pole assignment with time delays and partial pole assignment with time delays by using the unobservability condition are successful. Then the first twenty poles of the closed-loop systems in Case I - Case IV are determined by using TRACE-DDE toolbox in MATLAB (Breda et al. (2009)) as shown in Table 5.2. It is found that the required closed-loop poles are assigned precisely and the other poles generated by the effect of the time delays are located in the left-hand side of the complex plane for all cases. This indicates that the closed-loop systems may be stable. Nonetheless, the residual poles are unknown which may induced the instability. To ensure the stability, the frequency-sweeping test (Gu et al. (2003)) is applied. All cases are able to determine the critical time delay because the closed-loop systems without the time delay ($\lambda(\mathbf{A}_0 + \sum_{i=1}^{m} \mathbf{A}_i)$) are stable as shown in Table 5.3.

The critical time delay is obtained by using Eq.(5.25) and Eq.(5.30) for the single time delay and the multiple time delays respectively (see Table 5.4). It is clear that all closed-loop systems are stable because the critical time delay is smaller than the given time delay. In order to validate the critical time delays, displacement responses are plotted by using 'dde23' function in MATLAB. The initial conditions used to test this are taken to be zero displacement and zero velocity for all degrees-of-freedom except $x_2 = 0.01$ m.

The results are shown in Figure 5.1 - Figure 5.12 for Case I - Case IV respectively. For example Case III with the single time delay; $\tau_f = \tau_g = 0.10$, the critical time delay at $\overline{\tau} = 0.1757$ is validated by applying time delays $\tau_1 = 0.17$ ($\tau_1 < \overline{\tau}$) and $\tau_2 = 0.19$ ($\tau_2 > \overline{\tau}$). For Case III with the multiple commensurate time delays; $\tau_f = 0.05$, $\tau_g = 2\tau_f$, the critical time delay at $\overline{\tau} = 0.1179$ is validated by applying time delays $\tau_1 = 0.11$ ($\tau_1 < \overline{\tau}$) and $\tau_2 = 0.13$ ($\tau_2 > \overline{\tau}$). It is clear from Figure 5.8 and Figure 5.9 that the closed-loop systems are stable for τ_1 but they are unstable for τ_2.

Table 5.1: Control gains obtained by pole assignment and partial pole assignment with time delays by using the unobservability condition for the friction-induced vibration with the single friction force

Case	$\tau_f = \tau_g = 0.05$		$\tau_f = \tau_g = 0.10$		$\tau_f = 0.05, \tau_g = 2\tau_f$	
	g	**f**	**g**	**f**	**g**	**f**
I	−4.4771	−0.4745	9.0718	−0.3203	−0.4587	−0.5696
	−0.7689	3.3819	−22.020	2.1647	−0.6700	3.1361
	−17.941	1.7549	−20.227	0.1729	−20.400	0.5710
	−7.2313	3.1506	−43.849	1.1706	−19.861	2.2017
II	−9.0876	−0.6354	10.622	−0.5601	−7.9474	−1.0520
	0.3810	4.3864	−36.515	2.7771	−2.0394	4.2586
	−17.162	2.4363	−29.064	0.6065	−20.6566	1.3946
	6.4611	1.5852	−8.4730	1.3063	8.6388	1.9659
III	−13.601	0.6507	−8.6963	−0.1203	−15.407	−0.1034
	6.6597	4.0032	−27.274	2.9910	6.8405	4.3144
	−13.647	1.5917	−14.770	0.4837	−15.017	0.8414
	7.0605	1.7688	−10.270	1.4629	8.7870	2.1738
IV	−6.7473	1.9638	−13.459	1.2897	−7.6436	1.5776
	1.5996	−0.5320	3.4655	−0.3581	1.8673	−0.4379
	−7.5209	2.3608	−15.757	1.5581	−8.2725	1.9359
	1.6060	−0.6380	3.9468	−0.4292	1.5930	−0.5507

Table 5.2: First twenty poles of the closed-loop system with time delays obtained by TRACE-DDE toolbox in MATLAB (sorted by the real part) for the friction-induced vibration with the single friction force

Case	$\tau_f = \tau_g = 0.05$	$\tau_f = \tau_g = 0.10$	$\tau_f = 0.05, \tau_g = 2\tau_f$
I	$-1.0000 \pm 9.0000i$	$-1.0000 \pm 9.0000i$	$-1.0000 \pm 9.0000i$
	$-1.0000 \pm 12.500i$	$-1.0000 \pm 12.500i$	$-1.0000 \pm 12.500i$
	$-1.0000 \pm 17.000i$	$-1.0000 \pm 17.000i$	$-1.0000 \pm 17.000i$
	$-1.0000 \pm 20.000i$	$-1.0000 \pm 20.000i$	$-1.0000 \pm 20.000i$
	-42.978	-16.988	-28.140
	$-69.839 \pm 148.80i$	$-38.536 \pm 77.589i$	$-42.849 \pm 385.59i$
	$-81.372 \pm 277.39i$	$-45.631 \pm 140.96i$	$-43.183 \pm 385.28i$
	$-88.626 \pm 404.35i$	$-49.732 \pm 203.89i$	$-56.805 \pm 311.85i$
	$-93.937 \pm 530.77i$	$-52.010 \pm 1144.5i$	$-59.249 \pm 311.29i$
	$-98.131 \pm 656.94i$	$-52.607 \pm 266.75i$	$-59.582 \pm 81.434i$
II	$-0.1757 \pm 19.734i$	$-0.1757 \pm 9.734i$	$-0.1757 \pm 9.734i$
	$-1.0000 \pm 9.0000i$	$-1.0000 \pm 9.0000i$	$-1.0000 \pm 9.0000i$
	$-1.0000 \pm 12.500i$	$-1.0000 \pm 12.500i$	$-1.0000 \pm 12.500i$
	$-1.0000 \pm 17.000i$	$-1.0000 \pm 17.000i$	$-1.0000 \pm 17.000i$
	-50.428	-19.090	-40.775
	$-74.115 \pm 148.06i$	$-36.531 \pm 75.834i$	$-42.746 \pm 385.57i$
	$-85.458 \pm 276.95i$	$-42.819 \pm 139.63i$	$-43.183 \pm 385.28i$
	$-92.659 \pm 404.04i$	$-46.609 \pm 202.86i$	$-56.805 \pm 311.85i$
	$-97.949 \pm 530.53i$	$-49.336 \pm 265.92i$	$-58.565 \pm 310.08i$
	$-102.07 \pm 2288.7i$	$-51.168 \pm 1144.4i$	$-67.627 \pm 148.52i$
III	$-0.1757 \pm 19.734i$	$-0.1757 \pm 19.734i$	$-0.1757 \pm 19.734i$
	$-0.5259 \pm 16.823i$	$-0.5259 \pm 16.823i$	$-0.5259 \pm 16.823i$
	$-1.0000 \pm 9.0000i$	$-1.0000 \pm 9.0000i$	$-1.0000 \pm 9.0000i$
	$-1.0000 \pm 12.500i$	$-1.0000 \pm 12.500i$	$-1.0000 \pm 12.500i$
	-56.221	-21.366	$-42.786 \pm 385.53i$
	$-77.922 \pm 147.54i$	$-36.736 \pm 75.190i$	$-43.183 \pm 385.28i$
	$-89.129 \pm 276.65i$	$-42.800 \pm 139.21i$	-48.152
	$-96.293 \pm 403.83i$	$-46.518 \pm 202.55i$	$-56.805 \pm 311.85i$
	$-101.57 \pm 530.37i$	$-49.214 \pm 265.68i$	$-58.203 \pm 310.16i$
	$-103.01 \pm 2288.7i$	$-51.121 \pm 1144.4i$	$-72.316 \pm 147.97i$
IV	$-0.0553 \pm 12.134i$	$-0.0553 \pm 12.134i$	$-0.0553 \pm 12.134i$
	$-0.1757 \pm 19.734i$	$-0.1757 \pm 19.734i$	$-0.1757 \pm 19.734i$
	$-0.5259 \pm 16.823i$	$-0.5259 \pm 16.823i$	$-0.5259 \pm 16.823i$
	$-1.0000 \pm 9.0000i$	$-1.0000 \pm 9.0000i$	$-1.0000 \pm 9.0000i$
	-74.830	-31.057	$-43.003 \pm 385.40i$
	$-91.912 \pm 146.13i$	$-42.591 \pm 74.225i$	$-43.183 \pm 385.28i$
	$-102.72 \pm 275.81i$	$-48.400 \pm 138.64i$	$-56.805 \pm 311.85i$
	$-105.62 \pm 2288.8i$	$-52.047 \pm 202.15i$	-56.864
	$-108.91 \pm 2289.2i$	$-52.361 \pm 1144.4i$	$-57.538 \pm 311.18i$
	$-109.78 \pm 403.24i$	$-54.454 \pm 1144.6i$	$-78.016 \pm 147.30i$

Table 5.3: The closed-loop system without time delays for the friction-induced vibration with the single friction force

Case	$\tau_{\mathrm{f}} = \tau_{\mathrm{g}} = 0.05$	$\tau_{\mathrm{f}} = \tau_{\mathrm{g}} = 0.10$	$\tau_{\mathrm{f}} = 0.05, \tau_{\mathrm{g}} = 2\tau_{\mathrm{f}}$
I	$-0.9499 \pm 8.4243\mathrm{i}$	$-0.3790 \pm 7.8171\mathrm{i}$	$-0.5355 \pm 8.1906\mathrm{i}$
	$-0.8305 \pm 11.8630\mathrm{i}$	$-0.4164 \pm 11.5049\mathrm{i}$	$-0.6936 \pm 11.8597\mathrm{i}$
	$-0.8368 \pm 16.5697\mathrm{i}$	$-0.4742 \pm 16.4611\mathrm{i}$	$-0.6030 \pm 16.5208\mathrm{i}$
	$-0.5856 \pm 19.3872\mathrm{i}$	$-0.1521 \pm 19.2274\mathrm{i}$	$-0.3042 \pm 19.3429\mathrm{i}$
II	$-0.9409 \pm 8.4732\mathrm{i}$	$-0.4798 \pm 7.9232\mathrm{i}$	$-0.6168 \pm 8.3551\mathrm{i}$
	$-0.8204 \pm 11.9187\mathrm{i}$	$-0.4726 \pm 11.5825\mathrm{i}$	$-0.7978 \pm 11.9868\mathrm{i}$
	$-0.8237 \pm 16.6512\mathrm{i}$	$-0.5782 \pm 16.5301\mathrm{i}$	$-0.7710 \pm 16.6607\mathrm{i}$
	$-0.1757 \pm 19.7336\mathrm{i}$	$-0.1757 \pm 19.7336\mathrm{i}$	$-0.2446 \pm 19.7511\mathrm{i}$
III	$-0.9283 \pm 8.4992\mathrm{i}$	$-0.5268 \pm 8.0043\mathrm{i}$	$-0.6426 \pm 8.4220\mathrm{i}$
	$-0.8003 \pm 11.9555\mathrm{i}$	$-0.4948 \pm 11.6508\mathrm{i}$	$-0.8398 \pm 12.0284\mathrm{i}$
	$-0.5259 \pm 16.8229\mathrm{i}$	$-0.5259 \pm 16.8229\mathrm{i}$	$-0.5528 \pm 16.8265\mathrm{i}$
	$-0.1757 \pm 19.7336\mathrm{i}$	$-0.1757 \pm 19.7336\mathrm{i}$	$-0.2224 \pm 19.7426\mathrm{i}$
IV	$-0.8544 \pm 8.5724\mathrm{i}$	$-0.5575 \pm 8.2449\mathrm{i}$	$-0.6909 \pm 8.5478\mathrm{i}$
	$-0.0553 \pm 12.1336\mathrm{i}$	$-0.0553 \pm 12.1336\mathrm{i}$	$-0.0518 \pm 12.1323\mathrm{i}$
	$-0.5259 \pm 16.8229\mathrm{i}$	$-0.5259 \pm 16.8229\mathrm{i}$	$-0.5309 \pm 16.8257\mathrm{i}$
	$-0.1757 \pm 19.7336\mathrm{i}$	$-0.1757 \pm 19.7336\mathrm{i}$	$-0.1690 \pm 19.7297\mathrm{i}$

Table 5.4: Critical time delay for the friction-induced vibration with the single friction force

Case	$\tau_{\mathrm{f}} = \tau_{\mathrm{g}} = 0.05$	$\tau_{\mathrm{f}} = \tau_{\mathrm{g}} = 0.10$	$\tau_{\mathrm{f}} = 0.05, \tau_{\mathrm{g}} = 2\tau_{\mathrm{f}}$
I	0.0983	0.1590	0.0828
II	0.1301	0.1844	0.1204
III	0.1230	0.1757	0.1179
IV	0.1908	0.2422	0.1567

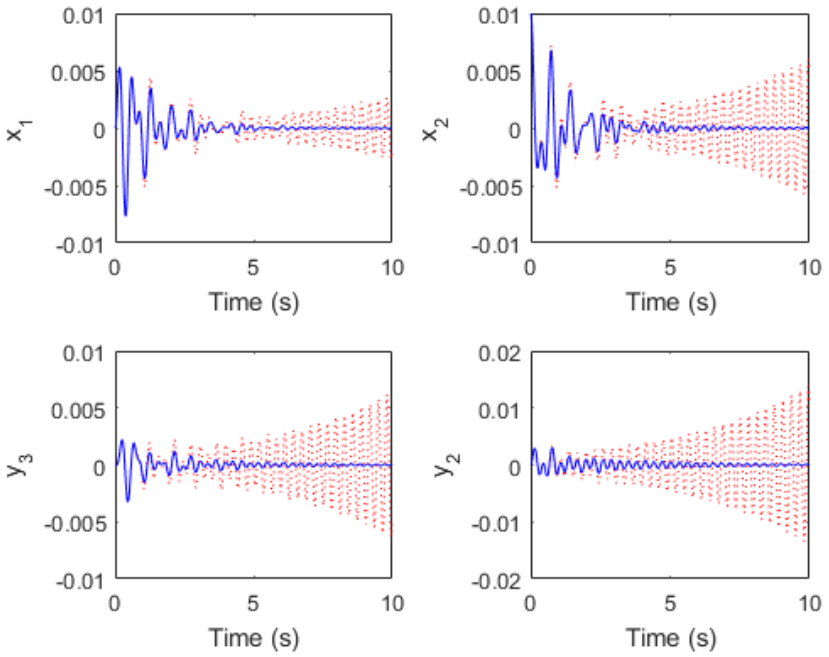

Figure 5.1: Displacement responses of the closed-loop system for Case I with $\tau_f = \tau_g = 0.05$: $\tau_1 = 0.09$ (blue solid line) and $\tau_2 = 0.11$ (red dotted line)

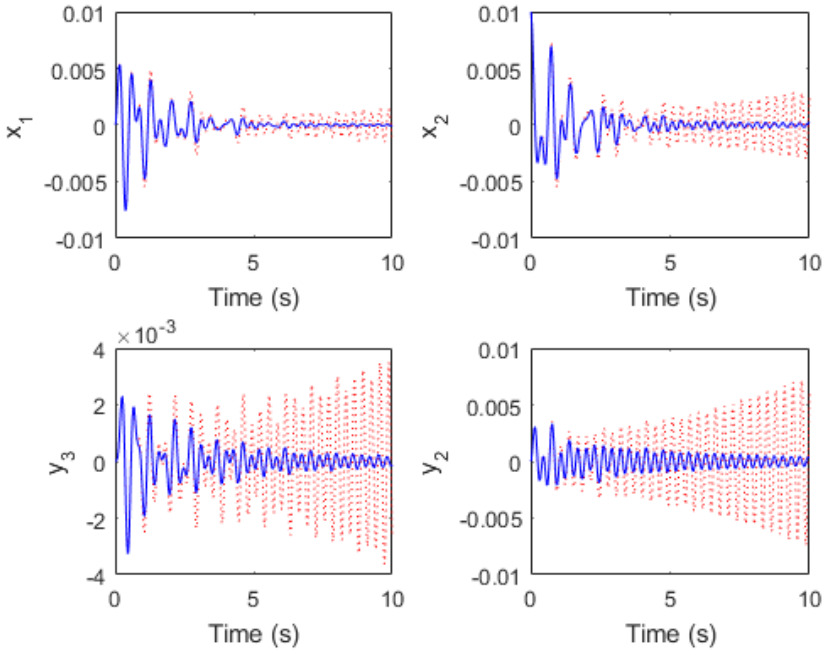

Figure 5.2: Displacement responses of the closed-loop system for Case I with $\tau_f = \tau_g = 0.10$: $\tau_1 = 0.15$ (blue solid line) and $\tau_2 = 0.17$ (red dotted line)

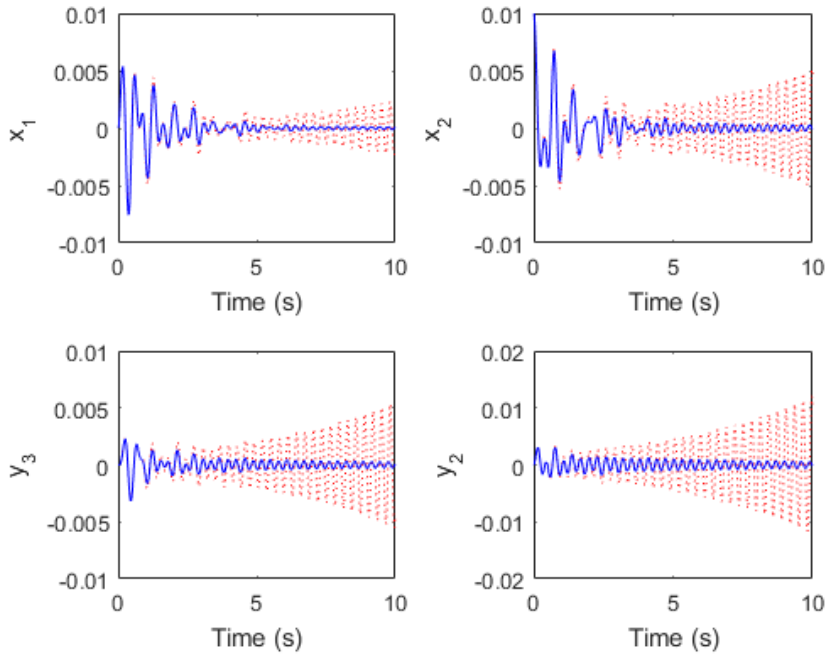

Figure 5.3: Displacement responses of the closed-loop system for Case I with $\tau_{\mathrm{f}} = 0.05, \tau_{\mathrm{g}} = 2\tau_{\mathrm{f}}$: $\tau_1 = 0.08$ (blue solid line) and $\tau_2 = 0.09$ (red dotted line)

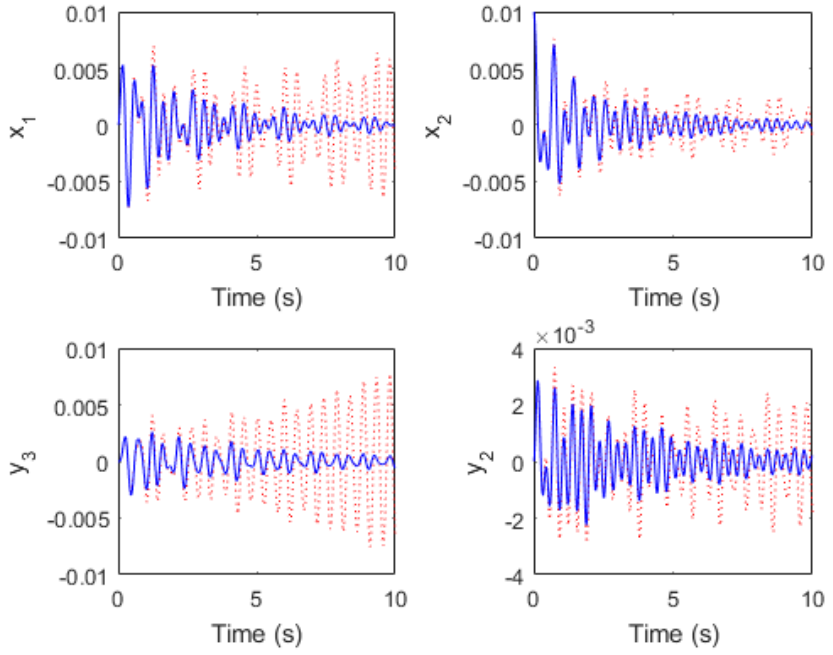

Figure 5.4: Displacement responses of the closed-loop system for Case II with $\tau_{\mathrm{f}} = \tau_{\mathrm{g}} = 0.05$: $\tau_1 = 0.12$ (blue solid line) and $\tau_2 = 0.14$ (red dotted line)

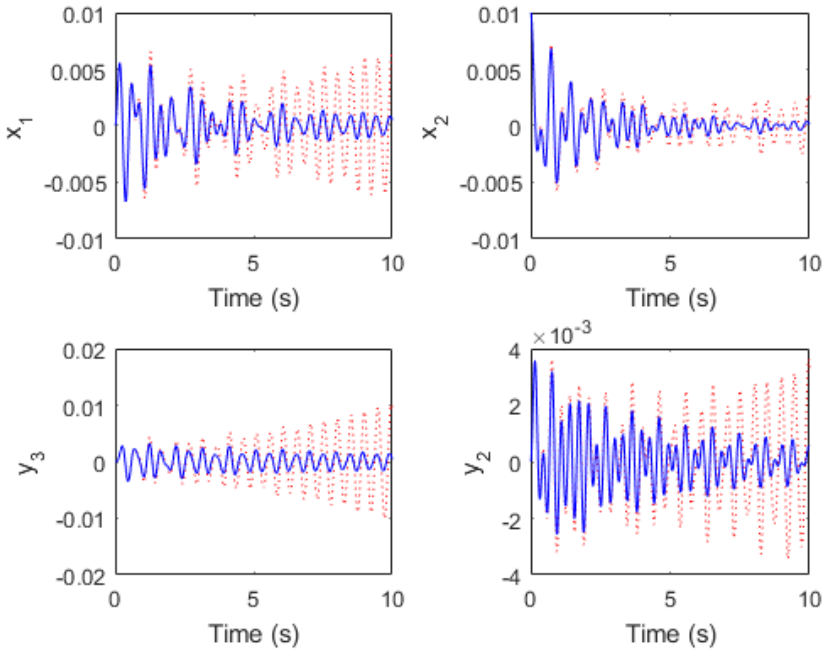

Figure 5.5: Displacement responses of the closed-loop system for Case II with $\tau_f = \tau_g = 0.10$: $\tau_1 = 0.18$ (blue solid line) and $\tau_2 = 0.20$ (red dotted line)

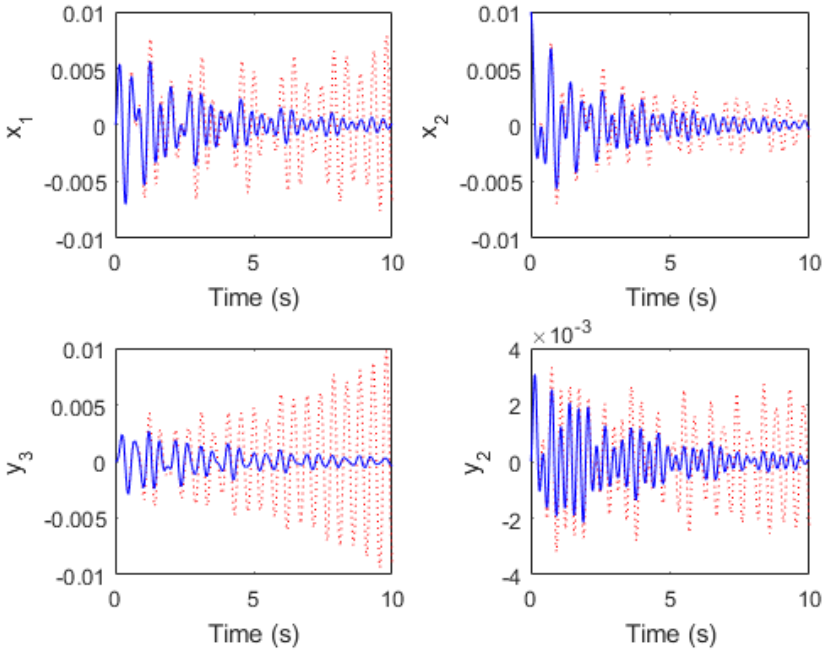

Figure 5.6: Displacement responses of the closed-loop system for Case II with $\tau_f = 0.05, \tau_g = 2\tau_f$: $\tau_1 = 0.11$ (blue solid line) and $\tau_2 = 0.13$ (red dotted line)

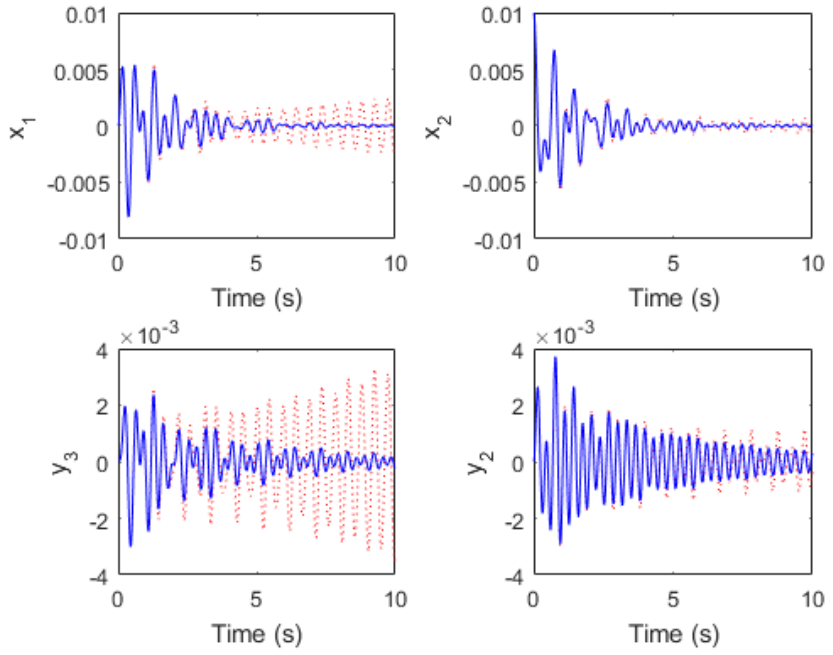

Figure 5.7: Displacement responses of the closed-loop system for Case III with $\tau_f = \tau_g = 0.05$: $\tau_1 = 0.11$ (blue solid line) and $\tau_2 = 0.13$ (red dotted line)

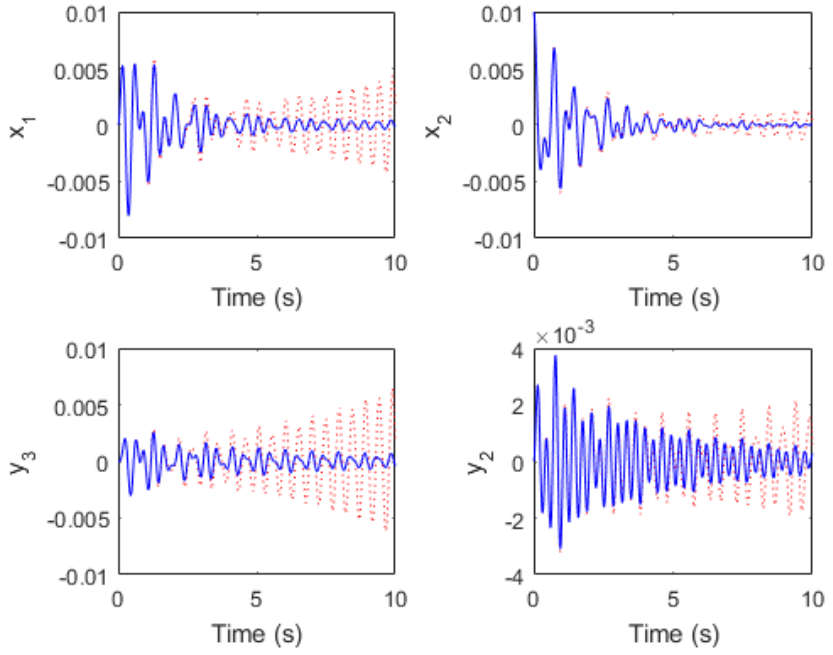

Figure 5.8: Displacement responses of the closed-loop system for Case III with $\tau_f = \tau_g = 0.10$: $\tau_1 = 0.17$ (blue solid line) and $\tau_2 = 0.19$ (red dotted line)

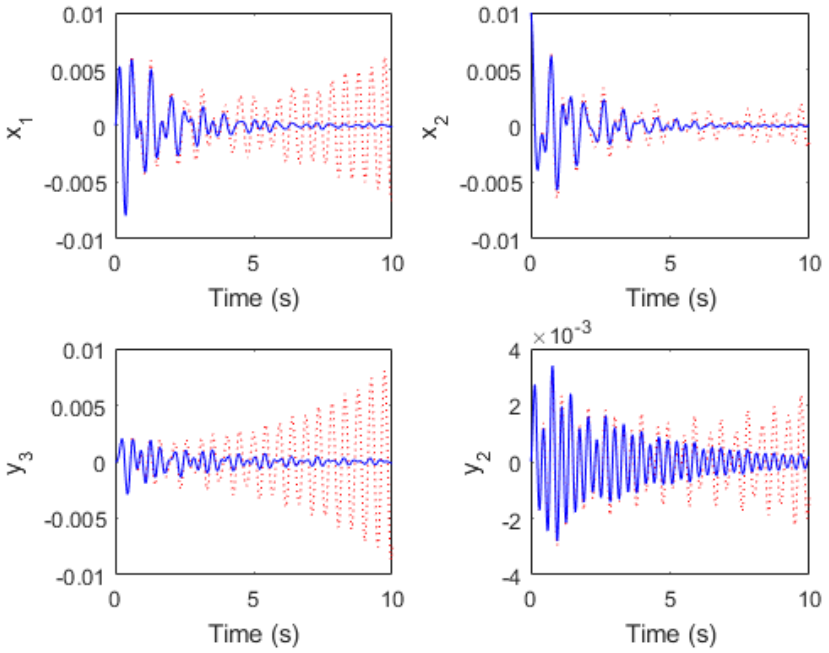

Figure 5.9: Displacement responses of the closed-loop system for Case III with $\tau_{\mathrm{f}} = 0.05, \tau_{\mathrm{g}} = 2\tau_{\mathrm{f}}$: $\tau_1 = 0.11$ (blue solid line) and $\tau_2 = 0.13$ (red dotted line)

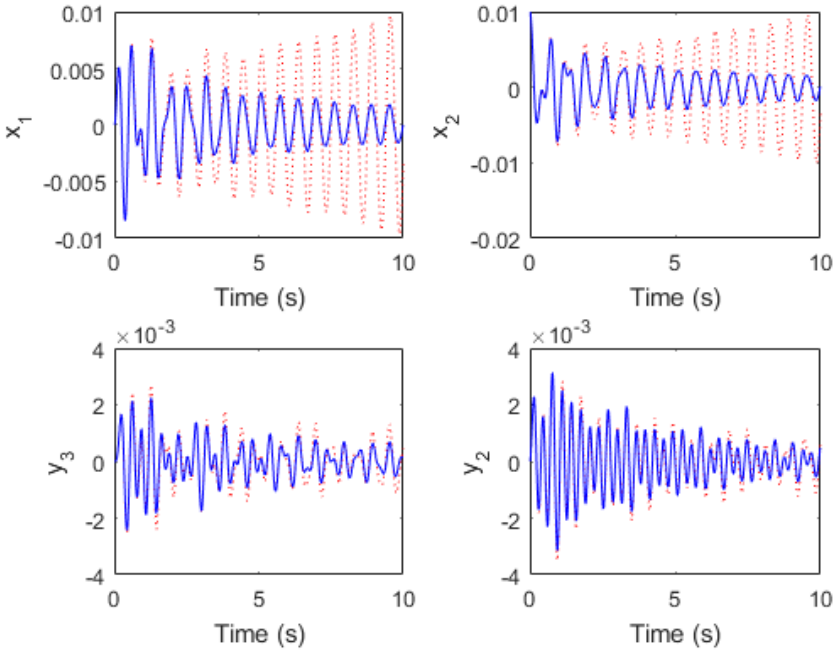

Figure 5.10: Displacement responses of the closed-loop system for Case IV with $\tau_{\mathrm{f}} = \tau_{\mathrm{g}} = 0.05$: $\tau_1 = 0.18$ (blue solid line) and $\tau_2 = 0.20$ (red dotted line)

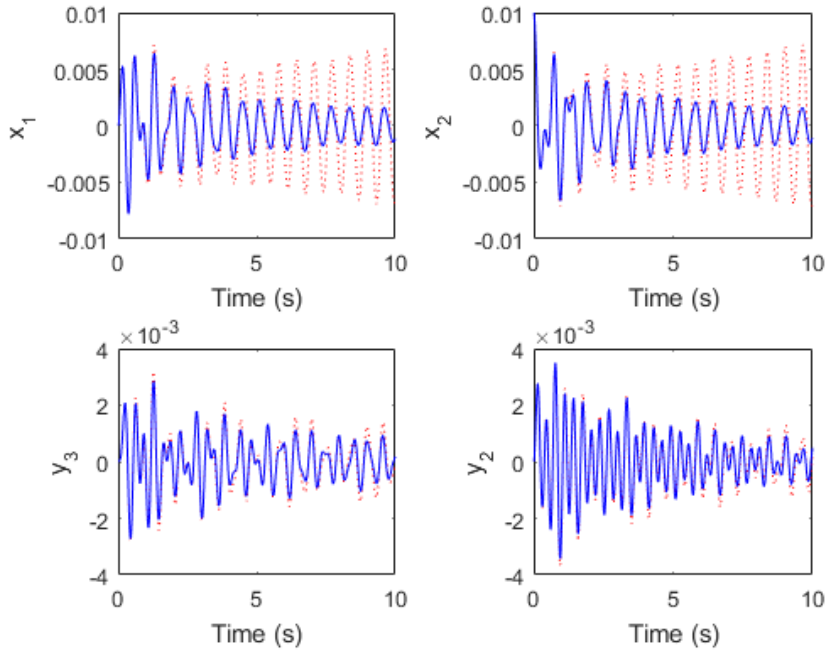

Figure 5.11: Displacement responses of the closed-loop system for Case IV with $\tau_{\mathrm{f}} = \tau_{\mathrm{g}} = 0.10$: $\tau_1 = 0.23$ (blue solid line) and $\tau_2 = 0.25$ (red dotted line)

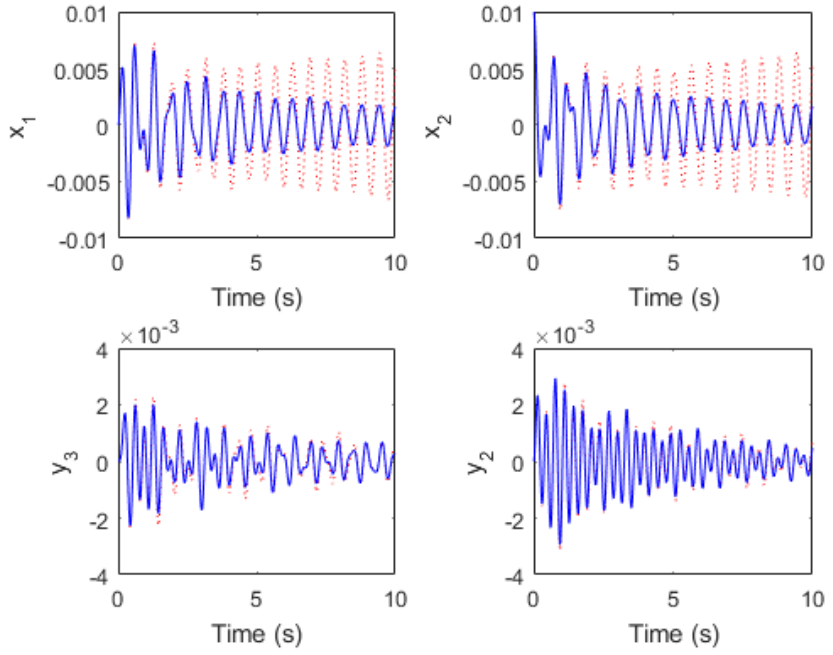

Figure 5.12: Displacement responses of the closed-loop system for Case IV with $\tau_{\mathrm{f}} = 0.05, \tau_{\mathrm{g}} = 2\tau_{\mathrm{f}}$: $\tau_1 = 0.15$ (blue solid line) and $\tau_2 = 0.16$ (red dotted line)

5.4.2 Friction-induced vibration with the multiple friction forces

The friction-induced vibration with the multiple friction forces modelled by a mass-spring-damper system on a conveyor belt as illustrated in Figure 5.13 is the asymmetric system under the present study. It is the same model studied in Ouyang (2009) (which made structural modifications). The system consists of four masses with m_1 having a degree-of-freedom in the horizontal direction, m_4 having a degree-of-freedom in the vertical direction, m_2 and m_3 having degrees-of-freedom in both directions attached with linear springs; k_5, k_7 and k_{10} at 45° relative to the vertical direction . When the belt is moving, friction forces are generated to produce an asymmetric stiffness matrix. To simplify the problem, Coulomb friction is considered and stick-slip phenomena is avoided. $\mathbf{M}$, $\mathbf{C}_\mathrm{s}$, $\mathbf{K}_\mathrm{s}$ and $\mathbf{K}_\mathrm{as}$ corresponding to the displacement vector, $\mathbf{x} = \{x_1, y_4, x_2, x_3, y_2, y_3\}^\mathrm{T}$ are given by,

$$\mathbf{M} = \begin{bmatrix} m_1 & 0 & 0 & 0 & 0 & 0 \\ 0 & m_4 & 0 & 0 & 0 & 0 \\ 0 & 0 & m_2 & 0 & 0 & 0 \\ 0 & 0 & 0 & m_3 & 0 & 0 \\ 0 & 0 & 0 & 0 & m_2 & 0 \\ 0 & 0 & 0 & 0 & 0 & m_3 \end{bmatrix}, \mathbf{C}_\mathrm{s} = \begin{bmatrix} c_1 & 0 & -c_1 & 0 & 0 & 0 \\ 0 & 0 & 0 & 0 & 0 & 0 \\ -c_1 & 0 & c_1+c_2 & -c_2 & 0 & 0 \\ 0 & 0 & -c_2 & c_2 & 0 & 0 \\ 0 & 0 & 0 & 0 & c_0 & 0 \\ 0 & 0 & 0 & 0 & 0 & c_3 \end{bmatrix},$$

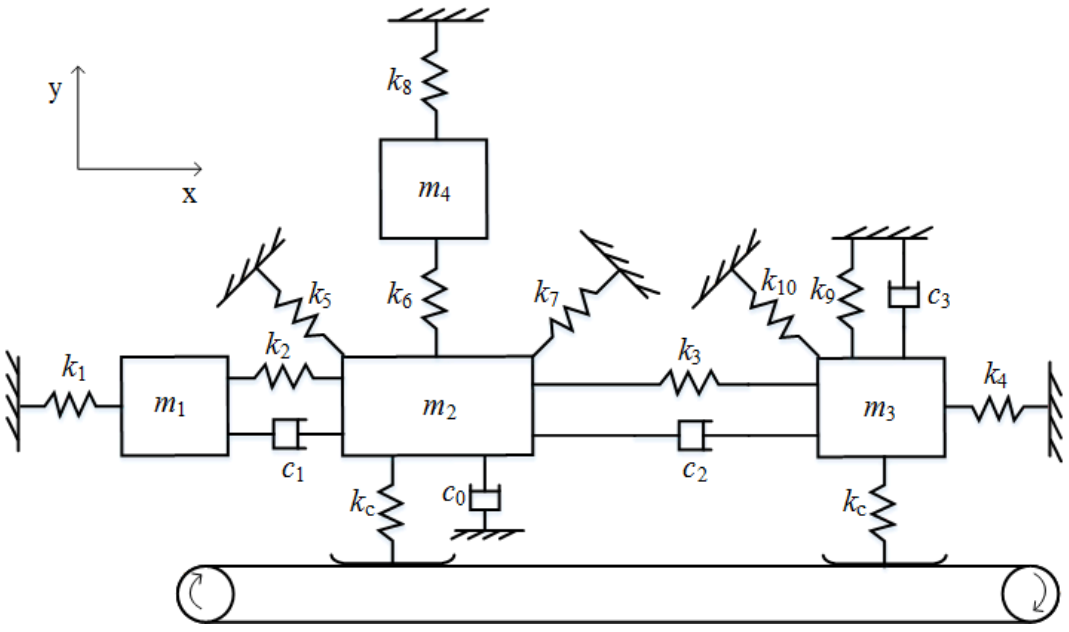

Figure 5.13: An asymmetric system of friction-induced vibration with multiple friction forces

$$\mathbf{K}_{\mathrm{s}} = \begin{bmatrix} k_{11} & 0 & k_{13} & 0 & 0 & 0 \\ 0 & k_{22} & 0 & 0 & k_{25} & 0 \\ k_{31} & 0 & k_{33} & k_{34} & k_{35} & 0 \\ 0 & 0 & k_{43} & k_{44} & 0 & k_{46} \\ 0 & k_{52} & k_{53} & 0 & k_{55} & 0 \\ 0 & 0 & 0 & k_{64} & 0 & k_{66} \end{bmatrix}, \mathbf{K}_{\mathrm{as}} = \mu_{\mathrm{c}} k_{\mathrm{c}} \begin{bmatrix} 0 & 0 & 0 & 0 & 0 & 0 \\ 0 & 0 & 0 & 0 & 0 & 0 \\ 0 & 0 & 0 & 0 & 1 & 0 \\ 0 & 0 & 0 & 0 & 0 & 1 \\ 0 & 0 & 0 & 0 & 0 & 0 \\ 0 & 0 & 0 & 0 & 0 & 0 \end{bmatrix}.$$

where $k_{11} = k_1 + k_2$, $k_{13} = k_{31} = -k_2$, $k_{22} = k_6 + k_8$, $k_{25} = k_{52} = -k_6$, $k_{33} = k_2 + k_3 + 0.5(k_5 + k_7)$, $k_{34} = k_{43} = -k_3$, $k_{35} = k_{53} = 0.5(k_7 - k_5)$, $k_{44} = k_3 + k_4 + 0.5k_{10}$, $k_{46} = k_{64} = -0.5k_{10}$, $k_{55} = k_{\mathrm{c}} + k_6 + 0.5(k_5 + k_7)$, $k_{66} = k_{\mathrm{c}} + k_9 + 0.5k_{10}$.

Assuming mass, $m_i = 1$ kg $(i = 1, 2, 3, 4)$; damping, $c_i = 0.5$ Ns/m $(i = 0, 1, 2, 3)$; stiffness, $k_i = 100$ N/m $(i = 1, 2, 3, 4, 5, 6, 8, 9, 10)$, $k_7 = 50$ N/m; contact stiffness, $k_{\mathrm{c}} = 110$ N/m; and friction coefficient; $\mu_{\mathrm{c}} = 0.5$, the open-loop poles are determined by using 'polyeig' function in MATLAB.

$$\{\lambda\}_1^{12} = \begin{Bmatrix} 0.0069 \pm 10.3843\mathrm{i} \\ -0.0903 \pm 11.4497\mathrm{i} \\ -0.2517 \pm 15.2078\mathrm{i} \\ -0.2465 \pm 15.9791\mathrm{i} \\ -0.0838 \pm 18.8646\mathrm{i} \\ -0.8346 \pm 19.6958\mathrm{i} \end{Bmatrix}.$$

Obviously, the open-loop system is unstable because the first pair of the open-loop poles is located on the right-hand side of the complex plane. To stabilise the system, they must be shifted to the left-hand side of the complex plane.

Four cases of required closed-loop poles are shown in Table 5.5. Pole assignment and partial pole assignment with different time delays (including single and multiple time delays) are demonstrated. The actuator distribution vector; $\mathbf{b} = \{0, 0, 1, 1, 1, 1\}^{\mathrm{T}}$ is assumed. Velocity and displacement gain vectors for assigning the required closed-loop poles including the time delays are determined by solving the linear equations expressed in Eq.(5.10) for pole assignment and Eq.(5.15) for partial pole assignment. The results are shown in Table 5.6. They are then substituted back into Eq.(5.16). It is found that $|D|$ is close to zero for all cases. Hence, the algorithms of pole assignment with time delays and partial pole assignment with time delays by using the unobservability condition are successful.

The stability can be investigated by examining the poles of the closed-loop system. By using TRACE-DDE toolbox in MATLAB (Breda et al. (2009)), the first twenty poles of the closed-loop system are determined (see Table 5.7). As can be seen, for all cases, the required closed-loop poles are placed precisely and the other poles have negative real parts. Although the closed-loop poles have negative real parts, the stability cannot be guaranteed due to the unidentified residue poles.

Alternatively, the stability is analysed by using the frequency-sweeping test (Gu et al. (2003)) described in Section 5.3.2. It is clear that the closed-loop systems for all cases are not delay-independent stable because of positive real parts of the open-loop poles ($\mathbf{A}_0$ is unstable). The closed-loop poles without time delay ($\lambda(\mathbf{A}_0 + \sum_{i=1}^{m} \mathbf{A}_i)$) are investigated as shown in Table 5.8. As can be seen, the closed-loop system without time delay is stable for Case V - Case VI with time delay $\tau_\mathrm{f} = \tau_\mathrm{g} = 0.05$ and Case VII - Case VIII with all time delay conditions which means the delay-dependent stability allowing to calculate the critical time delay.

The critical time delay is obtained by using Eq.(5.25) and Eq.(5.30) for the single time delay and the multiple time delays respectively. The results are shown in Table 5.9. For Case V and Case VI with the single time delay; $\tau_\mathrm{f} = \tau_\mathrm{g} = 0.10$ and multiple time delays; $\tau_\mathrm{f} = 0.05, \tau_\mathrm{g} = 2\tau_\mathrm{f}$, the critical time delay cannot be determined because $\mathbf{A}_0 + \sum_{i=1}^{m} \mathbf{A}_i$ is unstable. For other cases, the closed-loop systems are stable because the time delays are smaller than the critical ones.

In order to validate the critical time delays as shown in Table 5.9, displacement responses are plotted by using 'dde23' function in MATLAB. The initial conditions used to test this are taken to be zero displacement and zero velocity for all degrees-of-freedom except $x_3 = 0.01$ m. The results are shown in Figure 5.14, Figure 5.17 and Figure 5.20 - Figure 5.25. For example Case V with $\tau_\mathrm{f} = \tau_\mathrm{g} = 0.05$, the critical time delay at $\overline{\tau} = 0.0981$ is validated by applying time delays $\tau_1 = 0.08$ ($\tau_1 < \overline{\tau}$) and $\tau_2 = 0.11$ ($\tau_2 > \overline{\tau}$). It is clear from Figure 5.14 that the closed-loop system is stable for τ_1 but it is unstable for τ_2.

By using the same method, the closed-loop systems for Case V - Case VI with $\tau_\mathrm{f} = \tau_\mathrm{g} = 0.10$ and $\tau_\mathrm{f} = 0.05, \tau_\mathrm{g} = 2\tau_\mathrm{f}$ are stable if the time delays are the constant values (see Figure 5.15, Figure 5.16, Figure 5.18 and Figure 5.19).

Table 5.5: Required closed-loop poles of the friction induced vibration with the multiple friction forces

Case V	Case VI	Case VII	Case VIII
-1.0000 ± 10.5000i	-1.0000 ± 10.5000i	-1.0000 ± 10.5000i	-1.0000 ± 10.5000i
-1.0000 ± 11.5000i	-1.0000 ± 11.5000i	-1.0000 ± 11.5000i	-0.0903 ± 11.4497i
-1.0000 ± 15.0000i	-1.0000 ± 15.0000i	-1.0000 ± 15.0000i	-0.2517 ± 15.2078i
-1.0000 ± 16.0000i	-1.0000 ± 16.0000i	-0.2465 ± 15.9791i	-0.2465 ± 15.9791i
-1.0000 ± 18.5000i	-1.0000 ± 18.5000i	-0.0838 ± 18.8646i	-0.0838 ± 18.8646i
-1.0000 ± 20.0000i	-0.8346 ± 19.6958i	-0.8346 ± 19.6958i	-0.8346 ± 19.6958i

Table 5.6: Control gains obtained by pole assignment and partial pole assignment with time delays by using the unobservability condition for the friction-induced vibration with the multiple friction forces

Case	$\tau_{\mathrm{f}} = \tau_{\mathrm{g}} = 0.05$		$\tau_{\mathrm{f}} = \tau_{\mathrm{g}} = 0.10$		$\tau_{\mathrm{f}} = 0.05, \tau_{\mathrm{g}} = 2\tau_{\mathrm{f}}$	
	g	**f**	**g**	**f**	**g**	**f**
V	6.3954	−5.5626	68.2880	−2.6741	30.1636	−3.7518
	11.3052	3.9759	−15.3209	3.3982	11.5669	4.0462
	−10.9059	2.5366	−48.8595	0.4233	−13.4647	1.5465
	−55.4047	3.2902	−72.1743	−0.9000	−88.0116	−1.4803
	−10.0858	4.1461	−44.9679	1.9651	−31.9759	2.3075
	18.9242	−5.1110	74.2328	−1.7806	45.2496	−2.5424
VI	8.8756	−5.1007	61.2222	−2.4915	35.0940	−3.0658
	13.6525	4.0540	−15.7040	3.6150	14.1803	4.2553
	−21.9749	2.0511	−45.0928	−0.1745	−32.2067	0.1430
	−41.4140	3.4034	−68.3566	−0.1186	−65.6609	−0.2696
	−12.0039	3.7648	−38.9014	1.8174	−34.8242	1.7928
	14.9200	−4.8223	67.4949	−1.9479	39.1440	−2.5662
VII	−15.4097	−1.4658	2.2849	−1.7048	−14.1786	−2.1774
	19.1193	4.8153	−19.3657	4.3470	18.1490	5.5873
	−22.2576	0.0028	−16.2764	−1.1700	−25.1700	−1.2760
	−24.0482	0.5830	−23.4735	−0.9000	−29.8556	−0.9018
	18.3706	3.1316	−7.8771	3.0537	20.1041	4.0326
	2.1532	−0.1466	3.0501	0.0231	2.9517	0.0005
VIII	−5.5461	1.5305	−12.6243	0.9381	−6.5012	1.2013
	1.9129	−0.6826	5.1805	−0.4476	2.3218	−0.5650
	−5.1010	1.4081	−11.6325	0.8582	−5.7976	1.1113
	−4.0290	0.9744	−8.3916	0.5852	−4.8354	−0.7341
	1.4587	−0.6289	4.5753	−0.4118	1.5600	−0.5436
	0.0973	−0.0324	0.2529	−0.2010	0.1035	−0.0268

Table 5.7: First twenty poles of the closed-loop system with time delays obtained by TRACE-DDE toolbox in MATLAB (sorted by the real part) for the friction-induced vibration with the multiple friction forces

Case	$\tau_{\mathrm{f}} = \tau_{\mathrm{g}} = 0.05$	$\tau_{\mathrm{f}} = \tau_{\mathrm{g}} = 0.10$	$\tau_{\mathrm{f}} = 0.05, \tau_{\mathrm{g}} = 2\tau_{\mathrm{f}}$
V	$-1.0000 \pm 10.5000\mathrm{i}$	$-1.0000 \pm 10.5000\mathrm{i}$	$-1.0000 \pm 10.5000\mathrm{i}$
	$-1.0000 \pm 11.5000\mathrm{i}$	$-1.0000 \pm 11.5000\mathrm{i}$	$-1.0000 \pm 11.5000\mathrm{i}$
	$-1.0000 \pm 15.0000\mathrm{i}$	$-1.0000 \pm 15.0000\mathrm{i}$	$-1.0000 \pm 15.0000\mathrm{i}$
	$-1.0000 \pm 16.0000\mathrm{i}$	$-1.0000 \pm 16.0000\mathrm{i}$	$-1.0000 \pm 16.0000\mathrm{i}$
	$-1.0000 \pm 18.5000\mathrm{i}$	$-1.0000 \pm 18.5000\mathrm{i}$	$-1.0000 \pm 18.5000\mathrm{i}$
	$-1.0000 \pm 20.0000\mathrm{i}$	$-1.0000 \pm 20.0000\mathrm{i}$	$-1.0000 \pm 20.0000\mathrm{i}$
	-38.800	-19.871	-18.705
	$-69.699 \pm 149.553\mathrm{i}$	$-47.608 \pm 87.0881\mathrm{i}$	$-43.183 \pm 385.281\mathrm{i}$
	$-81.428 \pm 277.832\mathrm{i}$	$-54.454 \pm 1144.60\mathrm{i}$	$-43.284 \pm 385.475\mathrm{i}$
	$-88.739 \pm 404.666\mathrm{i}$	$-55.048 \pm 1144.88\mathrm{i}$	$-46.167 \pm 83.9970\mathrm{i}$
VI	$-0.8346 \pm 19.6958\mathrm{i}$	$-0.8346 \pm 19.6958\mathrm{i}$	$-0.8346 \pm 19.6958\mathrm{i}$
	$-1.0000 \pm 10.5000\mathrm{i}$	$-1.0000 \pm 10.5000\mathrm{i}$	$-1.0000 \pm 10.5000\mathrm{i}$
	$-1.0000 \pm 11.5000\mathrm{i}$	$-1.0000 \pm 11.5000\mathrm{i}$	$-1.0000 \pm 11.5000\mathrm{i}$
	$-1.0000 \pm 15.0000\mathrm{i}$	$-1.0000 \pm 15.0000\mathrm{i}$	$-1.0000 \pm 15.0000\mathrm{i}$
	$-1.0000 \pm 16.0000\mathrm{i}$	$-1.0000 \pm 16.0000\mathrm{i}$	$-1.0000 \pm 16.0000\mathrm{i}$
	$-1.0000 \pm 18.5000\mathrm{i}$	$-1.0000 \pm 18.5000\mathrm{i}$	$-1.0000 \pm 18.5000\mathrm{i}$
	-41.253	-22.519	-18.998
	$-71.699 \pm 149.518\mathrm{i}$	$-49.087 \pm 89.2780\mathrm{i}$	$-43.183 \pm 385.281\mathrm{i}$
	$-83.433 \pm 277.818\mathrm{i}$	$-54.454 \pm 1144.60\mathrm{i}$	$-43.389 \pm 385.432\mathrm{i}$
	$-90.746 \pm 404.658\mathrm{i}$	$-55.351 \pm 1144.93\mathrm{i}$	$-44.683 \pm 84.2841\mathrm{i}$
VII	$-0.0838 \pm 18.8646\mathrm{i}$	$-0.0838 \pm 18.8646\mathrm{i}$	$-0.0838 \pm 18.8646\mathrm{i}$
	$-0.2465 \pm 15.9791\mathrm{i}$	$-0.2465 \pm 15.9791\mathrm{i}$	$-0.2465 \pm 15.9791\mathrm{i}$
	$-0.8346 \pm 19.6958\mathrm{i}$	$-0.8346 \pm 19.6958\mathrm{i}$	$-0.8346 \pm 19.6958\mathrm{i}$
	$-1.0000 \pm 10.5000\mathrm{i}$	$-1.0000 \pm 10.5000\mathrm{i}$	$-1.0000 \pm 10.5000\mathrm{i}$
	$-1.0000 \pm 11.5000\mathrm{i}$	$-1.0000 \pm 11.5000\mathrm{i}$	$-1.0000 \pm 11.5000\mathrm{i}$
	$-1.0000 \pm 15.0000\mathrm{i}$	$-1.0000 \pm 15.0000\mathrm{i}$	$-1.0000 \pm 15.0000\mathrm{i}$
	-51.760	-22.566	-33.794
	$-76.375 \pm 148.296\mathrm{i}$	$-41.664 \pm 76.9644\mathrm{i}$	$-42.963 \pm 385.497\mathrm{i}$
	$-87.790 \pm 277.096\mathrm{i}$	$-48.599 \pm 140.603\mathrm{i}$	$-43.183 \pm 385.281\mathrm{i}$
	$-95.013 \pm 404.147\mathrm{i}$	$-52.557 \pm 1144.46\mathrm{i}$	$-56.805 \pm 311.847\mathrm{i}$
VIII	$-0.0838 \pm 18.8646\mathrm{i}$	$-0.0838 \pm 18.8646\mathrm{i}$	$-0.0838 \pm 18.8646\mathrm{i}$
	$-0.0903 \pm 11.4497\mathrm{i}$	$-0.0903 \pm 11.4497\mathrm{i}$	$-0.0903 \pm 11.4497\mathrm{i}$
	$-0.2465 \pm 15.9791\mathrm{i}$	$-0.2465 \pm 15.9791\mathrm{i}$	$-0.2465 \pm 15.9791\mathrm{i}$
	$-0.2517 \pm 15.2078\mathrm{i}$	$-0.2517 \pm 15.2078\mathrm{i}$	$-0.2517 \pm 15.2078\mathrm{i}$
	$-0.8346 \pm 19.6958\mathrm{i}$	$-0.8346 \pm 19.6958\mathrm{i}$	$-0.8346 \pm 19.6958\mathrm{i}$
	$-1.0000 \pm 10.5000\mathrm{i}$	$-1.0000 \pm 10.5000\mathrm{i}$	$-1.0000 \pm 10.5000\mathrm{i}$
	-74.707	-31.615	$-43.019 \pm 385.400\mathrm{i}$
	$-91.877 \pm 146.197\mathrm{i}$	$-43.467 \pm 74.4832\mathrm{i}$	$-43.183 \pm 385.281\mathrm{i}$
	$-102.72 \pm 275.863\mathrm{i}$	$-49.405 \pm 138.832\mathrm{i}$	-54.184
	$-105.63 \pm 2288.83\mathrm{i}$	$-52.554 \pm 1144.42\mathrm{i}$	$-56.805 \pm 311.847\mathrm{i}$

Table 5.8: The closed-loop system without time delays for the friction-induced vibration with the multiple friction forces

Case	$\tau_f = \tau_g = 0.05$	$\tau_f = \tau_g = 0.10$	$\tau_f = 0.05, \tau_g = 2\tau_f$
V	$-0.9649 \pm 9.3043i$	$0.2765 \pm 8.7067i$	$0.3413 \pm 8.5420i$
	$-0.5427 \pm 11.2012i$	$-0.3619 \pm 11.1206i$	$-0.4281 \pm 11.2852i$
	$-0.4218 \pm 14.4693i$	$0.2196 \pm 14.4687i$	$0.2850 \pm 14.0835i$
	$-0.6263 \pm 15.8035i$	$-0.5008 \pm 15.7003i$	$-0.4579 \pm 15.8836i$
	$-0.4164 \pm 18.3261i$	$-0.0353 \pm 18.2467i$	$-0.0646 \pm 18.1219i$
	$-0.9588 \pm 19.7873i$	$-0.9521 \pm 19.7028i$	$-1.0914 \pm 20.0045i$
VI	$-0.9456 \pm 9.3207i$	$0.2089 \pm 8.7806i$	$0.3557 \pm 8.5792i$
	$-0.5394 \pm 11.2069i$	$-0.3639 \pm 11.1331i$	$-0.4304 \pm 11.2864i$
	$-0.4062 \pm 14.4943i$	$0.1857 \pm 14.5324i$	$0.3140 \pm 14.1310i$
	$-0.6155 \pm 15.8113i$	$-0.4908 \pm 15.7159i$	$-0.4619 \pm 15.8894i$
	$-0.3573 \pm 18.3682i$	$0.0065 \pm 18.3428i$	$0.0425 \pm 18.1400i$
	$-0.8346 \pm 19.6958i$	$-0.8346 \pm 19.6958i$	$-0.8700 \pm 19.8118i$
VII	$-0.9926 \pm 9.5829i$	$-0.1982 \pm 8.9728i$	$-0.2810 \pm 9.2400i$
	$-0.5793 \pm 11.2653i$	$-0.4135 \pm 11.1839i$	$-0.6242 \pm 11.4170i$
	$-0.5485 \pm 14.7863i$	$-0.2268 \pm 14.7620i$	$-0.2979 \pm 14.7776i$
	$-0.2465 \pm 15.9791i$	$-0.2465 \pm 15.9791i$	$-0.2456 \pm 15.9792i$
	$-0.0838 \pm 18.8646i$	$-0.0838 \pm 18.8646i$	$-0.1432 \pm 18.8767i$
	$-0.8346 \pm 19.6958i$	$-0.8346 \pm 19.6958i$	$-0.8358 \pm 19.6955i$
VIII	$-0.8537 \pm 9.9950i$	$-0.4988 \pm 9.6246i$	$-0.6527 \pm 9.9523i$
	$-0.0903 \pm 11.4497i$	$-0.0903 \pm 11.4497i$	$-0.0845 \pm 11.4492i$
	$-0.2517 \pm 15.2078i$	$-0.2517 \pm 15.2078i$	$-0.2417 \pm 15.2035i$
	$-0.2465 \pm 15.9791i$	$-0.2465 \pm 15.9791i$	$-0.2471 \pm 15.9795i$
	$-0.0838 \pm 18.8646i$	$-0.0838 \pm 18.8646i$	$-0.0723 \pm 18.8527i$
	$-0.8346 \pm 19.6958i$	$-0.8346 \pm 19.6958i$	$-0.8391 \pm 19.7044i$

Table 5.9: Critical time delay for the friction-induced vibration with the multiple friction forces

Case	$\tau_f = \tau_g = 0.05$	$\tau_f = \tau_g = 0.10$	$\tau_f = 0.05, \tau_g = 2\tau_f$
V	0.0981	–	–
VI	0.1118	–	–
VII	0.1406	0.2015	0.1047
VIII	0.1688	0.2205	0.1334

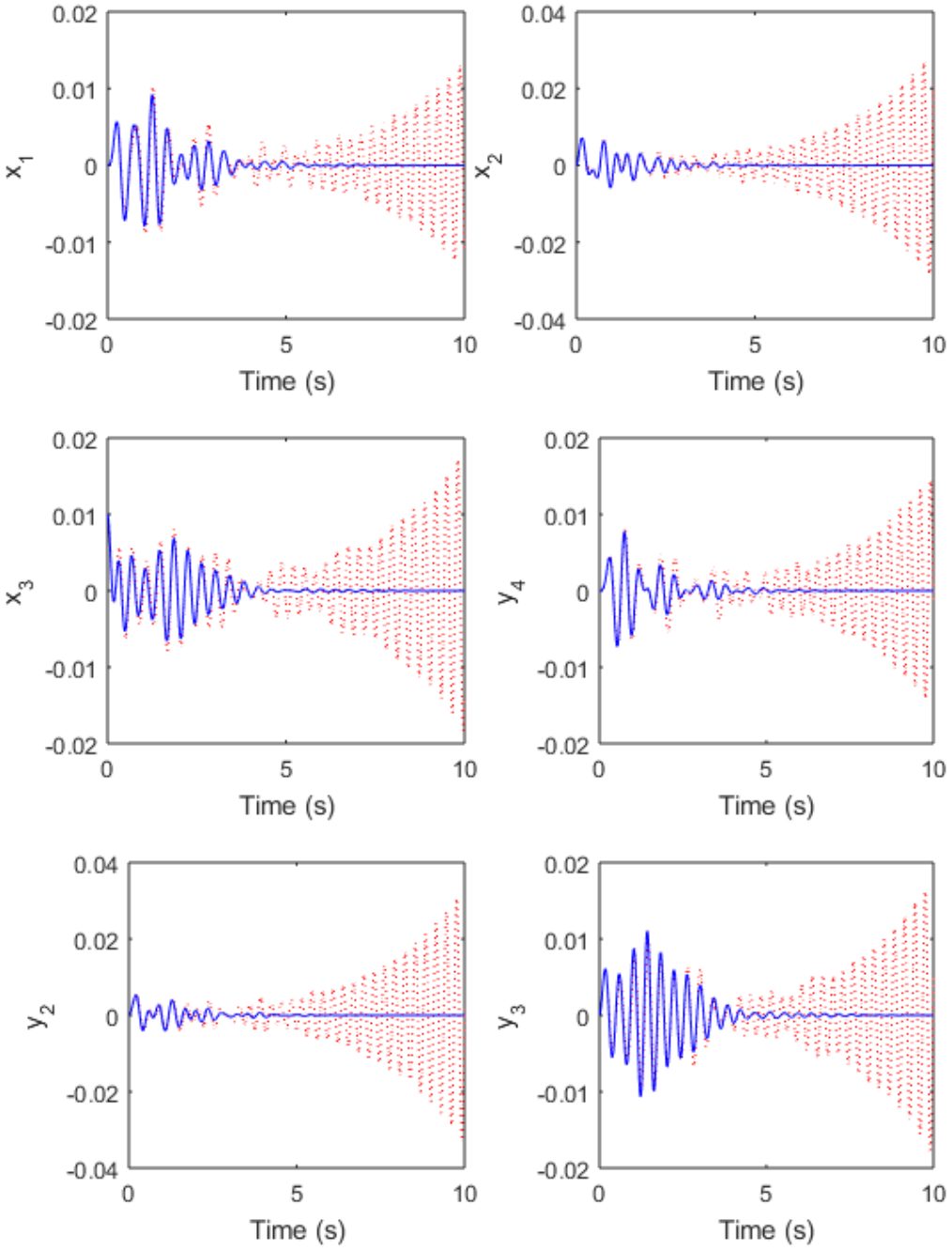

Figure 5.14: Displacement responses of the closed-loop system for Case V with $\tau_f = \tau_g = 0.05$: $\tau_1 = 0.08$ (blue solid line) and $\tau_2 = 0.11$ (red dotted line)

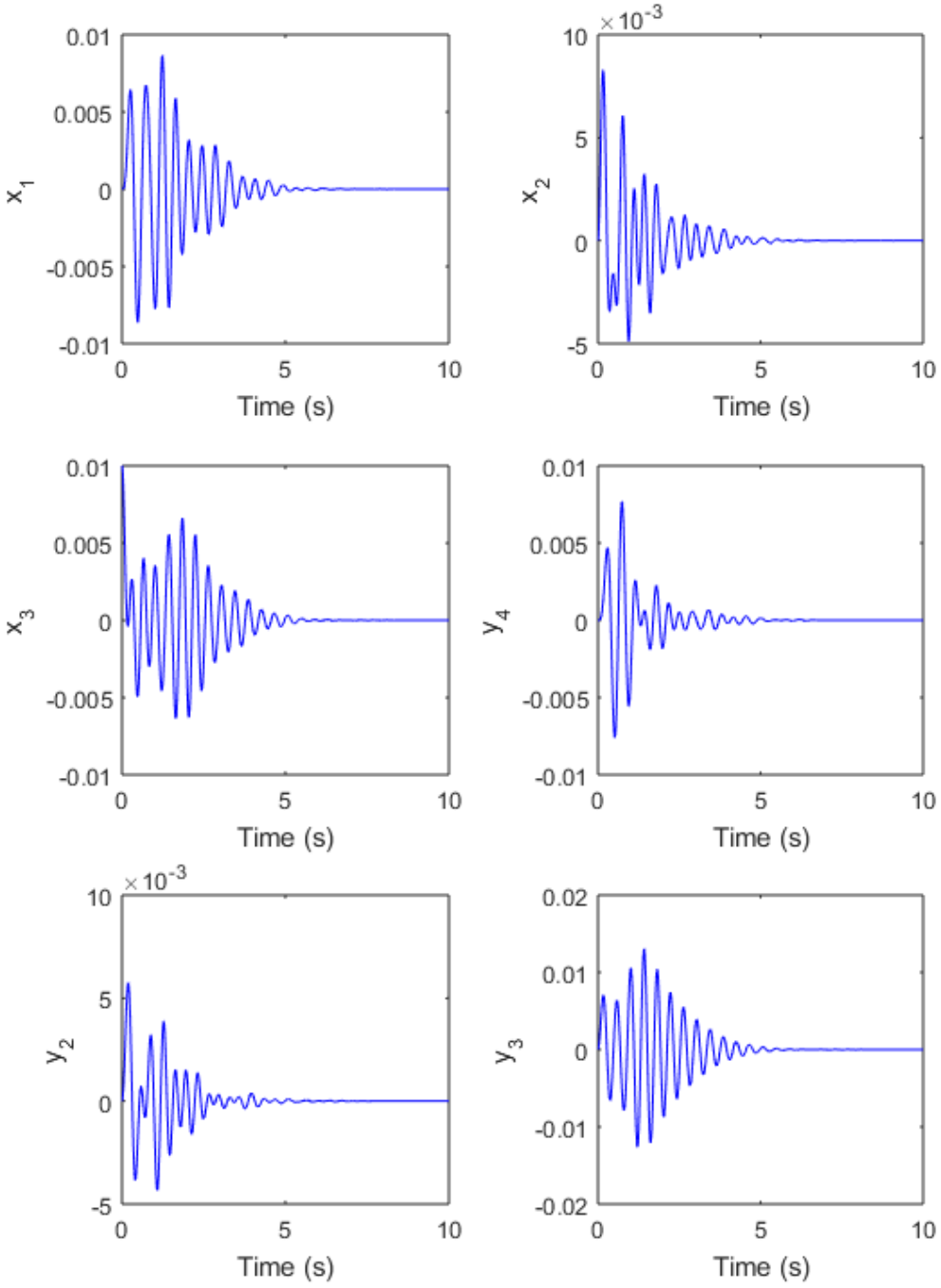

Figure 5.15: Displacement responses of the closed-loop system for Case V with $\tau_f = \tau_g = 0.10$: $\tau_1 = 0.10$ (blue solid line)

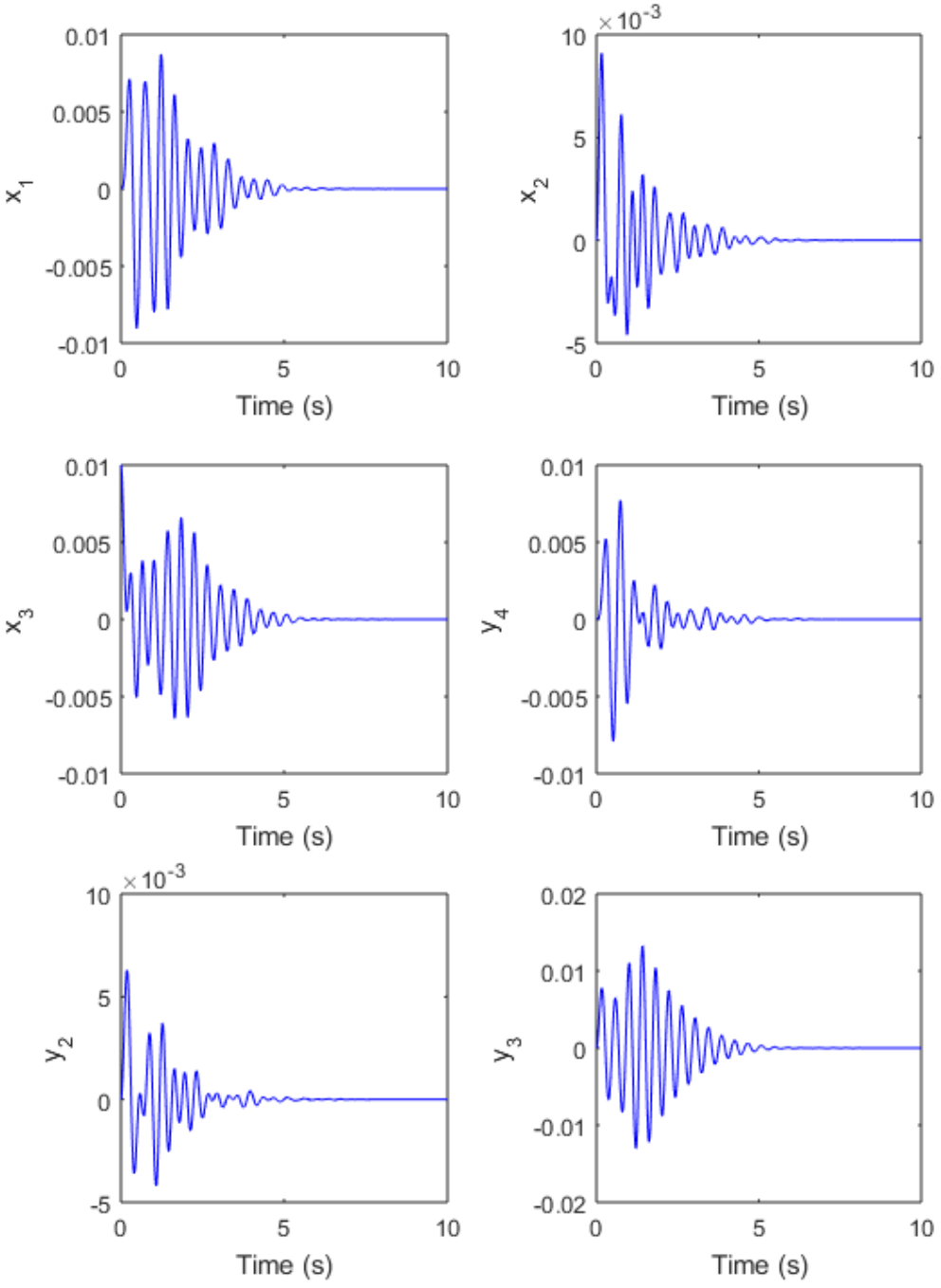

Figure 5.16: Displacement responses of the closed-loop system for Case V with $\tau_{\mathrm{f}} = 0.05, \tau_{\mathrm{g}} = 2\tau_{\mathrm{f}}$: $\tau_1 = 0.05$ (blue solid line)

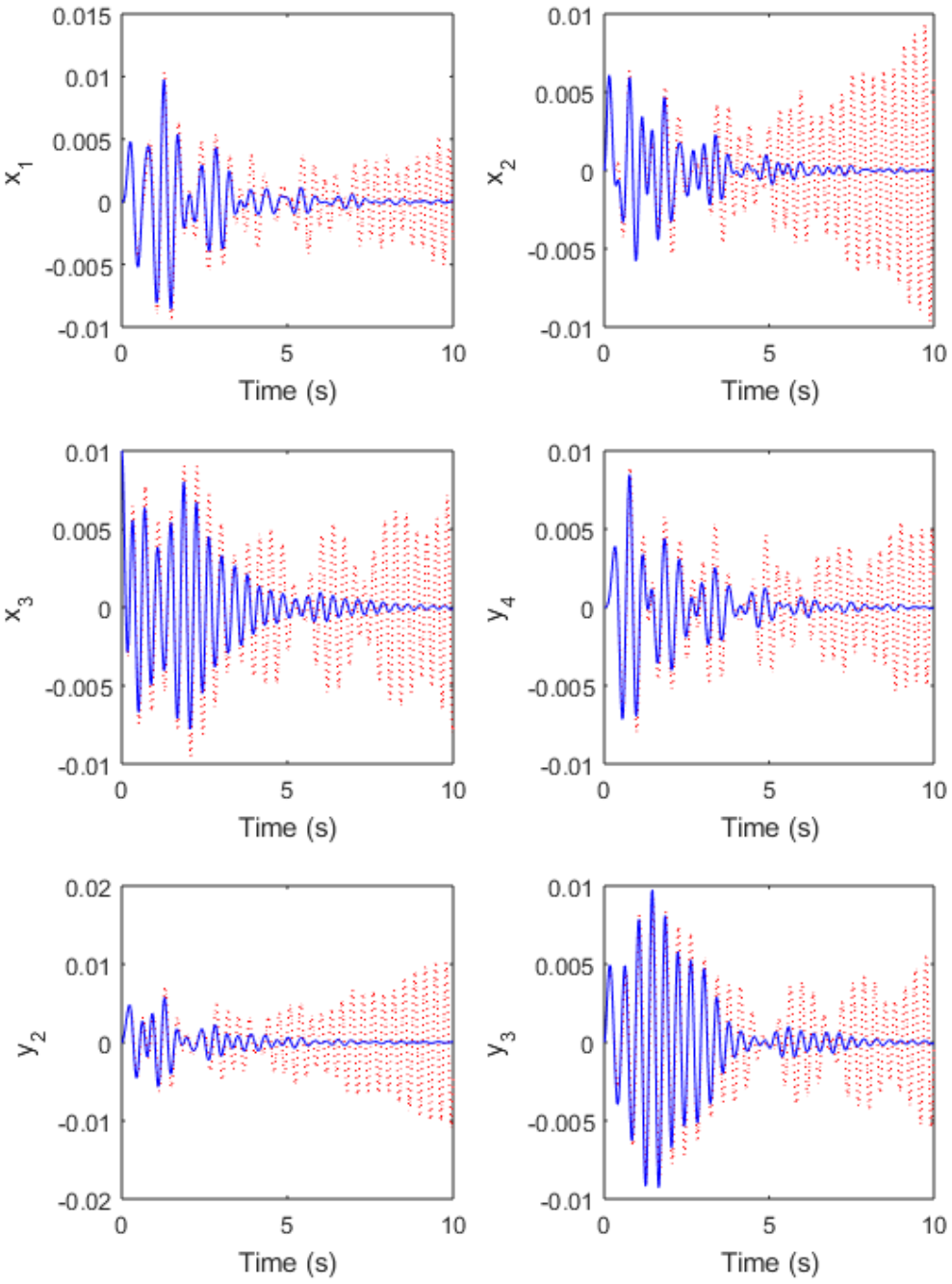

Figure 5.17: Displacement responses of the closed-loop system for Case VI with $\tau_f = \tau_g = 0.05$: $\tau_1 = 0.10$ (blue solid line) and $\tau_2 = 0.12$ (red dotted line)

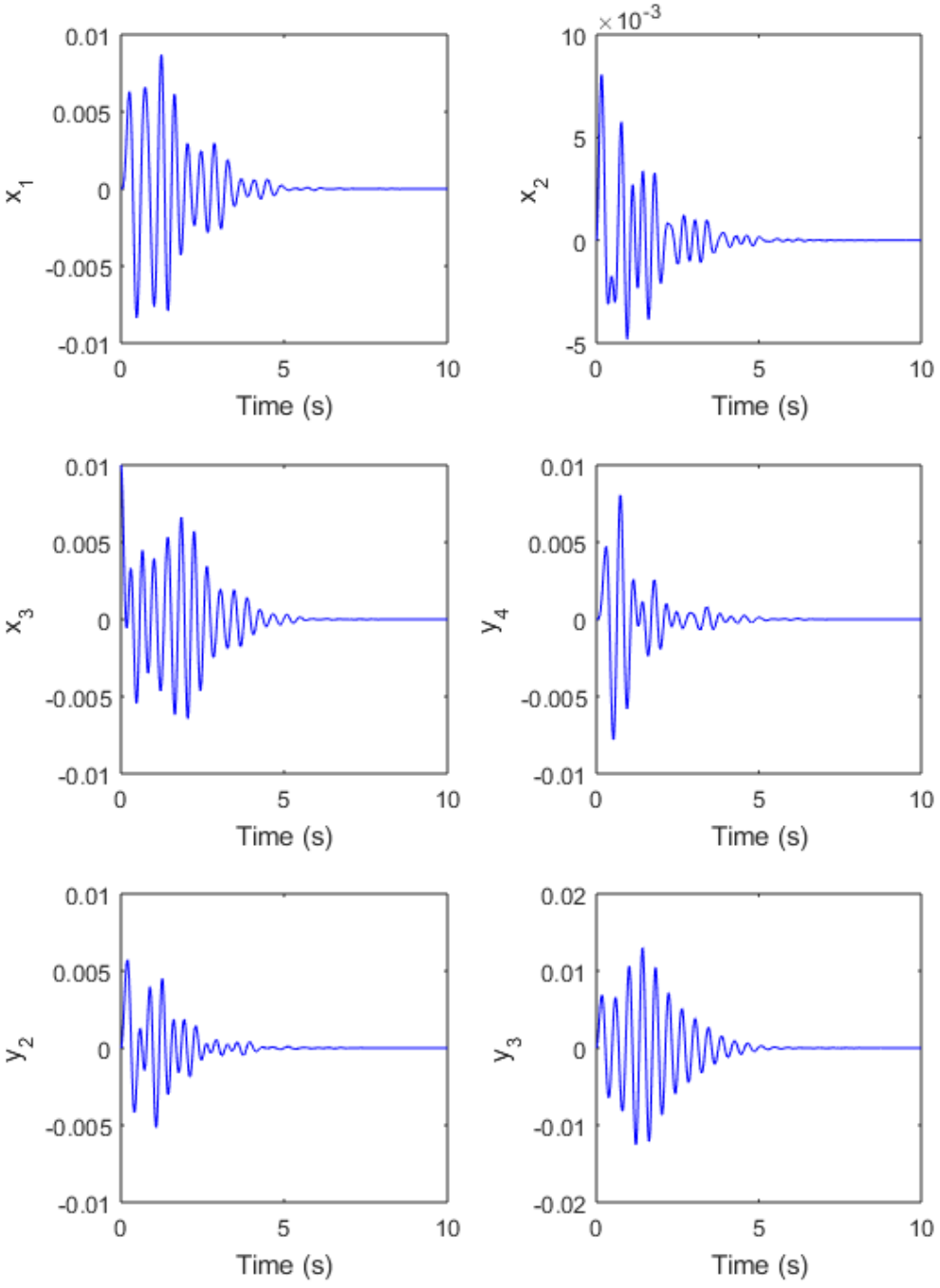

Figure 5.18: Displacement responses of the closed-loop system for Case VI with $\tau_f = \tau_g = 0.10$: $\tau_1 = 0.10$ (blue solid line)

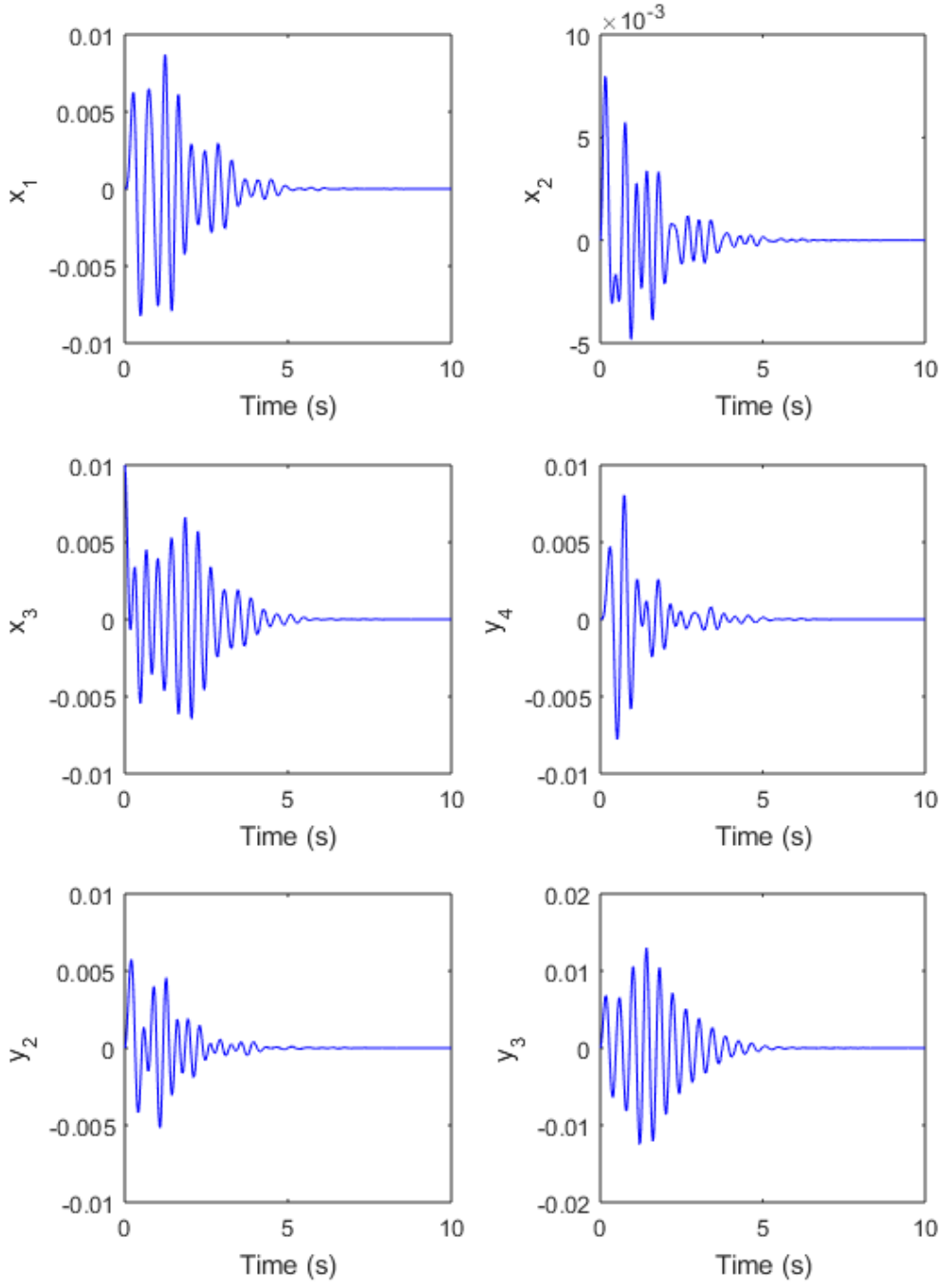

Figure 5.19: Displacement responses of the closed-loop system for Case VI with $\tau_{\mathrm{f}} = 0.05, \tau_{\mathrm{g}} = 2\tau_{\mathrm{f}}$: $\tau_1 = 0.05$ (blue solid line)

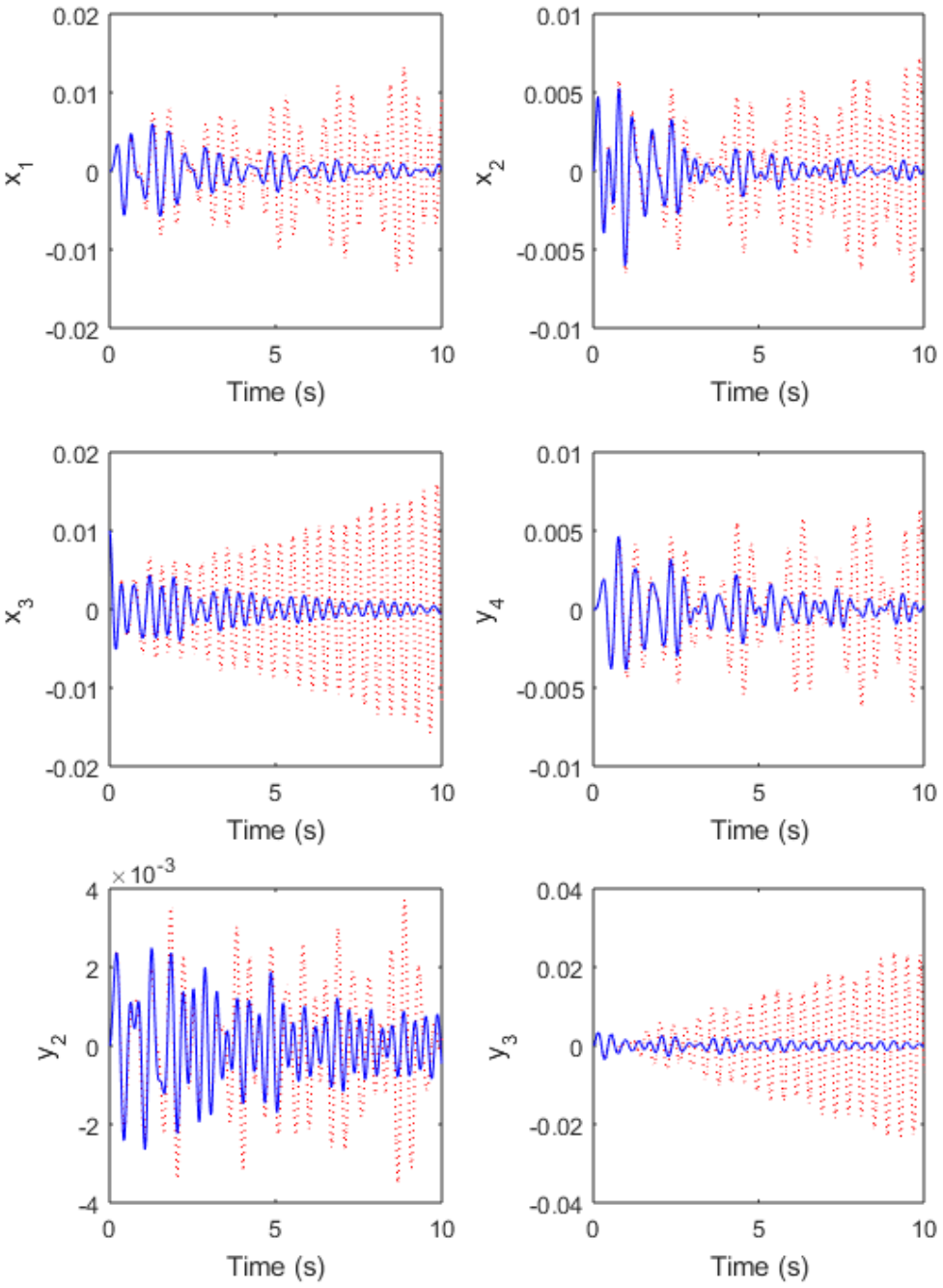

Figure 5.20: Displacement responses of the closed-loop system for Case VII with $\tau_f = \tau_g = 0.05$: $\tau_1 = 0.13$ (blue solid line) and $\tau_2 = 0.15$ (red dotted line)

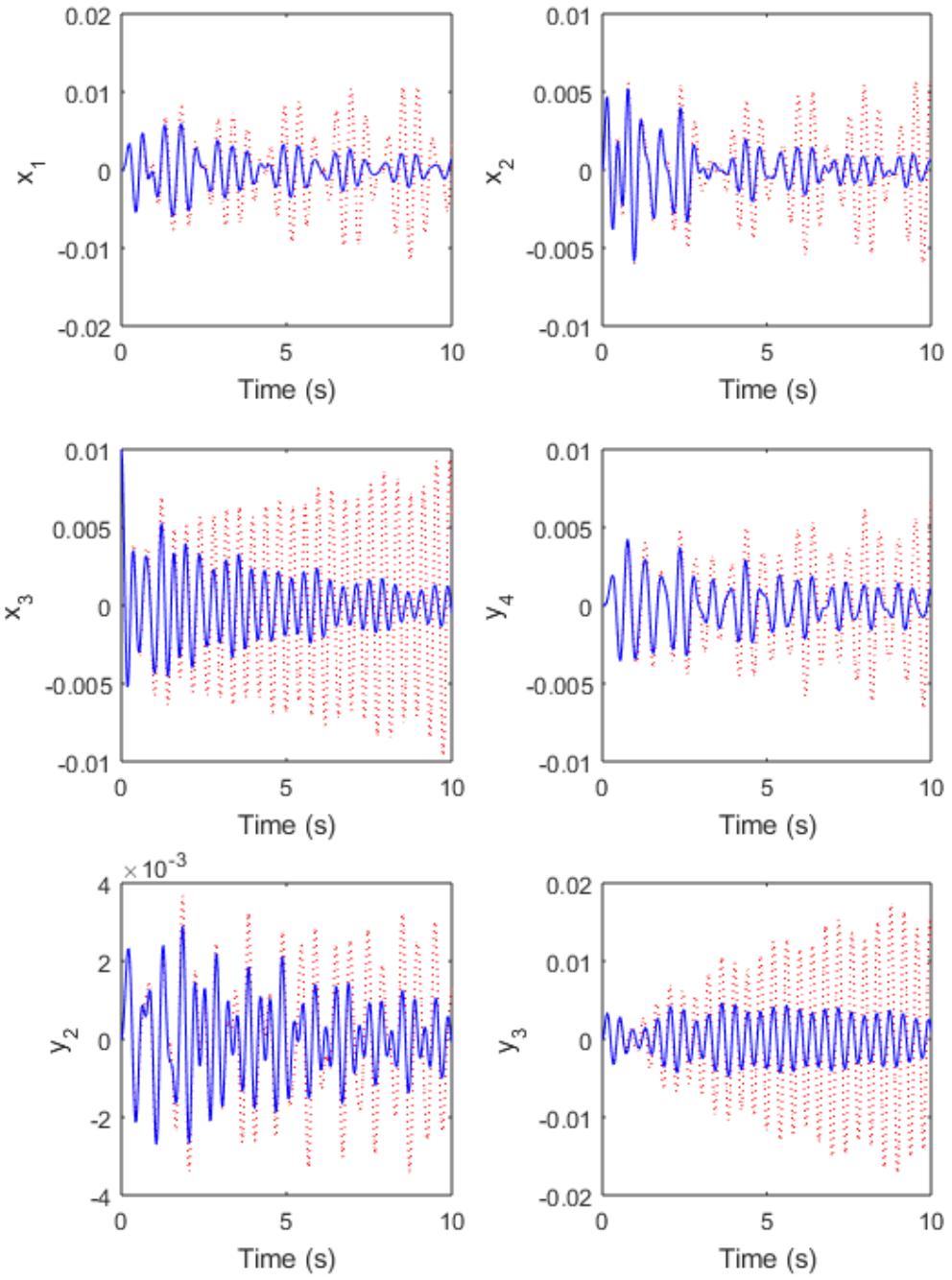

Figure 5.21: Displacement responses of the closed-loop system for Case VII with $\tau_{\mathrm{f}} = \tau_{\mathrm{g}} = 0.10$: $\tau_1 = 0.19$ (blue solid line) and $\tau_2 = 0.21$ (red dotted line)

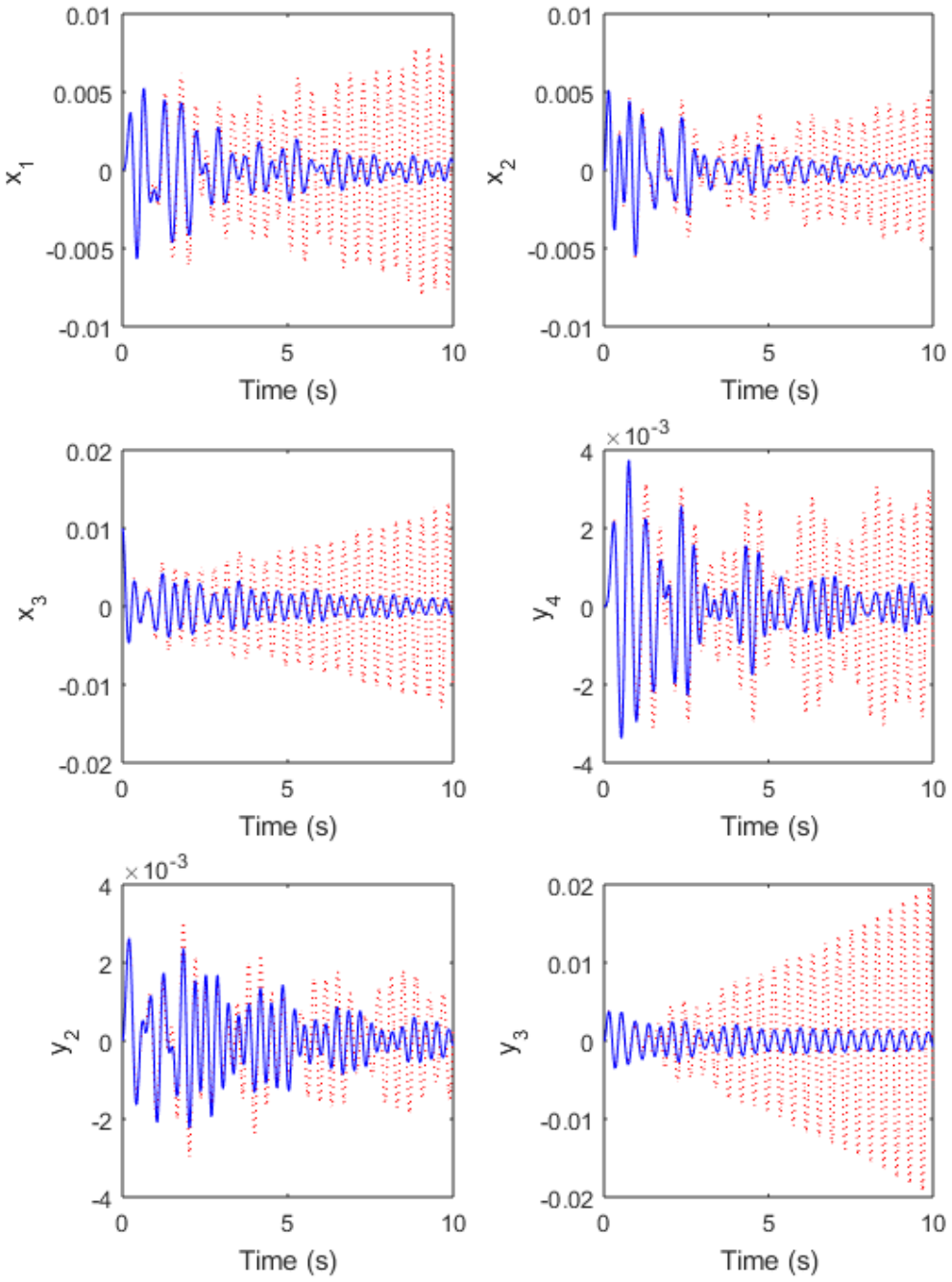

Figure 5.22: Displacement responses of the closed-loop system for Case VII with $\tau_{\mathrm{f}} = 0.05, \tau_{\mathrm{g}} = 2\tau_{\mathrm{f}}$: $\tau_1 = 0.10$ (blue solid line) and $\tau_2 = 0.11$ (red dotted line)

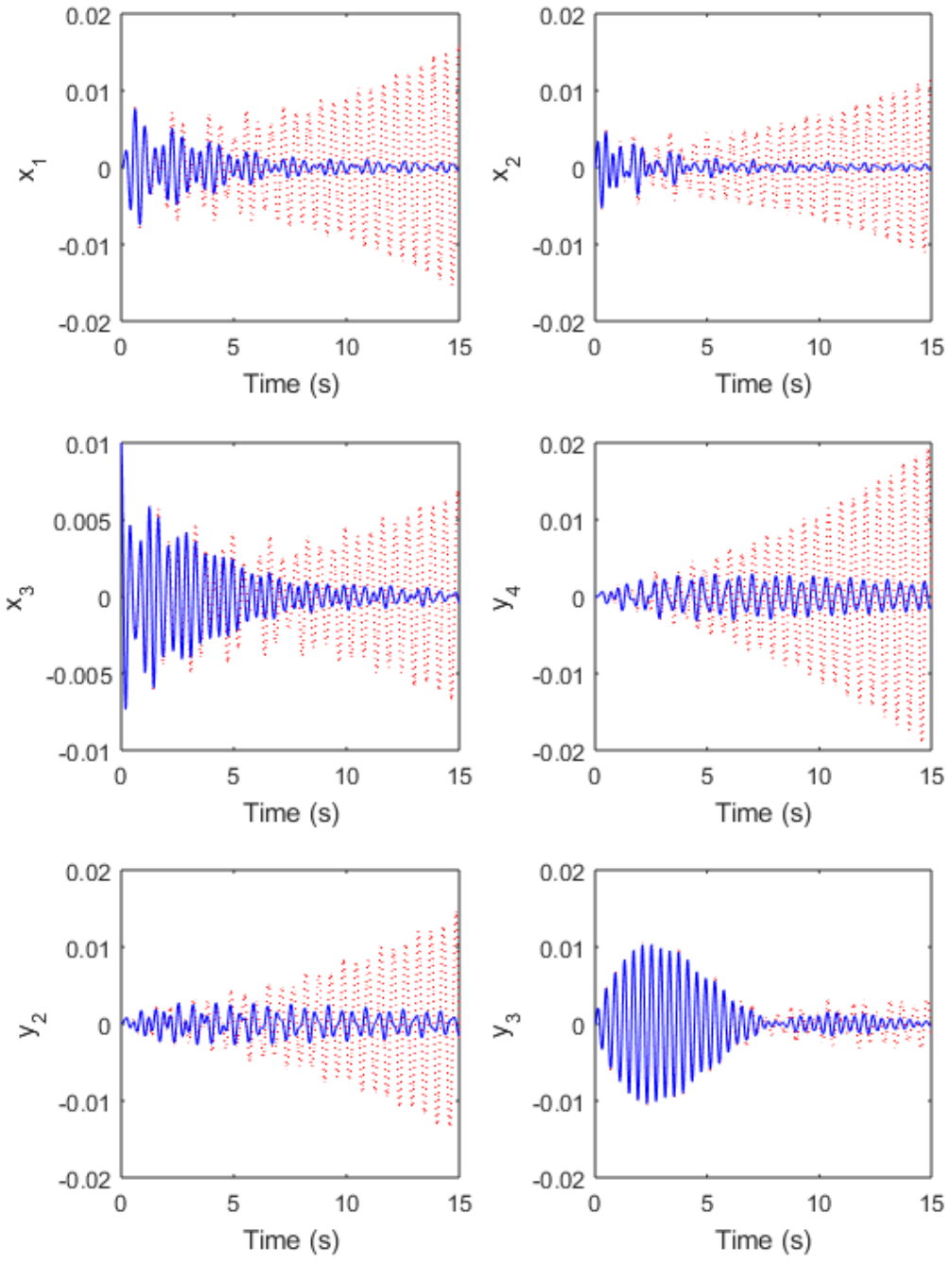

Figure 5.23: Displacement responses of the closed-loop system for Case VIII with $\tau_f = \tau_g = 0.05$: $\tau_1 = 0.15$ (blue solid line) and $\tau_2 = 0.18$ (red dotted line)

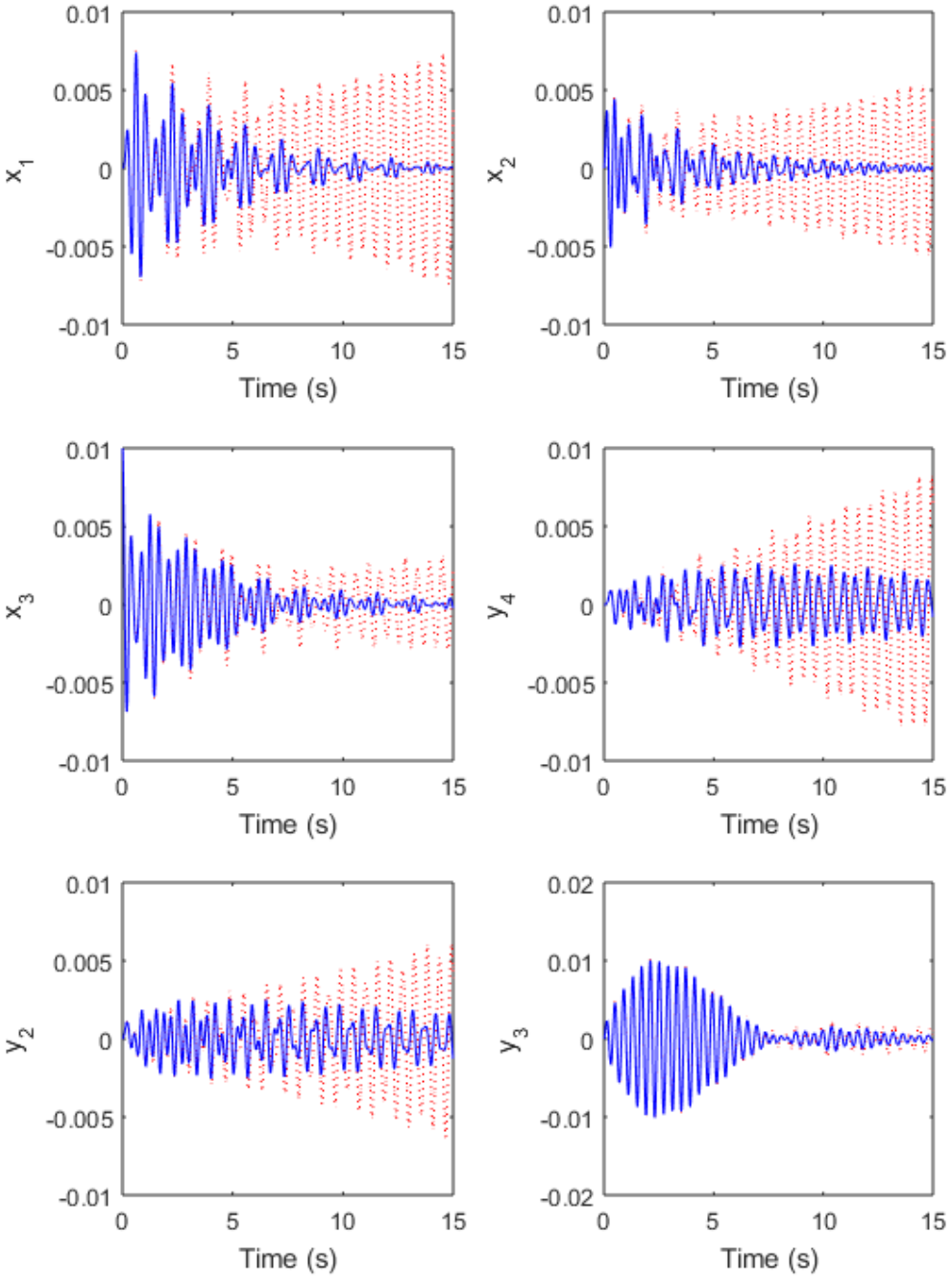

Figure 5.24: Displacement responses of the closed-loop system for Case VIII with $\tau_f = \tau_g = 0.10$: $\tau_1 = 0.21$ (blue solid line) and $\tau_2 = 0.23$ (red dotted line)

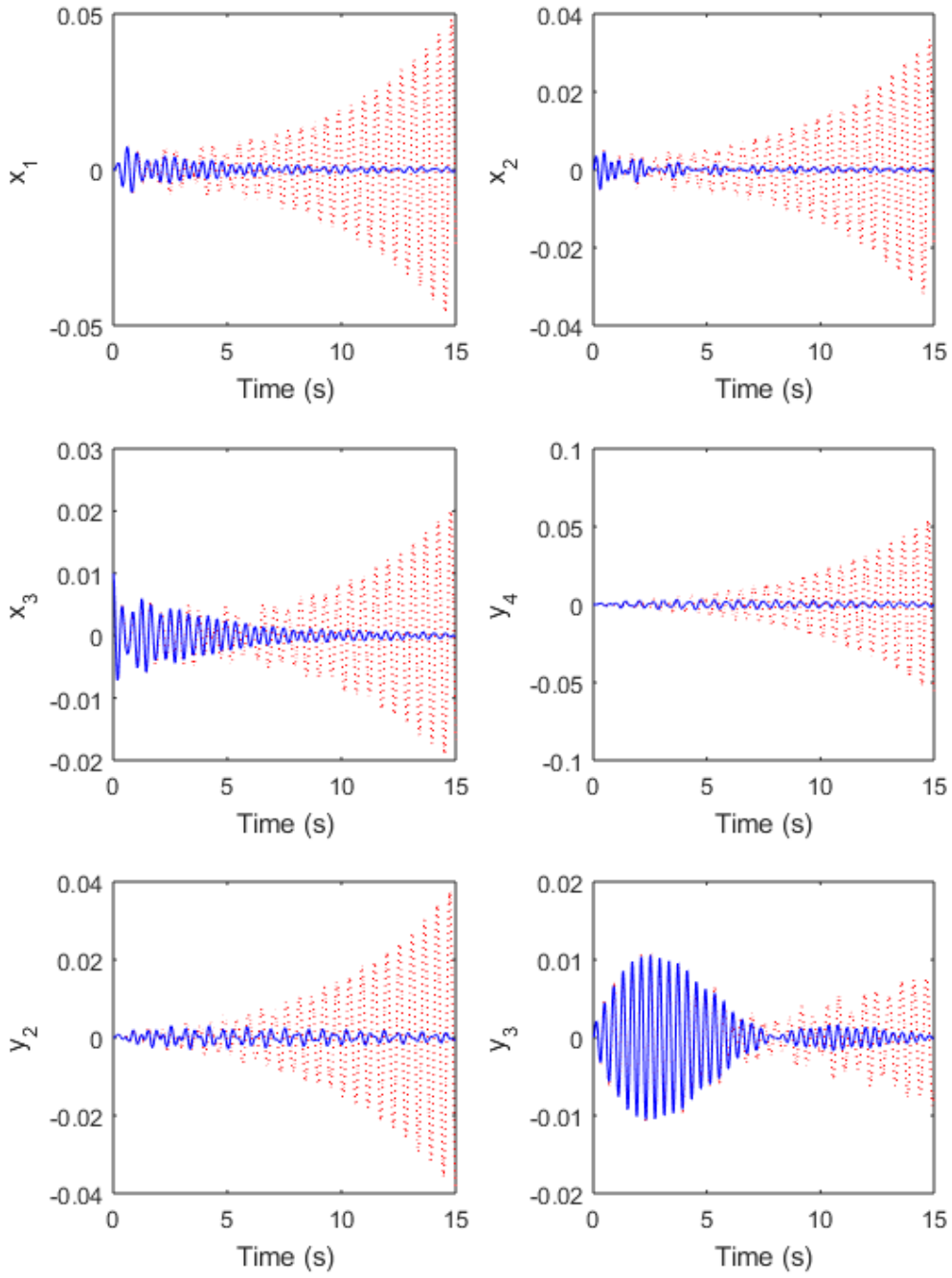

Figure 5.25: Displacement responses of the closed-loop system for Case VIII with $\tau_{\mathrm{f}} = 0.05, \tau_{\mathrm{g}} = 2\tau_{\mathrm{f}}$: $\tau_1 = 0.12$ (blue solid line) and $\tau_2 = 0.15$ (red dotted line)

5.4.3 Aerodynamic flutter

Flutter is an unstable oscillations which occurs in flexible structures because of aerodynamic, inertial and elastic forces. This phenomenon normally appears in aircraft, buildings, power lines and bridges. In the case of aircraft, flutter occurs when the airspeed increases over the critical point. This is because the damping of the wings is insufficient to absorb energy produced by the aerodynamic force. In order to solve this problem, the partial pole assignment with time delays is applied. A simple model of binary bending-torsion flutter of a rectangular cantilevered wing is shown in Figure 5.14. The aeroelastic equation of motion is given by Wright and Cooper (2008).

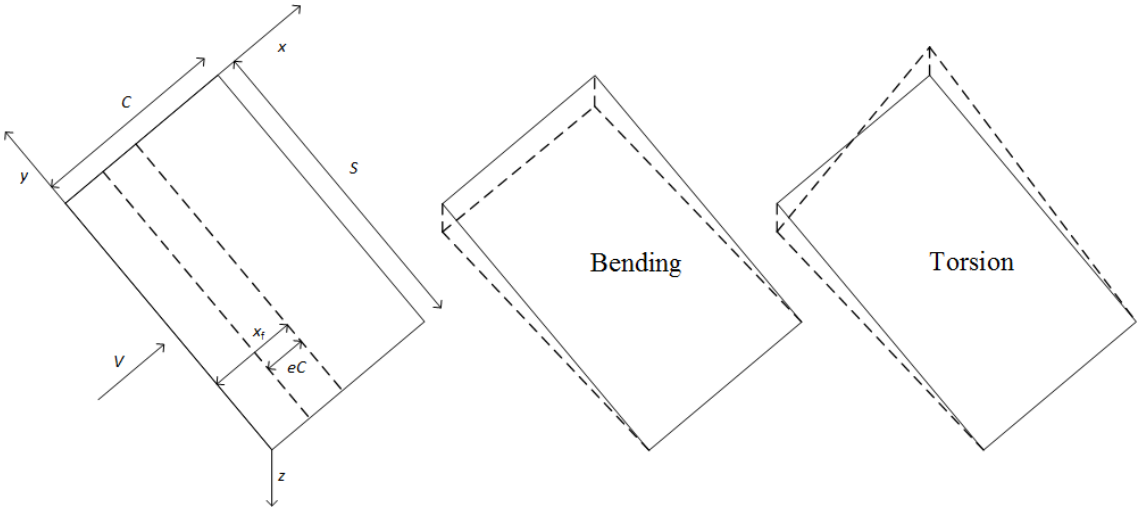

Figure 5.26: A rectangular wing showing bending and torsion modes

$$\mathbf{M}\ddot{\mathbf{q}} + (\rho V \mathbf{C}_{\text{as}} + \mathbf{C}_{\text{s}})\dot{\mathbf{q}} + (\rho V^2 \mathbf{K}_{\text{as}} + \mathbf{K}_{\text{s}})\mathbf{q} = 0, \tag{5.32}$$

$$\mathbf{M} = \begin{bmatrix} \frac{msc}{5} & \frac{ms}{4}(\frac{c^2}{2} - cx_{\text{f}}) \\ \frac{ms}{4}(\frac{c^2}{2} - cx_{\text{f}}) & \frac{ms}{3}(\frac{c^3}{3} - c^2x_{\text{f}} + cx_{\text{f}}^2) \end{bmatrix}, \mathbf{C}_{\text{as}} = \begin{bmatrix} \frac{csa_{\text{w}}}{10} & 0 \\ \frac{-c^2sea_{\text{w}}}{8} & \frac{-c^3sM_{\dot{\theta}}}{24} \end{bmatrix},$$

$$\mathbf{K}_{\text{as}} = \begin{bmatrix} 0 & \frac{csa_{\text{w}}}{8} \\ 0 & \frac{-c^2sea_{\text{w}}}{6} \end{bmatrix}, \mathbf{K}_{\text{s}} = \begin{bmatrix} \frac{4EI}{s^3} & 0 \\ 0 & \frac{GJ}{s} \end{bmatrix}, \mathbf{q} = \begin{pmatrix} q_b \\ q_t \end{pmatrix},$$

where $\mathbf{M}$, $\mathbf{C}_{\text{s}}$ and $\mathbf{K}_{\text{s}}$ are respectively the structural inertia, damping and stiffness (symmetric) matrices, $\mathbf{C}_{\text{as}}$ and $\mathbf{K}_{\text{as}}$ are the aerodynamic damping and stiffness (asymmetric) matrices and $\mathbf{q}$ is the generalised coordinate vector for bending q_{b} and torsion q_{t}, m is the mass per unit area of the wing, S is the wing span, C is the chord, x_{f} is the elastic axis location, EI is the bending rigidity, GJ is the torsional rigidity, a_{w} is the lift curve slope, $M_{\dot{\theta}}$ is the non-dimensional pitch damping derivative, e is the eccentricity between flexural axis and aero centre, ρ is the air density, and V is the air speed.

Parameters used are taken from Wright and Cooper (2008): mass per unit area of the wing, $m = 200$ kg/m^2; wing span, $S = 7.5$ m; chord, $C = 2$ m; elastic axis location, $x_\mathrm{f} = 0.48C$; bending rigidity, $EI = 2 \times 10^7$ Nm^2; torsional rigidity, $GJ = 2 \times 10^6$ Nm^2; lift curve slope, $a_\mathrm{w} = 2\pi$; non-dimensional pitch damping derivative, $M_{\dot{\theta}} = -1.2$; eccentricity between flexural axis and aero centre, $e = x_\mathrm{f}/C - 0.25$; air density, $\rho = 1.225$ kg/m^3; and air speed, $V = 150$ m/s. The damping matrix $\mathbf{C}_\mathrm{s}$ is ignored. The poles of the open-loop system are

$$\{\lambda\}_1^4 = \left\{ \begin{array}{c} 2.8961 \pm 18.7011\mathrm{i} \\ -5.2470 \pm 12.2944\mathrm{i} \end{array} \right\}.$$

This system is unstable because the first pair of poles has positive real parts. To stability this system pole assignment and partial pole assignment with time delays are implemented.

Two cases of required closed-loop poles are shown in Table 5.10. The actuator distribution vector; $\mathbf{b} = \{1, 1\}^\mathrm{T}$ is assumed. Velocity and displacement gain vectors for assigning the required closed-loop poles including the single time delay ($\tau_f = \tau_g = 0.02$ and 0.04) and the multiple time delays ($\tau_f = 0.02, \tau_g = 2\tau_\mathrm{f}$) are determined by solving the linear equations expressed in Eq.(5.10) for pole assignment and Eq.(5.15) for partial pole assignment. The control gains are shown in Table 5.11. The results are validated by applying Eq.(5.16). It is found that $|D|$ is close to zero for all cases. Hence, the algorithm of pole assignment with time delays and partial pole assignment with time delays by using the unobservability condition are successful to assign the required closed-loop poles in the aerodynamic flutter problem.

Then, TRACE-DDE toolbox in MATLAB (Breda et al. (2009)) is applied to determine the first ten closed-loop poles (see Table 5.12). As a result, the required closed-loop poles are placed precisely. The other poles are generated due to the effect of the time delays and located in the left-hand side of the complex plane. However, the stability does not guaranteed because the residue poles are not revealed. In order to ensure the stability, the frequency-sweeping test (Gu et al. (2003)) is also applied to determine the critical time delay.

Table 5.10: Required closed-loop poles of the aerodynamic flutter

Case IX	Case X
$-1.0000 \pm 20.0000\mathrm{i}$	$-1.0000 \pm 20.0000\mathrm{i}$
$-6.0000 \pm 13.0000\mathrm{i}$	$-5.2470 \pm 12.2944\mathrm{i}$

Table 5.11: Control gains obtained by pole assignment and partial pole assignment by using the unobservability condition for the aerodynamic flutter

Case	$\tau_f = \tau_g = 0.02$		$\tau_f = \tau_g = 0.04$		$\tau_f = 0.02, \tau_g = 2\tau_f$	
	$\mathbf{g} \times 10^3$	$\mathbf{f} \times 10^3$	$\mathbf{g} \times 10^3$	$\mathbf{f} \times 10^3$	$\mathbf{g} \times 10^3$	$\mathbf{f} \times 10^3$
IX	5.7940	0.8022	0.0399	0.8698	6.2112	0.9245
	10.9553	2.7483	−11.3750	2.1673	12.3345	3.0177
X	7.1391	0.8353	0.9122	0.9053	7.6689	0.9892
	5.8938	2.2573	−13.3718	1.7708	7.1139	2.4098

Table 5.12: First ten poles of the closed-loop system with time delays obtained by TRACE-DDE toolbox in MATLAB (sorted by the real part) for the aerodynamic flutter

Case	$\tau_f = \tau_g = 0.02$	$\tau_f = \tau_g = 0.04$	$\tau_f = 0.02, \tau_g = 2\tau_f$
IX	-1.0000 ± 20.0000i	-1.0000 ± 20.0000i	-1.0000 ± 20.0000i
	-6.0000 ± 13.0000i	-6.0000 ± 13.0000i	-6.0000 ± 13.0000i
	-138.72	-46.644	-106.61 ± 963.933i
	-191.44 ± 368.214i	-82.158 ± 186.339i	-107.96 ± 963.203i
	-219.22 ± 691.215i	-96.639 ± 346.919i	-142.01 ± 779.618i
X	-1.0000 ± 20.0000i	-1.0000 ± 20.0000i	-1.0000 ± 20.0000i
	-5.2470 ± 12.2944i	-5.2470 ± 12.2944i	-5.2470 ± 12.2944i
	-150.34	-52.893	-106.83 ± 963.818i
	-199.84 ± 367.372i	-86.093 ± 186.016i	-107.96 ± 963.203i
	-227.41 ± 690.728i	-100.53 ± 346.748i	-142.01 ± 779.618i

Table 5.13: The closed-loop system without time delays for the aerodynamic flutter

Case	$\tau_f = \tau_g = 0.02$	$\tau_f = \tau_g = 0.04$	$\tau_f = 0.02, \tau_g = 2\tau_f$
IX	-0.7660 ± 18.4347i	-0.1107 ± 17.0021i	-1.1560 ± 18.1666i
	-6.1115 ± 12.6191i	-5.9906 ± 12.1652i	-6.1985 ± 12.8793i
X	-0.9562 ± 18.3603i	-0.3165 ± 16.7487i	-1.5049 ± 18.0270i
	-5.2470 ± 12.2944i	-5.2470 ± 12.2944i	-5.0327 ± 12.6765i

Table 5.14: Critical time delay for the aerodynamic flutter

Case	$\tau_f = \tau_g = 0.02$	$\tau_f = \tau_g = 0.04$	$\tau_f = 0.02, \tau_g = 2\tau_f$
IX	0.0393	0.0548	0.0365
X	0.0387	0.0551	0.0352

Due to the stability of the closed-loop system without time delay (see Table 5.13), the critical time delay can be evaluated by using Eq.(5.25) and Eq.(5.30) for the single time delay and the multiple time delays respectively. As can be seen, the time delays are smaller than the critical ones which indicates the stability of the closed-loop system. The critical time delay is validated by plotting displacement responses with the given initial conditions: $\mathbf{q} = \{0, 0.01\}^{\mathrm{T}}$, $\dot{\mathbf{q}} = \{0, 0\}^{\mathrm{T}}$. It is clear from Figure 5.27 - Figure 5.32 that the closed-loop system with τ_1 is asymptotically stable ($\tau_1 < \overline{\tau}$), τ_2 is unstable ($\tau_2 > \overline{\tau}$) and τ_3 is marginally stable ($\tau_3 = \overline{\tau}$).

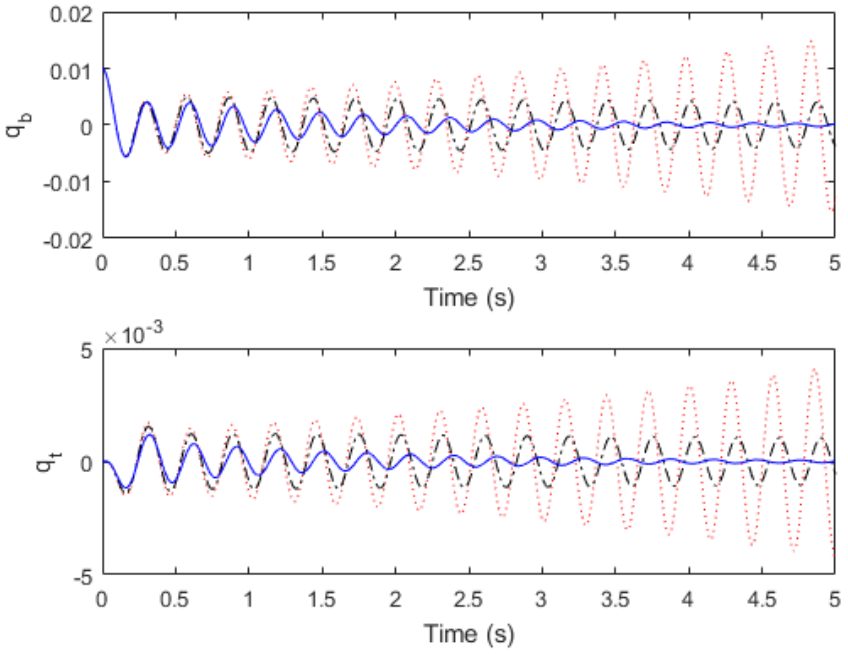

Figure 5.27: Displacement responses of the closed-loop system for Case IX with $\tau_{\mathrm{f}} = \tau_{\mathrm{g}} = 0.02$: $\tau_1 = 0.032$ (blue solid line), $\tau_2 = 0.042$ (red dotted line) and $\tau_3 = \overline{\tau}$ (black dashed line)

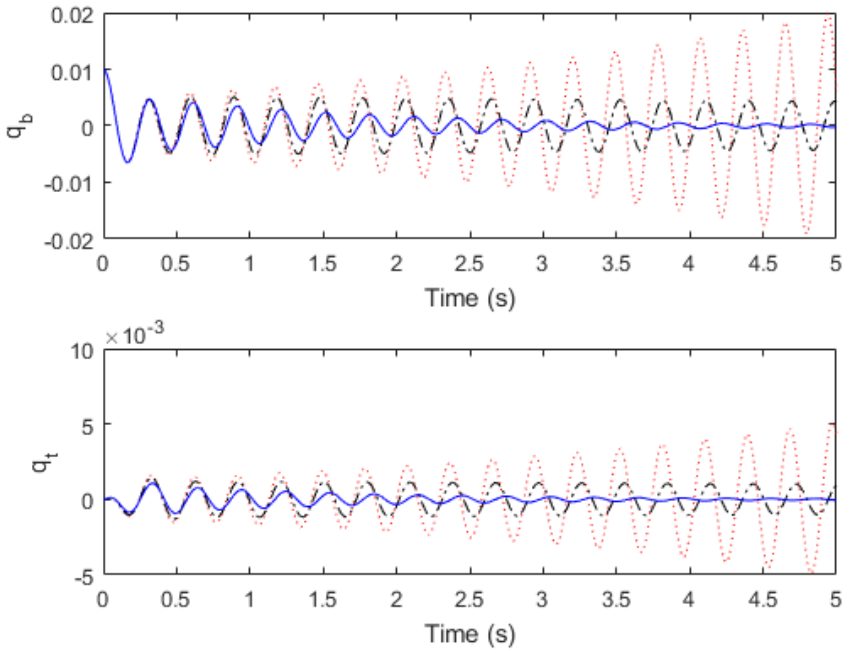

Figure 5.28: Displacement responses of the closed-loop system for Case IX with $\tau_f = \tau_g = 0.04$: $\tau_1 = 0.048$ (blue solid line), $\tau_2 = 0.058$ (red dotted line) and $\tau_3 = \overline{\tau}$ (black dashed line)

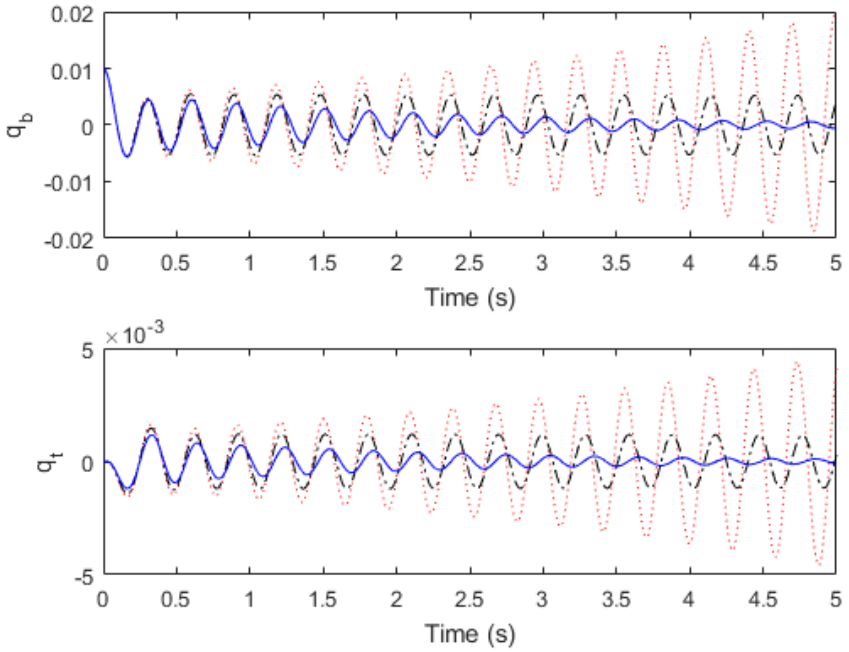

Figure 5.29: Displacement responses of the closed-loop system for Case IX with $\tau_f = 0.02, \tau_g = 2\tau_f$: $\tau_1 = 0.030$ (blue solid line), $\tau_2 = 0.040$ (red dotted line) $\tau_3 = \overline{\tau}$ (black dashed line)

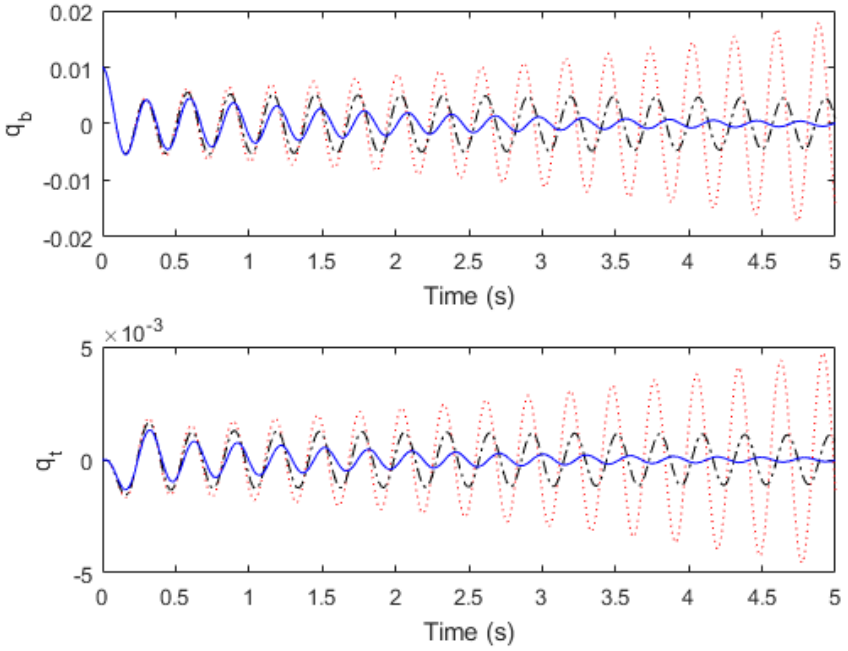

Figure 5.30: Displacement responses of the closed-loop system for Case X with $\tau_f = \tau_g = 0.02$: $\tau_1 = 0.032$ (blue solid line), $\tau_2 = 0.042$ (red dotted line) $\tau_3 = \overline{\tau}$ (black dashed line)

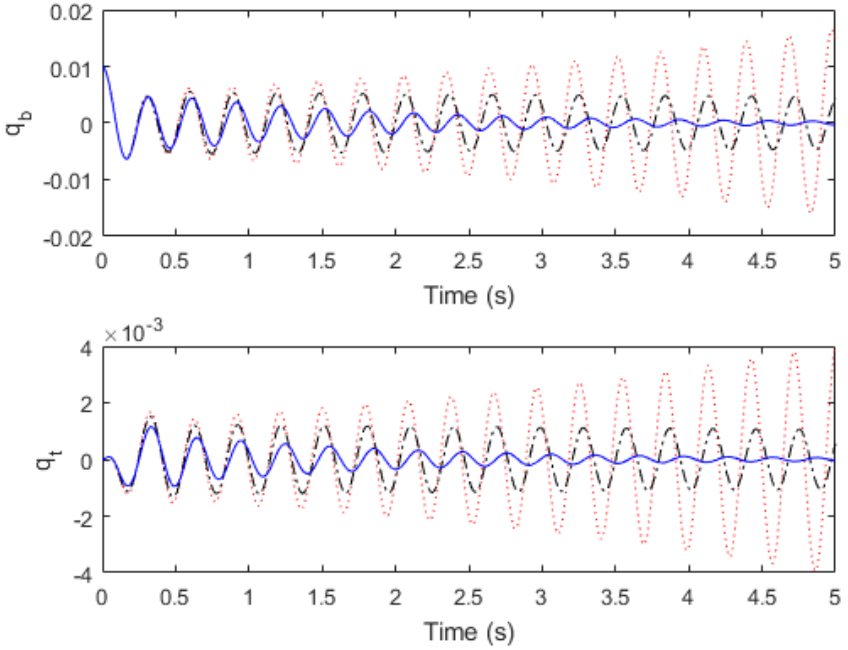

Figure 5.31: Displacement responses of the closed-loop system for Case X with $\tau_f = \tau_g = 0.04$: $\tau_1 = 0.048$ (blue solid line), $\tau_2 = 0.058$ (red dotted line) $\tau_3 = \overline{\tau}$ (black dashed line)

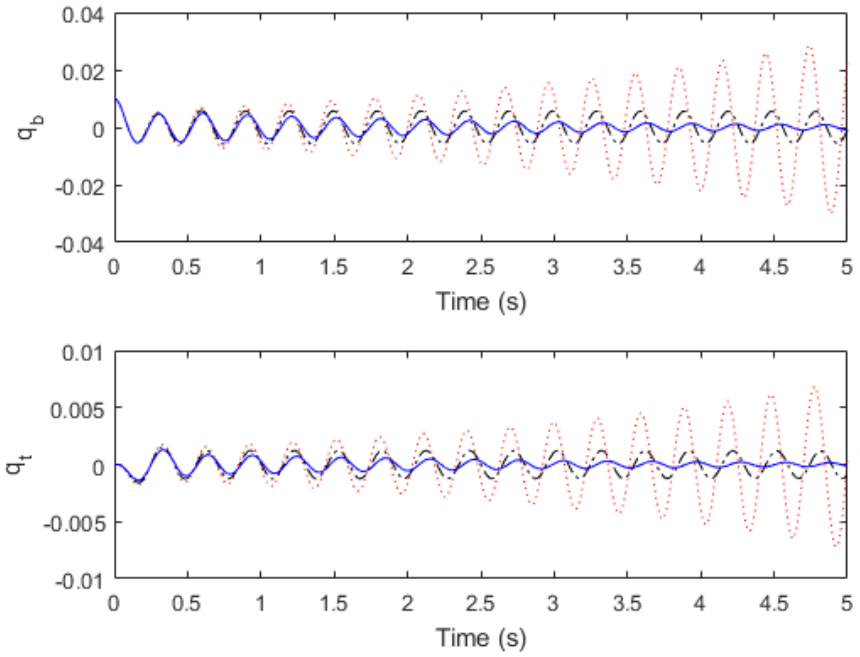

Figure 5.32: Displacement responses of the closed-loop system for Case X with $\tau_f = 0.02, \tau_g = 2\tau_f$: $\tau_1 = 0.030$ (blue solid line), $\tau_2 = 0.040$ (red dotted line) $\tau_3 = \overline{\tau}$ (black dashed line)

5.5 Summary

In this chapter, active partial pole assignment with time delays to the asymmetric system using the single-input state feedback control is developed. The unobservability condition is applied to keep some poles unchanged. The receptance method is used to avoid modelling errors from FEM and Sherman-Morrison formula is used to formulate the partial pole assignment problem in linear equations which can be solved directly. Both single time delay and multiple commensurate time delays are tested to ensure that the proposed method can assign the required closed-loop poles precisely without the spill-over effect.

Three numerical examples, two cases of friction-induced vibration and a case of aerodynamic flutter, show that the proposed method is capable to assign partial poles precisely although the time delays are included. Stability is investigated by using TRACE-DDE toolbox in MATLAB to determine the dominant closed-loop poles. It is clear that the number of the closed-loop poles is higher than $2n$ poles due to the effect of the time delays. Some closed-loop poles calculated by TRACE-DDE are exactly the same as the required ones and the others generated by the effect of the time delays are located in the left-hand side of the complex plane. This means that the closed-loop system may

be stable. However, the stability does not guarantee since the locations of the residual poles are not completely known yet.

To ensure the stability, the frequency-sweeping test is applied. In the case of the asymmetric system, the closed-loop system cannot be the delay-independent stability because the open-loop poles are unstable (Eq.(5.22) and Eq.(5.27) are unsatisfied). This indicates that the closed-loop system may be either the delay-dependent stability or instability. To identify the system, the critical time delay is determined. The results show that the closed-loop systems for all cases are stable because the given time delays are smaller than the critical ones.

Chapter 6

Robust Pole Assignment for Asymmetric Systems

An Asymmetric system exemplified by the friction-induced vibration and the aerodynamic flutter are stabilised by active pole assignment. Existing algorithms of pole assignment yields the high accuracy only when perturbations are disregarded. In fact, the perturbations are inevitable in the system and make the closed-loop poles shifted from their desired positions which cause the destabilisation of the system. To deal with this problem, sensitivities of the closed-loop poles with respect to uncertain parameters must be minimised. In this chapter, a new method of robust pole assignment for the asymmetric system is proposed. This method applies two control strategies, which are the single-input and the multiple-input state feedback controls. The uncertain parameters i.e. a friction coefficient, a contact damping, a contact stiffness (friction-induced vibration), an air density and an air speed (aerodynamic flutter) are processed by the generic algorithm in order to minimise Frobenius norm of the sensitivity matrix. The quantitative results demonstrate that closed-loop poles are assigned to the appropriate locations with their minimum sensitivities.

Although most structural systems are symmetric and naturally stable, some systems are asymmetric and prone to instability because of non-conservative forces such as friction and aerodynamic forces. These forces generate asymmetric damping and/or stiffness matrices exemplified by the friction-induced vibration problem (Hoffmann et al. (2002); Vahid-Araghi and Golnaraghi (2010)) and the aerodynamic flutter problem (Wright and Cooper (2008)). To stabilise the unstable friction-induced vibration, Ouyang (2009, 2010, 2011) introduced three control methods: a passive structural modification, an active pole assignment and a hybrid method (combination of the passive structural modification and the active pole assignment), to shift poles from positive to negative real parts of the complex plane.

For the symmetric system, pole assignment by the formulation of the first-order differential equation is mostly used in general control theory (Wonham (1967); Andry et al. (1983); Kautsky et al. (1985); Li and Yam (2001)) but it is not ideal for vibration control. Therefore, pole assignment formulated in the second-order differential equation having natural formulation for vibration problems, the improvement technique, was proposed (Juang and Maghami (1992); Chu and Datta (1996); Ram (1998); Chu (2002)). This formulation requires knowledge of mass, damping and stiffness matrices, which are evaluated by the numerical methods such as FEM.

Yang et al. (2016) proposed the finite element model updating method to maintain symmetric matrices and prevent spillover effect. However, due to assumptions of proportional damping, boundary condition, and model reduction, there are always modelling errors from FEM. To deal with these problems, Ram and Mottershead (2007) applied the receptance method in the single-input state feedback control to mitigate modelling errors. Based on their previous work, the same approach was adapted to variety of usages: pole-zero assignment to control the first two modes of a T-shaped plate (Mottershead et al. (2008)), pole assignment with time delay (Ram et al. (2009, 2011)), partial pole assignment (Tehrani et al. (2010); Ram et al. (2011); Ram and Mottershead (2013)), robust pole assignment (Mottershead et al. (2008); Tehrani et al. (2011)) and eigenstructure assignment (Liu et al. (2015)).

All above-mentioned works dealt with algorithms of pole/partial pole assignment, which are efficient only when the perturbations are absent. Nonetheless, the perturbations, which may destabilise a system, are always generated by the uncertain parameters, such as system matrices (mass, damping, stiffness) and control gains. Influences of perturbations are significant in the system and they are subjected to be reduced. One approach to achieve this goal is to decrease sensitivities of poles. Mottershead et al. (2009) and Tehrani et al. (2011) proposed a method to assign both closed-loop poles and their sensitivities with respect to control gains and measured receptances.

Furthermore, for the asymmetric system, Ouyang (2010, 2011) applied the receptance method to the active pole assignment for stabilising the friction-induced vibration. Tehrani and Ouyang (2012) and citeliang2016active extended previous works to partial pole assignment by using the uncontrollability and the unobservability conditions. Singh and Ouyang (2013) and citeariyatanapol2018partial introduced pole assignment with time delay and partial pole assignment with time delay respectively. Liang et al. (2017) studied pole sensitivity assignment for assigning both closed-loop poles and their sensitivities with respect to the friction coefficient by using the single-input state feedback control. However, both of them are not assigned precisely because the number of equations is higher than the number of the control gains.

In this work, a new method of robust pole assignment for the asymmetric system is proposed to assign the closed-loop poles with their minimum sensitivities. It aims to reduce the influences of the perturbations by minimising the sensitivities of the closed-loop poles. The receptance method is applied to derive the sensitivities of the closed-loop poles with respect to the uncertain parameters i.e. the coefficient of friction, the contact damping, the contact stiffness(friction-induced vibration), the air density and the air speed (aerodynamic flutter). Both cases: single-input and multiple-input state feedback controls are considered. The genetic algorithm, is implemented to minimise Frobenius norm of the sensitivity matrix. Numerical examples of the friction-induced vibration and the aerodynamic flutter are demonstrated to indicate the effectiveness of the proposed method.

6.1 Introductory of pole assignment by using the receptance method

6.1.1 Single-input control

The dynamic equation of the asymmetric system including velocity and displacement feedback for the single-input control presented in Ouyang (2010) can be written as

$$\left(s^2\mathbf{M} + s(\mathbf{C}_\mathrm{s} + \mathbf{C}_\mathrm{as}) + \mathbf{K}_\mathrm{s} + \mathbf{K}_\mathrm{as}\right)\mathbf{x}(s) = \mathbf{b}u(s) + \mathbf{p}(s), \tag{6.1}$$

$$u(s) = -(s\mathbf{f}^\mathrm{T} + \mathbf{g}^\mathrm{T})\mathbf{x}(s). \tag{6.2}$$

Then, combining Eq.(6.1) and Eq.(6.2) and rearranging, the closed-loop receptance is expressed as

$$\widehat{\mathbf{H}}_\mathrm{as}(s) = \mathbf{H}_\mathrm{as}(s) - \frac{\mathbf{H}_\mathrm{as}(s)\mathbf{b}(s\mathbf{f}^\mathrm{T} + \mathbf{g}^\mathrm{T})\mathbf{H}_\mathrm{as}(s)}{1 + (s\mathbf{f}^\mathrm{T} + \mathbf{g}^\mathrm{T})\mathbf{H}_\mathrm{as}(s)\mathbf{b}}. \tag{6.3}$$

It can be seen that the poles of the closed-loop system satisfy the following characteristic equation:

$$\Lambda = 1 + \mathbf{r}^\mathrm{T}(s\mathbf{f} + \mathbf{g}) = 0, \tag{6.4}$$

$$\mathbf{r} = \mathbf{H}_\mathrm{as}\mathbf{b}. \tag{6.5}$$

6.1.2 Multiple-input control

The dynamic equation of the asymmetric system including velocity and displacement feedback for with the multiple-input control can be written as

$$\big(s^2\mathbf{M} + s(\mathbf{C}_\mathrm{s} + \mathbf{C}_\mathrm{as}) + \mathbf{K}_\mathrm{s} + \mathbf{K}_\mathrm{as}\big)\mathbf{x}(s) = \mathbf{B}\mathbf{u}(s) + \mathbf{p}(s), \tag{6.6}$$

$$\mathbf{u}(s) = -(s\mathbf{F}^\mathrm{T} + \mathbf{G}^\mathrm{T})\mathbf{x}(s), \tag{6.7}$$

where $\mathbf{B}$, $\mathbf{F}$ and $\mathbf{G} \in \mathbb{R}^{n\times m}$ are respectively actuator distribution, velocity gain and displacement gain matrices; $\mathbf{u} \in \mathbb{C}^{m\times 1}$ is the multiple-input control.

Then, combining Eq.(6.6) and Eq.(6.7) and rearranging, the closed-loop receptance is expressed as

$$\widehat{\mathbf{H}}_\mathrm{as}(s) = \frac{\mathrm{adj}(\mathbf{H}_\mathrm{as}^{-1}(s) + s\mathbf{B}\mathbf{F}^\mathrm{T} + \mathbf{B}\mathbf{G}^\mathrm{T})}{\det(\mathbf{H}_\mathrm{as}^{-1}(s) + s\mathbf{B}\mathbf{F}^\mathrm{T} + \mathbf{B}\mathbf{G}^\mathrm{T})}, \tag{6.8}$$

where adj(•) and det(•) are respectively adjoint and determinant of the matrix. The poles of the closed-loop system satisfy the following characteristic equation:

$$\Lambda = \det(\mathbf{H}_\mathrm{as}^{-1}(s) + s\mathbf{B}\mathbf{F}^\mathrm{T} + \mathbf{B}\mathbf{G}^\mathrm{T}) = 0. \tag{6.9}$$

6.2 Sensitivities of the closed-loop poles

The previous section introduces pole assignment for the asymmetric system. It can assign the required closed-loop poles precisely when perturbations are excluded. Nonetheless, perturbations always exist in the system as aforementioned. The perturbation levels are associated with the sensitivities of the closed-loop poles in the directly proportional fashion. If the sensitivities are high, a large perturbation will appear in the system. Therefore, it is important to minimise the sensitivities of the closed-loop poles. This section shows the formulas to determine the sensitivities of the closed-loop poles with respect to the uncertain parameters, i.e., the friction coefficient, the contact damping, the contact stiffness (friction-induced vibration), the air density and the air speed (aerodynamic flutter).

6.2.1 Friction-induced vibration

The open-loop receptance of the friction-induced vibration is given by

$$\mathbf{H}_\mathrm{as} = \big(s^2\mathbf{M} + s(\mathbf{C}_\mathrm{s} + \mathbf{C}_\mathrm{as}) + \mathbf{K}_\mathrm{s} + \mathbf{K}_\mathrm{as}\big)^{-1}. \tag{6.10}$$

The asymmetric damping and stiffness matrices of the friction-induced vibration, for example a disc brake model, can be expressed as (Ouyang (2009))

$$\mathbf{C}_{\text{as}} = \sum_{k=1}^{m} \mu_{\text{c},k} c_{\text{c},k} \mathbf{E}_k, \tag{6.11}$$

$$\mathbf{K}_{\text{as}} = \sum_{k=1}^{m} \mu_{\text{c},k} k_{\text{c},k} \mathbf{E}_k, \tag{6.12}$$

where μ_{c} is the friction coefficient, c_{c} and k_{c} are respectively the contact damping and the contact stiffness and $\mathbf{E}$ is the asymmetric matrix contained only one non-zero element corresponding to μ_{c}.

Three uncertain parameters: the friction coefficient, the contact damping and the contact stiffness, are applied to derive the sensitivity of the closed-loop pole. Considering a small perturbation of the friction coefficient, Eq.(6.4) for the single-input control and Eq.(6.9) for the multiple-input control can be rewritten by using the first-order Taylor expansion (Liang et al. (2017)):

$$\Lambda(\mu_{\text{c}} + \delta\mu_{\text{c}}, s + \delta s) = \Lambda(\mu_{\text{c}}, s) + \frac{\partial \Lambda}{\partial \mu_{\text{c}}} \delta\mu_{\text{c}} + \frac{\partial \Lambda}{\partial s} \delta s = 0. \tag{6.13}$$

Rearranging Eq.(6.13), the sensitivity of the closed-loop pole with respect to the friction coefficient is expressed as

$$S_{\mu_{\text{c},k},i} = \left.\frac{\partial s}{\partial \mu_{\text{c},k}}\right|_{s=\mu_i} = -\left.\frac{\partial \Lambda}{\partial \mu_{\text{c},k}} \Big/ \frac{\partial \Lambda}{\partial s}\right|_{s=\mu_i}, \tag{6.14}$$

where μ_i is the closed-loop pole.

Similarly, the sensitivities of the closed-loop poles with respect to the contact damping and the contact stiffness are expressed as

$$S_{c_{\text{c},k},i} = \left.\frac{\partial s}{\partial c_{\text{c},k}}\right|_{s=\mu_i} = -\left.\frac{\partial \Lambda}{\partial c_{\text{c},k}} \Big/ \frac{\partial \Lambda}{\partial s}\right|_{s=\mu_i}, \tag{6.15}$$

$$S_{k_{\text{c},k},i} = \left.\frac{\partial s}{\partial k_{\text{c},k}}\right|_{s=\mu_i} = -\left.\frac{\partial \Lambda}{\partial k_{\text{c},k}} \Big/ \frac{\partial \Lambda}{\partial s}\right|_{s=\mu_i}. \tag{6.16}$$

For the single-input control, the parameters in Eq.(6.14) - Eq.(6.16) are given by

$$\frac{\partial \Lambda}{\partial s} = \left(\frac{\partial \mathbf{r}}{\partial s}\right)^{\text{T}} \mathbf{g} + \left(s\left(\frac{\partial \mathbf{r}}{\partial s}\right)^{\text{T}} + \mathbf{r}^{\text{T}}\right)\mathbf{f}, \tag{6.17}$$

$$\frac{\partial \Lambda}{\partial \mu_{\text{c},k}} = \left(\frac{\partial \mathbf{r}}{\partial \mu_{\text{c},k}}\right)^{\text{T}} \mathbf{g} + s\left(\frac{\partial \mathbf{r}}{\partial \mu_{\text{c},k}}\right)^{\text{T}} \mathbf{f}, \tag{6.18}$$

$$\frac{\partial \Lambda}{\partial c_{\mathrm{c},k}} = \Big(\frac{\partial \mathbf{r}}{\partial c_{\mathrm{c},k}}\Big)^{\mathrm{T}}\mathbf{g} + s\Big(\frac{\partial \mathbf{r}}{\partial c_{\mathrm{c},k}}\Big)^{\mathrm{T}}\mathbf{f}, \tag{6.19}$$

$$\frac{\partial \Lambda}{\partial k_{\mathrm{c},k}} = \Big(\frac{\partial \mathbf{r}}{\partial k_{\mathrm{c},k}}\Big)^{\mathrm{T}}\mathbf{g} + s\Big(\frac{\partial \mathbf{r}}{\partial k_{\mathrm{c},k}}\Big)^{\mathrm{T}}\mathbf{f}, \tag{6.20}$$

where

$$\frac{\partial \mathbf{r}}{\partial s} = -\mathbf{H}_{\mathrm{as}}(2s\mathbf{M} + \mathbf{C}_{\mathrm{s}} + \mathbf{C}_{\mathrm{as}})\mathbf{H}_{\mathrm{as}}\mathbf{b}, \tag{6.21}$$

$$\frac{\partial \mathbf{r}}{\partial \mu_{\mathrm{c},k}} = -\mathbf{H}_{\mathrm{as}}(sc_{\mathrm{c},k}\mathbf{E}_k + k_{\mathrm{c},k}\mathbf{E}_k)\mathbf{H}_{\mathrm{as}}\mathbf{b}, \tag{6.22}$$

$$\frac{\partial \mathbf{r}}{\partial c_{\mathrm{c},k}} = -\mathbf{H}_{\mathrm{as}}(s\mu_{\mathrm{c},k}\mathbf{E}_k)\mathbf{H}_{\mathrm{as}}\mathbf{b}, \tag{6.23}$$

$$\frac{\partial \mathbf{r}}{\partial k_{\mathrm{c},k}} = -\mathbf{H}_{\mathrm{as}}(\mu_{\mathrm{c},k}\mathbf{E}_k)\mathbf{H}_{\mathrm{as}}\mathbf{b}. \tag{6.24}$$

For the multiple-input control, the parameters in Eq.(6.14) - Eq.(6.16) are derived by using Jacobi's formula.

$$\frac{\partial \Lambda}{\partial s} = \mathrm{tr}\big(\mathrm{adj}(\mathbf{H}_{\mathrm{as}}^{-1} + s\mathbf{B}\mathbf{F}^{\mathrm{T}} + \mathbf{B}\mathbf{G}^{\mathrm{T}})(2s\mathbf{M} + \mathbf{C}_{\mathrm{s}} + \mathbf{C}_{\mathrm{as}} + \mathbf{B}\mathbf{F}^{\mathrm{T}})\big), \tag{6.25}$$

$$\frac{\partial \Lambda}{\partial \mu_{\mathrm{c},k}} = \mathrm{tr}\big(\mathrm{adj}(\mathbf{H}_{\mathrm{as}}^{-1} + s\mathbf{B}\mathbf{F}^{\mathrm{T}} + \mathbf{B}\mathbf{G}^{\mathrm{T}})(sc_{\mathrm{c},k}\mathbf{E}_k + k_{\mathrm{c},k}\mathbf{E}_k)\big), \tag{6.26}$$

$$\frac{\partial \Lambda}{\partial c_{\mathrm{c},k}} = \mathrm{tr}\big(\mathrm{adj}(\mathbf{H}_{\mathrm{as}}^{-1} + s\mathbf{B}\mathbf{F}^{\mathrm{T}} + \mathbf{B}\mathbf{G}^{\mathrm{T}})(s\mu_{\mathrm{c},k}\mathbf{E}_k)\big), \tag{6.27}$$

$$\frac{\partial \Lambda}{\partial k_{\mathrm{c},k}} = \mathrm{tr}\big(\mathrm{adj}(\mathbf{H}_{\mathrm{as}}^{-1} + s\mathbf{B}\mathbf{F}^{\mathrm{T}} + \mathbf{B}\mathbf{G}^{\mathrm{T}})(\mu_{\mathrm{c},k}\mathbf{E}_k)\big), \tag{6.28}$$

where $\mathrm{tr}(\bullet)$ denotes trace of the matrix.

The sensitivities of closed-loop poles with respect to the friction coefficient, the contact damping and the contact stiffness can be expressed in matrix form as shown below:

$$\mathbf{S}_{\mathrm{FIV}} = \begin{bmatrix}\mathbf{S}_{\mu_{\mathrm{c}}} & \mathbf{S}_{c_{\mathrm{c}}} & \mathbf{S}_{k_{\mathrm{c}}}\end{bmatrix}, \tag{6.29}$$

where

$$\mathbf{S}_{\mu_{\mathrm{c}}} = \begin{bmatrix} S_{\mu_{\mathrm{c},1},1} & S_{\mu_{\mathrm{c},2},1} & \cdots & S_{\mu_{\mathrm{c},m},1} \\ S_{\mu_{\mathrm{c},1},2} & S_{\mu_{\mathrm{c},2},2} & \cdots & S_{\mu_{\mathrm{c},m},2} \\ \vdots & \vdots & \ddots & \vdots \\ S_{\mu_{\mathrm{c},1},2n} & S_{\mu_{\mathrm{c},2},2n} & \cdots & S_{\mu_{\mathrm{c},m},2n} \end{bmatrix}, \tag{6.30}$$

$$\mathbf{S}_{c_c} = \begin{bmatrix} S_{c_{c,1},1} & S_{c_{c,2},1} & \dots & S_{c_{c,m},1} \\ S_{c_{c,1},2} & S_{c_{c,2},2} & \dots & S_{c_{c,m},2} \\ \vdots & \vdots & \ddots & \vdots \\ S_{c_{c,1},2n} & S_{c_{c,2},2n} & \dots & S_{c_{c,m},2n} \end{bmatrix}, \tag{6.31}$$

$$\mathbf{S}_{k_c} = \begin{bmatrix} S_{k_{c,1},1} & S_{k_{c,2},1} & \dots & S_{k_{c,m},1} \\ S_{k_{c,1},2} & S_{k_{c,2},2} & \dots & S_{k_{c,m},2} \\ \vdots & \vdots & \ddots & \vdots \\ S_{k_{c,1},2n} & S_{k_{c,2},2n} & \dots & S_{k_{c,m},2n} \end{bmatrix}. \tag{6.32}$$

6.2.2 Aerodynamic flutter

The open-loop receptance of the aerodynamic flutter is given by (Wright and Cooper (2008))

$$\mathbf{H}_{\text{as}} = \left(s^2\mathbf{M} + s(\mathbf{C}_{\text{s}} + \rho V \mathbf{C}_{\text{as}}) + \mathbf{K}_{\text{s}} + \rho V^2 \mathbf{K}_{\text{as}}\right)^{-1}, \tag{6.33}$$

where ρ and V are respectively the air density and the air speed.

The sensitivity of the closed-loop pole with respect to the air density and the air speed are expressed as

$$S_{\rho,i} = \left.\frac{\partial s}{\partial \rho}\right|_{s=\mu_i} = -\frac{\partial \Lambda}{\partial \rho} \Big/ \left.\frac{\partial \Lambda}{\partial s}\right|_{s=\mu_i}. \tag{6.34}$$

$$S_{V,i} = \left.\frac{\partial s}{\partial V}\right|_{s=\mu_i} = -\frac{\partial \Lambda}{\partial V} \Big/ \left.\frac{\partial \Lambda}{\partial s}\right|_{s=\mu_i}. \tag{6.35}$$

Considering on the single-input control, the parameters in Eq.(6.34) and Eq.(6.35) are given by

$$\frac{\partial \Lambda}{\partial s} = \left(\frac{\partial \mathbf{r}}{\partial s}\right)^{\text{T}} \mathbf{g} + \left(s\left(\frac{\partial \mathbf{r}}{\partial s}\right)^{\text{T}} + \mathbf{r}^{\text{T}}\right)\mathbf{f}, \tag{6.36}$$

$$\frac{\partial \Lambda}{\partial \rho} = \left(\frac{\partial \mathbf{r}}{\partial \rho}\right)^{\text{T}} \mathbf{g} + s\left(\frac{\partial \mathbf{r}}{\partial \rho}\right)^{\text{T}} \mathbf{f}, \tag{6.37}$$

$$\frac{\partial \Lambda}{\partial V} = \left(\frac{\partial \mathbf{r}}{\partial V}\right)^{\text{T}} \mathbf{g} + s\left(\frac{\partial \mathbf{r}}{\partial V}\right)^{\text{T}} \mathbf{f}, \tag{6.38}$$

where

$$\frac{\partial \mathbf{r}}{\partial s} = -\mathbf{H}_{\text{as}}(2s\mathbf{M} + \mathbf{C}_{\text{s}} + \rho V \mathbf{C}_{\text{as}})\mathbf{H}_{\text{as}}\mathbf{b}, \tag{6.39}$$

$$\frac{\partial \mathbf{r}}{\partial \rho} = -\mathbf{H}_{\text{as}}(sV\mathbf{C}_{\text{as}} + V^2\mathbf{K}_{\text{as}})\mathbf{H}_{\text{as}}\mathbf{b}, \tag{6.40}$$

$$\frac{\partial \mathbf{r}}{\partial V} = -\mathbf{H}_{\text{as}}(s\rho\mathbf{C}_{\text{as}} + 2\rho V\mathbf{K}_{\text{as}})\mathbf{H}_{\text{as}}\mathbf{b}. \tag{6.41}$$

For the multiple-input control, the parameters in Eq.(6.34) - Eq.(6.35) are derived by using Jacobi's formula.

$$\frac{\partial \Lambda}{\partial s} = \mathrm{tr}\big(\mathrm{adj}(\mathbf{H}_{\mathrm{as}}^{-1} + s\mathbf{B}\mathbf{F}^{\mathrm{T}} + \mathbf{B}\mathbf{G}^{\mathrm{T}})(2s\mathbf{M} + \mathbf{C}_{\mathrm{s}} + \rho V\mathbf{C}_{\mathrm{as}} + \mathbf{B}\mathbf{F}^{\mathrm{T}})\big), \tag{6.42}$$

$$\frac{\partial \Lambda}{\partial \rho} = \mathrm{tr}\big(\mathrm{adj}(\mathbf{H}_{\mathrm{as}}^{-1} + s\mathbf{B}\mathbf{F}^{\mathrm{T}} + \mathbf{B}\mathbf{G}^{\mathrm{T}})(sV\mathbf{C}_{\mathrm{as}} + V^2\mathbf{K}_{\mathrm{as}})\big), \tag{6.43}$$

$$\frac{\partial \Lambda}{\partial V} = \mathrm{tr}\big(\mathrm{adj}(\mathbf{H}_{\mathrm{as}}^{-1} + s\mathbf{B}\mathbf{F}^{\mathrm{T}} + \mathbf{B}\mathbf{G}^{\mathrm{T}})(s\rho\mathbf{C}_{\mathrm{as}} + 2\rho V\mathbf{K}_{\mathrm{as}})\big). \tag{6.44}$$

The sensitivities of closed-loop poles with respect to the air density and the air speed can be expressed in matrix form as shown below:

$$\mathbf{S}_{\mathrm{AF}} = \begin{bmatrix} S_{\rho,1} & S_{V,1} \\ S_{\rho,2} & S_{V,2} \\ \vdots & \vdots \\ S_{\rho,2n} & S_{V,2n} \end{bmatrix}. \tag{6.45}$$

6.3 Robust pole assignment

In this section, the sensitivities of the closed-loop poles with respect to the uncertain parameters are minimised to make the closed-loop system robust by solving the optimisation problems based on the single-input and multiple-input controls.

For the single-input control,

$$\mathbf{S} = \mathbf{S}_{\mathrm{FIV}}(\mu_{\mathrm{c}}, c_{\mathrm{c}}, k_{\mathrm{c}}, \mathbf{b}, \mathbf{g}, \mathbf{f}) \text{ or } \mathbf{S}_{\mathrm{AF}}(\rho, V, \mathbf{b}, \mathbf{g}, \mathbf{f}). \tag{6.46}$$

It is clear that the sensitivities are functions of the uncertain parameters, the actuator distributions and the control gains. Assuming the uncertain parameters and the actuator distributions are constants, the optimisation problem of the single-input control to minimise the sensitivity is given below

$$\min_{\mathbf{g},\mathbf{f}} \|\mathbf{S}(\mathbf{g}, \mathbf{f})\|_{\mathrm{F}} \text{ subjected to } \Re(\mu_{\max,i}) \leq 0, \tag{6.47}$$

where $\mu_{\max}$ is the closed-loop pole with the maximum uncertain parameters, $\Re(\bullet)$ indicates the real part of a complex number and $\| \bullet \|_{\mathrm{F}}$ denotes the Frobenius norm. The nonlinear constraint as shown above guarantees the stability of the closed-loop system under the maximum perturbations of the uncertain parameters.

Furthermore, the control effort constraint should be regarded to confine the energy supplied to the actuators. It is expressed by

$$\eta = \sqrt{\|\mathbf{b}\mathbf{g}^{\mathrm{T}}\|_{\mathrm{F}}^2 + \|\mathbf{b}\mathbf{f}^{\mathrm{T}}\|_{\mathrm{F}}^2} \leq \beta \tag{6.48}$$

where η is the control effort and β denotes the control effort margin. Although the control effort constraint is able to save energy supplied to the actuators, it reduces the robustness.

Similarly, the optimisation problem of the multiple-input control to minimise the sensitivity with the control effort constraint is given by

$$\min_{\mathbf{G},\mathbf{F}} \|\mathbf{S}(\mathbf{G},\mathbf{F})\|_{\mathrm{F}} \text{ subjected to } \begin{cases} \Re(\mu_{\max,i}) \leq 0 \\ \eta = \sqrt{\|\mathbf{B}\mathbf{G}^{\mathrm{T}}\|_{\mathrm{F}}^2 + \|\mathbf{B}\mathbf{F}^{\mathrm{T}}\|_{\mathrm{F}}^2} \leq \beta \end{cases}. \tag{6.49}$$

It should be noted that the proposed method attempt to minimise the sensitivity matrix by searching the optimal pole locations which are unpredictable. An additional constraint should be considered in order to assign the closed-loop poles within the elliptical region (Tehrani et al. (2011)).

$$\frac{(x - x_{\mathrm{c}})^2}{a^2} + \frac{(y - y_{\mathrm{c}})^2}{b^2} \leq 1 \tag{6.50}$$

where x and y are respectively real and imaginary parts of the closed-loop poles, x_{c} and y_{c} are respectively real and imaginary parts of the ellipse's centre and a and b are respectively radius along the horizontal and vertical directions.

6.4 Numerical examples

In this section, three numerical examples: the friction-induced vibration with single and multiple friction forces and the aerodynamic flutter, are studied as a goal of assigning the closed-loop poles with the minimum sensitivities (robustness). The results are validated by plotting the closed-loop poles perturbed by the uncertainties of the friction coefficient, the contact damping, the contact stiffness (friction-induced vibration), the air density and the air speed (aerodynamic flutter).

6.4.1 Friction-induced vibration with the single friction force

Friction-induced vibration with the single friction force is generally modelled by a mass-spring-damper system on a conveyor belt as illustrated in Figure 6.1 (Liang et al. (2017)).

This model is modified from Ouyang (2010) by adding the contact damping. The system consists of three masses with m_1 having a degree-of-freedom in the horizontal direction, m_3 having a degree-of-freedom in the vertical direction and m_2 having degrees-of-freedom in both directions attached with a linear spring k_3 at 45° relative to the vertical direction. When the belt is moving, a friction force is generated between the belt and the slider. To simplify the problem, Coulomb friction is considered and stick-slip phenomenon is avoided. $\mathbf{M}$, $\mathbf{C}_{\mathrm{s}}$, $\mathbf{K}_{\mathrm{s}}$ and $\mathbf{E}$ corresponding to the displacement vector, $\mathbf{x} = \{x_1, y_3, x_2, y_2\}^{\mathrm{T}}$ are given by,

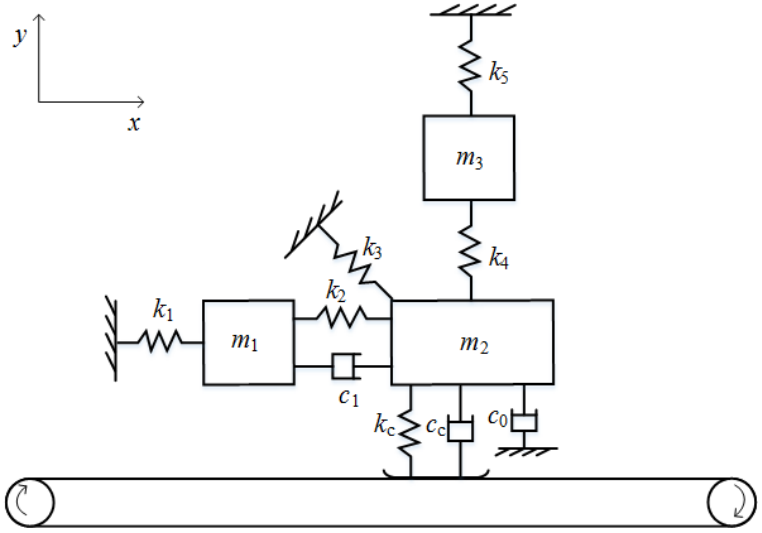

Figure 6.1: Friction-induced vibration with the single friction force

$$\mathbf{M} = \begin{bmatrix} m_1 & 0 & 0 & 0 \\ 0 & m_3 & 0 & 0 \\ 0 & 0 & m_2 & 0 \\ 0 & 0 & 0 & m_2 \end{bmatrix}, \quad \mathbf{C}_{\mathrm{s}} = \begin{bmatrix} c_1 & 0 & -c_1 & 0 \\ 0 & 0 & 0 & 0 \\ -c_1 & 0 & c_1 & 0 \\ 0 & 0 & 0 & c_0 + c_{\mathrm{c}} \end{bmatrix},$$

$$\mathbf{K}_{\mathrm{s}} = \begin{bmatrix} k_1 + k_2 & 0 & -k_2 & 0 \\ 0 & k_4 + k_5 & 0 & -k_4 \\ -k_2 & 0 & k_2 + 0.5k_3 & -0.5k_3 \\ 0 & -k_4 & -0.5k_3 & k_4 + 0.5k_3 + k_{\mathrm{c}} \end{bmatrix},$$

$$\mathbf{E} = \begin{bmatrix} 0 & 0 & 0 & 0 \\ 0 & 0 & 0 & 0 \\ 0 & 0 & 0 & 1 \\ 0 & 0 & 0 & 0 \end{bmatrix}.$$

Parameters used are taken from Liang et al. (2017): mass, $m_i = 1$ kg ($i = 1, 2, 3$); damping, $c_i = 0.5$ Ns/m ($i = 0, 1$); stiffness, $k_i = 100$ N/m ($i = 1, 2, ..., 5$); contact damping, $c_c = 0.1$ Ns/m; contact stiffness, $k_c = 200$ N/m; and friction coefficient, $\mu_c = 0.5$. The open-loop poles are determined by using 'polyeig' function in MATLAB.

$$\{\lambda\}_1^8 = \begin{Bmatrix} 0.0050 \pm 8.9462\text{i} \\ -0.0655 \pm 12.1341\text{i} \\ -0.5174 \pm 16.8229\text{i} \\ -0.2122 \pm 19.7324\text{i} \end{Bmatrix}.$$

The open-loop poles indicate that the system is unstable because the first pair of poles is located on the right-hand side of the complex plane. To make the system stable and robust, the robust pole assignment as mentioned in Section 6.3 is applied to relocate the poles on the left-hand side of the complex plane and minimise their sensitivities.

$$\{\mu\}_1^8 = \begin{Bmatrix} -0.2000 \pm 9.0000\text{i} \\ -0.4000 \pm 12.0000\text{i} \\ -0.5500 \pm 17.0000\text{i} \\ -0.2500 \pm 20.0000\text{i} \end{Bmatrix}.$$

The results are compared with Liang et al. (2017). Based on Liang's work, the perturbations of the contact damping and the contact stiffness are disregarded because of less significant in comparison with the friction coefficient. Bounds of the control gains are set between -40 and 40 and the control effort margin is given at 79 (smaller than the control effort obtained by Liang's work). The uncertain friction coefficient is assumed to vary between 0.35-0.65, which indicates the high level of the perturbations. The radius along the horizontal and vertical directions of the ellipse are 0.1 and 1.7 respectively. The actuator distributions for the single-input and multiple-input controls are given by

$$\mathbf{b} = \begin{Bmatrix} 0 \\ 0 \\ 1 \\ 1 \end{Bmatrix}, \mathbf{B} = \begin{bmatrix} 0 & 0 \\ 0 & 0 \\ 1 & 0 \\ 0 & 1 \end{bmatrix}.$$

Applying Liang's method, the control gains are

$$\mathbf{g}_{\text{Liang}} = \begin{Bmatrix} -6.4253 \\ -29.275 \\ 44.958 \\ -14.650 \end{Bmatrix}, \mathbf{f}_{\text{Liang}} = \begin{Bmatrix} 0.1941 \\ 1.4551 \\ 0.0946 \\ 0.7974 \end{Bmatrix}.$$

Then, the genetic algorithm is applied to Eq.(6.47) for the single-input control and Eq.(6.49) for the multiple-input control to minimise the sensitivities of the closed-loop poles. As a result, the control gains are

$$\mathbf{g}_\eta = \begin{Bmatrix} 3.5570 \\ -12.077 \\ 40.000 \\ 36.854 \end{Bmatrix}, \mathbf{f}_\eta = \begin{Bmatrix} 0.4252 \\ 1.7535 \\ 0.2876 \\ 0.5159 \end{Bmatrix},$$

$$\mathbf{G}_\eta = \begin{bmatrix} 39.934 & 8.1568 \\ 15.346 & -21.864 \\ -21.480 & 39.998 \\ -11.036 & 39.973 \end{bmatrix}, \mathbf{F}_\eta = \begin{bmatrix} 0.0372 & -0.0006 \\ 5.9247 & 1.1683 \\ 0.4135 & -0.0281 \\ 6.8596 & 0.5471 \end{bmatrix}.$$

By using these control gains, the closed-loop poles, the sensitivities of the closed-loop poles, Frobenius norm of the sensitivity matrix and the control effort are obtained as shown in Table 6.1. As can be seen, the closed-loop systems without the perturbations are stable due to all negative real parts of the close-loop poles. Frobenius norm of the sensitivity matrix obtained by the single-input control is about 0.63 being smaller than Liang's method at 0.87.

On the other hand, the smallest norm of the sensitivity matrix is about 0.38 obtained by the multiple-input control. This indicates that the closed-loop poles obtained by the single-input control is less sensitive than Liang's method and the closed-loop poles obtained by the multiple-input control is the least sensitive. In order to gain the confidence level of the results of the robustness of the closed-loop system, 200 samples of the friction coefficient within the range of 0.35-0.65 are generated. The closed-loop poles with the afore-mentioned perturbations are plotted in Figure 6.2.

As a result, the closed-loop poles without the perturbations for all cases are located within the elliptical region. The closed-loop systems with the perturbations are stable because all closed-loop poles are located in the left-hand side of the complex plane. For Liang's method (green crosses) and the single-input control (red circles), the closed-loop poles under the perturbations are moderately shifted from the desired locations (black crosses and circles). For the multiple-input control, the closed-loop poles under the perturbations (yellow triangles) are slightly shifted from the closed-loop poles without the perturbations (black triangles). This means that the multiple-input control is the most effective method to assign the closed-loop poles with their minimum sensitivities.

Table 6.1: Closed-loop poles, sensitivities of closed-loop poles, Frobenius norm of sensitivity matrix and control effort for the friction-induced vibration with the single friction force

Method	μ	S_{μ_c}	$\|\mathbf{S}\|_{\mathrm{F}}$	η
Liang	$-0.1130 \pm 9.7480\mathrm{i}$ $-0.3960 \pm 11.628\mathrm{i}$ $-0.4850 \pm 17.326\mathrm{i}$ $-0.2520 \pm 19.971\mathrm{i}$	$0.1987 \pm 0.4740\mathrm{i}$ $-0.1765 \mp 0.2753\mathrm{i}$ $-0.0221 \mp 0.0316\mathrm{i}$ $-0.0001 \mp 0.0410\mathrm{i}$	0.87	79.21
Single	$-0.1158 \pm 9.9179\mathrm{i}$ $-0.4454 \pm 12.310\mathrm{i}$ $-0.4798 \pm 17.212\mathrm{i}$ $-0.1607 \pm 40.735\mathrm{i}$	$0.2369 \pm 0.1632\mathrm{i}$ $-0.1452 \pm 0.0188\mathrm{i}$ $-0.0880 \pm 0.1757\mathrm{i}$ $-0.0037 \mp 0.2319\mathrm{i}$	0.63	79.00
Multiple	$-0.2351 \pm 8.9207\mathrm{i}$ $-0.3738 \pm 12.242\mathrm{i}$ $-0.4880 \pm 15.770\mathrm{i}$ $-0.1824 \pm 20.966\mathrm{i}$	$0.0119 \pm 0.1218\mathrm{i}$ $0.0025 \pm 0.0660\mathrm{i}$ $-0.0518 \pm 0.1210\mathrm{i}$ $0.0374 \mp 0.1806\mathrm{i}$	0.38	78.99

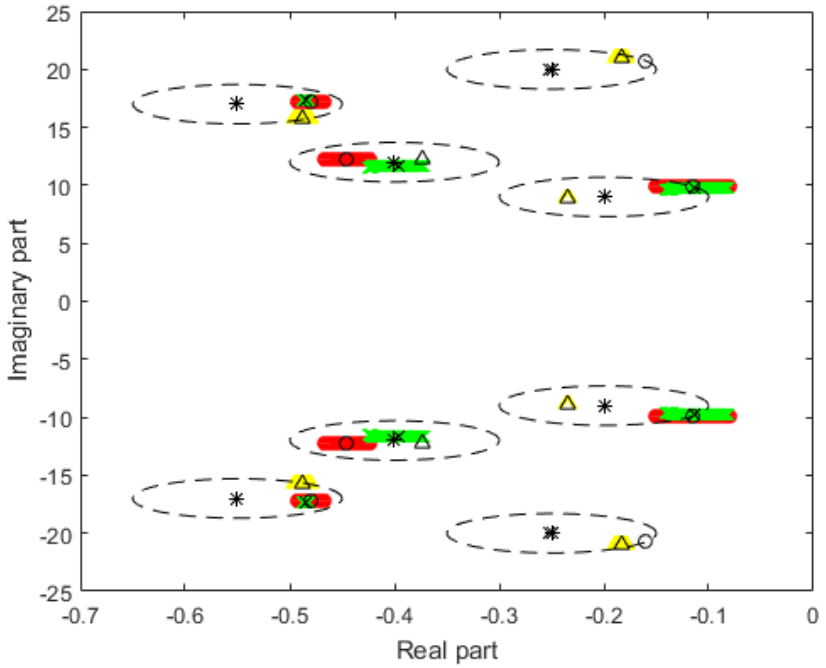

Figure 6.2: The closed-loop poles under the perturbations obtained by Liang's method (green crosses), the single-input (red circles) and the multiple-input (yellow triangles) for the friction-induced vibration with the single friction force

6.4.2 Friction-induced vibration with the multiple friction forces

The next example focuses on the friction-induced vibration with the multiple friction forces as illustrated in Figure 6.3. This model is modified from Ouyang (2009) by adding two contact dampers. The system consists of four masses with m_1 having a degree-of-freedom in the horizontal direction, m_4 having a degree-of-freedom in the vertical direction, m_2 and m_3 having degrees-of-freedom in both directions attached with linear springs; k_5, k_7 and k_{10}, at 45° relative to the vertical direction. When the belt is moving, friction forces are generated to produce asymmetric stiffness and damping matrices. To simplify the problem, Coulomb friction is considered and stick-slip phenomenon is avoided. $\mathbf{M}$, $\mathbf{C}_\mathrm{s}$, $\mathbf{K}_\mathrm{s}$, $\mathbf{E}_1$ and $\mathbf{E}_2$ corresponding to the displacement vector, $\mathbf{x} = \{x_1, y_4, x_2, x_3, y_2, y_3\}^\mathrm{T}$ are given by,

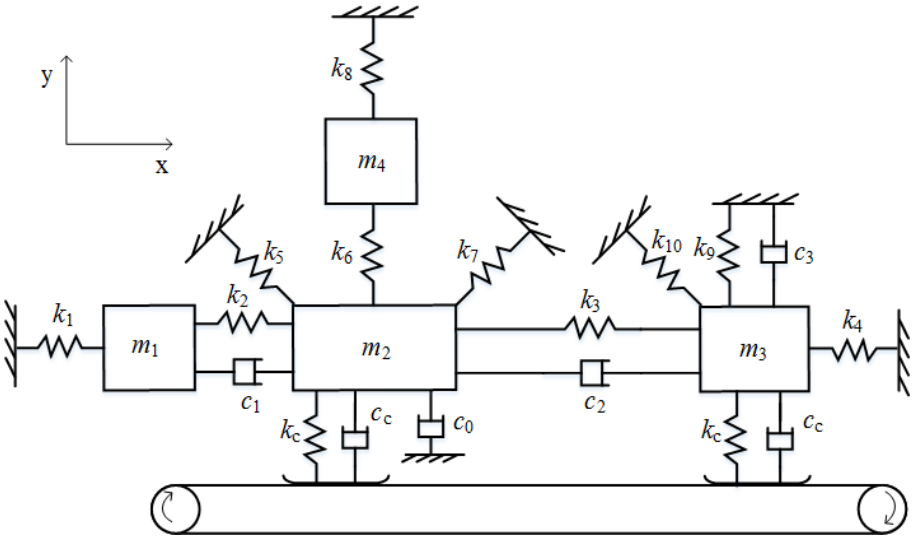

Figure 6.3: Friction-induced vibration with the multiple friction forces

$$\mathbf{M} = \begin{bmatrix} m_1 & 0 & 0 & 0 & 0 & 0 \\ 0 & m_4 & 0 & 0 & 0 & 0 \\ 0 & 0 & m_2 & 0 & 0 & 0 \\ 0 & 0 & 0 & m_3 & 0 & 0 \\ 0 & 0 & 0 & 0 & m_2 & 0 \\ 0 & 0 & 0 & 0 & 0 & m_3 \end{bmatrix},$$

$$\mathbf{C}_\mathrm{s} = \begin{bmatrix} c_1 & 0 & -c_1 & 0 & 0 & 0 \\ 0 & 0 & 0 & 0 & 0 & 0 \\ -c_1 & 0 & c_1 + c_2 & -c_2 & 0 & 0 \\ 0 & 0 & -c_2 & c_2 & 0 & 0 \\ 0 & 0 & 0 & 0 & c_0 + \mathrm{c}_0 & 0 \\ 0 & 0 & 0 & 0 & 0 & c_3 + \mathrm{c}_0 \end{bmatrix},$$

$$\mathbf{K}_{\mathrm{s}} = \begin{bmatrix} k_{11} & 0 & k_{13} & 0 & 0 & 0 \\ 0 & k_{22} & 0 & 0 & k_{25} & 0 \\ k_{31} & 0 & k_{33} & k_{34} & k_{35} & 0 \\ 0 & 0 & k_{43} & k_{44} & 0 & k_{46} \\ 0 & k_{52} & k_{53} & 0 & k_{55} & 0 \\ 0 & 0 & 0 & k_{64} & 0 & k_{66} \end{bmatrix},$$

$$\mathbf{E}_1 = \begin{bmatrix} 0 & 0 & 0 & 0 & 0 & 0 \\ 0 & 0 & 0 & 0 & 0 & 0 \\ 0 & 0 & 0 & 0 & 1 & 0 \\ 0 & 0 & 0 & 0 & 0 & 0 \\ 0 & 0 & 0 & 0 & 0 & 0 \\ 0 & 0 & 0 & 0 & 0 & 0 \end{bmatrix}, \mathbf{E}_2 = \begin{bmatrix} 0 & 0 & 0 & 0 & 0 & 0 \\ 0 & 0 & 0 & 0 & 0 & 0 \\ 0 & 0 & 0 & 0 & 0 & 0 \\ 0 & 0 & 0 & 0 & 0 & 1 \\ 0 & 0 & 0 & 0 & 0 & 0 \\ 0 & 0 & 0 & 0 & 0 & 0 \end{bmatrix},$$

where $k_{11} = k_1 + k_2$, $k_{13} = k_{31} = -k_2$, $k_{22} = k_6 + k_8$, $k_{25} = k_{52} = -k_6$, $k_{33} = k_2 + k_3 + 0.5(k_5 + k_7)$, $k_{34} = k_{43} = -k_3$, $k_{35} = k_{53} = 0.5(k_7 - k_5)$, $k_{44} = k_3 + k_4 + 0.5k_{10}$, $k_{46} = k_{64} = -0.5k_{10}$, $k_{55} = k_{\mathrm{c}} + k_6 + 0.5(k_5 + k_7)$, $k_{66} = k_{\mathrm{c}} + k_9 + 0.5k_{10}$.

Assuming mass, $m_i = 1$ kg $(i = 1, 2, 3, 4)$; damping, $c_i = 0.5$ Ns/m $(i = 0, 1, 2, 3)$; stiffness, $k_i = 100$ N/m $(i = 1, 2, 3, 4, 5, 6, 8, 9, 10)$, $k_7 = 50$ N/m; contact damping, $c_{\mathrm{c}} = 0.1$ Ns/m; contact stiffness, $k_{\mathrm{c}} = 110$ N/m; and friction coefficient, $\mu_{\mathrm{c}} = 0.5$, the open-loop poles are determined by using 'polyeig' function in MATLAB.

$$\lambda = \begin{Bmatrix} 0.0047 \pm 10.384\mathrm{i} \\ -0.1058 \pm 11.450\mathrm{i} \\ -0.2703 \pm 15.208\mathrm{i} \\ -0.2789 \pm 15.978\mathrm{i} \\ -0.1259 \pm 18.873\mathrm{i} \\ -0.8239 \pm 19.685\mathrm{i} \end{Bmatrix}.$$

Obviously, the open-loop poles indicate that the system is unstable because the first pair of poles is located on the right-hand side of the complex plane. To make the system stable and robust, the robust pole assignment as mentioned in Section 6.3 is applied. The closed-loop poles are set as follow:

$$\mu = \begin{Bmatrix} -0.2000 \pm 11.000\mathrm{i} \\ -0.2000 \pm 13.000\mathrm{i} \\ -0.3000 \pm 15.000\mathrm{i} \\ -0.3000 \pm 17.000\mathrm{i} \\ -0.5000 \pm 19.000\mathrm{i} \\ -0.9000 \pm 21.000\mathrm{i} \end{Bmatrix}.$$

Three cases i.e. the single-input with and without the control effort constraint, and the multiple-input with the control effort constraint, are considered. Bounds of the control gains are set between -40 and 40 and the control effort margin is given at 95. The uncertain friction coefficient, uncertain contact damping and uncertain stiffness are respectively assumed to vary between 0.35-0.65, 0.07-0.13 Ns/m and 77-143 N/m which indicate the high level of the perturbations. The radius along the horizontal and vertical directions of the ellipse are 0.2 and 1.0 respectively. The actuator distributions for the single-input and multiple-input controls are given by

$$\mathbf{b} = \begin{Bmatrix} 0 \\ 0 \\ 1 \\ 1 \\ 1 \\ 1 \end{Bmatrix}, \mathbf{B} = \begin{bmatrix} 0 & 0 & 0 & 0 \\ 0 & 0 & 0 & 0 \\ 1 & 0 & 0 & 0 \\ 0 & 1 & 0 & 0 \\ 0 & 0 & 1 & 0 \\ 0 & 0 & 0 & 1 \end{bmatrix}.$$

Then, the genetic algorithm is applied to Eq.(6.47) for the single-input control and Eq.(6.49) for the multiple-input control to minimise the sensitivities of the closed-loop poles. As a result, the control gains are

$$\mathbf{g} = \begin{Bmatrix} -20.938 \\ 26.149 \\ 38.557 \\ 23.844 \\ 25.520 \\ -23.760 \end{Bmatrix}, \mathbf{f} = \begin{Bmatrix} -0.0063 \\ -0.3682 \\ 0.6523 \\ 0.1828 \\ 0.5539 \\ -0.5353 \end{Bmatrix},$$

$$\mathbf{g}_\eta = \begin{Bmatrix} -12.960 \\ 17.624 \\ 34.754 \\ 19.728 \\ 8.6852 \\ -10.073 \end{Bmatrix}, \mathbf{f} = \begin{Bmatrix} 0.7817 \\ -0.8985 \\ 1.0739 \\ 0.4411 \\ -0.1366 \\ 0.1740 \end{Bmatrix},$$

$$\mathbf{G}_\eta = \begin{bmatrix} 0.8884 & 1.0279 & 0.9866 & -2.9343 \\ 4.0235 & 0.9207 & 2.4543 & -0.6765 \\ 7.7985 & -0.5098 & 12.692 & 6.3039 \\ 0.6861 & 6.9234 & -0.1744 & 22.302 \\ -6.9809 & 0.4847 & 12.125 & -2.0627 \\ 3.3896 & -1.9655 & 4.2186 & 14.509 \end{bmatrix},$$

$$\mathbf{F}_\eta = \begin{bmatrix} -1.1538 & 0.8262 & -2.2783 & -0.7309 \\ 4.1290 & 2.8009 & 0.7593 & -1.3378 \\ -1.1020 & 0.3598 & 0.5877 & -0.8380 \\ 0.8453 & 1.3417 & 2.7740 & -0.4793 \\ 0.6649 & 1.3693 & 1.0771 & -0.5751 \\ 2.8478 & -1.5413 & 1.0079 & 0.8695 \end{bmatrix}.$$

By using these control gains, the closed-loop poles, the sensitivities of the closed-loop poles, Frobenius norm of the sensitivity matrix and the control effort are obtained as shown in Table 6.2 and Table 6.3. As can be seen, the closed-loop systems without the perturbations are stable due to all negative real parts of the closed-loop poles. The sensitivities of the closed-loop poles with respect to the friction coefficient are the largest whereas the sensitivities of the closed-loop poles with respect to the stiffness are the smallest. This means that the sensitivities significantly depend on the friction coefficient rather than the stiffness.

Frobenius norm of the sensitivity matrix obtained by the single-input control without the control effort constraint at 0.96, is smaller than the single-input control with the control effort constraint at 2.77. However, the control effort obtained by the single-input control without the control effort constraint at 132.58, is larger than the single-input control with the control effort constraint at 94.98. This is because the control effort constraint limits the control gains which slightly increase the sensitivities (acceptable) but cost problems are improved. Then, the multiple-input control with the control effort constraint is implemented to gain sensitivity and cost problem improvement. The norm of the sensitivity matrix at 0.73, is the smallest and the control effort is confined at 36.75 (see Table 6.3).

In order to investigate the robustness of the closed-loop system, 200 samples of the uncertain friction coefficients in the range of 0.35-0.65, the uncertain contact damping in the range of 0.07-0.13 Ns/m and the uncertain contact stiffness in the range of 77-143 N/m are generated. The closed-loop poles with the aforementioned perturbations are plotted in Figure 6.4. As a result, all closed-loop systems under the perturbations are stable due to all negative real parts of the closed-loop poles.

Obviously, the uncertainties of the closed-loop poles depend on the norm of the sensitivity matrix. The closed-loop poles under the perturbations for the single-input control with the control effort constraint (red circles) are moderately shifted from the desired locations (black circles). Nonetheless, the closed-loop poles under the perturbations for the single-input control without the control effort constraint (green crosses) and the multiple-input control with the control effort constraint (yellow triangles) are slightly shifted from the desired locations (black crosses and triangles).

Table 6.2: Closed-loop poles and their sensitivities for the friction-induced vibration with the multiple friction forces

Parameters	Single-input without control effort constraint	Single-input with control effort constraint	Multiple-input with control effort constraint
μ	-0.0702 ± 10.916i	-0.2216 ± 10.955i	-0.1083 ± 10.500i
	-0.2018 ± 12.274i	-0.2165 ± 12.008i	-0.3199 ± 12.202i
	-0.1208 ± 15.402i	-0.4410 ± 15.696i	-0.4571 ± 14.382i
	-0.2276 ± 16.301i	-0.2273 ± 16.200i	-0.4875 ± 16.722i
	-0.5089 ± 18.953i	-0.3691 ± 18.663i	-0.4529 ± 18.939i
	-0.8976 ± 20.026i	-0.9008 ± 20.000i	-0.8676 ± 20.038i
$S_{\mu_{c,1}}$	0.1342 ∓ 0.0270i	0.5206 ∓ 0.1388i	0.0233 ± 0.1708i
	-0.0789 ∓ 0.0871i	-0.3873 ± 0.0419i	0.1473 ∓ 0.0189i
	0.0088 ± 0.0029i	-0.0001 ± 0.0135i	0.0050 ± 0.0732i
	0.0237 ∓ 0.2221i	0.0044 ∓ 0.1412i	-0.0745 ± 0.0168i
	0.1833 ± 0.0473i	0.1577 ± 0.0139i	-0.0360 ∓ 0.0556i
	-0.2710 ± 0.2077i	-0.2952 ± 0.1477i	-0.0651 ∓ 0.0907i
$S_{\mu_{c,2}}$	0.0324 ± 0.0240i	0.1324 ∓ 0.0239i	-0.1111 ± 0.0865i
	0.0271 ± 0.1739i	0.0871 ± 0.0906i	-0.0327 ± 0.2944i
	0.0767 ± 0.2086i	-0.4999 ± 1.4265i	0.0279 ± 0.1097i
	-0.0509 ± 0.1822i	0.2883 ∓ 0.8261i	0.0701 ± 0.0025i
	-0.0659 ∓ 0.1530i	0.0133 ∓ 0.1706i	0.0758 ∓ 0.1574i
	-0.0193 ∓ 0.2817i	-0.0214 ∓ 0.3275i	-0.0300 ∓ 0.1571i
$S_{c_{c,1}}$	0.0014 ± 0.0067i	0.0066 ± 0.0260i	-0.0082 ± 0.0011i
	0.0049 ∓ 0.0044i	-0.0021 ∓ 0.0212i	0.0009 ± 0.0082i
	-0.0002 ± 0.0006i	-0.0010 ∓ 0.0000i	-0.0048 ± 0.0002i
	0.0165 ± 0.0017i	0.0104 ± 0.0003i	-0.0012 ∓ 0.0057i
	-0.0042 ± 0.0158i	-0.0012 ± 0.0134i	0.0048 ∓ 0.0031i
	-0.0183 ∓ 0.0252i	-0.0127 ∓ 0.0272i	0.0084 ∓ 0.0057i
$S_{c_{c,2}}$	-0.0012 ± 0.0016i	0.0011 ± 0.0066i	-0.0041 ∓ 0.0053i
	-0.0097 ± 0.0015i	-0.0050 ± 0.0047i	-0.0163 ∓ 0.0021i
	-0.0146 ± 0.0055i	-0.1013 ∓ 0.0371i	-0.0072 ± 0.0017i
	-0.0135 ∓ 0.0038i	0.0609 ± 0.0212i	-0.0003 ± 0.0053i
	0.0132 ∓ 0.0056i	0.0145 ± 0.0012i	0.0135 ± 0.0066i
	0.0257 ∓ 0.0011i	0.0299 ∓ 0.0011i	0.0144 ∓ 0.0024i
$S_{k_{c,1}}$	0.0006 ∓ 0.0001i	0.0024 ∓ 0.0007i	0.0001 ± 0.0008i
	-0.0004 ∓ 0.0004i	-0.0018 ± 0.0002i	0.0007 ∓ 0.0001i
	0.0000 ± 0.0000i	0.0000 ± 0.0001i	0.0000 ± 0.0003i
	0.0001 ∓ 0.0010i	0.0000 ∓ 0.0006i	-0.0003 ± 0.0001i
	0.0008 ± 0.0002i	0.0007 ± 0.0001i	-0.0002 ∓ 0.0003i
	-0.0012 ± 0.0010i	-0.0013 ± 0.0007i	-0.0003 ∓ 0.0004i
$S_{k_{c,2}}$	0.0001 ± 0.0001i	0.0006 ∓ 0.0001i	-0.0005 ± 0.0004i
	0.0001 ± 0.0008i	0.0004 ± 0.0004i	-0.0001 ± 0.0013i
	0.0004 ± 0.0009i	-0.0022 ± 0.0065i	0.0001 ± 0.0005i
	-0.0002 ± 0.0008i	0.0013 ∓ 0.0038i	0.0003 ± 0.0000i
	-0.0003 ∓ 0.0007i	0.0000 ∓ 0.0008i	0.0003 ∓ 0.0007i
	-0.0001 ∓ 0.0013i	-0.0001 ∓ 0.0015i	-0.0001 ∓ 0.0007i

Table 6.3: Frobenius norm of sensitivity matrix and control effort for the friction-induced vibration with the multiple friction forces

Parameters	Single-input without control effort constraint	Single-input with control effort constraint	Multiple-input with control effort constraint
$\|S\|_{\mathrm{F}}$	0.96	2.77	0.72
η	132.58	94.98	36.75

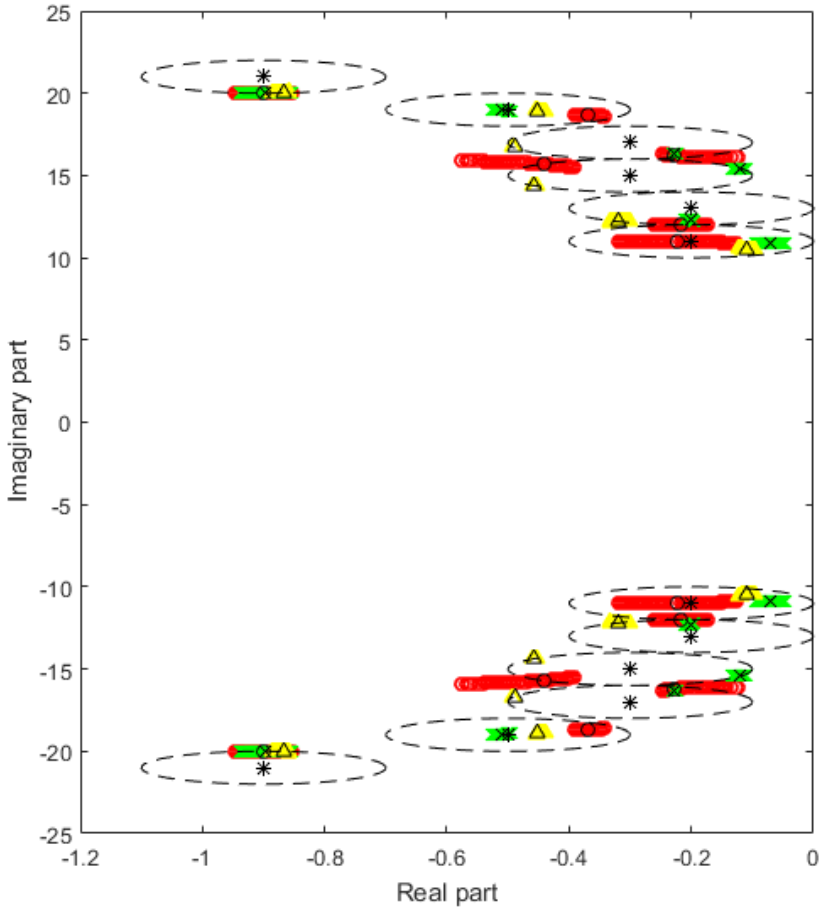

Figure 6.4: The closed-loop poles under the perturbations obtained by the single-input without the control effort constraint (green crosses), the single-input with the control effort constraint (red circles) and the multiple-input with the control effort constraint (yellow triangles) for the friction-induced vibration with the multiple friction forces

6.4.3 Aerodynamic flutter

In this section, the robust pole assignment technique is applied to the aerodynamic flutter problem of a simple rectangular cantilever wing as shown in Figure 5.14 (Wright and Cooper (2008)). The parameters are used as the same with Section 5.4.2 which make the system unstable. Bounds of the control gains are set between -6×10^3 and 6×10^3 and the control effort margin is given at 8×10^3. The uncertain air density and the uncertain air speed are respectively assumed to vary between 1.1515-1.2985 kg/m^3 and 141-159 m/s, which indicate the high level of the perturbations. The radius along the horizontal and vertical directions of the ellipse are 1.5 and 2.0 respectively. The actuator distributions of the single-input and multiple-input controls are given by

$$\mathbf{b} = \begin{Bmatrix} 1 \\ 1 \end{Bmatrix}, \mathbf{B} = \begin{bmatrix} 1 & 0 \\ 0 & 1 \end{bmatrix}.$$

The closed-loop poles are set as follow:

$$\mu = \begin{Bmatrix} -2.0000 \pm 13.000\mathrm{i} \\ -9.0000 \pm 18.000\mathrm{i} \end{Bmatrix}.$$

By using the proposed method, the control gains are

$$\mathbf{g} = \begin{Bmatrix} 5.6191 \\ 5.6037 \end{Bmatrix} \times 10^3, \mathbf{f} = \begin{Bmatrix} 2.4186 \\ 4.0007 \end{Bmatrix} \times 10^3,$$

$$\mathbf{g}_\eta = \begin{Bmatrix} 3.0954 \\ 2.5655 \end{Bmatrix} \times 10^3, \mathbf{f}_\eta = \begin{Bmatrix} 2.0078 \\ 3.4358 \end{Bmatrix} \times 10^3,$$

$$\mathbf{G}_\eta = \begin{bmatrix} -0.2819 & -2.9826 \\ 1.5616 & 3.2860 \end{bmatrix} \times 10^3, \mathbf{F}_\eta = \begin{bmatrix} 3.8004 & 1.9301 \\ -2.0876 & 3.4989 \end{bmatrix} \times 10^3.$$

It is clear from Table 6.4 that the single-input without the control effort constraint gives the small norm of the sensitivity matrix at 21.94, but it requires the large control effort at 13.03×10^3. Then, the single-input with the control effort constraint is applied. The norm of the sensitivity matrix slightly increases to 22.43 but the control effort considerably reduces to 8.00×10^3. Finally, the multiple-input with the control effort constraint is implemented. The norm of the sensitivity matrix is the smallest at 18.796, and the control effort confines at 7.55×10^3. Therefore, robust pole assignment by using the multiple-input control with the control effort constraint is the most effective method among the others. It should be noted that the sensitivities of the closed-loop poles depend on the the air density rather than the air speed.

In order to validate the results, 200 samples of the uncertain air density in range 1.1515-1.2985 kg/m^3 and the uncertain air speed in range 141-159 m/s are generated. The closed-loop poles under the perturbations are plotted as shown in Figure 6.5. As can be seen, the multiple-input control with the control effort constraint under the perturbations (yellow triangles) are slightly shifted from the closed-loop poles without the perturbations (black triangles) which directly refers to the smallest norm of the sensitivity matrix as mentioned above.

Table 6.4: The closed-loop poles, the sensitivities of the closed-loop poles, the norm of the sensitivity matrix and the control effort for the aerodynamic flutter

Parameters	Single-input without control effort constraint	Single-input with control effort constraint	Multiple-input with control effort constraint
μ_c	$-0.5504 \pm 12.8345i$ $-9.3431 \pm 16.9961i$	$-0.5781 \pm 13.6371i$ $-8.1975 \pm 16.3695i$	$-0.6717 \pm 13.5215i$ $-10.119 \pm 17.0213i$
S_ρ	$-4.9035 \mp 11.182i$ $2.9844 \mp 9.0865i$	$-5.9199 \mp 9.4751i$ $4.0008 \mp 10.522i$	$-1.7721 \mp 8.2370i$ $-0.1471 \mp 10.266i$
S_V	$-0.0580 \mp 0.1920i$ $0.0424 \mp 0.1342i$	$-0.0738 \mp 0.1686i$ $0.0581 \mp 0.1533i$	$-0.0128 \mp 0.1463i$ $-0.0029 \mp 0.1466i$
$\|S\|_F$	21.94	22.43	18.79
η	13.03×10^3	8.00×10^3	7.55×10^3

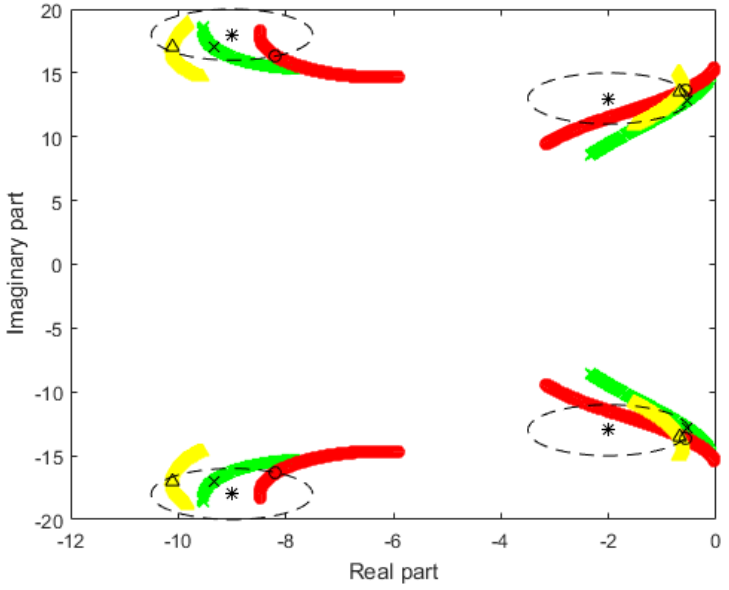

Figure 6.5: The closed-loop poles under perturbations of air density and air speed: the single-input without the control effort constraint (green crosses), the single-input with the control effort constraint (red circles) and the multiple-input with the control effort constraint (yellow triangles) for the aerodynamic flutter

6.5 Summary

In conclusions, robust pole assignment for the asymmetric system is proposed to assign the closed-loop poles with as small sensitivities as possible under a certain constraint. Both the single-input control and the multiple-input control are applied to derive the sensitivities of the closed-loop poles with respect to uncertain parameters i.e. the friction coefficient, the contact damping, the contact stiffness (friction-induced vibration), the air density and the air speed (aerodynamic flutter). The proposed method is achieved by applying the genetic algorithm to minimise Frobenius norm of the sensitivity matrix. Numerical examples of the friction-induced vibration with both single and multiple friction forces and the aerodynamic flutter of the rectangular wing are shown that the robust pole assignment by using the multiple-input control is the most effective method to assign the closed-loop poles with their minimum sensitivities.

Chapter 7

Conclusions and future work

7.1 Conclusions

In this research, power flow mode theory based on damping distribution is applied to determine the optimal locations of poles for minimising the vibration (see Chapter 3). The basic concept of this theory is to minimise vibration by maximising time-averaged power dissipation per unit characteristic velocity or the trace of the damping matrix. To archive this theory, damping coefficients (passive control) or velocity gains (active control) must be maximised. Numerical results show that this theory is capable to reduce the vibration especially around resonances in passive control but the high damping coefficients may change the underdamped system to the overdamped system. For single-input and multiple-input velocity feedback controls, maximum velocity gains cannot minimise the vibration. This means that power flow mode theory based on damping distribution is only suitable for the passive control. Therefore, this theory cannot apply to the active pole assignment to determine the optimal locations of poles for minimising the vibration.

Then, partial pole assignment for the asymmetric system by using the unobservability condition is developed (see Chapter 4). It requires only unassigned poles to keep them unchanged. The control strategies are considered on velocity and displacement feedback, acceleration and velocity feedback, as well as acceleration and displacement feedback. The receptance method is applied to avoid modelling errors from evaluating mass, damping and stiffness matrices by using FEM. The solutions to determine the control gains are rearranged in the linear equations by using Sherman-Morrison formula which can be solved directly. The proposed method with three control strategies implemented to the asymmetric system modelled by the disc brake, is capable to assign the poles precisely and keep other unchanged except acceleration and displacement feedback. This

is because partial pole assignment by using acceleration and displacement feedback is ill-conditioned.

Various sets of the actuator distribution vectors are considered to determine the optimal actuator distribution vector for minimising the energy supplied to the actuators. Alternatively, the genetic algorithm is also implemented to determine the optimal one. The results show that the optimal actuator distribution vector is modified when the location of poles are changed. In addition, velocity and displacement feedback and acceleration and velocity feedback are compared to determine the most effective method for minimising the energy index. It is found that both methods give the same energy index.

In fact, the time delay always exists in active pole assignment due to sensing and actuating in the feedback loop. It may degrade the control performance and destabilise the closed-loop system. To cope with this problem, partial pole assignment with time delays for the asymmetric system is proposed (see Chapter 5). Both single and multiple commensurate time delays are considered. The unobservability condition as mention in Chapter 4 is applied to keep unassigned poles unchanged. The receptance method is used to avoid modelling errors from FEM and the Sherman-Morrison formula is applied to reformulate the partial pole assignment problem in the linear equations which can be solved directly.

Three numerical examples: friction-induced vibration and aerodynamic flutter, show that the proposed method can assign the required closed-loop precisely without spillover effect. The stability of the closed-loop system is analysed by evaluating the first few dominant poles and determining the critical time delay. By using TRACE-DDE toolbox in MATLAB, the dominant closed-loop poles are determined. Some of them shows that the required closed-loop poles are assigned accurately and the others produced by the effect of the time delays are located on the left-hand side of the complex plane which indicate the stability. Nonetheless, they cannot guarantee the stability because the residual poles have unknown yet. To ensure stability, the frequency-sweeping test is applied to determine the critical time delay.

Finally, robust pole assignment for the asymmetric system is proposed to assign the closed-loop poles with their minimum sensitivities (see Chapter 6). Algorithms of partial pole assignment with and without time delays as mentioned above are capable to assign the required closed-loop poles precisely when perturbations are disregarded. Nonetheless, the perturbations are inevitable and make the closed-loop poles shifted from the desired positions. They may destabilise the system when the closed-loop poles shifted to the right-hand side of the complex plane. To solve the problem, the sensitivities of the closed-loop poles with respect to the uncertain parameters must be minimised.

Both single-input and the multiple-input controls are applied. The sensitivities of the closed-loop poles with respect to the uncertain parameters i.e. the friction coefficient, the contact damping, the contact stiffness (friction-induced vibration), the air density and the air speed (aerodynamic flutter) are derived. The solution is formulated in the optimisation problem in order to search the control gains for minimising Frobenius norm of the sensitivity matrix. Additional control effort constraint is also considered to confine energy supplied to the actuators. Numerical examples of the friction-induced vibration with both single and multiple friction forces and the aerodynamic flutter of the rectangular wing are shown that the robust pole assignment by using the multiple-input control is the most effective method to assign the closed-loop poles with the smallest sensitivities.

7.2 Future work

The next research should be considered on hybrid partial pole assignment (combination of passive structural modification and active pole assignment) and pole assignment for non-linear asymmetric systems. An experimental work for the real disc brake system is also focus. The number of future works is listed below.

- Partial pole assignment by using a combination of passive structural modification and active pole assignment is considered to gain advantages of both methods. Basically, the active pole assignment allows to assign the required closed-loop poles precisely but it requires the large control effort which reflects to the cost. To deal with this problem, the passive structural modification by adding mass, damping and stiffness is combined into the active pole assignment.
- Pole assignment for non-linear asymmetric systems challenges to the next research. Normally, linear springs and linear dampers are assumed. In fact, they are non-linear. In order to solve this problem, pole assignment for the nonlinear system should be considered.
- The next step is to consider on the experimental work. The proposed methods are applied to stabilise the real disc brake system.

References

Andry, A., Shapiro, E., and Chung, J. (1983). Eigenstructure assignment for linear systems. *IEEE Transactions on Aerospace and Electronic Systems*, (5):711–729.

Ariyatanapol, R., Xiong, Y., and Ouyang, H. (2018). Partial pole assignment with time delays for asymmetric systems. *Acta Mechanica*, 229(6):2619–2629. doi.org/10.1007/s00707-018-2118-2.

Bai, Z.-J., Chen, M.-X., and Yang, J.-K. (2012). A multi-step hybrid method for multi-input partial quadratic eigenvalue assignment with time delay. *Linear Algebra and its Applications*, 437(7):1658–1669.

Baumann, O. N. and Elliott, S. J. (2007). Destabilization of velocity feedback controllers with stroke limited inertial actuators. *The Journal of the Acoustical Society of America*, 121(5):211–217.

Beshara, M. and Keane, A. (1998). Vibrational energy flows between plates with compliant and dissipative couplings. *Journal of Sound and Vibration*, 213(3):511–535.

Billah, K. Y. and Scanlan, R. H. (1991). Resonance, tacoma narrows bridge failure, and undergraduate physics textbooks. *American Journal of Physics*, 59(2):118–124.

Brahma, S. and Datta, B. (2009). An optimization approach for minimum norm and robust partial quadratic eigenvalue assignment problems for vibrating structures. *Journal of Sound and Vibration*, 324(3):471–489.

Breda, D., Maset, S., and Vermiglio, R. (2009). TRACE-DDE: a tool for robust analysis and characteristic equations for delay differential equations. In *Topics in Time Delay Systems*, pages 145–155. Springer.

Choi, W., Xiong, Y., and Shenoi, R. (2009). Power flow analysis for a floating sandwich raft isolation system using a higher-order theory. *Journal of Sound and Vibration*, 319(1):228–246.

Chu, E. (2002). Pole assignment for second-order systems. *Mechanical Systems and Signal Processing*, 16(1):39–59.

Chu, E. and Datta, B. (1996). Numerically robust pole assignment for second-order systems. *International Journal of Control*, 64(6):1113–1127.

Clarkson, B. (1991). Estimation of the coupling loss factor of structural joints. *Proceedings of the Institution of Mechanical Engineers, Part C: Mechanical Engineering Science*, 205(1):17–22.

Cuschieri, J. (1990a). Structural power-flow analysis using a mobility approach of an l-shaped plate. *The Journal of the Acoustical Society of America*, 87(3):1159–1165.

Cuschieri, J. (1990b). Vibration transmission through periodic structures using a mobility power flow approach. *Journal of Sound and Vibration*, 143(1):65–74.

Datta, B. and Sarkissian, D. (1999). Multi-input partial eigenvalue assignment for the symmetric quadratic pencil. In *American Control Conference, 1999. Proceedings of the 1999*, volume 4, pages 2244–2247. IEEE.

Datta, B. N., Elhay, S., and Ram, Y. M. (1997). Orthogonality and partial pole assignment for the symmetric definite quadratic pencil. *Linear Algebra and its Applications*, 257:29–48.

Davison, E. and Wang, S. (1975). On pole assignment in linear multivariable systems using output feedback. *IEEE Transactions on Automatic Control*, 20(4):516–518.

Elliott, S., Serrand, M., and Gardonio, P. (2001). Feedback stability limits for active isolation systems with reactive and inertial actuators. *Journal of Vibration and Acoustics*, 123(2):250–261.

Farag, N. and Pan, J. (1996). Dynamic response and power flow in two-dimensional coupled beam structures under in-plane loading. *The Journal of the Acoustical Society of America*, 99(5):2930–2937.

Gardonio, P., Bianchi, E., and Elliott, S. (2004). Smart panel with multiple decentralized units for the control of sound transmission. Part II: design of the decentralized control units. *Journal of Sound and Vibration*, 274(1):193–213.

Gardonio, P., Elliott, S., and Pinnington, R. (1997a). Active isolation of structural vibration on a multiple-degree-of-freedom system, Part I: the dynamics of the system. *Journal of Sound and Vibration*, 207(1):61–93.

Gardonio, P., Elliott, S., and Pinnington, R. (1997b). Active isolation of structural vibration on a multiple-degree-of-freedom system, Part II: effectiveness of active control strategies. *Journal of Sound and Vibration*, 207(1):95–121.

Gardonio, P. and Elliott, S. J. (1999). Active control of structure-borne and airborne sound transmission through double panel. *Journal of Aircraft*, 36(6):1023–1032.

Gardonio, P. and Elliott, S. J. (2005). Modal response of a beam with a sensor–actuator pair for the implementation of velocity feedback control. *Journal of Sound and Vibration*, 284(1):1–22.

Gatti, G., Brennan, M. J., and Gardonio, P. (2007). Active damping of a beam using a physically collocated accelerometer and piezoelectric patch actuator. *Journal of Sound and Vibration*, 303(3):798–813.

Goyder, H. and White, R. (1980a). Vibrational power flow from machines into built-up structures, Part I: introduction and approximate analyses of beam and plate-like foundations. *Journal of Sound and Vibration*, 68(1):59–75.

Goyder, H. and White, R. (1980b). Vibrational power flow from machines into built-up structures, Part III: power flow through isolation systems. *Journal of Sound and Vibration*, 68(1):97–117.

Goyder, H. and White, R. (1980c). Vibrational power flow from machines into built-up structures,Part II: Wave propagation and power flow in beam-stiffened plates. *Journal of Sound and Vibration*, 68(1):77–96.

Gu, K., Chen, J., and Kharitonov, V. L. (2003). *Stability of time-delay systems*. Springer Science & Business Media.

Guzzardo, C., Pang, S., and Ram, Y. (2013). Optimal actuation in vibration control. *Mechanical Systems and Signal Processing*, 35(1):279–290.

Hambric, S. (1990). Power flow and mechanical intensity calculations in structural finite element analysis. *Journal of Vibration and Acoustics*, 112(4):542–549.

Hambric, S. and Taylor, P. (1994). Comparison of experimental and finite element structure-borne flexural power measurements for a straight beam. *Journal of Sound and Vibration*, 170(5):595–605.

Hoffmann, N., Fischer, M., Allgaier, R., and Gaul, L. (2002). A minimal model for studying properties of the mode-coupling type instability in friction induced oscillations. *Mechanics Research Communications*, 29(4):197–205.

Hong, C., Gardonio, P., and Elliott, S. J. (2007). Active control of resiliently mounted beams using triangular actuators. *Journal of Sound and Vibration*, 301(1):297–318.

Huh, Y. C., Chung, T. Y., Lee, J. W., and Kim, J. K. (2015). Damage identification in plates using vibratory power estimated from measured accelerations. *Journal of Sound and Vibration*, 336:106–131.

Jayachandran, V. and Sun, J. (1997). Unconditional stability domains of structural control systems using dual actuator–sensor pairs. *Journal of Sound and Vibration*, 208(1):159–166.

Ji, L., Mace, B., and Pinnington, R. (2003). A power mode approach to estimating vibrational power transmitted by multiple sources. *Journal of Sound and Vibration*, 265(2):387–399.

Juang, J. and Maghami, P. G. (1992). Robust eigensystem assignment for state estimators using second-order models. *Journal of Guidance, Control, and Dynamics*, 15(4):920–927.

Kautsky, J., Nichols, N. K., and Van Dooren, P. (1985). Robust pole assignment in linear state feedback. *International Journal of Control*, 41(5):1129–1155.

Kessissoglou, N. J. (2004). Power transmission in L-shaped plates including flexural and in-plane vibration. *The Journal of the Acoustical Society of America*, 115(3):1157–1169.

Kimura, H. (1975). Pole assignment by gain output feedback. *IEEE Transactions on Automatic Control*, 20(4):509–516.

Koh, Y. and White, R. (1996a). Analysis and control of vibrational power transmission to machinery supporting structures subjected to a multi-excitation system, part i: Driving point mobility matrix of beams and rectangular plates. *Journal of Sound and Vibration*, 196(4):469–493.

Koh, Y. and White, R. (1996b). Analysis and control of vibrational power transmission to machinery supporting structures subjected to a multi-excitation system, part ii: Vibrational power analysis and control schemes. *Journal of Sound and Vibration*, 196(4):495–508.

Koh, Y. and White, R. (1996c). Analysis and control of vibrational power transmission to machinery supporting structures subjected to a multi-excitation system, part iii: Vibrational power cancellation and control experiments. *Journal of Sound and Vibration*, 196(4):509–522.

Li, T., Zhang, W., and Liu, T. (2001). Vibrational power flow analysis of damaged beam structures. *Journal of Sound and Vibration*, 242(1):59–68.

Li, W. and Lavrich, P. (1999). Prediction of power flows through machine vibration isolators. *Journal of Sound and Vibration*, 224(4):757–774.

Li, Y. and Yam, L. (2001). A robust design method of active controller for uncertain vibration systems. *Journal of Vibration and Control*, 7(3):453–466.

Liang, Y., Ouyang, H., and Yamaura, H. (2016). Active partial eigenvalue assignment for friction-induced vibration using receptance method. In *Journal of Physics: Conference Series*, volume 744, page 012008. IOP Publishing.

Liang, Y., Yamaura, H., and Ouyang, H. (2017). Active assignment of eigenvalues and eigen-sensitivities for robust stabilization of friction-induced vibration. *Mechanical Systems and Signal Processing*, 90:254–267.

Linjama, J. and Lahti, T. (1992). Estimation of bending wave intensity in beams using the frequency response technique. *Journal of Sound and Vibration*, 153(1):21–36.

Liu, Z., Li, W., Ouyang, H., and Wang, D. (2015). Eigenstructure assignment in vibrating systems based on receptances. *Archive of Applied Mechanics*, 85(6):713–724.

Mace, B. and Shorter, P. (2000). Energy flow models from finite element analysis. *Journal of sound and vibration*, 233(3):369–389.

Ming, R., Pan, J., and Norton, M. (1999). The mobility functions and their application in calculating power flow in coupled cylindrical shells. *The Journal of the Acoustical Society of America*, 105(3):1702–1713.

Moore, B. C. (1975). On the flexibility offered by state feedback in multivariable systems beyond closed loop eigenvalue assignment. In *Decision and Control Including the 14th Symposium on Adaptive Processes*, volume 14, pages 207–214. IEEE.

Mottershead, J. E., Tehrani, M. G., James, S., and Ram, Y. M. (2008). Active vibration suppression by pole-zero placement using measured receptances. *Journal of Sound and Vibration*, 311(3):1391–1408.

Mottershead, J. E., Tehrani, M. G., and Ram, Y. M. (2009). Assignment of eigenvalue sensitivities from receptance measurements. *Mechanical Systems and Signal Processing*, 23(6):1931–1939.

Noiseux, D. (1970). Measurement of power flow in uniform beams and plates. *The Journal of the Acoustical Society of America*, 47(1B):238–247.

Olgac, N. and Sipahi, R. (2002). An exact method for the stability analysis of time-delayed linear time-invariant (LTI) systems. *IEEE Transactions on Automatic Control*, 47(5):793–797.

Ouyang, H. (2009). Prediction and assignment of latent roots of damped asymmetric systems by structural modifications. *Mechanical Systems and Signal Processing*, 23(6):1920–1930.

Ouyang, H. (2010). Pole assignment of friction-induced vibration for stabilisation through state-feedback control. *Journal of Sound and Vibration*, 329(11):1985–1991.

Ouyang, H. (2011). A hybrid control approach for pole assignment to second-order asymmetric systems. *Mechanical Systems and Signal Processing*, 25(1):123–132.

Ouyang, H., Richiedei, D., and Trevisani, A. (2013). Pole assignment for control of flexible link mechanisms. *Journal of Sound and Vibration*, 332(12):2884–2899.

Pan, J., Hansen, C. H., and Pan, J. (1993). Active isolation of a vibration source from a thin beam using a single active mount. *The Journal of the Acoustical Society of America*, 94(3):1425–1434.

Pan, J. and Pan, J. (1998). A comparison of modal expansion and travelling wave methods for predicting energy flow in beam structures. *Journal of sound and vibration*, 214(1):1–15.

Pan, J., Pan, J., and Hansen, C. H. (1992). Total power flow from a vibrating rigid body to a thin panel through multiple elastic mounts. *The Journal of the Acoustical Society of America*, 92(2):895–907.

Park, D.-H., Hong, S.-Y., Kil, H.-G., and Jeon, J.-J. (2001). Power flow models and analysis of in-plane waves in finite coupled thin plates. *Journal of Sound and Vibration*, 244(4):651–668.

Pavić, G. (1976). Measurement of structure borne wave intensity, part i: Formulation of the methods. *Journal of Sound and Vibration*, 49(2):221–230.

Pratt, J. M., Singh, K. V., and Datta, B. N. (2009). Quadratic partial eigenvalue assignment problem with time delay for active vibration control. In *Journal of Physics: Conference Series*, volume 181, page 012092. IOP Publishing.

Preumont, A. (2011). *Vibration control of active structures: an introduction*, volume 179. Springer Science & Business Media.

Ram, Y. and Elhay, S. (2000). Pole assignment in vibratory systems by multi-input control. *Journal of Sound and Vibration*, 230(2):309–321.

Ram, Y., Mottershead, J., and Tehrani, M. G. (2011). Partial pole placement with time delay in structures using the receptance and the system matrices. *Linear Algebra and its Applications*, 434(7):1689–1696.

Ram, Y. and Mottershead, J. E. (2013). Multiple-input active vibration control by partial pole placement using the method of receptances. *Mechanical Systems and Signal Processing*, 40(2):727–735.

Ram, Y., Singh, A., and Mottershead, J. E. (2009). State feedback control with time delay. *Mechanical Systems and Signal Processing*, 23(6):1940–1945.

Ram, Y. M. (1998). Pole assignment for the vibrating rod. *The Quarterly Journal of Mechanics and Applied Mathematics*, 51(3):461–476.

Ram, Y. M. and Mottershead, J. E. (2007). Receptance method in active vibration control. *AIAA Journal*, 45(3):562.

Rao, S. S. (2004). Mechanical vibrations. 4th.

Shankar, K. and Keane, A. (1995a). Energy flow predictions in a structure of rigidly joined beams using receptance theory. *Journal of Sound and Vibration*, 185(5):867–890.

Shankar, K. and Keane, A. (1995b). A study of the vibrational energies of two coupled beams by finite element and green function (receptance) methods. *Journal of Sound and Vibration*, 181(5):801–838.

Shankar, K. and Keane, A. (1997). Vibrational energy flow analysis using a substructure approach: The application of receptance theory to fea and sea. *Journal of Sound and Vibration*, 201(4):491–513.

Shin, C., Hong, C., and Jeong, W. B. (2013). Active vibration control of beams using filtered-velocity feedback controllers with moment pair actuators. *Journal of Sound and Vibration*, 332(12):2910–2922.

Singh, K. V., Dey, R., and Datta, B. N. (2014). Partial eigenvalue assignment and its stability in a time delayed system. *Mechanical Systems and Signal Processing*, 42(1):247–257.

Singh, K. V. and Ouyang, H. (2013). Pole assignment using state feedback with time delay in friction-induced vibration problems. *Acta Mechanica*, 224(3):645.

Singh, K. V. and Ram, Y. M. (2002). Transcendental eigenvalue problem and its applications. *AIAA Journal*, 40(7):1402–1407.

Soong, T. (1990). *Active structural control: theory and practice*. Longman Structural Engineering and Struc Series. Longman Scientific & Technical.

Srinathkumar, S. (1978). Eigenvalue/eigenvector assignment using output feedback. *IEEE Transactions on Automatic Control*, 23(1):79–81.

Sun, L., Leung, A., Lee, Y., and Song, K. (2007). Vibrational power-flow analysis of a mimo system using the transmission matrix approach. *Mechanical Systems and Signal Processing*, 21(1):365–388.

Tehrani, M. G., Elliott, R. N., and Mottershead, J. E. (2010). Partial pole placement in structures by the method of receptances: theory and experiments. *Journal of Sound and Vibration*, 329(24):5017–5035.

Tehrani, M. G., Mottershead, J. E., Shenton, A. T., and Ram, Y. M. (2011). Robust pole placement in structures by the method of receptances. *Mechanical Systems and Signal Processing*, 25(1):112–122.

Tehrani, M. G. and Ouyang, H. (2012). Receptance-based partial pole assignment for asymmetric systems using state-feedback. *Shock and Vibration*, 19(5):1135–1142.

Tehrani, M. G., Wilmshurst, L., and Elliott, S. J. (2013). Receptance method for active vibration control of a nonlinear system. *Journal of Sound and Vibration*, 332(19):4440–4449.

Tehrani, M. G., Wilmshurst, L. I., and Elliott, S. J. (2015). Bifurcation control of a duffing oscillator using pole placement. *Journal of Vibration and Control*, 21(14):2838–2851.

Vahid-Araghi, O. and Golnaraghi, F. (2010). *Friction-induced vibration in lead screw drives*. Springer Science & Business Media.

Verheij, J. (1980). Cross spectral density methods for measuring structure borne power flow on beams and pipes. *Journal of Sound and Vibration*, 70(1):133–138.

Vyhlidal, T. and Zitek, P. (2009). Mapping based algorithm for large-scale computation of quasi-polynomial zeros. *IEEE Transactions on Automatic Control*, 54(1):171–177.

Wang, Z., Xing, J., and Price, W. (2002a). An investigation of power flow characteristics of L-shaped plates adopting a substructure approach. *Journal of Sound and Vibration*, 250(4):627–648.

Wang, Z., Xing, J., and Price, W. (2002b). Power flow analysis of indeterminate rod/beam systems using a substructure method. *Journal of Sound and Vibration*, 249(1):3–22.

Wang, Z., Xing, J., and Price, W. (2004). A study of power flow in a coupled plate–cylindrical shell system. *Journal of Sound and Vibration*, 271(3):863–882.

Wei, X., Maha, A., Ram, Y., and Mottershead, J. (2014). The role of controllability and observability in partial pole placement by the method of receptance. In *International Conference on Noise and Vibration Engineering (ISMA)*.

Wong, W., Wang, X., and Cheng, L. (2009). Modal power flow analysis of a damaged plate. *Journal of Sound and Vibration*, 320(1-2):84–100.

Wonham, W. (1967). On pole assignment in multi-input controllable linear systems. *IEEE Transactions on Automatic Control*, 12(6):660–665.

Wright, J. R. and Cooper, J. E. (2008). *Introduction to aircraft aeroelasticity and loads*, volume 20. John Wiley & Sons.

Wu, C. and White, R. (1995). Vibrational power transmission in a finite multi-supported beam. *Journal of Sound and Vibration*, 181(1):99–114.

Xiang, J., Zhen, C., and Li, D. (2016). Partial pole assignment with time delay by the receptance method using multi-input control from measurement output feedback. *Mechanical Systems and Signal Processing*, 66:743–755.

Xing, J.-T. and Price, W. (1999). A power–flow analysis based on continuum dynamics. In *Proceedings of the Royal Society of London A: Mathematical, Physical and Engineering Sciences*, volume 455, pages 401–436. The Royal Society.

Xiong, Y., Xing, J., and Price, W. (2001). Power flow analysis of complex coupled systems by progressive approaches. *Journal of Sound and Vibration*, 239(2):275–295.

Xiong, Y.-P. (2015). Novel approach for structural dynamic topology optimizations based on power flow mode theory. In *Vibration Engineering and Technology of Machinery*, pages 1065–1076. Springer.

Xiong, Y.-P., Xing, J., and Price, W. (2005). A power flow mode theory based on a system's damping distribution and power flow design approaches. In *Proceedings of the Royal Society of London A: Mathematical, Physical and Engineering Sciences*, volume 461, pages 3381–3411. The Royal Society.

Xu, S. and Qian, J. (2008). Orthogonal basis selection method for robust partial eigenvalue assignment problem in second-order control systems. *Journal of Sound and Vibration*, 317(1):1–19.

Yang, J., Ouyang, H., and Zhang, J.-F. (2016). A new method of updating mass and stiffness matrices simultaneously with no spillover. *Journal of Vibration and Control*, 22(5):1181–1189.

Zhang, J., Ouyang, H., and Yang, J. (2014). Partial eigenstructure assignment for undamped vibration systems using acceleration and displacement feedback. *Journal of Sound and Vibration*, 333(1):1–12.

Zhang, J., Ouyang, H., Zhang, Y., and Ye, J. (2015). Partial quadratic eigenvalue assignment in vibrating systems using acceleration and velocity feedback. *Inverse Problems in Science and Engineering*, 23(3):479–497.

Zhang, J.-h. and Li, D.-s. (2016). Mobility power flows of thin circular plate carrying concentrated masses based on structural circumferential periodicity. *Proceedings of the Institution of Mechanical Engineers, Part C: Journal of Mechanical Engineering Science*, 230(17):2996–3011.

Zhen, C., Jiffri, S., Li, D., Xiang, J., and Mottershead, J. E. (2018). Feedback linearisation of nonlinear vibration problems: A new formulation by the method of receptances. *Mechanical Systems and Signal Processing*, 98:1056–1068.

Zilletti, M., Elliott, S. J., and Gardonio, P. (2010). Self-tuning control systems of decentralised velocity feedback. *Journal of Sound and Vibration*, 329(14):2738–2750.